

Rapid load testing of piles in sand

Effects of loading rate and excess pore pressure

PROEFSCHRIFT

ter verkrijging van de graad van doctor
aan de Technische Universiteit Delft,
op gezag van de Rector Magnificus prof. dr. ir. J. T. Fokkema,
voorzitter van het College voor Promoties,
in het openbaar te verdedigen op dinsdag 23 september 2008 om 15.00 uur

door

Quang Huy NGUYEN
Master of Engineering, Hanoi University of Civil Engineering
geboren te Hanoi, Vietnam

Dit manuscript is goedgekeurd door de promotor:
Prof. ir. A. F. van Tol

Samenstelling promotiecommissie:

Rector Magnificus
Prof. ir. A. F. van Tol
Prof. dr. A. Hyde
Prof. dr. ir. F.B.J. Barends
Prof. ir. C.A. Willemse
Dr. A.V. Metrinkine
Dr. P. Hölscher
Ir. P. Middendorp
Reservelid Prof. ir. J.W. Bosch

Voorzitter
Technische Universiteit Delft, promotor
University of Sheffield, The United Kingdom
Technische Universiteit Delft
Technische Universiteit Delft
Technische Universiteit Delft
Deltares, Delft, the Netherlands
Profound, the Netherland
Technische Universiteit Delft

Copyright © 2008 by Nguyen Quang Huy
ISBN
Printed in the Netherlands

To my family

Acknowledgement

This research is supported by the Vietnamese Ministry of Education and Training, CICAT Management Centre for International Cooperation, Delft Cluster and CUR commission “Rapid pile load test” (CUR-H410). Their contributions are gratefully acknowledged.

The hospitality of the Geotechnical Laboratory of the Civil Engineering department of Delft University of Technology is greatly appreciated.

I would like to express my thankfulness to my promotor, Prof. van Tol, for his tolerance, continuous encouragement and profound comments. I would also like to thank Dr. Hölscher for his guidance, incisive advice, questions and patience. Without the support from you all this thesis will not become reality.

I am thankful to many people who have contributed to the work presented in this thesis. Especially, Mr. Aad Schappers for your help with the triaxial tests; Jelke Dijkstra and Archeewa for the model pile tests; Haike van Lottum, Adam Bezuijen and the centrifuge technical team in Deltares for the centrifuge test; Michelle Simpson for the reviewing english of this thesis; Tuan for the cover. Thanks also given to Veronique van der Varst and Theda Olsder from CICAT; Dao Tang Kiem from Hanoi University of Civil Engineering for their administrative support.

Thank you very much for you all VCID’ers, who accompany me in many recreative activities. Big expression is given to you Liems, who had shortened their time to lengthen my time.

Lastly but never enough I am deeply indebted to my family. Especially, to my parents for their continuous support and encouragement; to my two little stars: Huong and TuTu, for their endless love and patience. They are always my inspiration and motivation; this thesis is dedicated to them.

Nguyen Quang Huy
Delft, August 2008

Summary

With the aim to create a load test method for piles, which is less time-consuming than the conventional static load test and less complicated to analyze than the dynamic load test, the rapid pile load test was developed. However, the broad acceptance of this test method is limited due to the fact that the treatment of the rate effect and excess pore pressure effect in the utilized interpretation methods is not clear. This research aims to clarify these two effects for the case of a pile founded in sand, subjected to the rapid load test. The work described in this thesis includes laboratory tests, numerical investigations, and model tests at 1 g and in the centrifuge.

The laboratory tests involve triaxial tests on soil samples. Dry and saturated sand specimen were tested statically (loading velocity = 0.0125 mm/s) and rapidly (loading velocity as fast as 550 mm/s). In dry sand, the loading rate does increase the shear strength of the sand and this increment is mainly due to the increase of friction angle with the loading rate. The effect increases with higher relative density (the maximum increase is 20% at a relative density of about 80%). In saturated sand only a small increase in shear strength is found, but it is believed that the true effect is obscured by cavitation of pore water pressure.

The model pile load test under 1g condition was performed on a model pile in a calibration chamber filled with unsaturated or saturated sand. The loading rates were varied from 1 mm/s (constant rate of penetration test) to more than 1 m/s (dynamically loaded). Almost no rate effect on bearing capacity of the model pile was found in this test series. This confirms the findings from the literature, where it is found that the rate effect is significant at a relatively slow rate, up to about 1 mm/s. In this test series the rates are all above this value, the rate effect was therefore not observed.

The numerical investigations aim to point out the effect of excess pore pressure on the resistance of a pile installed in sand. In the first phase, the FE package Plaxis is used to consider the difference of the pile resistance in the fully drained and fully undrained cases. It shows that due to the excess pore pressure in the undrained case, both the shaft resistance and toe resistance of a pile are significantly affected. In dilatant sand, the pile resistance increases due to the negative excess pore pressure. In the second phase, the FE code Titan, which couples the wave propagation and consolidation theories, is used to evaluate the importance of drainage condition on pile resistance. The results show the dependency of the pile toe resistance on the loading duration and the consolidation characteristics of the soil region under the pile toe. This dependency can be evaluated by the value of the defined drainage factor, which is related to a certain fraction of consolidation during the loading period of the test.

The geo-centrifuge model test, which is considered as the most appropriate method to model the soil behavior at a reduced scale, is performed to obtain more knowledge about mobilised pile resistance during a rapid load test and to validate the numerical results. The salient feature of this test series is that the drainage condition of the soil around the pile is scaled correctly by the usage of viscous fluid as pore fluid in the sand. Three centrifuge tests were performed, two with a viscous fluid and one with

water. This makes it possible to evaluate the effect of drainage condition in a wide range of values of drainage factor. Tests with different loading rates were carried out. The loading velocity ranged from 0.00167 mm/s to about 300 mm/s. The results significantly increase the understanding of the characteristics of excess pore pressure in the soil region near the pile tip and the effect of the penetration rate on the pile resistance. It appears that immediately after loading an increase of pore pressure in region right under the pile toe occurs, followed by a drop to negative values of excess pore pressure. This is due to generation of the negative excess pore pressure caused by dilation of sand in the shearing zone close to pile toe. The excess pore pressure strongly depends on the water flow between different soil regions; i.e. depends on the drainage conditions. As the penetration rate increases, the pile resistance also increases. Two components contribute to this effect: the rate effect and the negative excess pore pressure. The rate effect is limited to 10% increment of the pile resistance. The negative excess pore pressure can cause a 30% increase in pile resistance, depending on the displacement magnitude and the drainage condition. This conclusion is very significant as it is the first time the effect of excess pore pressure is clearly pointed out. The results also confirm the numerical results that the effect of excess pore pressure can be evaluated considering the value of the defined dimensionless drainage factor and a value of 10 can be seen as a boundary value (i.e. as the value is larger than 10, the effect of excess pore pressure is negligible).

Based on the obtained results, the application of the unloading point (UP) method to analyse the rapid pile load test results is evaluated. In cases the effect of excess pore pressure is negligible (drainage factor is larger than 10), the pile resistance at the unloading point is not affected by the loading rate. The unloading point method can be used in a straightforward way; and the rate effect correction factor as suggested by Paikowsky et al, (2006) is not necessary. In cases with a drainage factor smaller than 10, the effect of excess pore pressure is not negligible. This effect leads to an over-estimation of bearing capacity and correction factor for the effect is needed. Although the experiment results need further refinement and validation, it has been shown that the defined drainage factor can be used to estimate the correction factor. The estimation of the correction factor, which depends on the value of drainage factor and displacement of the pile, is suggested.

Samenvatting

Met het doel een test methode voor het draagvermogen van palen te ontwikkelen, waarvan de uitvoering minder tijd kost dan een conventionele statische proefbelasting en de interpretatie minder complex is dan een dynamische proefbelasting, is de snelle paalttest ontwikkeld. Echter, de algemene acceptatie van deze test methode is beperkt doordat de behandeling van de snelheidsafhankelijkheid en de invloed van de wateroverspanningen niet duidelijk is. Dit onderzoek heeft tot doel deze twee effecten te verduidelijken voor een paal in zand, onderworpen aan een snelle paalttest. Het werk, beschreven in dit proefschrift, omvat laboratorium proeven, numerieke berekeningen en modelproeven bij 1g conditie en in de geo-centrifuge.

De laboratorium proeven bestaan uit triaxiaal proeven op zand. Er zijn droge en verzadigde monsters beproefd, zowel statisch (belastingssnelheid = 0.0125 mm/s) als snel (belastingssnelheid tot 550 mm/s). In droog zand verhoogt de belastingssnelheid de schuifsterkte van zand. De toename wordt vooral veroorzaakt door de toename van de hoek van interne wrijving bij toenemende belastingssnelheid. Dit effect wordt sterker bij hogere relatieve dichtheid van het zand (maximale toename is 20% bij een relatieve dichtheid van ongeveer 80%). In verzadigd zand wordt slechts een kleine toename van de schuifspanning gevonden, maar vermoedelijk wordt het echte effect versluierd door cavitatie van het poriewater.

De model paal proeven onder 1g conditie zijn uitgevoerd op een model in een calibratie tank gevuld met onverzadigd en met verzadigd zand. De belastingssnelheid is gevarieerd van 1 mm/s (penetratieproef met constante snelheid) tot meer dan 1 m/s (dynamische belasting). Het draagvermogen van de model paal was vrijwel onafhankelijk van de belastingssnelheid. Dit bevestigt de bevindingen in de literatuur, waaruit blijkt dat de snelheidsafhankelijkheid vooral van belang is bij relatief lage snelheden, tot ongeveer 1 mm/s. In deze proevenserie lag de belastingssnelheid steeds boven deze waarde, wat verklaart dat er geen snelheidseffecten optreden.

De numerieke berekeningen hadden tot doel het effect van de (dynamische) waterspanningen op het draagvermogen van een paal in zand te onderzoeken. In de eerste fase is het eindige elementen pakket Plaxis gebruikt om het verschil in weerstand tussen een paal in een volledig gedraineerde en een volledig ongedraineerde situatie te bepalen. Hieruit bleek dat zowel de schachtwrijving als de puntweerstand van een paal sterk worden beïnvloed door het optreden van wateroverspanningen in de ongedraineerde situatie. In dilatant zand neemt de weerstand van de paal toe door het ontstaan van wateronderspanningen. In de tweede fase is het eindige elementen pakket Titan (dat golfvoortplanting en consolidatie gekoppeld berekend) gebruikt om het belang van de drainage op de weerstand van de paal te evalueren. De resultaten tonen de afhankelijkheid van de paalweerstand van de duur van de belasting en de consolidatie-eigenschappen van de grond rondom de paalpunt. Deze afhankelijkheid kan beoordeeld worden op basis van de waarde van de dimensieloze drainage factor die gerelateerd is aan de verhouding tussen consolidatie tijd van de grond en duur van de belasting tijdens de test.

De modelproeven in de geo-centrifuge (die beschouwd wordt als het beste instrument om schaalproeven op grond uit te voeren) zijn uitgevoerd om meer kennis te

verwerven over de gemobiliseerde weerstand van een paal tijdens een snelle proef en om de resultaten van de numerieke berekeningen te valideren. Het meest saillante aspect van deze proevenserie is de schaling van de drainage conditie van de grond rondom de paal door de toepassing van een viskeuze vloeistof in het zand. Drie centrifuge proeven zijn uitgevoerd; bij twee proeven is de viskeuze vloeistof gebruikt als porie vloeistof, en bij één test is water gebruikt. Hierdoor is het mogelijk een brede range van de drainage factor te beschouwen. De testen zijn met verschillende belastingsnelheden uitgevoerd. De belastingsnelheid varieerde van 0.00167 mm/s tot ongeveer 300 mm/s. Uit de proeven blijkt dat direct na het begin van de belasting de waterspanning onder de paalpunt toeneemt, maar deze toename wordt direct gevolgd door een snelle afname. Deze afname wordt veroorzaakt door het ontstaan van wateronderspanning (negatieve wateroverspanningen) ten gevolge van de dilatantie in het zand in de afschuifzones rondom de paalpunt. De wateroverspanningen hangen nauw samen met de waterstroming in de verschillende deelgebieden rondom de paal, zij hangen dus af van de drainage conditie. Als de penetratiesnelheid toeneemt, neemt de paalweerstand ook toe. Twee effecten dragen hieraan bij: het snelheidsafhankelijke effect en de wateronderspanning. Het snelheidsafhankelijke effect is beperkt tot een toename van 10 % op de paalweerstand. De negatieve wateroverspanningen kunnen een toename van de paalweerstand tot 30% veroorzaken, afhankelijk van de grootte van de paalverplaatsing en de drainage conditie. Deze conclusie is belangrijk, omdat het de eerste keer is dat de invloed van de wateroverspanningen volledig uitgewerkt is. De resultaten bevestigen de numerieke resultaten dat de invloed van de waterspanning geëvalueerd kan worden met de dimensieloze drainage factor. Een waarde van 10 kan beschouwd worden als de grenswaarde (d.w.z. als de waarde van de drainage factor groter dan 10 is, dan is het effect van de wateroverspanning verwaarloosbaar).

Gebaseerd op de behaalde onderzoeksresultaten is de toepassing van de *unloading point* methode voor de analyse van de resultaten van een snelle paaltest beoordeeld. Als de wateroverspanning verwaarloosbaar is (drainage factor is groter dan 10), wordt de paalweerstand in het ontlastingspunt niet beïnvloed door de belastingsnelheid. De *unloading point* methode kan zonder correctie toegepast worden, en de correctiefactor die Paikowsky et al (2006) voorstelt, is niet nodig. Als de drainage factor kleiner dan 10 is, dan is de invloed van de wateroverspanningen niet meer verwaarloosbaar. Dit effect leidt tot een overschatting van het draagvermogen en een correctiefactor voor deze invloed is noodzakelijk. Hoewel de experimentele resultaten nog verder verfijnd en gevalideerd moeten worden, wordt aangetoond dat de drainage factor gebruikt kan worden om de correctiefactor te schatten. Deze correctiefactor is afhankelijk van de drainage factor en de grootte van de paalverplaatsing.

TABLE OF CONTENTS

SUMMARY

SAMENVATING

TABLE OF CONTENTS

1	INTRODUCTION	1
1.1	Overview	1
1.2	Objectives of the thesis	2
1.3	Outline of the thesis	2
2	LITERATURE REVIEW	5
2.1	Introduction	5
2.2	Description of rapid load testing method	5
2.2.1	Definition of the rapid pile load test	5
2.2.2	Rapid pile load test method	5
2.3	Interpretation of the rapid pile load test results	8
2.3.1	The concentrated mass model	8
2.3.2	Alternative methods based on the concentrated mass model	12
2.3.3	One-dimensional stress wave analysis	13
2.3.4	Finite element analysis	14
2.3.5	Evaluating the interpretation methods	14
2.4	Rate effects in sand	16
2.4.1	Rate effects on sand strength	17
2.4.2	Rate effects on pile resistance	20
2.4.3	Generalization	22
2.5	Excess pore pressure	24
2.6	Summary	27
3	LABORATORY EXPERIMENTS ON RATE EFFECTS IN SAND	29
3.1	Introduction	29
3.2	Triaxial tests	29
3.2.1	Testing programme	29
3.2.2	Testing system	30
3.2.3	Sand properties	31
3.2.4	Specimen preparation and testing procedure	31
3.2.4.1	Specimen preparation	31
3.2.4.2	Testing procedures	32
3.2.5	Analysis of test data	33
3.2.5.1	Actual testing rate	33
3.2.5.2	Existence of the cavitation phenomenon	34
3.2.5.3	Evaluation of the dynamic effects	35
3.2.5.4	Density of specimen	36
3.2.5.5	Elaboration of the test results	36

3.2.6	Rate effect in dry sand	38
3.2.7	Rate effect in saturated sand	40
3.2.8	Summary	41
3.3	Model pile tests	42
3.3.1	Introduction	42
3.3.2	Test set-up	42
3.3.2.1	Calibration chamber and sand bed	42
3.3.2.2	Model pile	43
3.3.2.3	Load test methods and loading system	44
3.3.2.4	Measurements devices	45
3.3.2.5	Notes on the model scale	45
3.3.3	Test results	46
3.3.3.1	Tests in unsaturated sand	46
3.3.3.2	Tests in saturated sand	51
3.3.4	Evaluation of the rate effects	55
3.3.4.1	Rate effect in unsaturated sand	56
3.3.4.2	Rate effect in saturated sand	57
3.3.5	Summary and discussion	60
4	NUMERICAL INVESTIGATION INTO THE EFFECT OF EXCESS PORE PRESSURE	61
4.1	Introduction	61
4.2	Pile resistance in drained and undrained conditions	61
4.2.1	Introduction	61
4.2.2	Numerical simulation of the pile load tests	62
4.2.3	Simulation results	64
4.2.4	Effect of drainage condition on tip resistance and shaft friction	68
4.2.5	Summary	73
4.3	Consideration of the partially drained condition	73
4.3.1	Introduction	73
4.3.2	Validation of the Titan finite element code	73
4.3.3	Effect of different drainage conditions on dynamic stiffness	76
4.3.4	Effect of different drainage condition on pile resistance	79
4.3.5	Summary	80
5	MODEL PILE LOAD TESTS IN THE GEOTECHNICAL CENTRIFUGE	81
5.1	Introduction	81
5.2	Test programme	82
5.3	Scaling rules	83
5.4	Experimental set-up	85
5.4.1	Test set-up	85
5.4.2	Soil material	87
5.4.3	Measurement set-ups	88
5.4.4	Discussion of the set-up effects	89
5.5	Test results	91
5.5.1	Static load test (SLT)	92
5.5.2	Rapid load test (RLT)	93

5.5.3	Response of pore pressure during a RLT	99
5.6	Effect of penetration rate on pile resistance	103
5.6.1	Effect of penetration rate on shaft resistance	104
5.6.2	Effect of penetration rate on tip resistance	105
5.7	Characteristics of excess pore pressure and its effects on tip resistance	106
5.7.1	Characteristics of excess pore pressure	107
5.7.2	Effects of excess pore pressure	108
5.8	Validating the numerical results	110
5.9	Concluding remarks	111
6	IMPLICATIONS FOR THE ANALYSIS OF RAPID PILE LOAD TESTS	113
6.1	Introduction	113
6.2	Elaboration of the centrifuge test results	113
6.2.1	Small displacement RLTs	114
6.2.2	Medium displacement RLTs	115
6.2.3	Large displacement RLTs	116
6.2.4	Integration of all displacement results	116
6.3	Implications	119
6.4	Conclusions	119
7	CONCLUSIONS AND RECOMMENDATIONS	121
7.1	Conclusions	121
7.1.1	Rate effect in sand	121
7.1.2	Excess pore pressure effect	122
7.1.3	The UP method	123
7.2	Recommendations	124
	REFERENCES	125
	LIST OF ABBREVIATIONS AND SYMBOLS	133
	APPENDIX 5A	135
	CURRICULUM VITAE	

Chapter 1

Introduction

1.1 Overview

It is vital for all pile designers to know the bearing capacity and load–displacement relationship of a pile during its working lifetime. This can be achieved using theoretical formulas and/or in-situ pile load test data. However, theoretical formulas often show large discrepancies in their results due to the many uncertainties involved with soil conditions and construction of the pile. Pile load tests are used to give a more effective and reliable pile design. Pile load testing is one of the more effective methods for dealing with these uncertainties (Poulos, 1998), and plays an important role in pile foundation design.

In practical pile load testing, three testing methods are most widely used: the static load test, the dynamic load test, and the rapid load test. The static load test is generally considered to be the most reliable method, but is time-consuming and expensive. The result, however, is straightforward. By contrast, the dynamic load test and the rapid load test are much faster and more cost-effective, but their results need to be analysed and interpreted to derive the pile's static capacity and load displacement behaviour. Analysis of the results aims to eliminate the dynamic force components related to the high loading rate of these tests in order to achieve the equivalent static result.

The analysis technique for the dynamic load test has been well documented, and the test itself is accepted in many building codes. The rapid pile load test has been developed more recently, and aims to incorporate the benefits of both the static and the dynamic method, i.e. analysis of this test is simpler than for the dynamic load test, and is much less time-consuming than the conventional static load test.

The first rapid loading device dates back to 1984 (Gonin et al, 1984). However, use of the rapid load testing method only started to increase significantly following development of the Statnamic testing device in 1989 (Bermingham and Janes, 1989). The Statnamic load test is currently the most widely used internationally of the rapid pile testing methods. The rapid load testing method is frequently used in countries outside the European Union and is accepted in several building codes, but its use within the European Union is limited. A general inventory of the reasons for not using this type of test has shown that certain technical questions cause doubts about the test's applicability for deriving the static pile capacity. The main reasons for this uncertainty are interpreting the test with respect to the influence of rate effects related to soil strength, and the possibility of generating excess pore water pressure under and close to the pile toe. The needs of relevant parties, important clients, main contractors, and building authorities meant that a well-defined interpretation rule was required.

Throughout the European Union, other relevant research has been carried out in Belgium and the United Kingdom. In Belgium, research concentrated on validating the rapid test method in over-consolidated clay at Limelette (Charue, 2004). In the United Kingdom, a research group at the University of Sheffield investigated Statnamic testing of piles in clay deposits (Brown, 2004).

The work described in this thesis is part of the Delft Cluster work package “Validation of the Rapid Load Test for piles” [www.rapidloadtesting.eu, 2008]. The main aim of this work package is to evaluate the applicability of the rapid load test on piles to assess the static bearing capacity. The ultimate objective is to produce a standard that describes proper execution of the test, and a guideline that describes reliable interpretation methods. The work package is supervised by a CUR (Civieltechnisch Centrum Uitvoering Research en Regelgeving - Centre for Civil Engineering Research and Codes) commission “Rapid pile load test” (CUR-H410). The standard for rapid load testing and the guideline will be developed with the assistance of an international expert group.

Deltares (formerly GeoDelft) and the Delft University of Technology are working together in this work package. Deltares is responsible for project management, the collection of empirical data, and the initiation and organisation of a demonstration project. This PhD-study at the Delft University of Technology aims to answer the more fundamental questions about rate effects and excess pore water pressure. Because of the characteristics of geotechnical conditions in the Netherlands, where the bearing capacity layer of most piles is dense sand, this research concentrates on the rapid load testing of piles in sand.

1.2 Objectives of the thesis

The objective of this thesis is to answer two fundamental questions that are relevant to the response of sand, and to a pile founded in sand under the high loading rate of a rapid load test:

- (1) The effect of the loading rate on sand strength and on the mobilised resistance of a pile founded in sand.
- (2) The effect of excess pore pressure on the mobilised resistance of a pile founded in sand during the rapid load test.

1.3 Outline of the thesis

Chapter 2 presents a review of background information considered to be relevant to the study in this thesis. The rapid load testing method is defined, the rapid tests are described, and the interpretation methods to derive the static bearing capacity are given. Particular focus is given to the validity and evaluation of the most commonly used interpretation method: the unloading point method (UP method). Previous studies relevant to rate effects and excess pore pressure are reviewed in detail.

Chapter 3 presents two series of laboratory experiments. The rapid triaxial test series in dry and saturated sand aims to assess the rate effect on the shear strength of sand, and the characteristics of excess pore pressure inside the sand specimen under a high loading rate. The model pile load test series in a calibration chamber under 1-g condition aims to determine the effect of loading rate on the mobilised resistance of a model pile and the effect of excess pore pressure on pile resistance.

Chapter 4 presents investigations into the effect of excess pore pressure using numerical simulations of a rapid pile load test. The finite element package Plaxis V 8.0 is used to study the mobilised resistance of a pile in two limiting cases of soil behaviour: fully drained and fully undrained. The results highlight the difference between the mobilised pile resistance in these two limiting cases. The real situation will lie in between, due to the partially drained condition during a rapid load test. The finite element code (Titan code), which is capable of coupling wave propagation and consolidation, is employed to evaluate the effect of drainage conditions on the mobilised resistance.

Chapter 5 describes the investigation into the evolution of pile resistance and excess pore pressure during a rapid load test by means of geotechnical centrifuge tests. The results of three centrifuge tests are presented and discussed. The rate effect and the effect of excess pore pressure on the resistance of a model pile are given.

Chapter 6 presents some of the implications of this study's findings for the interpretation method (the UP method) used for rapid load testing.

Chapter 7 presents the conclusions and recommendations.

Chapter 2

Literature review

2.1 Introduction

This literature review aims to study current knowledge of the rapid pile load test method. The review starts with a short introduction that defines the rapid testing method and describes its performance. The review then examines current methods for interpreting the rapid pile load test and its assumptions, as well as their validity. The study focuses on assessing the relevance of analysis methods for rapid load testing of piles in sand, in particular regarding the rate effect and excess pore pressure effect. Finally, previous studies of the rate effect in sand and excess pore water pressure at elevated loading rate are reviewed.

2.2 Description of rapid load testing method

2.2.1 Definition of the rapid pile load test

The rapid pile load test method (sometimes known as the kinematic pile load test method) works by exerting a long duration pulse load (commonly 50 - 200 milliseconds) on the pile head (Holeyman, 1992). Such a long loading duration is 10 to 20 times longer than the typical loading duration of a conventional dynamic pile load test. This means there is a significant reduction in stress-wave effects, and that simpler analysis methods are possible. This will be discussed in section 2.3. However, the rapid pile load test is still recognised as a dynamic event. The distinction between the rapid load testing method and the conventional dynamic load testing method is generally based on the so-called wave number $N_w = \frac{T \cdot c}{L}$, which represents the ratio between the length of the applied pulse load and the length of the pile (Holeyman, 1992; Middendorp and Bielefeld, 1995); or the relative duration $t_r = \frac{T}{\left(\frac{2L}{c}\right)}$, which represents the ratio between the duration of the applied pulse

load and the duration needed for a stress wave to propagate forwards and backwards through the pile (Karkee et al., 1997). In these equations, T is the duration of the applied load (s), L is the length of the tested pile (m), and c is the velocity of stress wave propagation in the pile (m/s). According to the Research Committee on Rapid Load Test Methods in Japan, any load testing method with a wave number N_w ranging from 10 to 1000 or with the relative duration t_r from 5 to 500, is regarded as a rapid load test. If a test has a value $N_w < 10$, it will be regarded as a dynamic load test. If N_w is larger than 1000, it will be regarded as a static load test (Kusakabe et al., 1998).

2.2.2 Rapid pile load testing methods

In practical pile load testing, two types of load testing are regarded as a rapid pile load test. The first type relates to a mass falling on the pile head, and is known as the Dynatest (Gonin et al, 1984) or the Pseudo Static Pile Load Tester (Schellingerhout et al, 1996). The second type relates to launching a mass from the pile head, and is known as the Statnamic test (Birmingham & Janes,

1989; Middendorp, 2000). The Statnamic test is the most frequently used internationally for rapid pile load test methods. A brief description of the two tests methods is presented below.

The Dynatest and Pseudo Static Pile Load Tester

A reduction in spring stiffness and an increase of the drop mass are feasible ways to lengthen the duration of the impact force (Holeyman, 1992). The Dynatest and the Pseudo Static Pile Load Tester (PSPLT) work by dropping a heavy mass on the pile head with a coiled spring placed in between. The coiled spring is attached to the pile head in the Dynatest, or to the bottom of the falling mass in the Pseudo Static Pile Load Tester. The force applied on the pile head during the test is measured by a load cell. The displacement and acceleration at the pile head are measured by an optical displacement transducer and accelerometers respectively. An example of signals measured during a Pseudo Static Pile Load Tester is shown in figure 2.1.

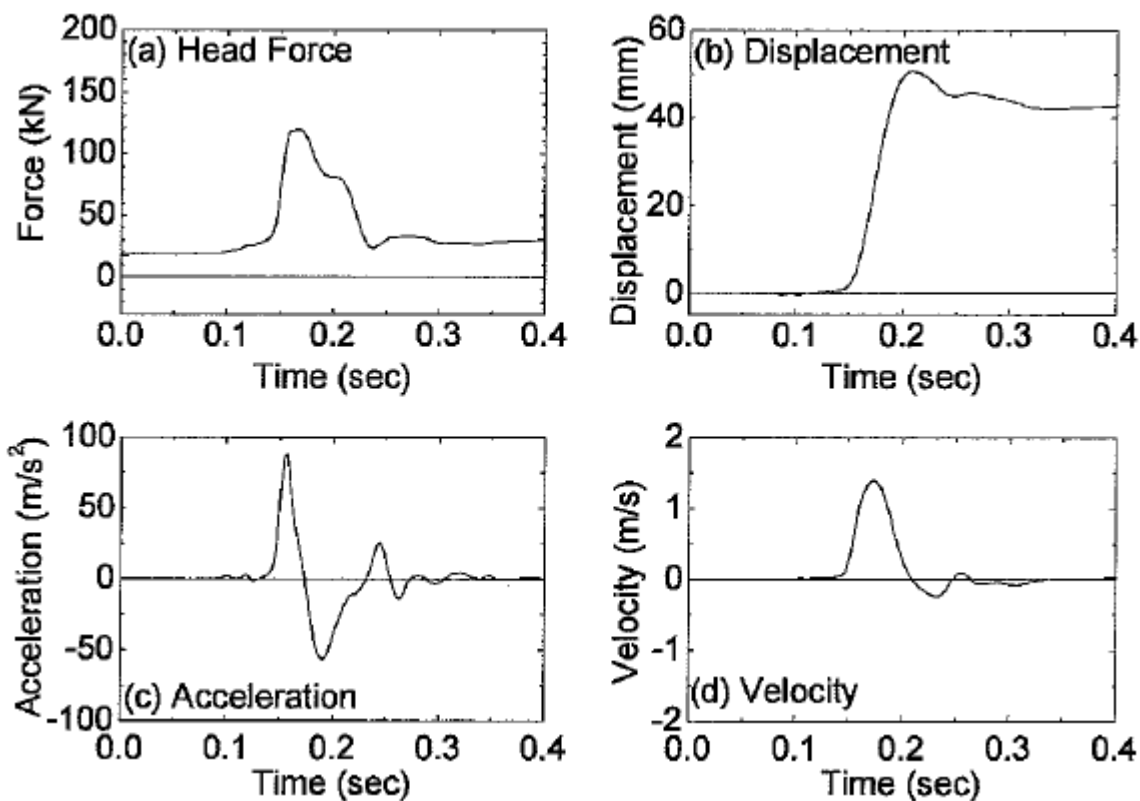


Figure 2.1: Measurements in a pseudo-static load test (after Matsumoto, 2005)

The Statnamic pile load test

The Statnamic pile load test method was jointly developed by Bermingham Corporation Limited (Canada) and TNO Building & Construction Research (The Netherlands) in 1988. It is seen as an efficient alternative to the high-cost and time-consuming static pile load test method, especially for high capacity deep foundations (Bermingham, 1989). The first small model of the Statnamic device was built and tested in Hamilton, Ontario in 1988. The first Statnamic test was introduced onto the market in 1992, when it was originally known as Inertial Load Testing. Middendorp re-named it the Statnamic test, to reflect the intermediate characteristics of the test between the STATIC and dyNAMIC pile load tests (Middendorp, 2000). The Statnamic pile load test method has been described in detail in numerous publications and will only be presented briefly here.

Figure 2.2 shows a Statnamic pile load test set-up with a gravel catching system. A Statnamic loading device consists of a pressure chamber, a reaction mass, and a catching system. Solid fuel is burned in the pressure chamber to produce high pressure. This creates an upward force to launch the reaction mass, and an equal downward reaction force on the pile head to push the pile into the ground. The catching system is used to prevent the reaction mass from again falling down onto the pile head. The reaction mass is launched upwards at approximately 20g, so the required weight of the reaction mass is only 5 – 10% of the required force. The applied load, the displacement, and the acceleration at the pile head are measured during the test. The pile head force is measured by a load cell, which is mounted directly between the loading device and the pile head. Displacement of the pile head is measured by a displacement transducer, which is capable of measuring displacement directly and continuously. The displacement transducer consists of a light-sensitive cell placed at the central longitudinal axis of the pile, and a remote laser light source whose distance from the pile is such that it is not influenced by ground vibrations. The acceleration is measured by an accelerometer mounted near the pile head. A typical measurement result of the pile head load and the displacement as a function of time from a STN test is shown in figure 2.3.

Statnamic loading devices with an applied force capacity ranging from 0.1 to 30 MN have been used in practice, and devices with a higher capacity are possible. The test can be performed in a vertical direction, as well as in a horizontal or inclined direction (Middendorp, 2000^b). Statnamic load testing is increasingly being used in foundation engineering, and the test is considered as a potential replacement for the conventional static load test method (Poulos, 1998).

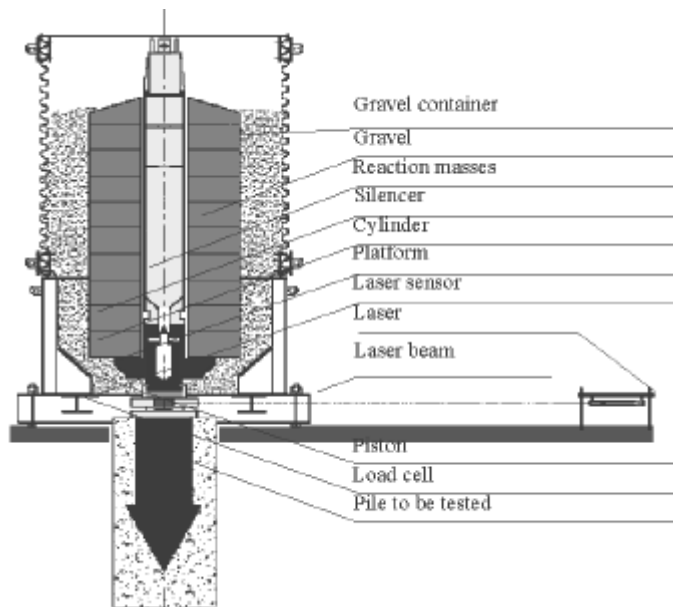


Figure 2.2: The Statnamic test set-up (after Poulos, 1998)

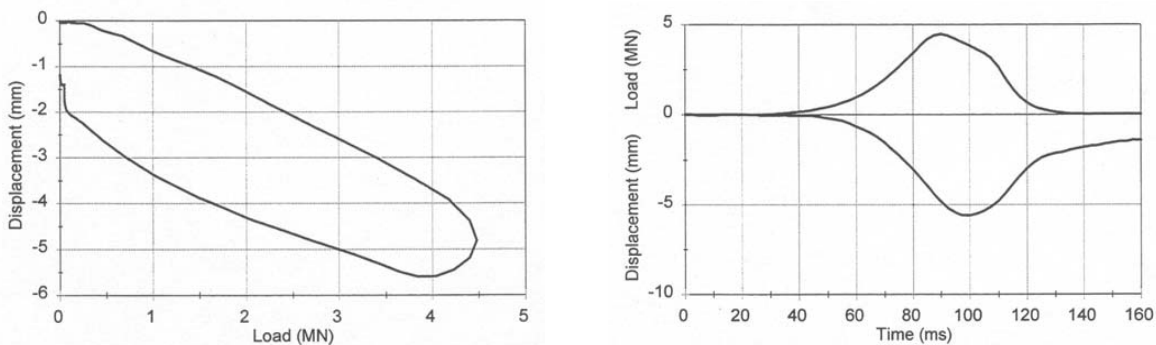


Figure 2.3: Typical measured results of a Statnamic pile load test

2.3 Interpretation of the rapid pile load test results

If the rapid load test is used to derive the equivalent static load–displacement curve of a pile, its results need to be analysed. Since the rapid pile load test is in fact a dynamic event (Middendorp et al. 1992), dynamic effects exist in the results. In a broad sense, these dynamic effects may include: (1) the stress-wave effect, (2) the inertial effect, (3) the radiation of energy due to vibration of the pile-soil system (4) the rate effect, and (5) the effect of excess pore pressure. The analysis methods aim to estimate and eliminate these dynamic effects from the measurement results. The methods that are available for analysing the rapid pile load test are presented here.

2.3.1 The concentrated mass model

The concentrated mass model is based on the significant assumption that the stress-wave phenomenon in the pile is negligible due to the long wavelength of the test. As a result, the pile behaves as a rigid body during a Statnamic test and its behaviour can be modelled with a single degree of freedom system. The force acting on the pile and the rheological model of the pile-soil interaction during a loading test are shown in figure 2.4. In the model, the spring stiffness represents the pile's static response including the elastic shortening of the pile, the viscous damping dashpot represents the dynamic resistance developed during penetration of the pile, and the mass represents the pile mass, i.e. the inertial effect is considered for the pile mass only.

The equilibrium equation for the pile mass (Middendorp et al. 1992) is

$$F_{\text{stn}}(t) = F_{\text{soil}}(t) + F_{\text{a}}(t) = F_{\text{u}}(t) + F_{\text{v}}(t) + F_{\text{p}}(t) + F_{\text{a}}(t) \quad (1)$$

where:

$F_{\text{stn}}(t)$ is the applied Statnamic load (measured)

$F_{\text{a}}(t)$ is the inertial force of the pile mass, $F_{\text{a}}(t) = m_{\text{pile}} \cdot a(t)$, where m_{pile} is the total mass of the pile and $a(t)$ is acceleration of pile head.

$F_{\text{soil}}(t)$ is the soil resistance of the pile shaft and toe, $F_{\text{soil}}(t) = F_{\text{u}}(t) + F_{\text{v}}(t) + F_{\text{p}}(t)$, which is composed of static resistance $F_{\text{u}}(t)$, damping resistance $F_{\text{v}}(t)$ and water pore pressure force $F_{\text{p}}(t)$.

$F_{\text{v}}(t) = C_{\text{v}} \cdot v(t)$, where C_{v} is a damping coefficient; $v(t)$ is velocity of the pile, which is derived by differentiation of the measured pile head displacement $u(t)$.

This approach takes into account the pore pressure force as part of the damping force, and is presumed to be linear with the pile velocity $v(t)$ (Middendorp et al. 1992). So that:

$$(F_{\text{v}}(t) + F_{\text{p}}(t)) = (C_{\text{v}} + C_{\text{p}}) \cdot v(t) = C \cdot v(t)$$

Rewriting equation (1), this gives the static resistance $F_{\text{u}}(t)$:

$$F_{\text{u}}(t) = F_{\text{stn}}(t) - F_{\text{v}}(t) - F_{\text{a}}(t) = F_{\text{stn}}(t) - C \cdot v(t) - m_{\text{pile}} \cdot a(t) \quad (2)$$

All parameters on the right-hand side of the equation (2), except the damping coefficient (C), are known from measurements and pile properties. Proposed methods to determine the damping coefficient (C) are described below.

Unloading Point method (Middendorp et al, 1992)

The Unloading Point Method (the UP method) is the first published interpretation method for the Statnamic pile load test, and has become the most widely used. In the original publication, the authors divide the Statnamic load-displacement curve in figure 2.5 into five key parts. The damping

coefficient (C) is determined for each part. Hereafter, the subscript number indicates the value during the particular period with that number.

+ In part 1, the Statnamic reaction mass is placed on the pile top. The load displacement behaviour is fully static. The measured load and displacement at the end of area 1 are referred to as F_{stat} and u_{stat} . The spring stiffness k_1 in this area can be calculated as:

$$k_1 = F_{stat} / u_{stat}$$

+ In part 2, the reaction mass is launched. Statnamic loading starts. The soil behaviour is elastic. The assumption is that the spring stiffness k_2 at the start of area 2 equals k_1 . The damping coefficient (C) is expressed as:

$$C_2 = (F_{stn2} - k_1 \cdot u_2 - m \cdot a_2) / v_2$$

+ In part 3, the damping and inertia force increase. The maximum Statnamic load is reached at the end of this part, and the static soil resistance is assumed to reach its ultimate value F_{uy} . The damping coefficient is taken from the calculated value in part 4 below.

+ In part 4, the Statnamic load decreases but the pile's displacement still increases (due to the inertia force) to reach the maximum value u_{max} at the end of this part. The point where maximum displacement is reached is referred to as the unloading point, since the pile displacement changes from downwards to upwards. At that point, the pile velocity is zero and so is the damping force in equation (2). Therefore, at the time of the unloading point, the equation (2) is written as:

$$F_u(t_{umax}) = F_{stn}(t_{umax}) - m \cdot a(t_{umax})$$

The value $F_u(t_{umax})$ is considered as the maximum static soil resistance and is equivalent to the yielding value F_{uy} throughout the area 4, $F_{uy} = F_u(t_{umax})$. The damping coefficient (C) at any time within part 4 is:

$$C_4 = (F_{stn4} - F_{uy} - m \cdot a_4) / v_4$$

Finally, the damping coefficient (C) in part 3 and in part 5 is assumed to be equivalent to the mean value of (C) in part 4. The static resistance F_u is then calculated in part 3 and 5 as:

$$F_u(t) = F_{stn}(t) - C_4 \cdot v(t) - m \cdot a(t)$$

Use of the UPM in current practise is more simplified. The UPM determines the damping coefficient (C) in part 4 only, and a representative value (generally the average value) is used to derive the hold static load-displacement curve from the measured load-displacement curve during a Statnamic test.

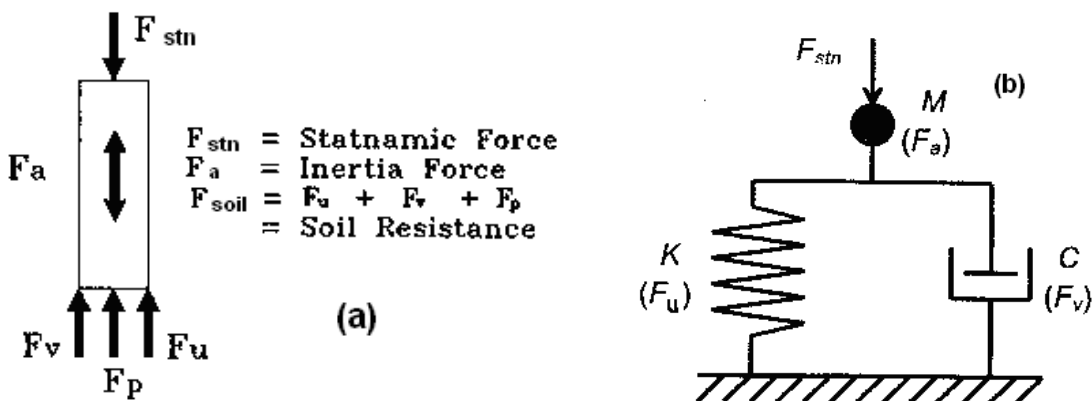


Figure 2.4: (a) Force components on pile; (b) The SDOF rheological model

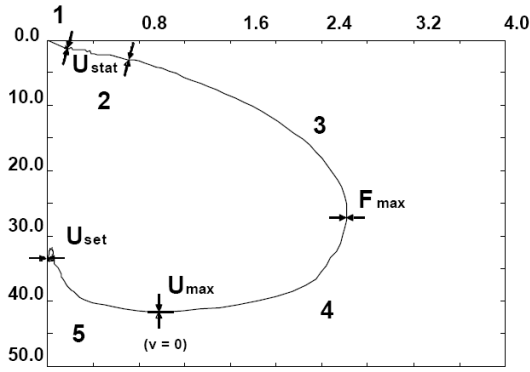


Figure 2.5: Key areas for the UPM analysis (after Middendorp et al, 1992)

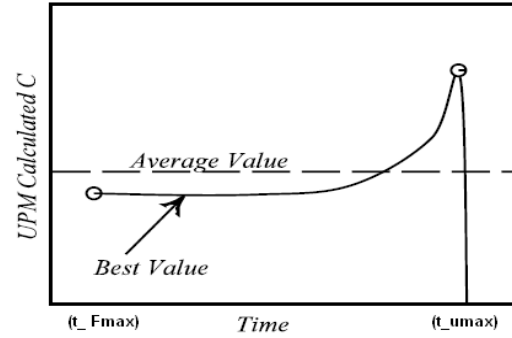


Figure 2.6: Variation of damping (C) in part 4 (after Mullins et al, 2002)

An example of variation of the calculated damping coefficient (C) with time in part 4 when using the UP method is shown in figure 2.6. It shows that the value of the damping coefficient is extremely high near the unloading point due to the zero velocity. Use of the average value may therefore not be adequate. In cases where a constant value of the calculated damping coefficient (C) appears for a long period of time (shown as 'best value' in figure 2.6), it is advisable to use this value instead of the average value (Mullins et al. 2002).

Non-linear damping method (Matsumoto et al. 2005)

Matsumoto et al. 2005 proposed an analytical method where both the damping value (C) and spring stiffness (k) are treated as non-linear. In this method, the whole measured load-displacement curve as shown figure 2.5 is first divided into a number of small steps. The spring stiffness k and damping value C are then determined in consecutive steps, in the same way as the UPM in part 1 and part 2 of the curve. In the first step (i = 1), the spring stiffness is calculated in the same way as the UPM method:

$$k_1 = F_{stat} / u_{stat} = F_{u-1} / u_1$$

In the next step (i=2), the spring stiffness k_2 is assumed to be equal to k_1 . The static soil resistance and the damping value C_2 are then calculated as:

$$\begin{aligned} k_2 &= k_1 \\ F_{u-2} &= F_{u-1} + k_2 \cdot (u_2 - u_1) \\ C_2 &= (F_{soil-2} - F_{u-2}) / v_2 \end{aligned}$$

in which F_{soil} is the total soil resistance and known from the Statnamic and pile mass inertial forces.

In the following step (i = 3), the damping value C_3 is assumed to be equal to C_2 . The static soil resistance and the spring stiffness are then calculated as:

$$\begin{aligned} C_3 &= C_2 \\ F_{u-3} &= F_{soil-3} - C_3 \cdot v_3 \\ k_3 &= \frac{F_{u-3} - F_{u-2}}{u_3 - u_2} \end{aligned}$$

The procedure is repeated in subsequent steps, ending at the step of maximum displacement in the load-displacement diagram. The static load-displacement curve is constructed from the values of static soil resistance calculated in each step.

According to the authors of this method, the constructed static load-displacement curve is identical to the total soil resistance at the unloading point, and prediction of the pile head stiffness is more accurate. However, the authors did not provide instructions to determine the initial stiffness k_1 ,

which is often not easy to find. Also, they did not describe how to choose the step size in the analysis. This may strongly affect the assumption about equalising the spring stiffness and damping value of the present step to the next step.

Models from Sheffield University, United Kingdom

These models were developed to analyse the results of a Statnamic test in clay, where the rate effect is highly non-linear (Hyde et al, 1998). The models require the relationship between the dynamic soil resistance and the penetration rate of the pile, as well as the damping coefficient values, to be known beforehand. These criteria are determined using laboratory tests at different loading rates.

To determine the damping value for rapid pile tests in clay, Brown (2004) performed a series of model pile tests at different loading rates in a calibration chamber. The results from his experiments have led to the following relationship between the ratio of the ultimate dynamic shaft friction over the static value and the pile velocity (equation 3), and its application for analysing the Statnamic pile load test results (equation 4)

$$\frac{\tau_d}{\tau_s} = 1 + \alpha \cdot (v)^\beta - \alpha \cdot (v_s)^\beta \quad (3)$$

$$F_{STA} = \frac{F_{STN} - M \cdot a}{1 + \alpha (v)^\beta - \alpha (v_s)^\beta} \quad (4)$$

where τ_d and τ_s are the limiting values of the dynamic and static pile shaft friction.

F_{STA} is the derived static pile resistance

F_{STN} is the total measured Statnamic load

M is the pile mass

a is the pile acceleration

v is the pile velocity

v_s is the lowest pile velocity, used to determine the ultimate static shaft friction

α & β are the damping coefficients determined from the model pile tests ($\alpha = 1.22$, $\beta = 0.32$ in his study).

The proposed model has been validated by a series of full-scale Statnamic tests on an instrumented bored concrete pile, with a diameter of 600 mm and a length of 12 m, embedded in clay at the Grimsby test site. Details of the case history and analysis results can be found in Brown et al. (2006). Application of the new model gives reasonable correlation between the predicted ultimate pile resistance and that of a maintained load test for the same pile, but significantly under-predicts stiffness in the load-displacement curve in the elastic range (Hanh, 2006).

With the aim of improving the prediction, the Sheffield University research group has proposed two damping model variations. The first model incorporates a proportional exponent of the velocity term (equation 5), the second model incorporates a proportional multiplier of the velocity term (equation 6) (Anderson et al, 2006).

$$F_{STA} = \frac{F_{STN} - m \cdot a}{1 + \alpha \left(\frac{v}{v_s} \right)^\beta \left(\frac{F_{STN}}{F_{STN \text{ ultimate}}} \right)} \quad (5)$$

and/or

$$F_{STA} = \frac{F_{STN} - m * a}{1 + \alpha \left(\frac{F_{STN}}{F_{STN}^{ultimate}} \right) \left(\frac{v}{v_s} \right)^\beta} \quad (6)$$

in which F_{STA} is the static pile resistance, F_{STN} is the Statnamic pile load, $F_{STN}^{ultimate}$ is the ultimate Statnamic load, v is the pile velocity, v_s is the reference static velocity ($=0.01$ mm/s), m is the pile mass, a is the pile acceleration; and α and β are the damping coefficients. The value of β is taken as 0.2 for clay (identical to the finding of Gibson and Coyle, 1968; Randolph and Deeks, 1992).

These models were applied to the above-mentioned Statnamic test case history at the Grimsby research test site to validate the new model. The analysis shows improved prediction of the static load-displacement curve, and better performance of the proportional exponent model works compared to the proportional multiplier model (Anderson et al, 2006).

Although the models proposed by the research group at Sheffield University adequately take into account the non-linear nature of clay's rate dependency, their approach requires the rate effect of the test site soil to be known in advance. The disadvantage of these models is that they require additional tests (model pile test, high speed triaxial tests, or multi-cycle Statnamic test) to determine the damping factors α & β for every test site (Anderson et al, 2006).

2.3.2 Alternative methods based on the concentrated mass model

The concentrated mass model has been proven to be a useful tool for analysing rapid pile load test results, if the rigid body assumption is valid (Paikowsky et al. 2006). Middendorp and Bielefeld (1995) have pointed out that the concentrated mass model can be applied accurately for cases where the wave number N_w is larger than 12. Using the average loading duration of a Statnamic test of 100 ms, and a stress wave velocity in steel pile and concrete pile of 5000 m/s and 4000 m/s respectively, the value of the wave number (12) limits the applicability of the concentrated mass model for the steel pile to shorter than 42 m and the concrete pile to shorter than 33 m. However, there are many cases where the assumption is violated in practical rapid pile load testing. To maintain the simplicity of the concentrated mass model, alternative methods have therefore been proposed for these cases.

The first method is known as the Modified Unloading Point method (MUP method - Lewis, 1999), proposed for testing a short pile where the wave number is larger than 12, but where the rigid body assumption is violated. This occurs in cases where the lower part of the pile and/or the pile tip is placed in a strong bearing stratum. As a result, the pile toe movement is restrained and causes the pile top response to significantly differ from the pile toe response. To determine the damping value in this case, the MUP method uses an additional accelerometer at the pile toe, which is combined with the pile head measurements to calculate the average acceleration and velocity of the pile. The standard UPM is then carried out using the pile head load. The average acceleration and velocity of the pile determines the equivalent static load- displacement relationship of the pile.

The second method is known as the Segmental Unloading Point method (the SUPM - Justason, 2000), which is proposed for load testing a long pile where the wave number N_w is smaller than 12. In such cases, the rigid body assumption is negated by the significance of stress wave propagation. The average motion values of the pile top and toe are therefore not adequate to represent the motion of the whole pile. In the SUP method, the pile is divided into smaller segments. Each segment fulfils the rigid body assumption, and the standard UPM can thus be applied for each segment. This method requires the use of instrument strain gauges between each pile segment in order to

determine the displacement and the force applied on every segment. The standard UPM is then carried out on each segment to derive the static response. The results from each segment are added together to produce the derived static load-displacement behaviour of the pile. One disadvantage of the UPM is the need for pile instrumentation, as this leads to higher test costs and limits the possibility to randomly test piles in a project.

2.3.3 One-dimensional stress wave analysis

The application of one-dimensional stress wave analysis for a Statnamic test is based on the well-documented method for analysing the dynamic pile load test described by El.Naggar et al, (1992), and was the first analysis method proposed for Statnamic testing. Nishimura et al (1995), Ochiai et al (1996), Matsumoto et al (1996), Matsumoto et al (1998) and van Foeken et al (2000) confirmed that one-dimensional stress-wave analysis with an automatic signal-matching technique can be used to interpret the Statnamic test results, and to derive the static load-displacement behaviour of the tested pile. Details of the pile model and soil interaction can be found in numerous papers and will therefore not be repeated here. The most commonly used shaft and toe models are shown in figure 2.7. In general, the initial value of the model parameters (spring stiffness, damping factor, lumped mass etc.) is taken from standard soil investigation (see Randolph and Deeks, 1992) or from engineering practice.

Although the one-dimensional stress wave analysis has long been used to interpret the Statnamic test, none of the authors have provided any assurance for the uniqueness of the solution. Hayashi et al, 1998 showed that different shaft resistance distribution and magnitude can give a virtually identical pile head response from the one-dimensional stress wave analysis. The long duration of Statnamic loading means that the reflection of the front wave at the pile toe arrives at the pile top before the main portion of the Statnamic loading enters the pile. This makes it difficult to determine the distribution of soil resistance along the pile shaft. However, the one-dimensional stress wave analysis is still mandatory for interpreting a Statnamic test in the case of a long pile (wave number smaller than 12) , without the additional instruments needed in the SUP method.

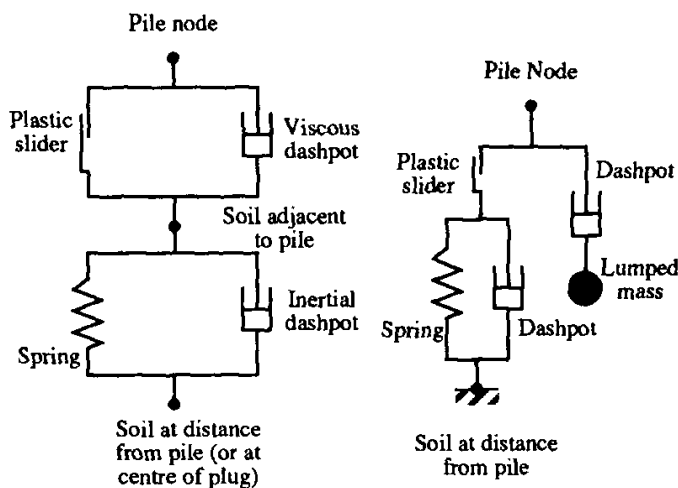


Figure 2.7. The shaft and base soil model for one-dimensional stress-wave analysis (Randolph and Deeks, 1992)

2.3.4 Finite element analysis

Finite element analysis is applicable for analysing the axial Statnamic pile load test (Matsumoto, 1998; Horikoshi et al., 1998). The analytical input soil parameters are determined from standard soil investigation. The Statnamic pile head force is used as input to calculate the pile response in finite element analysis, i.e. pile head displacement - time or pile head velocity - time. The shear modulus of the soil is reduced by multiplication with a reduction factor η ($\eta \leq 1$) to allow for the effects of the larger strain level on the soil response. The dynamic analysis of the Statnamic load test is conducted iteratively, until there is agreement between the calculated and observed pile behaviour in order to find the best reduction factor. In the final step, the static pile behaviour is analysed using the derived reduction factor.

2.3.5 Evaluating the interpretation methods

Many researchers have proven in numerous publications on the subject that the above-mentioned interpretation methods can be used to analyse the Statnamic test results, which is the major testing method for the rapid pile load test. However, the most widely used and most accepted methods are the UP method and derived related methods such as MUP and SUP (Paikowsky et al, 2006). This section therefore focuses on evaluating the validation of the UP method.

A number of researchers evaluated the general validation of assumptions made for the UP method, which are supposed to affect the accuracy of a pile's predicted bearing capacity. The following assumptions were considered as significant:

- Neglect of stress waves in the pile
- Damping coefficient assumed to be constant throughout the test
- Soil resistance at the unloading point coincides with static ultimate capacity of the pile.

The validity of these assumptions varies from case to case, and cannot be generally guaranteed. Goble et al (1995) and Seidel (1996) have commented on the UP method, focusing on the validity of the rigid body assumption during the unloading phase of Statnamic loading and the aspect of constant damping. During the loading phase, the loading rate can be controlled by the amount of explosive fuel and reaction mass, but the unloading phase occurs in a very short time period and cannot be controlled. As a result, an appreciable stress wave may exist in the pile. This may violate the rigid body assumption, hence causing errors in the prediction. Moreover, the very short period of the unloading phase may cause high deceleration of the pile. As the bearing capacity is evaluated around that time, the prediction will be relatively sensitive to the acceleration reading. Seidel (1996) has also proved that dashpot damping is not constant in part 2 and part 4 of the load-displacement curve (see the numbers in figure 2.5), which may lead to an error of 20% in the predicted bearing capacity. Moreover, he pointed out that the predicted static load-displacement curve largely depends on the choice of damping constant, which may vary by a factor of 2 in part 4, as shown in figure 2.6.

Hyde et al (1998) have described the use of a linear damping model in the UP method as an oversimplification of the phenomenon, since the peak resistance of soil is a non-linear function of velocity as shown by Coyle and Gibson (1970); Heerema (1979); Lithouhi and Poskitt (1980). The non-linear relationship has long been accepted for analysing the dynamic load test (Randolph and Deeks, 1992). It has recently been applied to analyse the Statnamic test, as proposed by researchers at Sheffield University.

On the other hand, some authors have made the evaluation based on a selected database of pile load tests, where both a Statnamic test and a static load test were performed on the same or nearby piles. Brown (1994) reviewed and re-analysed nine Statnamic load test case histories in United States and Canada using the UP method. The predicted static resistance was compared to results from the static load test. Of the nine cases, there were five where the piles were founded on sand and the rest were founded on clay. Brown concluded that in terms of the ultimate bearing capacity, the UP method agrees closely with the results of conventional static pile load tests for the piles in sand, but over-predicts between 25% and 30% for piles in clay. The predicted load-displacement curves generally agree well with those measured. However, no ultimate bearing capacity criterion was given in Brown's paper, and the maximum resistance in each test was taken to be the bearing capacity. This is inadequate since the displacement range of tests presented in the paper is quite different in most cases. Brown's later conclusion is also not clearly supported, i.e. no comparison was made between the predicted static load-displacement curve and that measured in the same graph.

McVay et al. (2003) collected and examined a larger database of Statnamic test case histories from test sites in Japan, North America and Europe. There were 61 tests in their database. In 31 of these tests, the piles were loaded to failure point according to the FDOT (Florida Department of Transportation) or Davisson failure criteria. Both the Statnamic test and the static test were performed on the same or nearby piles. The Statnamic test results were analysed using the UP method to derive the static load-displacement curves, and were compared to results from conventional static load tests. For the piles primarily founded in clay soil (8 cases), a larger deviation was found between the predicted static capacity by the UPM and the measured value: the predicted bearing capacity ($F_{(u)}$) is higher than the measured value. This larger difference is thought to be due to the loading rate effect. Mc Vay et al. also suggested that the Statnamic load test for a pile in clay soil should always be calibrated using the static load test. For piles founded in sand and silt (23 cases), the comparison between the predicted and measured bearing capacity is shown in figure 2.8. The figure shows good correlation for the piles founded in sand, but the deviation seems to be more pronounced in cases with a high capacity pile. Figure 2.8 also shows that the over-prediction for cases where the piles founded in silt is quite clear. The general validity of the assumption 'The soil resistance at the unloading point coincides with static ultimate capacity of the pile' is not valid in this case. It is believed to be the effect of a high loading rate in the Statnamic test, since soils often show higher strength under rapid loading than under static loading (Whitman, 1957).

Paikowsky et al, (2006) reviewed and extended the database for the Statnamic load test case histories. They concluded that the Statnamic test (with data analysed by the UPM, the MUPM, and the SUPM) can currently be used to determine the design value of a pile's static bearing capacity if the loading rate correction factor (η) is used to account for the over-predicted bearing capacity from the UP method. The loading rate factor (η) varies with the soil type. For rock, the factor is $\eta = 0.96$; for sand, $\eta = 0.91$; for silt, $\eta = 0.69$; for clay, $\eta = 0.65$. It should be noted that the values of loading rate factor (η) are statistically determined from the database to produce one unique safety factor ($SF = 2.0$) for the pile design in all soil types, without taking into account the nature of a soil's loading rate effect. However, as its values correspond to soil types, this implies that it should have a certain correlation with the nature of the loading rate dependency of the shear strength of soils (hereby referred to as the rate effect). This is because it is widely accepted that the magnitude of the rate effect strongly depends on soil type, and that this effect is more pronounced in silt and clay than in sand (Hyde et al, 1998; Brown, 2004; Holeyman, 2006 and many others).

Evaluation of the rapid pile load test method using the database presented above, especially the work of Paikowsky et al (2006), suggests that the testing method can be used to determine a pile's static bearing capacity, despite several assumptions that had been made and the lack of their general validity. However, the need to incorporate the loading rate correction factor in the analysis reflects the implicit over-prediction of a pile's bearing capacity using the rapid load testing method. Over-prediction can be seen even in cases where piles are founded in sand, as shown in figure 2.8 where there are two cases of significant over-prediction. This may be due to the fact that the loading rate effect in sand is sometimes minor, but sometimes not (Charue, 2004). A more fundamental understanding of the mobilised shear strength of soils at the elevated loading therefore seems to be essential, in order to predict a pile's static bearing capacity more reliably using the rapid testing method.

Moreover, as noted by Matsumoto (2004), the predicted static load-displacement curve from the rapid load test results generally deviates considerably from the static load test results. This is also the case with results introduced by Mc Vay et al (2003) and Paikowsky et al (2006), even when the loading rate correction factor was applied during the analysis. This may be caused by the constant damping coefficient, or linear damping model assumptions in the UP method. This deviation increases the need for greater understanding of soil response under the high loading rate of the rapid load test.

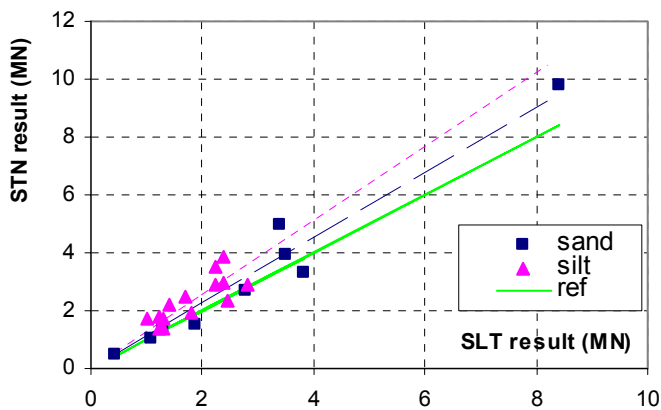


Figure 2.8: Comparison of the predicted and measured static bearing capacity (modified after McVay et al., 2003)

2.4 Rate effects in sand

This section reviews and discusses previous studies into the effect of loading rate in soils. The term 'rate effect' used here is also referred as 'strain rate effect' in literature, and was defined by Whitman (1957) as "the relationship between the rapidity of loading and the shearing strength of a soil". The review focuses on studies with sand. This is because an extensive study on clay has been carried out at Sheffield University, and because sand is the bearing capacity strata of most pile foundations in the Netherlands.

The review is divided into two categories: rate effects on sand strength and rate effects on the resistance of a pile founded in sand.

2.4.1 Rate effects on sand strength

Rate effects in shear tests

Two studies of rate effects in shear tests can be found in literature. They both report the independence of shear strength on the applied loading rate, i.e. no rate effects.

Schimming et al, (1966) studied the loading rate effects on the shear strength of sand in a direct shear device. ASTM C-190 sand was used with a sample size of 1.9 cm (3/4 inches) in thickness and 10 cm (4 inches) in diameter. Three loading rates were applied: the dynamic test (where the maximum shear force is reached within a period of 1 to 5 minutes), the rapid static test (where the time to failure is between 30 and 50 minutes), and the static test. The tests were performed on a dry loose sample, a dry dense sample, and a dense saturated sample with unrestricted drainage condition. No rate effect was found on maximum shear resistance and friction angle of the tested sand, but the maximum shear resistance in the dynamic test on dense saturated sand was slightly higher than that of dense dry sand. This was thought to be caused by a change in pore pressure, although this was not measured during the experiment.

Hungr & Morgenstern (1984) used the ring shear device to examine the behaviour of sand at high shear rates and different normal stresses. Shear rates between 0.1 cm/s and 98 cm/s were applied, and the normal stresses varied between 20 kPa and 200 kPa. Two types of coarse Ottawa sand (grain diameter 1.5-2 mm and 2-3 mm) were used in the study in wet and dry condition. In the range of test conditions, they concluded that rate effects do not influence the shear strength and friction angle.

Rate effects in triaxial tests

The triaxial testing device is used extensively to examine rate effects on the shear strength of sand. Test conditions and the magnitude of the measured rate effects vary from study to study. These studies are presented here in chronological order.

Casagrande & Shannon (1948) performed a series of triaxial compression tests on dry Manchester sand. The confining pressures were between 30 and 90 kPa. The size of sand sample was 7.1 cm in diameter and 18 cm in height. The densest sample was at a void ratio of 0.61, and the loosest was at 0.88. By varying the time to failure between 0.02 seconds and 10 minutes, a nearly 10% increase was found in the internal friction angle and a 15% increase in the sand's shear strength.

Seed & Lundgren (1954) carried out drained and undrained tests on specimens of fine and coarse saturated sand at different void ratios ($e = 0.58 - 0.83$). Three loading rates were used for the tests: static tests where the time to reach maximum load was between 10 and 15 minutes; medium tests with a constant deformation rate of 0.25 cm per second (6 inches per minute); and rapid tests with a deformation rate of 102 cm per second (40 inches per second). A confining pressure of 200 kPa was applied for all tests. The general rate effects from the study are shown in figure 2.9. The main conclusions from the study are:

- No rate effect was found up to a deformation rate of 0.25 cm per second.
- As the deformation rate increases to the rapid rate, the shear strength can exceed the static value by about 40%. Of this, approximately 20% is due to rate effect, while the remainder is due to the generation of negative pore pressure.
- As the void ratio increases, the rate effect decreases.
- The modulus of deformation (defined as 2% of axial strain) increases approximately 30% in a comparison between the rapid tests and the static tests.

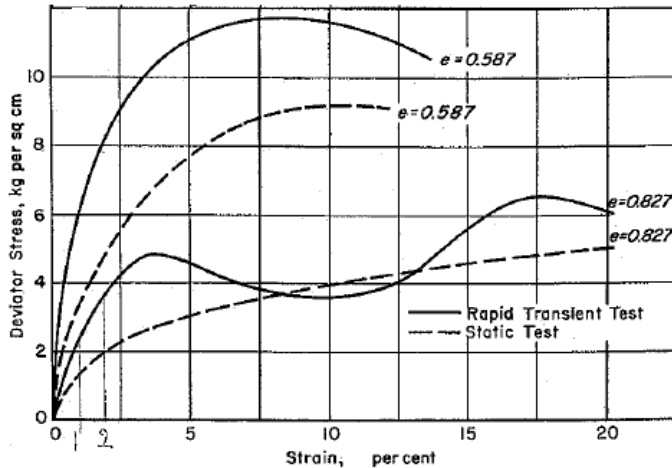


Figure 2.9: Loading rate effects in sand (after Seed & Lundgren, 1954)

Whitman & Healy (1962) reported the results from an extensive study into rate effects in non-cohesive soils at the M.I.T between 1951 and 1962. The tests were performed on three different dry sands: standard Ottawa sand, Fort Peck sand, and Nevada sand in a loose and dense state. The time to failure ranges between 5 minutes and 5 milliseconds (equivalent to a loading velocity from $15 \cdot 10^{-4}$ – 0.51m/s). They also performed the tests on dense saturated sand using three different tested loading velocities ($3 \cdot 10^{-4}$ m/s; $2 \cdot 10^{-3}$ m/s and 0.46 m/s), on loose saturated Ottawa sand with failure times of 5 seconds and 0.025 seconds and on loose Camp Cooke sand with failure times of 3 minutes and 0.2 seconds. Their main findings are:

- There is virtually no rate effect on the strength of dry sand.
- No significant effect is found in saturated dense sand. However, if the magnitude of excess pore pressure depends on the loading velocity, some increment in the shear strength is observed.
- There are noticeable rate effects in saturated loose sand that are dependent on the sand type. The strength of Ottawa sand and Camp Cooke sand increases approximately 40% and 100% respectively.

Lee et al, (1969) tested dry sand samples of different densities, where the confining pressure varied between 1 kPa and 15 kPa. A clean, uniformly-graded fine sand was used with fairly angular grains. By varying the loading velocity up to 0.22 m/s, they found an increase in strength and a nearly 100% increase in initial tangent modulus. The increment of 7% was found in the strength of loose sand at all confining pressures, and in dense sand at low confining pressure. In contrast, dense sand at high confining pressure showed a 20% increase in strength with the same loading velocity range.

Gibson & Coyle (1968) carried out a study into the rate effects of sand in order to determine the soil damping constant of sand in correlation with the damping constant used in dynamic pile load testing. The tests were conducted on Ottawa sand, Arkansas sand, and Victoria sand, which varied in grain size and angularity. Slow (static) tests were consolidated drained, with a loading velocity of 0.05 inches per minute; dynamic tests were an undrained test, where loading was applied by dropping a weight into the soil samples. By varying the drop height, the dynamic loading velocities ranged from 0 to 3 m/sec. The effective confining pressure was 100 kPa in all tests. A summary of their findings on rate effects is shown in figure 2.10. An increase in shear strength of up to 100% can be seen when the loading velocity varies from nearly zero to 0.6 m/sec. A further increase in loading velocity to 3 m/sec causes another 40% increase in strength. The study also concluded that the rate effects could be expressed by the power law

$$R_d = R_s \cdot (1 + J \cdot v^N)$$

where R_d is total dynamic resistance

R_s is total static resistance

J is a constant damping parameter

v is shearing velocity

N is a parameter optimised to keep the damping factor constant. $N = 0.2$ is determined from the test results in sand.

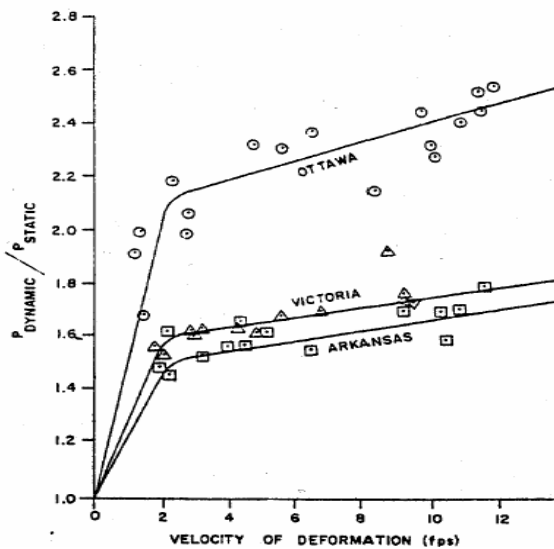


Figure 2.10: $P_{dynamic}/P_{static}$ vs. loading velocity (after Gibson and Coyle, 1968)

Ibsen (1995) studied the rate effects in saturated loose and dense sand using the constant deformation rate test. The rates ranged from 4 to 100.000 % per hour (loading velocity from $8 \cdot 10^{-7}$ to $2 \cdot 10^{-2}$ m/s). Three effective confining pressures were applied: 100 kPa, 500 kPa, and 1000 kPa. The study found rate effects of approximately 10% on shear strength (as shown in figure 2.11), and a substantial effect on the modulus of the stress-strain relationship (although no specific number was given).

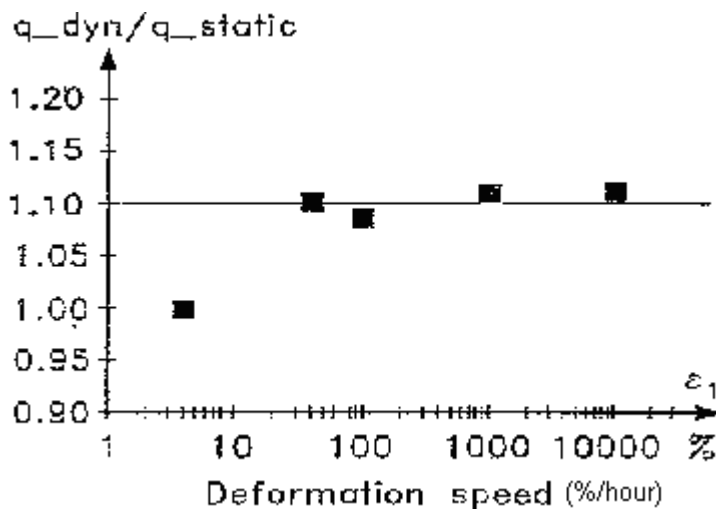


Figure 2.11: Loading rate effect on shear strength of sand (after Ibsen, 1995)

Abrantes & Yamamuro (2002) performed a series of tests in loose dry sand ($D_r = 38\%$) at a confining pressure of 100 kPa. The high rates of loading were created by a drop weight, and the maximum loading velocity was as high as 2.67 m/sec. They found rate effects in the sand of 30% in shear strength, and of 100% in secant modulus.

2.4.2 Rate effects on pile resistance

This section reviews and evaluates previous research into the effects of loading rate on the axial capacity of a pile founded in sand.

Fleming (1958) performed a series of model pile tests in sand where the loading velocity was varied between $2 \cdot 10^{-3}$ mm/min and 100 mm/min. The increment of skin friction with loading velocity is clearly visible from these tests, as shown in figure 2.14. The maximum increment is approximately 20%.

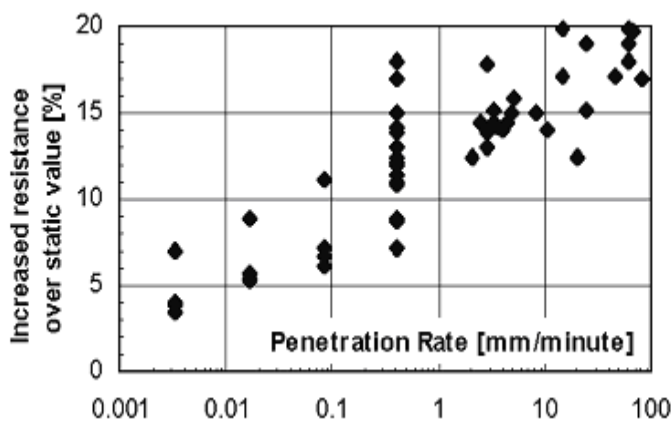
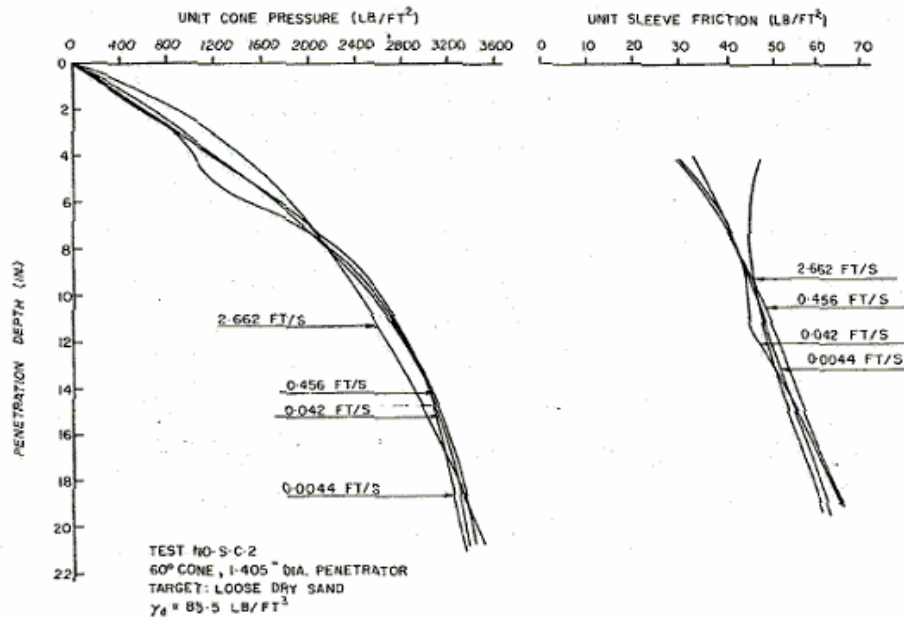


Figure 2.14: The variation of model pile resistance with loading rates (after Fleming, 1958).

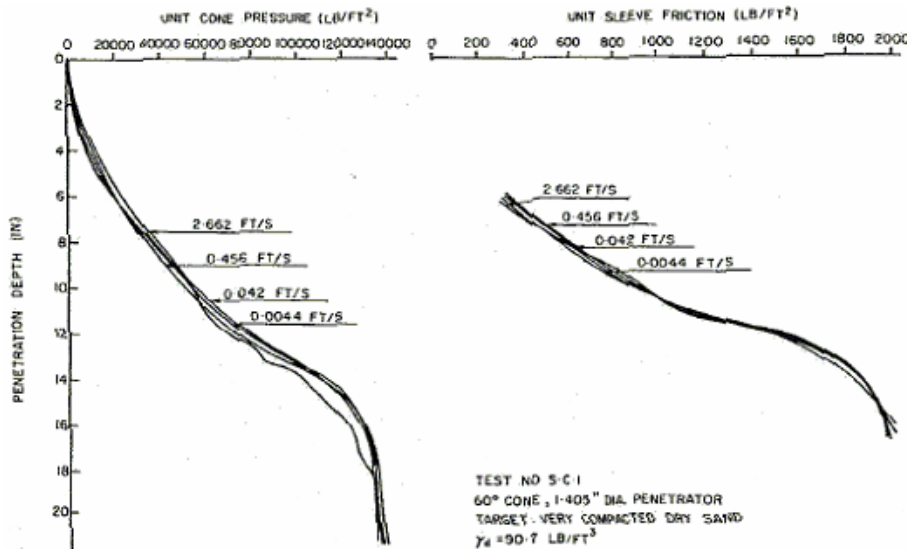
Jezequel (1969) carried out cone penetrometer tests in medium dense sand that was dry and submerged, where the loading velocities were varied between 0.002 m/sec and 0.02 m/sec. His results showed that a ten-fold increase in loading velocity led to a 7% increase in total cone resistance in dry sand, and a 20% increase in submerged sand.

Brumund & Leonards (1973) studied the static and dynamic friction between sand and a steel rod. In the experiments, a steel rod was located along the axis of a cylinder sand sample and was made to slip relative to the sand by static and dynamic forces. The static force was applied so that the slip occurred in approximately 5 minutes. The dynamic force was applied by a shock tube so that the slip occurred in 1 or 2 milliseconds. An increase of about 26% in the limit friction of the dynamic tests over the static test was observed. The paper does not report a loading velocity.

Dayal & Allen (1975) studied the subject using instrumented (cone load cell, sleeve friction load cell, and velocity measuring device) impact cone penetrometer tests. The cone penetrated a sand chamber at constant velocities ranging from 0.13 cm/sec to 81.44 cm/sec. The tests using dense and loose sand showed no significant rate effects on cone resistance. Typical measurement results of tests in sand are shown in figure 2.15.



a) loose sand



b) dense sand

Figure 2.15: Results of the test in sand from Dayal & Allen (1975)

Heerema (1979) carried out research to determine the relationship between the sleeve friction of a steel pile and horizontal stress and pile velocity in sand. The sand samples were taken from a North Sea site in a wetted state. The steel pile wall was modelled using a steel plate that was equipped with strain gauges and displacement gauge. An hydraulic oscillator movement controlled its movement. The velocity of the tests in sand varied from 7.10^{-4} m/sec to 0.6 m/s. The applied horizontal stresses ranged from 50 to 240 kPa. The results demonstrated that the magnitude of the steel pile wall friction was independent of the loading velocity.

Eiksund and Nordal (1996) performed loading rate tests on a model pile in a calibration chamber. The model pile was 1.07 metres in length, with a cross section area of 406 mm^2 . The tests were performed in F-75 Ottawa sand. Tests using different actuator loading velocities in saturated Ottawa sand showed an increase of less than 10 %, with velocities between 0.8 mm/s and 1100 mm/s (as shown in figure 2.16).

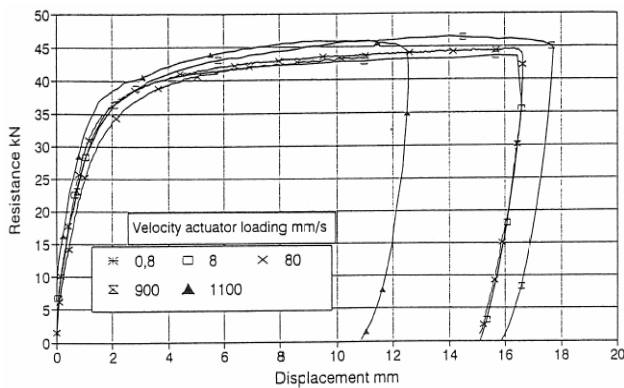


Figure 2.16: Penetration resistance with different velocities (after Eiksund and Nordal, 1996)

Al – Mhaidib (1999) performed 45 capacity tests on a model pile embedded in sand in a cylindrical tank. The model pile was made of steel and measured 3 cm in diameter. The embedded lengths were 7, 10, and 15 times the diameter. Three densities of sand samples were prepared for the investigation: loose ($D_r = 30\%$), medium ($D_r = 55\%$), and dense ($D_r = 80\%$). As the applied loading velocities were increased from 0.01 mm/min to 1 mm/min, the model pile resistance increased 90% for tests carried out in loose sand and 40% in medium and dense sand.

Gennaro et al, (2001) studied the effects of the loading rate on pile resistance by performing a series of model pile tests in a calibrated sand chamber. The loading velocities were between 1 mm/min and 60 mm/min. Two length/diameter ratios were tested, namely $D/B=17.25$ ($D=345\text{mm}$) and $D/B=25$ ($D=500\text{mm}$) (D = embedded length [mm], B =diameter [mm]). The results are shown in figure 2.17. The rate effects on the model pile's toe resistance are insignificant (less than 10%). Surprisingly however, the sleeve friction of the model pile decreases notably as the loading rate increases (approximately 30%).

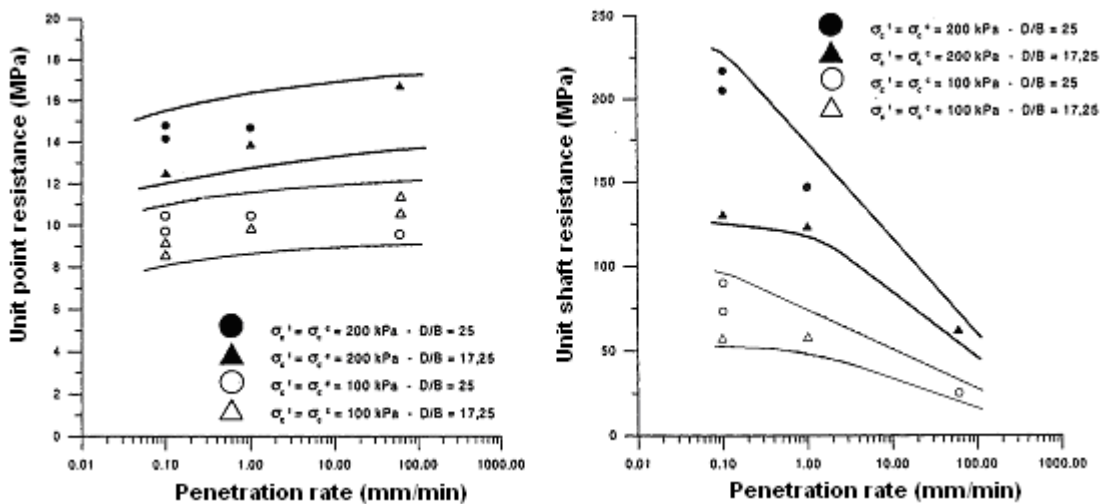


Figure 2.17: Results of loading rate effects from Gennaro et al, (2001)

2.4.3 Generalisation

The reviews presented above show different magnitudes of rate effects on sand strength, as well as on the resistance of a pile founded in sand. Results from the triaxial tests, however, show that the magnitude of the rate effect depends on the sand type, the sand state (density), and the applied

loading rates. In order to make a general evaluation of rate effects throughout the literature, an approximate generalisation of the results can be made with respect to two factors that are considered important to this study. The first factor is the range of applied loading rate in terms of strain rate, which is defined by the loading velocity over the length of the specimen (% per second). The second factor is the ratio between resistance at maximum (R_v) and minimum velocity (R_s). On the basis of this configuration, results from all the above studies have been combined and are presented in figures 2.18 and 2.19. Certain conclusions about the rate effects can be derived from these figures. Rate effects on sand strength do exist, in particular:

- The shear strength of dry sand increases approximately 20% over the static value at the strain rate $\approx 1000\%$ per hour (loading velocity approximately 1 m/sec).
- At the same strain rate, the shear strength of saturated sand increases from 40% to more than 100%.

Similar figures have been plotted for resistance of a pile founded in sand, but the loading rate is presented in terms of the absolute value of loading velocity for the sake of convenience in linking with the prototype rapid load test, where the pile velocity is known. Figure 2.20 presents the relationship between total pile resistance and the penetration velocity. Figure 2.21 presents the relationship between skin friction and the penetration rate. A similar picture cannot be plotted for pile tip resistance because of a lack of information within the literature. Contrary to the effect on sand strength, pile resistance seems to be affected less by loading rates, and the rate effect is more pronounced at a low velocity rather than a high velocity. At slow rates (e.g. less than 0.002 m/s), increments in total pile resistance due to the rate effect of 20% and 40% are observed. But there is no rate effect, or only a minimal rate effect, at higher rates. This differs from observations in the in-situ Statnamic tests, where all the tests recorded higher pile resistance compared to that in static loading (e.g. Kusakabe, 1998).

Table 2.1 presents the summarization of the previous study on the loading rate effect on resistance of a model pile in sand. For a better comparison, the loading rate is normalised by the diameter. It is interesting to see from the table that the pile resistance may increase significant as the rate increase from very slow rate to the magnitude of 10^{-2} (D/s); at the more rapid rate, the pile resistance seems less affected by the loading rate.

Table 2.1: Overview of loading rate effect on pile resistance from the literature

Literature	Test type	Sand sample	D_{pile} (mm)	Rate (D/s)	Resistance increase
Fleming (1958)	Model pile	- Saturated	40	$8.3 \cdot 10^{-7} - 4.17 \cdot 10^{-2}$	Up to 20% in shaft resistance
Jezequel (1969)	Penetrometer test	- Dry - Saturated	36	$5.56 \cdot 10^{-2} - 5.56 \cdot 10^{-1}$	- 7% - 20%
Brumund (1973)	Sand – steel interface	- Dry	N/A	N/A (Time to failure: 5 min – 1 msec)	Up to 26%
Dayal & Allen (1975)	Penetrometer test		36	$3.61 \cdot 10^{-2} - 2.25 \cdot 10^1$	Not increase
Heerema (1979)	Sand – steel interface	Saturated	N/A	N/A (Velocity: $7 \cdot 10^{-4} - 0.6$ m/sec)	Not increase
Eiksund & Nordal (1996)	Model pile	Saturated	63.5	$1.26 \cdot 10^{-2} - 1.73 \cdot 10^1$	Less then 10%
Al-Mhaidib (1999)	Model pile	- Loose - Dense	30	$2.77 \cdot 10^{-5} - 5.57 \cdot 10^{-4}$	- 90% - 40%
Gennaro et al, (2001)	Model pile		20	$3.85 \cdot 10^{-5} - 5 \cdot 10^{-2}$	- Tip increase 5% - Shaft decrease 30%

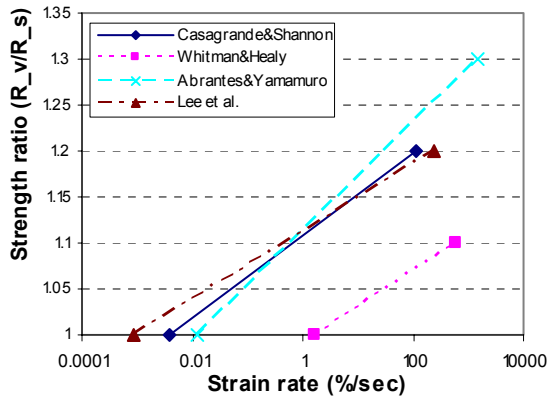


Figure 2.18: Summary of the rate effects in dry sand (triaxial tests)

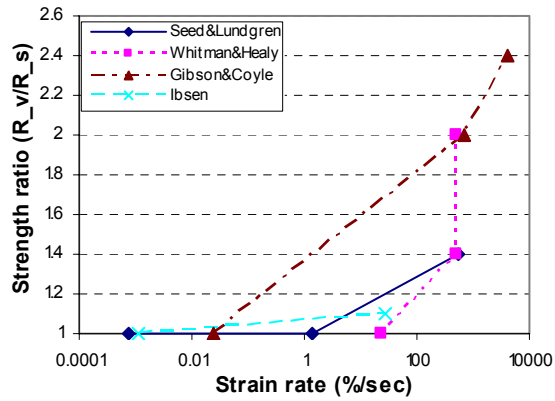


Figure 2.19: Summary of the rate effects in saturated sand (triaxial tests)

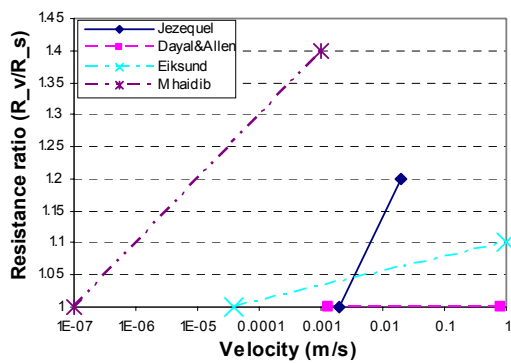


Figure 2.20: Summary of the rate effects on total pile resistance

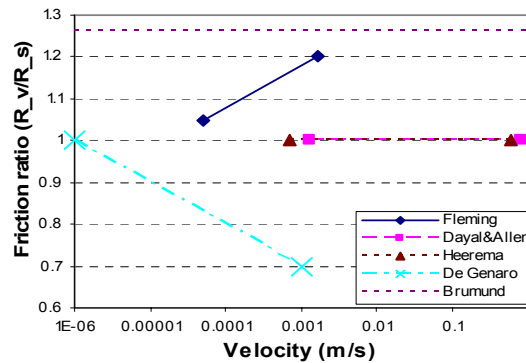


Figure 2.21: Summary of the rate effects on skin friction

2.5 Excess pore pressure

With regard to excess pore pressure during the loading time of a rapid load test, Holeyman (1992) indicated that there is no difference between the dynamic and the rapid load testing methods in terms of 90% of excess pore pressure dissipation. In both tests, excess pore pressure does not have enough time to dissipate sufficiently, even if the pile is founded in sand. In several projects, excess pore pressure in the soil around the pile has been measured. Some researchers have made attempts to point out the effect of excess pore pressure on the bearing capacity of a pile, but no clear effect has been found. Their work will be reviewed and discussed in this section. For the convenience, from now on in this thesis, the compression pore pressure is positive; and the term ‘positive pore pressure’ refers to compressive pore pressure; the term ‘negative pore pressure’ refers to suction (tension) pore pressure; the term ‘positive excess pore pressure’ refers to the increase of pore pressure in comparison to the initial value; and the term ‘negative excess pore pressure’ refers to the decrease of pore pressure in comparison to the initial value.

Hölscher (1992) measured excess pore pressure near the pile toe during pile driving, a dynamic load test, and a Statnamic load test at the testing event of the Stress Wave Conference 1992, Delft, the Netherlands. The pile was a pre-fabricated reinforced concrete pile, with a cross section of $25 \times 25 \text{ cm}^2$. The final depth of the pile toe was 18.2 m below the surface, and the pile toe was penetrated 3.2 m into a dense sand layer. The pore pressure transducer was placed at a location of 0.5 m away and 0.2 m below the centre of the pile toe. Figure 2.22 shows the excess pore pressure measurements for the last pile driving blow, the dynamic test three days later, and the Statnamic test five days later. Negative values represent an increase in pore pressure and are thus the result of

compression. The measurements show the same pore pressure response during all types of loading. The pore pressure increases (compressive) when loading begins, then decreases to a negative value (suction). It is noticeable that the consolidation time of excess pore pressure ranges from 100 ms to 200 ms, which is comparable with the Statnamic loading duration. It can therefore be concluded that soil behaviour is partially drained during the Statnamic test in this case. As the measured pile head force data is unfortunately missing, it is not possible to evaluate the importance of excess pore pressure in relation to the pile capacity (Hölscher, 1995).

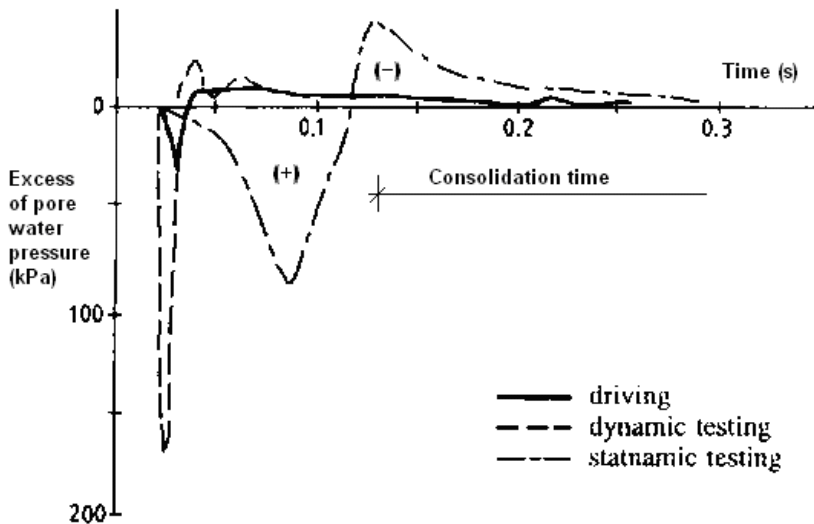


Figure 2.22: Excess pore pressure during pile driving, dynamic, and Statnamic tests (after Hölscher, 1992).

Maeda et al, (1998) measured excess pore water pressure in soil during a Statnamic test on a cast-in-place pile. The pile had a diameter of 1.2 m and length of 13.4 m. The pile toe was penetrated 1.2 m into a diluvial gravel sand layer. Two pore pressure transducers were placed at a distance of 1.05 m from the pile's axis, and 0.5 m and 1.1 m below the pile toe level. Their measurements show the pore pressure increased simultaneously with applied Statnamic loading by up to 80 kPa (compressive), then dissipated immediately after completion of the test. The consolidation time estimated from Maeda et al, (1998) is approximately 300 msec to 500 msec, which is far longer than the Statnamic loading duration. The soil can therefore be considered as almost undrained. The force at the pile toe was also measured in the Statnamic test and in a static test. The pile toe resistance at the unloading point in the Statnamic test was approximately 12 MN, and at the same displacement in the static test was approximately 9 MN. The difference of 3 MN cannot be explained by the simplified pore pressure force of 0.09 MN on the pile toe (production of the excess pore pressure and pile toe area), and no further clarification is given in the paper.

Hajduk et al, (1998) also measured pore water pressure at the pile shaft and in the sand layer near the pile toe during Statnamic loading. The pore water pressure in the sand layer at approximately 1.5 m and 2.5 m from the pile reached dynamic values up to 2 kPa, which is extremely small in comparison with the pile resistance. This pore water pressure decreased (consolidation) in approximately 10-15 minutes. This is relatively slow for a sand layer, but no explanation is given.

Matsumoto (1998) measured excess pore pressure during a Statnamic test in an open-ended pipe pile driven into a diatomaceous mudstone (a type of soft rock). A large pore pressure built-up and dissipation was also observed in the period between 100 ms and 200 ms. The excess pore pressure was negative at the pile shaft, and positive below the pile toe. The ratio between peak pore pressure

force and soil resistance at the unloading point was approximately 0.2% in this case, which is again too small.

Eiksund & Nordal (1996) also measured excess pore pressure near the model pile tip in their experiments. Examples of test measurements using different loading velocities are shown in figure 2.23. The overall pore pressure response is the same: a small increase is observed initially, but the excess pore pressure turns into a negative value after approximately 1 mm of model pile movement. This is explained by the dilatancy of the sand. A comparison of the two figures shows that a higher loading velocity caused a higher negative excess pore pressure value. The largest excess pore pressure for the test series in sand was approximately -30 kPa, which is extremely small in comparison with the average total stress at the pile tip of 10000 kPa. The study concludes that the excess pore pressure induced by pile penetration has a minor influence on resistance.

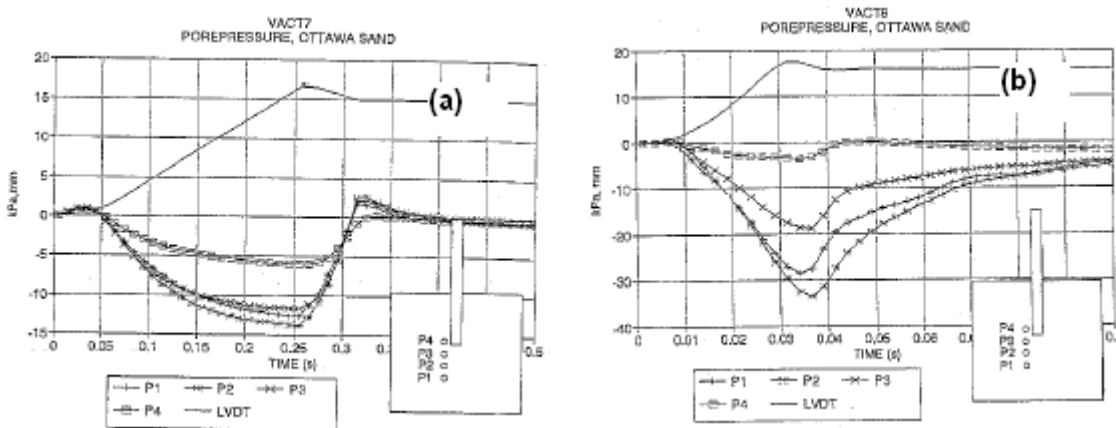


Figure 2.23: Pore pressure response in constant rate of penetration tests (after Eiksund and Nordal, 1996) (a) $v = 80$ mm/s; (b) $v = 900$ mm/s

Discussion

From the investigations described above, it is possible to generalise that excess pore pressure is generated during a Statnamic test even if the pile is founded in sand, and that soil behaviour is partially drained during the loading time of the Statnamic test. The pore pressure first increases (compressive), and then decreases to a negative value (suction) which is perhaps mainly due to the dilatancy of the sand. The magnitude of excess pore pressure depends on the loading rate and sand properties. However, in comparison to the total stress underneath the pile tip, it can be concluded that the magnitude of excess pore pressure is extremely small and seems to have little effect on pile resistance.

On the other hand, it can be expected that excess pore pressure may influence the shear strength of the surrounding sand and subsequently affect the pile's mobilised resistance. This has been reported in several experiments with a footing, and a contradictory effect is found. Finnie and Randolph (1994) reported the results of centrifuge tests when studying the effect of the penetration rate on a footing's bearing capacity in saturated uncemented sand. The penetration rate ranged from 0.1 mm/s to 3 mm/s. They found that within the penetration range, the footing's response changed from a drained to an undrained condition. The bearing capacity in the undrained condition was up to two times lower than that in the drained condition. Although no pore pressure response was measured in their experiments, they blamed positive excess pore pressure during the fast loading for the reduction in bearing capacity. However, their situation was quite different from the investigation

mentioned above, where pile velocity was much higher (≈ 1 m/s) and where negative excess pore pressure was measured. By contrast, Vesic et al (1965) reported test results from experiments into the dynamic bearing capacity of footings in dry and submerged sand. For tests in submerged sand, the loading velocity ranged from $2.5 \cdot 10^{-6}$ mm/s to 25.4 mm/s. The relationship between the bearing capacity factor and the loading velocity in their experiments is shown in figure 2.24. In the case of submerged sand, the bearing capacity at maximum loading velocity was significantly higher than the static bearing capacity. Although no pore pressure measurements were reported and no clear evidence is given in their paper, they explained that the significant increment of bearing capacity in submerged sand must be caused by negative pore water pressure, which increases the sand's shear strength as does the footing capacity. Therefore, if negative excess pore pressure exists during a Statnamic test, the same effect can be expected on pile resistance.

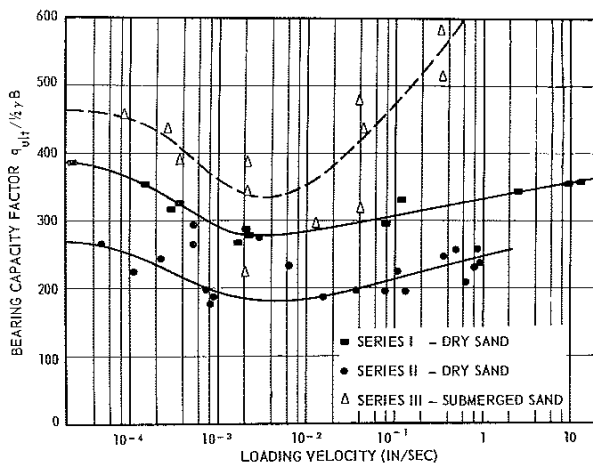


Figure 2.24: Effect of loading velocity on bearing capacity of footing (after Vesic et al. 1965)

2.6 Summary

The rapid pile load test method (especially the Statnamic test) is capable of predicting the static bearing capacity of a pile when used with the UP method to interpret the results, but only if the loading rate effect factor (η) proposed by Paikowsky et al, (2006) is applied in the analysis. However, resorting to the loading rate effect factor (which is smaller than 1) implies that a pile's mobilised resistance at the unloading point of a rapid load test is larger than the pile's static resistance at the same displacement. This is thought to be related to the high loading rate of the rapid test. Indeed, the loading rate can affect the mobilised strength of soils, a phenomenon that has been referred to in literature as the 'rate effect'. The rate effect has been defined by Whitman (1957) as "the relationship between the rapidity of loading and shearing strength of a soil". Although a high loading rate can increase the shear strength of soil, its effects on a pile's mobilised resistance are different for cases where the pile is founded in sand, as reported in literature. One of the objectives of this study will be to examine the rate effect. Throughout this thesis, the term 'rate effect' is taken to be the definition made by Whitman. This rate effect is distinguished from other dynamic effects such as inertial, damping, and excess pore pressure. It is seen as constitutive soil behaviour.

In addition, the occurrence of excess pore pressure in the surrounding soil during the test has been confirmed, which may influence pile resistance. Measurements made in some previous studies reveal that excess pore pressure has a minor effect in terms of reaction force on the pile toe. However, its effects on the shear strength of surrounding soil and subsequently on the pile's mobilised resistance are not discussed in literature. To facilitate worldwide use of the rapid pile

load test in cases where sand forms the main bearing capacity stratum for the pile, answers must therefore be found to two fundamental questions that are studied in this thesis:

1. The rate effect on resistance of a pile founded in sand and its incorporation into analysis models, such as described in the UP method.
2. The effects of excess pore pressure on the shear strength of soil near the pile toe, and its subsequent effects on the mobilisation of pile resistance during the test.

Moreover, some researchers have indicated that prediction of the static load-displacement curve is generally poor. The reason is thought to be the constant damping factor used in the analysis model. It is expected that further insight into these two questions will increase the prediction reliability of a pile's static load-displacement curve derived from a rapid load test.

Chapter 3

Laboratory experiments on rate effects in sand

3.1. Introduction

Two series of laboratory experiments were carried out: triaxial tests and model pile load tests. These tests focused on the effects of loading rate on the resistance of a pile founded in sand. The experiments and results are presented in this chapter.

The first series of experiments described in this chapter are the triaxial strain controlled tests, which were performed at different rates of deformation. Dry and unsaturated sand samples were used in the tests. The aim of the test series was to study the rate effects on the shear strength of sand and the characteristics of excess pore pressure under different loading rates.

The second series of experiments described are the model pile load tests, where the pile was embedded in a calibration chamber filled with unsaturated or saturated sand. Both constant rate of penetration load tests and dynamic load tests were performed. The main objective of the test series was to study the rate effects on pile resistance.

3.2. Triaxial tests

3.2.1. Testing programme

The testing programme was designed in such a way that the behaviour of the sand specimen could be determined at different loading rates. The main objectives of the test series were:

- To examine the rate effects on stress-strain behaviour and the shear strength of sand.
- To investigate excess pore pressure in a sand specimen at high loading rates.

The tests were performed under the same conditions, but the applied loading rate was varied from a very slow rate (static) to higher rates. The pore pressure was measured during all tests. The choice of testing rates was based on the rates to which soil is subjected during a static pile load test and a rapid pile load test in the prototype situation. In practise, the velocity field of surrounding soil during a pile load test is generally unknown but deformation rates in the soil at the contact interface would be virtually identical to the observed pile head velocity. The testing rates were therefore chosen in correlation with the pile head velocity. In conventional static pile load tests such as the maintained load test (MLT) or the constant rate of penetration load test (CRP), the pile is penetrated into the soil at a very slow rate. For example, the British Standard (BS 8004:1986) recommends a rate of 0.25 mm/hour for the MLT, and a rate of 0.025 mm/sec for the CRP. On the other hand, the peak velocity of a pile during a full-scale rapid load test may be as high as 0.5 to 1 m/sec (Holeyman, 1992). Based on these velocities, the minimum testing rate was chosen as 0.0125 mm/sec and the highest testing rate was 0.6 m/sec. Some tests were also performed using intermediate rates. The rate of deformation was constant in all tests. This helped to minimise dynamic effects such as the inertial and stress wave at high rate tests, as will be shown later.

An effective confining pressure of 100 kPa was applied throughout the test series. The same sand type and specimen preparation procedure were used. The following were measured during a test:

- Applied force on the specimen
- Downward displacement at the top of specimen
- Applied confining pressure
- Pore pressure at the bottom of the specimen.

In some high rate tests, the forces were measured at both ends of the specimen in order to verify the measurement and to examine the dynamic effects on the test results.

3.2.2. Testing system

An overview of the testing system is shown in figure 3.1. The testing system included four main components: the triaxial cell, the hydraulic loading system with control box, the data acquisition system, and a desktop computer for visualising the recorded data.

The triaxial cell

The triaxial cell was designed as a conventional triaxial cell for testing a soil sample of 66 mm in diameter and 150 mm in height. The only difference was an additional waterproof load cell placed on the bottom plate to measure the axial force at the bottom end of the specimen. This load cell was used in several tests to verify the measurement and the existence of dynamic effects.

The hydraulic loading system and loading control box

A hydraulic loading system was used to apply a selected loading velocity pattern to the specimen. The loading plunger was operated by high-pressure oil. Oil flow was controlled by the loading control box. The maximum designed loading velocity of the loading system was 0.6 m/sec and the minimum loading velocity had a magnitude of 10^{-5} m/sec. There is the second load cell embedded in the loading plunger to measure the applied load on the top of specimen in all tests. The displacement transducer was also embedded inside the loading plunger to supervise its downward movement, which is seen as the axial displacement of the tested specimen.

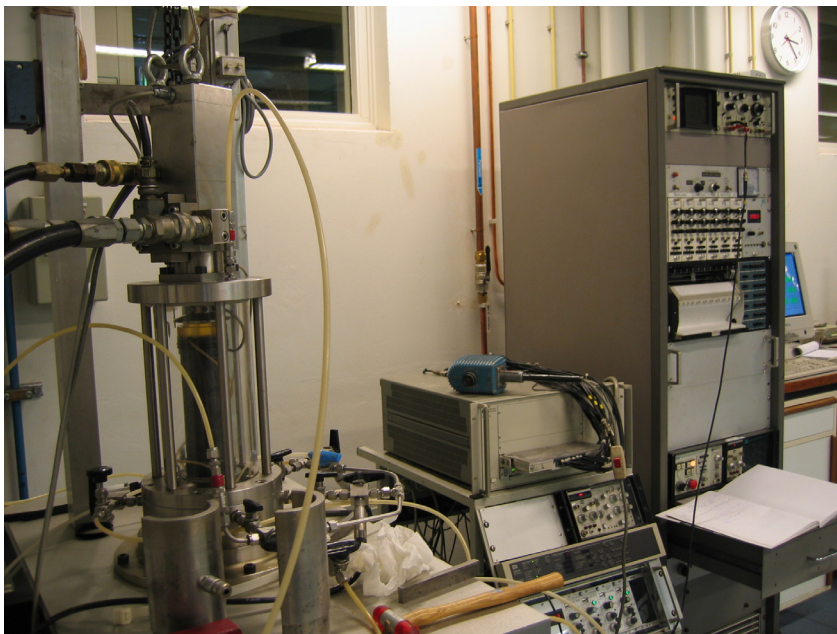


Figure 3.1: Overview of testing and data acquisition system

3.2.3. Sand properties

The sand used in this triaxial test series is known as Itterbeck sand. The grain size distribution is shown in figure 3.2 and the classification parameters, that were determined in TU Delft's Geotechnical Laboratory according to the procedures described in Head (1998), are presented in table 3.1.

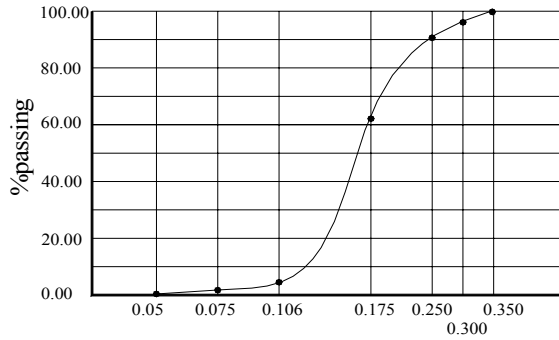


Figure 3.2: Grain size distribution curve of Itterbeck sand

Table 3.1: Classification parameters of Itterbeck sand

Property	Value
Specific gravity, ρ_s	2.613
Max. dry density, ρ_{\max}	1.731 Mg/m ³
Min. dry density, ρ_{\min}	1.415 Mg/m ³
Mean grain size, D_{50}	0.165 mm
Uniformity coefficient, D_{60}/D_{10}	1.7

3.2.4. Specimen preparation and testing procedure

To avoid unexpected errors, the specimen preparation and testing procedures closely followed procedures described in the laboratory manual (Head, 1998). Details of the procedures are presented below.

3.2.4.1 Specimen preparation

All specimens were prepared using the same dimensions (66 mm in diameter and 150 mm in height). The amount of each sand specimen was calculated from a desired relative density (I_d) and placed in a separate cup. Before use, the sand was dried in an oven for a minimum of 12 hours and was then cooled at room temperature. A brief description of the preparation of a dry and a saturated sand specimen is given.

Preparation of a dry sand specimen

A dense dry specimen was prepared in a cylindrical split mould using the multi-stage vibration method, which was acceptable for a routine laboratory triaxial test. The vibration was applied to the outer side of the mould by tamping with a hammer and a vibration machine. During vibration, the mould was kept full of sand until all the sand had been added. The upper surface of the specimen was then carefully flattened and closed with a porous stone disk. A vacuum (-20 kPa) was applied

to the specimen through the drainage connection so that the specimen remained stable when the mould was removed. Once the mould had been removed, the precise specimen dimensions were recorded at vacuum pressure. The dimension measurements were initially made at two vacuum pressure values: a “stay stable” value of -20 kPa, and the effective confining pressure of 100 kPa. The differences were negligible. The triaxial cell was then assembled and tightened to the base by screws. In the following step, the vacuum pressure inside the specimen was replaced by the triaxial cell air pressure. The cell pressure was increased to +50 kPa before release of the vacuum pressure. The cell pressure was again increased to the desired effective confining value of +100 kPa. The cell pressure was supplied by air pressure. Before starting a test, the top loading plunger was lowered to a space of approximately 2 mm above the top of the specimen. This was to minimise the inertial effect of the loading plunger on the tested specimen’s response.

Preparation of a saturated sand specimen

The first step in preparing a saturated specimen was to prepare a dry specimen with the desired relative density as described previously, so only the saturated step is described here.

Once a dry specimen had been prepared and the triaxial cell had been tightened in place, the cell pressure was increased to approximately 30kPa to ensure that the specimen remained stable during the saturation process. Initially, CO₂ gas was slowly pumped into the specimen at low pressure (less than 5kPa) over a 5-minute period to replace air in the specimen voids. The specimen was then slowly saturated using de-aerated water until no gas bubbles were visible in the drainage connection. Finally, the pore water pressure and cell pressure were gradually increased to 300 kPa and 400 kPa respectively using a routine laboratory back pressure procedure. At every step of cell pressure increase, the cell pressure and pore water pressure values were recorded to calculate the Skempton’s factor (B), i.e. to verify the specimen’s degree of saturation. When the pore pressure reached 300 kPa of back pressure, any remaining gas in the void was dissolved and the Skempton’s factor was close to unity, i.e. the specimen was 100% saturated. Once the back pressure procedure had been completed, the cell pressure was 400 kPa and the pore pressure was 300 kPa, i.e. the effective confining pressure is 100 kPa.

3.2.4.2 Testing procedures

In general, the testing procedure was identical for tests on dry and saturated specimens. There were only minor differences in the applied loading velocities and the test conditions, due to the limitation of the testing system which will be described later. Before starting a test, a prescribed loading program was selected and executed in the loading control box. The test was performed until the vertical displacement of the loading plunger reached approximately 30 mm ($\approx 20\%$ of axial strain) to ensure specimen failure. All measurement data were recorded and stored via the data acquisition system. The sampling rate of the data acquisition system was specifically set for each test (usually 1 kHz for a rapid test and 1 Hz for a static test).

The static tests for both dry and saturated specimens were performed using a constant loading velocity of 0.0125 mm/sec. The rapid tests with dry and saturated specimens were performed using a maximum constant loading velocity of 0.6 m/sec and 0.4 m/sec respectively. The test series on saturated specimens was also carried out with an intermediate loading velocity of 1 mm/s.

Drainage valves were opened for all tests with dry specimens, i.e. the tests were in a drained condition so that excess air pore pressure could be considered during the rapid tests. The drainage valves were closed during tests with saturated specimens, i.e. the tests were in an undrained condition to prevent the drainage condition of the testing system affecting the measured values of pore water pressure.

3.2.5. Analysis of test data

This section first considers the validity of the measurement data. It includes the determination of the actual deformation rate of a test;; the occurrence and confirmation of cavitation for tests in saturated sand; the evaluation of dynamic effects in a rapid test; and the error in the relative density of a specimen. It concludes by elaborating the test results.

3.2.5.1 Actual testing rate

Tests on dry sand

After a review of the test data, it was clear that the actual testing rate of a rapid test differed slightly from the desired rate. The actual loading rate therefore needs to be verified for later evaluation of the rate effect. Figure 3.3 shows an example of the desired and measured displacement-time graphs of a rapid test. The desired velocity is 0.6 m/sec. However, it was determined that the actual velocity of the test was approximately 0.525 m/sec. The actual deformation rate in all rapid tests on dry specimens has been determined and is elaborated in table 3.2. For the static tests on dry specimens, the actual rate of deformation is the same as the desired value and does not need to be adjusted.

The reason for the difference between the desired velocity and the actual velocity of a rapid test is that the oil pressure in the loading system was insufficiently high to speed-up the loading plunger to the desired value in the rapid tests. For the test shown in figure 3.3, the oil pressure was initially set to 120 bars. When the oil pressure was increased to 200 bars, the actual velocity was very close to the desired value (approximately 0.59 m/sec).

Tests on saturated sand

In the tests on saturated sand, the loading velocity of the first test was set at the loading system's highest velocity (≈ 0.6 m/sec) in order to check the operation. The measured displacement-time is shown in figure 3.4. Verification of the loading velocity shows that the actual velocity was approximately 0.44 m/sec at the first 15 mm of displacement. The velocity then increased to ≈ 0.75 m/sec. This differs markedly from the desired velocity pattern. After several attempts, it was found out that the loading system could not exert sufficient force to reach the desired velocity at the start of the test. The maximum loading velocity in this case was only approximately 0.44 m/sec. The maximum velocity of 0.4 m/sec was therefore applied for rapid tests on saturated specimens. The actual deformation rate in every rapid test on saturated sand has been determined and is shown in table 3.3.

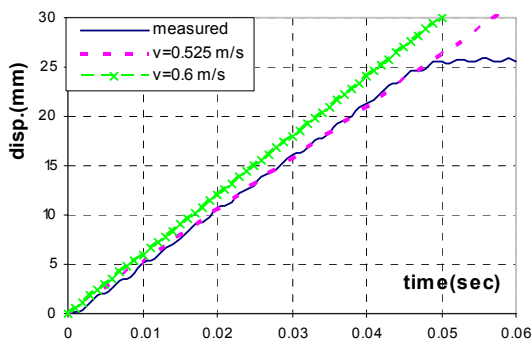


Figure 3.3: Example of displacement-time graph in a high rate test (dry sand)

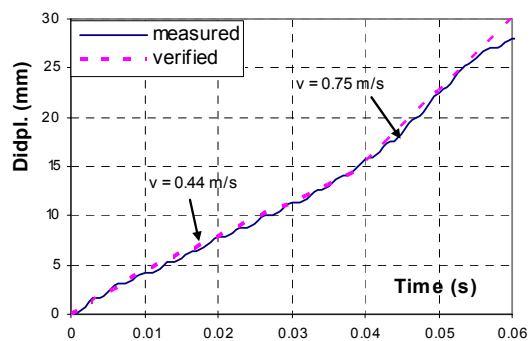


Figure 3.4: Example of displacement-time graph in a high rate test (saturated sand)

3.2.5.2 Existence of the cavitation phenomenon

The saturated sand test series was performed using dense specimens in an undrained condition. Negative excess pore pressure due to dilatancy and volume expansion inside the sand sample were therefore expected. If pore water pressure reaches its vapour pressure (approximately -100 kPa at laboratory room temperature), the cavitation phenomenon will occur. Once it occurs, air will be present in the pores of the specimen and the validity of pore pressure measurement can no longer be ensured whether or not the measured value is the pore water pressure or the pore air pressure or the pore pressure. The existence of the cavitation phenomenon therefore needs to be verified to evaluate the test results.

A typical graph plotting measured pore pressure against axial strain during a saturated test is shown in figure 3.5. Initially, the specimen was isotropically compressed and pore water pressure increased. After some time, pore pressure quickly decreased to a constant value of approximately -80 kPa, which is still higher than the theoretical cavitation pressure. To check the existence of cavitation, an extra test was performed using a 62% relative density specimen. The extra test was performed at static velocity, the back pressure was 600 kPa, and the cell pressure was 700 kPa. Displacement and pore water pressure measurements taken during the ‘extra test’ are shown in figures 3.6 and 3.7. In the ‘extra test’, the loading plunger was unable to move further than about 5 mm ($\approx 3.5\%$ of axial strain) since the loading system had reached its limiting force. Fortunately, the value of excess pore pressure was high enough to verify the cavitation phenomenon. Figure 3.5 shows that the total excess pore pressure (Δu) was approximately 400 kPa, whereas that of the ‘extra test’ in figure 3.7 was approximately 600 kPa at 3.5% of axial strain. As both specimens had the same relative density and were tested under the same conditions, the degree of dilatancy would be virtually identical (i.e. the total change in pore water pressure should be the same). The difference in these figures confirms that cavitation occurred. The vapour pressure at the test condition was approximately -80 kPa.

Because cavitation occurred in the tests on saturated sand, it was not possible to guarantee that pore pressure inside the specimen was identical to measured pore pressure due to the existence of pore air. As a result, the effective confining stress was unknown and the friction angle cannot be determined. The rate effects in the saturated sand will therefore be evaluated based on the deviator stress-strain relationship and the maximum deviator stress.

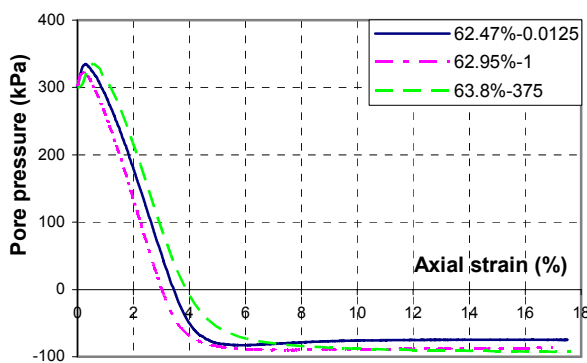


Figure 3.5: Pore pressure vs. ϵ_1 at different rates

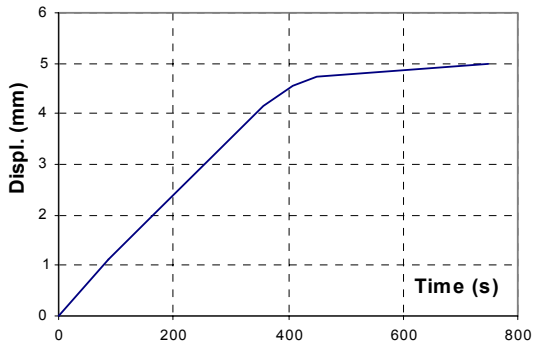


Figure 3.6: Displacement-time graph of the 'extra test'

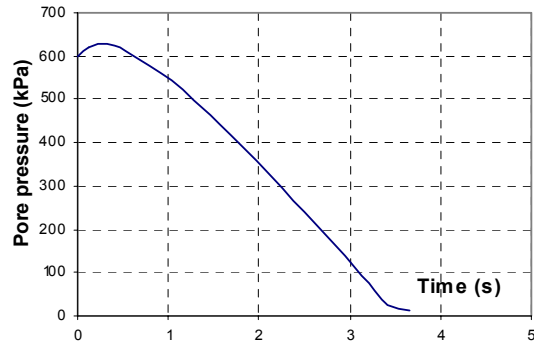


Figure 3.7: Pore pressure-strain graph of the 'extra test'

3.2.5.3 Evaluation of the dynamic effects

As the rapid tests were performed with high velocity, dynamic effects such as stress wave propagation and inertial forces may be exerted on the specimen. If significant, these dynamic effects can create a non-uniform stress distribution in the specimen and influence the test results. This section evaluates the significance of these effects.

If the stress wave is significant in a rapid test, the measured force at the top and bottom of the specimen will differ markedly at the start of the test. This is due to the propagation of stress waves backwards and forwards in the specimen. Moreover, the force recorded by the top load cell at the start of the test will include the inertial force resulting from the accelerating loading plunger and specimen. These inertial forces will disappear once deformation is in a steady-state condition. As a consequence of these two phenomena, the load at the top load cell will be larger than that at the bottom load cell at the start of a rapid test. The evaluation of dynamic effects can therefore be based on a comparison of the forces measured at both ends of the specimen during the fastest test.

Figure 3.8 shows the forces measured during the rapid test with the highest velocity ($v = 0.58$ m/sec). Figure 3.9 shows a close-up of the values measured at the start of the test. These figures show that the difference between the force measured at the top and bottom load cell is insignificant. There is only a time lag between these measurements, which relates to the compression wave velocity in the specimen. As the height of the specimen is ≈ 150 mm and the time lag in figure 3.9 is ≈ 0.001 s, the compression wave velocity will be approximately 150 m/sec. This is a reasonable value for dry sand (Hölscher, 1995). The dynamic effects are negligible in this case, and are therefore also negligible in the other rapid tests with lower velocities. As a result, the distribution of stresses in a rapid test is uniform and a single measurement is sufficient to analyse the results.

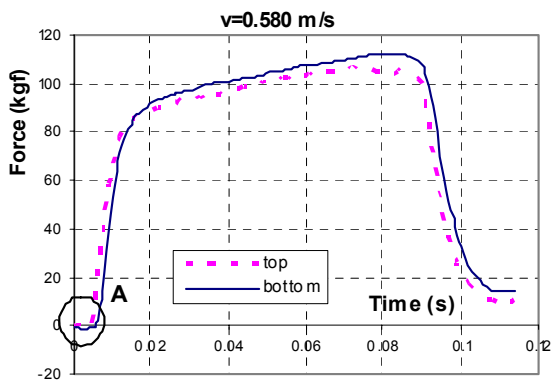


Figure 3.8: Forces measured at the top and bottom load cells

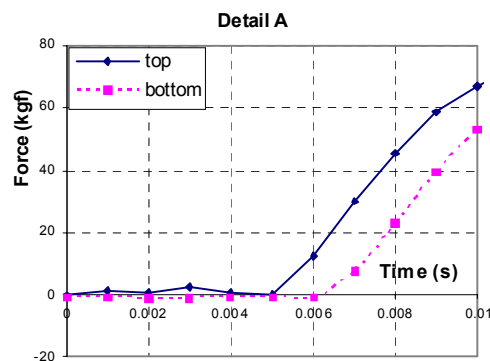


Figure 3.9: Close-up A (start of the test)

3.2.5.4 Density of specimen

From the measured dimensions and mass of a prepared specimen, the relative density of the specimen can be calculated as (Head, 1998):

$$I_D = \frac{\rho_D - \rho_{D,min}}{\rho_{D,max} - \rho_{D,min}} \cdot \frac{\rho_{D,max}}{\rho_D}$$

where

I_D : relative density (%)

$\rho_{D,max}$: maximum volumetric mass of the sand (= 1.731 Mg/m³) in densest state e_{min}

$\rho_{D,min}$: minimum volumetric mass of the sand (= 1.415 Mg/m³) at loosest state e_{max}

ρ_D : actual volumetric mass of the specimen (Mg/m³) = $\frac{m}{V}$

m: mass of sand in the specimen (g)

V: measured volume of the specimen (m³).

Tables 3.2 and 3.3 present the density of tested specimens for the test series in dry and saturated sand respectively. The objective of the test programme was to perform tests on specimens with three different densities: 60% (dense specimen), 70% (medium dense), and 80% (very dense). For the test series in dry sand, however, there was a large deviation between the proposed density and the actual density as shown in table 3.2. This was due to a lack of adherence between the rubber membrane and the inside wall of the split mould, and the radius for the prepared specimens was therefore not as expected. This situation was solved for the test series in saturated sand by attaching a thin textile lining to the mould's inside wall, so improving adherence with the membrane. This resulted in densities for prepared specimens that were easier to reproduce and that were nearly the same as the proposal shown in table 3.3.

Some deviation is unavoidable since the dimensions of a specimen were measured manually. Assuming an inaccuracy of 0.2 mm in the measurements, the calculated deviation in relative density (I_D) of each specimen will be $\pm 2.5\%$.

3.2.5.5 Elaboration of the test results

A total of 22 tests were performed on dry sand specimens. This included nine static tests and 13 rapid tests with different loading velocities. The relative density ranged from 63% to 85%. The results of the tests are presented in table 3.2.

A total of 10 tests were performed on saturated sand specimens. This included three static tests, three intermediate tests ($v = 1$ mm/sec) and four rapid tests. The results of these tests are presented in table 3.3.

Table 3.2: Results of the tests in dry sand

Test No. (mm:dd-hh:mm)	V (m/sec)	I_D (%)	σ_3 (kPa)	Max. ($\sigma_1 - \sigma_3$) (kPa)	φ (deg.)	ϵ_{1-max} (%)
1 (0614-1137)	static	75.4 ± 2.4	100	386.4	41.2	2.85
2 (0614-1523)	0.525	75.1 ± 2.4	101	411.5	42.1	3.90
3 (0615-1116)	static	64.2 ± 2.5	101	343.4	39.0	3.64
4 (0615-1359)	0.178	66.8 ± 2.5	102	357.5	39.5	4.42

Table 3.2: Results of the tests in dry sand (continue)

Test No. (mm:dd-hh:mm)	V (m/sec)	I _D (%)	σ_3 (kPa)	Max. ($\sigma_1 - \sigma_3$) (kPa)	ϕ (deg.)	ϵ_{1-max} (%)
5 (0615-1502)	0.182	64.5 ± 2.5	101	357.2	39.7	4.82
6 (0615-1556)	0.550	64.2 ± 2.5	102	358.5	39.6	6.90
7 (0616-1407)	static	76.4 ± 2.5	102	387.9	41.4	3.05
8 (0616-1525)	0.178	68.1 ± 2.5	102	372.6	40.3	5.40
9 (0617-0958)	0.580	71.5 ± 2.4	102	388.6	41.0	4.80
10 (0617-1050)	0.590	83.3 ± 2.4	102	484.8	44.7	4.53
11 (0617-1142)	0.195	83.5 ± 2.4	102	456.4	43.7	4.50
12 (0617-1355)	static	84.6 ± 2.3	100	401.7	41.9	2.48
13 (0617-1515)	0.405	81.2 ± 2.4	102	414.2	42.1	3.23
14 (0614-1420)	0.180	76.3 ± 2.4	100	398.2	41.4	3.81
15 (0830-1110)	static	70.5 ± 2.5	100	347.6	39.4	2.68
16 (0907-1529)	0.585	65.6 ± 2.5	102	356.3	39.9	4.80
17 (0908-1416)	static	70.0 ± 2.5	100	340.7	39.3	2.50
18 (0909-1419)	static	79.4 ± 2.4	100	388.4	41.7	2.90
19 (0909-1536)	0.480	74.8 ± 2.4	102	401.4	41.6	4.80
20 (0910-1257)	static	71.0 ± 2.5	100	367.3	40.3	3.10
21(0910-1418)	0.195	69.0 ± 2.5	102	372.0	40.2	3.40
22 (0910-1515)	static	63.0 ± 2.6	100	319.5	38.0	30
<i>“static” = tests with loading rate of 0.0125 mm/s</i>						

Table 3.3: Results of the tests in saturated sand

Test No. (mm:dd-hh:mm)	V (m/sec)	I _D (%)	σ'_3 (kPa)	Max. ($\sigma_1 - \sigma_3$) (kPa)	ϕ (deg.)	ϵ_{1-max} (%)
1 (1004-1502)	static	62.5 ± 2.5	x	1293	N/A	6.5
2 (1003-1149)	0.001	63.0 ± 2.5	x	1284	N/A	7.5
3 (1004-1206)	0.375	63.8 ± 2.5	x	1328	N/A	9.0
4 (929-1115)	static	71.3 ± 2.5	x	1442	N/A	6.5
5 (0928-1506)	0.001	71.5 ± 2.5	x	1420	N/A	7.5
6 (0929-1508)	0.380	71.2 ± 2.5	x	1485	N/A	7.7
7 (1003-1530)	0.0007	75.0 ± 2.5	x	1450	N/A	7.7
8 (0829-1157)	static	80.5 ± 2.5	x	1553	N/A	6.5
9 (0831-1115)	0.350	80.3 ± 2.5	x	1647	N/A	5.5
10 (0823-1129)	0.440	80.9 ± 2.5	x	1648	N/A	6.5
<i>“static” = tests with loading rate of 0.0125 mm/s; N/A : not available</i>						

3.2.6. Rate effect in dry sand

Rate effect on shear strength of dry sand

To determine the rate effect on the shear strength of dry sand, the test results in table 3.2 are divided into two groups: the first group includes all the static tests, the second group includes all the rapid tests. Figure 3.10a shows a graph of the peak friction angles against the relative density of these two groups. As the test conditions were the same for the entire test series, evaluation of the rate effect is straightforward from the figure. Overall, peak friction angles derived from the rapid tests are higher than those derived from the static tests. The linear trend lines of the two groups show an average increment of the peak friction angle due to the rate effect of approximately one degree, and a slight increase of the rate effect with relative density. The loading rate does affect the shear strength of the dry sand, and the magnitude of the rate effect increases as the specimen's relative density increases.

The results in table 3.2 can also be divided into three groups based on the loading velocity: group 1 contains all static tests (known as 'static'), group 2 contains all rapid tests with loading velocities of approximately 0.2 m/s (known as 'v=0.2 m/s'), and group 3 contains all tests with loading velocities between 0.525 m/s and 0.595 m/s (known as 'v=0.55 m/s'). Figure 3.10b shows a graph of the peak friction angle against the relative density of these three groups. It also includes the linear trend lines of each group. The peak friction angle of group 3 'v=0.55m/s' seems to be higher than that of group 2 'v=0.2 m/s', hence the load rate effect increases with loading velocity. However, the number of data points from groups 2 and 3 with a high density is limited. The observation from figure 3.10b therefore requires further verification.

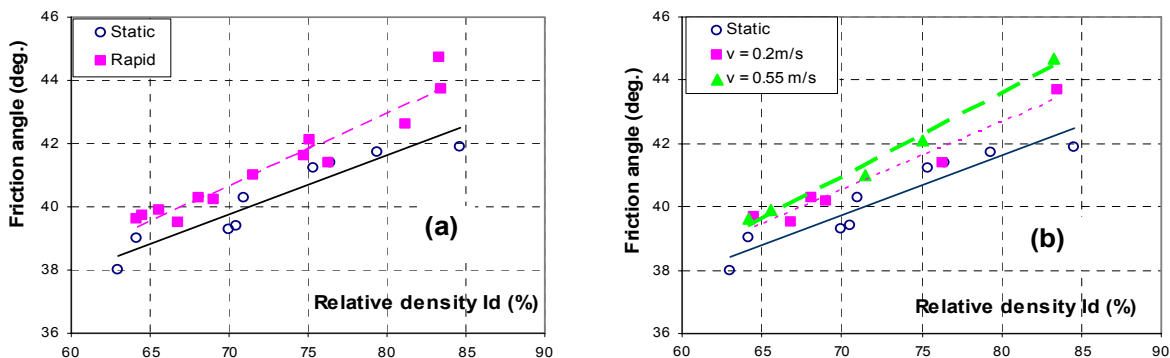


Figure 3.10: Rate effect on internal friction angle of dry sand (a): static vs. rapid; (b): different velocities

Rate effect on stress-strain relationship and excess pore pressure

Figures 3.11 to 3.16 show representative graphs of the stress-strain relationship and measured excess pore pressure-time relationship of tests on dry specimens with virtually identical density but different loading rates. Figures 3.11 and 3.12 present test results from specimens with a relative density of approximately 64% (test No. 3, 5, and 6 – table 3.2). Figures 3.13 and 3.14 present test results from specimens with a relative density of 76% (test No. 2, 7, and 14). Figures 3.15 and 3.16 show test results from a specimen with a relative density of 83% (test No. 10, 11, and 12). Only the rate effect on peak shear strength is clearly seen in these figures; the maximum increase of the peak shear stress is approximately 20% (figure 3.15). In the range of applied strain rate for this test series (0.008%/sec - 400 %/sec), the observed rate effect is very similar to what in the literature shown in figure 2.18; especially the results of Casagrande & Shannon (1948) and Lee et al (1969). The

effect on stiffness is not particularly clear, but the figures seem to suggest that stiffness in the rapid tests is not higher than in the static tests.

A negative excess pore air pressure is observed during the rapid tests. This observation confirms the fact that even air has insufficient time to fully drain during rapid loading, i.e. dry sand behaviour during rapid loading is not in a fully drained condition. These figures (for tests in specimens of virtually identical density) show that excess pore pressure becomes lower as the tests become faster. The negative excess pore air pressure will increase the effective confining stress, thus increase the shear strength. To determine the role of the negative excess pore air pressure, the results presented in figure 3.15 and 3.16, where the maximum increase in peak shear strength of 20% is observed, will be considered. In figure 3.15, the peak shear strength of the rapid tests is reached at the axial strain of approximately 5% (equivalent to the displacement of nearly 7.5 mm). This corresponding to the time of peak shear strength of 0.038sec and 0.013sec for the test with loading velocity of 0.195 m/s and 0.590 m/s, respectively. At this time, the value of excess pore air pressure is less than 4kPa (i.e. less than 4% of the confining pressure). Therefore, the contribution of the negative excess pore air pressure on the increment of the peak shear strength in this case is less than 4%. The role of excess air pore pressure in this case is minor and most of the observed increment in the peak shear strength should be deduced by the increase of friction angle with the increase of loading velocity. This differs from the conclusion from Casagrande & Shannon (1948) and Lee et al (1969) that the excess pore pressure is the main contribution in the total increment of strength.

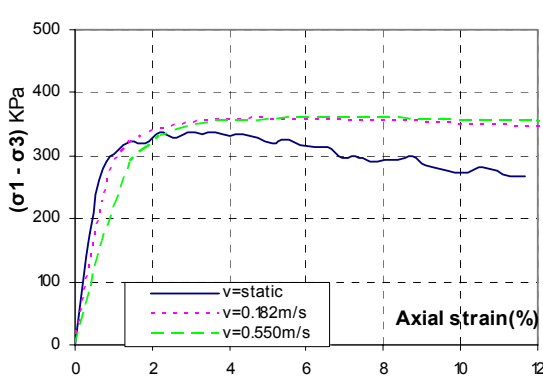


Figure 3.11: Stress-strain relationships at different loading rates ($I_d \approx 64\%$)

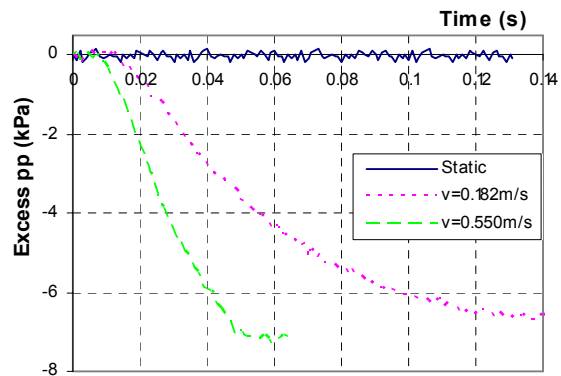


Figure 3.12: Excess pore air pressure-time at different loading rates ($I_d = 64\%$)

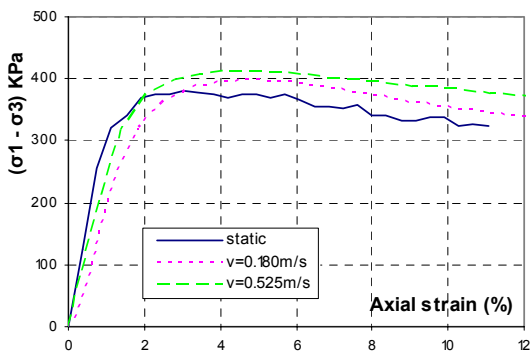


Figure 3.13: Stress-strain relationships at different loading rates ($I_d \approx 76\%$)

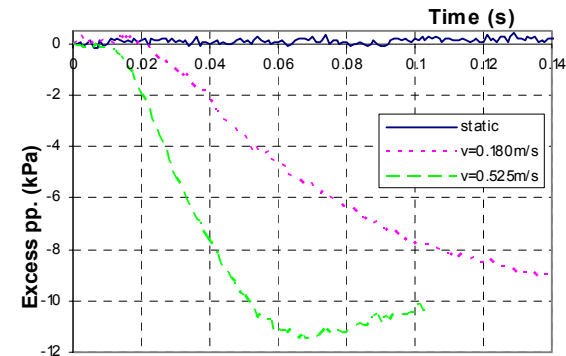


Figure 3.14: Excess pore air pressure-time at different loading rates ($I_d \approx 76\%$)

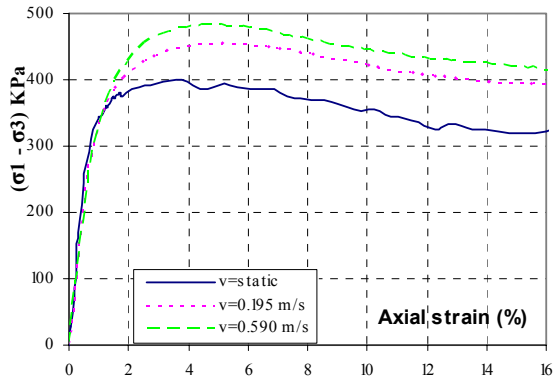


Figure 3.15: Stress-strain relationships at different loading rates ($I_d \approx 83\%$)

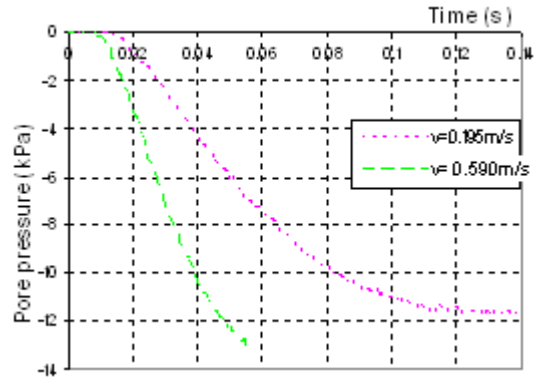


Figure 3.16: Excess pore air pressure-time at different loading rates ($I_d \approx 83\%$)

3.2.7. Rate effects in saturated sand

The stress-strain relationship and pore pressures measured during tests on saturated sand are shown in figures 3.17 to 3.22. The graphs are divided into three groups that correspond to three different densities: 63%, 71%, and 80%. No significant difference is seen between the curves in these figures, so there is therefore no effect on stiffness. Only some increment in the peak deviator stress with increasing loading rate can be seen. Figure 3.23 plots the absolute values of peak stress against the relative density of the specimens. This figure shows that the values of the static tests and tests with a loading rate of 1 mm/sec are virtually the same, and that values of the rapid tests (loading rate higher than 300 mm/sec) are higher than the static values. The increment is approximately 2% at a specimen with the relative density of 63%, and increases as density increases. The increment is approximately 6% at a relative density of 80%. It can therefore be concluded that the rate effect has no influence on the stress-strain relationship of saturated sand, but that it does affect the value of peak strength by up to 6%.

As demonstrated earlier, cavitation of pore water occurred during all tests on saturated specimens. Mcmanus and Davis (1997) noted that the undrained nature of the test changes to a drained condition once cavitation occurs, as inferred by Whitman and Healy (1962). However, the consequences for the test results and/or the sand's rate effect have currently not been clarified. This means that the true effect of the deformation rate on the strength of saturated sand (the rate effect) in this test series may be obscured by cavitation of the pore water.

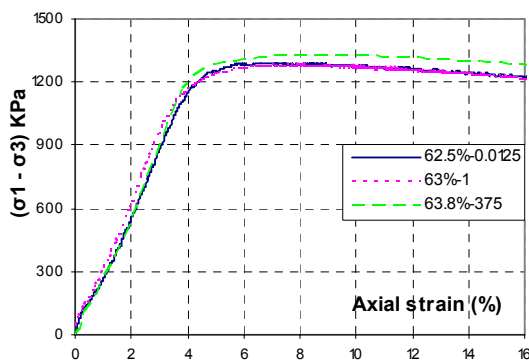


Figure 3.17: Stress-strain relationships at different loading rates ($I_d \approx 63\%$)

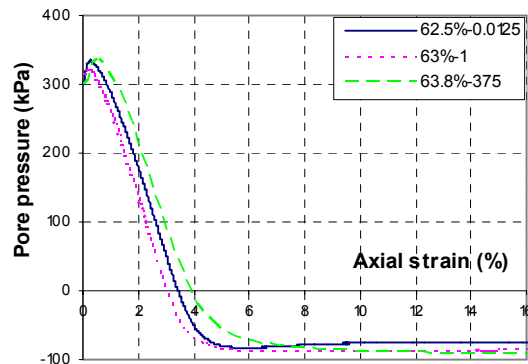


Figure 3.18: Excess pore air pressure-strain at different loading rates ($I_d = 63\%$)

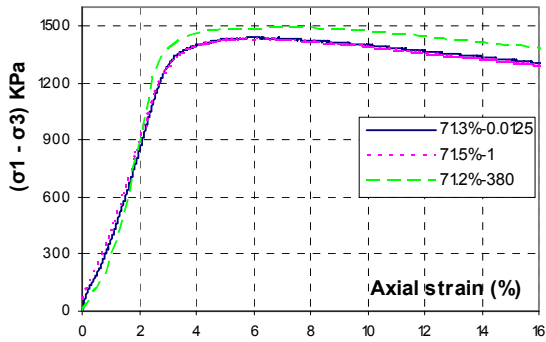


Figure 3.19: Stress-strain relationships at different loading rates ($I_d \approx 71\%$)

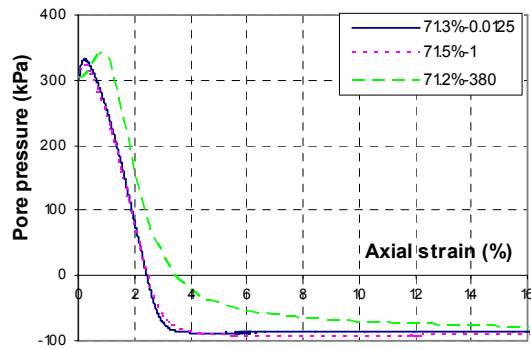


Figure 3.20: Excess pore air pressure-strain at different loading rates ($I_d = 71\%$)

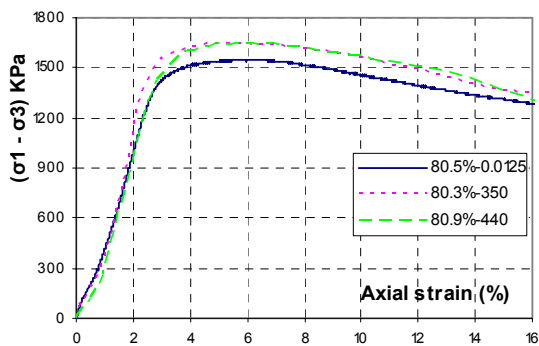


Figure 3.21: Stress-strain relationships at different loading rates ($I_d \approx 80\%$)

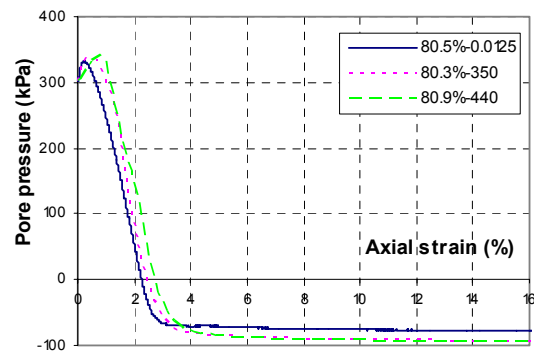


Figure 3.22: Excess pore air pressure-strain at different loading rates ($I_d = 80\%$)

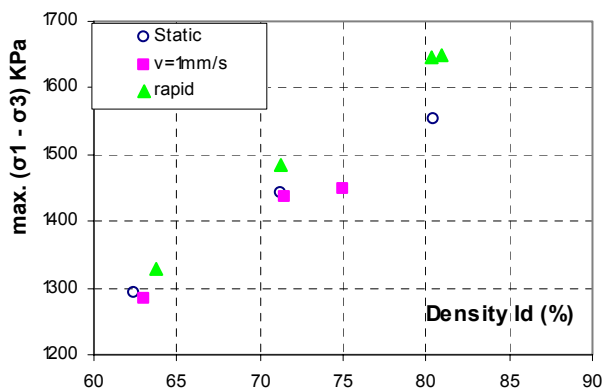


Figure 3.23: Effect of loading rate on peak strength (saturated sand)

3.2.8. Summary

Results from the tests series show the ability of the high speed triaxial test facility to study rate effects on the shear strength of dry and saturated sand. The main results of the test series are summarised below.

For dry sand:

- The loading rate affects the strength of dry sand. At a loading velocity of approximately 0.2 m/sec, the friction angle of dry sand increases one degree over the static value due to the rate

effect. The significance of the rate effect seems to increase with the density of the specimen. The maximum increment in peak shear strength is approximately 20%.

- There is excess pore air pressure during a high rate loading test on dry sand, but the role it plays on the rate effects is small. The excess pore pressure implies that sand behaviour at the high loading rate is not in a fully air-drained condition.

For saturated sand:

- Rate effects on the peak strength of saturated sand are small (approximately 6%), but the true rate effect in saturated sand may be obscured by cavitation of the pore water.
- The loading rate has no influence on the first stage of the stress-strain relationship of the sand, and thus on the stiffness.

3.3 Model pile tests

3.3.1 Introduction

A series of load tests on a model pile founded in a sand bed were carried out to investigate loading rate effects on pile resistance. The tests were performed using a 1-g model test in a calibration chamber at a target scale of 1:10. The sand bed was in a both unsaturated and saturated condition. Two types of loading rate test were performed: a constant rate of penetration test, and a dynamic test. The test set-up and tests in unsaturated sand were carried out by Dijkstra (Dijkstra, 2004). The tests in saturated sand were carried out by Archeewa (Archeewa, 2005). This section briefly describes the test set-up and presents the test results.

3.3.2 Test set-up

An overview of the test set-up and the sand used for the model pile test series is shown in figures 3.24 and 3.25. The loading device shown in figure 3.24 was used for the dynamic load test. The model pile used in this study is a Dutch standard penetration cone (CPT). Details of the set-up are given below.

3.3.2.1 Calibration chamber and sand bed

The calibration chamber

A rigid steel wall calibration chamber was used measuring 1.9 m in diameter and 3.23 m in height. It was equipped with two steel beams on the top to act as a support frame for the loading system. At the bottom, a number of drains were embedded in a filter bed and connected to a pumping system. This system was used to saturate the sand bed from below and to fluidise the sand. Two vibrators were attached to the sides of the chamber (figure 3.24) to increase sand density during draining.

The design of the calibration chamber described here differs from most calibration chambers used worldwide in a number of ways (Broere, 2004). The first and most noticeable difference is the lateral and bottom rigid boundaries. The effect of these boundaries on the test results was minimised by the large chamber-to-cone diameter ratio ($R_d = 56$), and the fact that the top boundary was free. Secondly, the sand bed was not prepared using the commonly-used pluviation method but by a fluidisation and vibration procedure, which leads to less uniform densification of the sand bed. For the purposes of this study, this effect can be minimised by executing different tests (static and dynamic) in the same sand bed preparation and at the same test location i.e. the test conditions are identical. Any difference in the resistance can therefore be seen as the loading rate effect.

The sand bed

The calibration chamber was filled with a sand layer of approximately 1.6 m in height. The sand was coarse river sand with a grain size distribution as shown in figure 3.25. The mean grain size, D_{50} , was 0.27 mm. The maximum and minimum densities were 1.788 Mg/m^3 and 1.467 Mg/m^3 .

The sand bed was prepared using fluidisation and vibration procedures. The sand bed was first saturated and fluidised with an upwards water flow created by the pumping system from the bottom of the chamber to the sand surface. This redistributed the sand grains to a loose state, and a sufficiently homogeneous sand sample was expected after 1.5 hours of fluidisation. After fluidisation, the chamber was vibrated using two vibrators. At the same time, the water was drained to obtain greater compaction. The vibration time was usually between 5 minutes and 20 minutes. After the period of vibration, the remaining water was drained to create an unsaturated sand bed condition or a partially saturated sand bed condition.

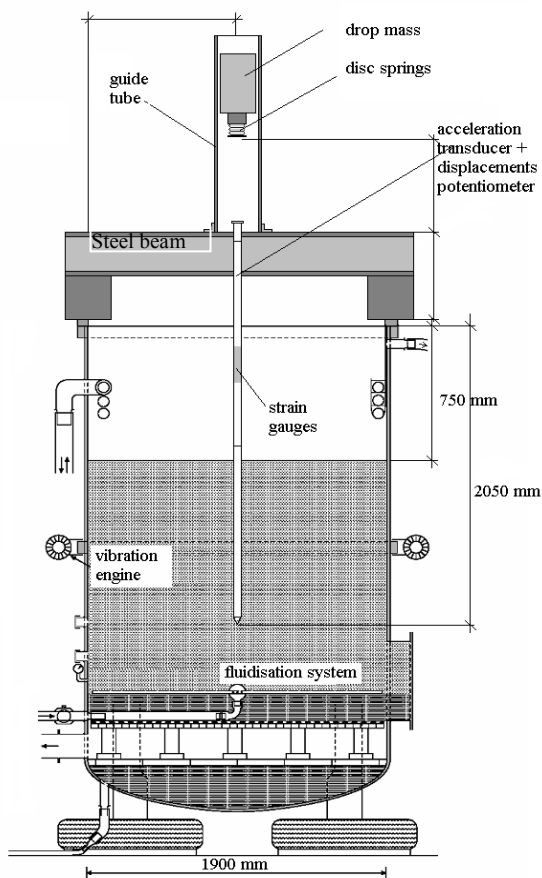
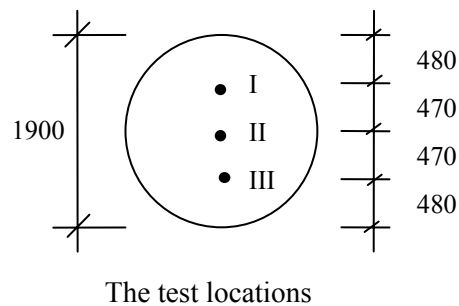


Figure 3.24: Sketch of test set-up



The test locations

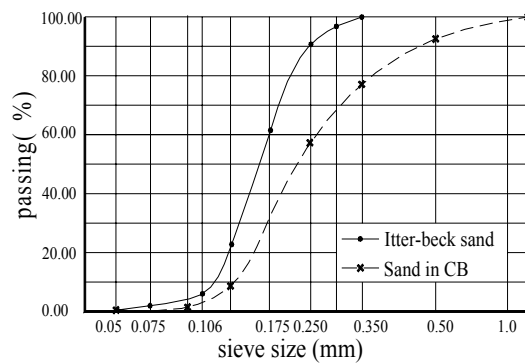


Figure 3.25: Grain size distribution of the sand

3.3.2.2 Model pile

The model pile used for the test series in unsaturated sand was a Dutch standard penetration cone (CPT), and a piezometer cone (CPTu) was used for the test series in saturated sand. The cone measured 36 mm in diameter, the point surface was 10 cm^2 , and the friction sleeve area was 150 cm^2 . The total length including the rods was 2.65 m, of which 1.3 m was embedded in the sand. The rod above the sand bed surface was equipped with strain gauges, an acceleration transducer, and a displacement sensor (linear stroke potentiometer). In the case of the piezometer cone, the pore pressure sensor was located between the tip and friction sleeve.

3.3.2.3 Load test methods and loading systems

Load test methods

The objectives of this study are to determine the effect of loading rate on either the bearing capacity of a pile or the response of pore water pressure near the pile toe. The tests therefore had to be performed using different loading rates on the model pile, where the soil condition remained the same. The same preparation procedure was used in order to achieve the same soil condition, i.e. identical periods of fluidisation and vibration, as well as the same test location. Three different loading rate tests were employed: the CPT test, the static test, and the rapid test.

- The CPT test involved installing the cone (the model pile) into the sand bed. The penetration rate of the pile was kept constant at 20 mm/s, which is the standard rate of the CPT test in the Netherlands. Resistance was recorded during the last 160 mm of penetration.
- The static test was performed in the same manner as the CPT test, but the target rate of penetration was 1 mm/s. Since the test was manually operated, the actual velocity was slightly slower or faster. The maximum displacement was approximately 20 mm in the static test, which is more than 50% of the model pile diameter.
- The pseudo-static test in this study was performed by dropping a heavy mass from a certain height onto the model pile head. A series of steel disc springs were installed between the drop mass and pile head to extend the duration of the blow. The number of disc springs was pre-determined to create a loading pulse on the model pile head that lasted approximately 22 ms. This can be considered similar to the Statnamic loading in the current model scale.

The loading systems

Two loading systems were used in this test series: a constant loading rate apparatus, and a dynamic loading apparatus. The constant loading rate system was a hydraulic rig (figure 3.26). It was used to install the model pile into the sand bed at a constant rate of 20 mm/s (the CPT test), and to perform the static tests at a constant velocity of 1 mm/s. The dynamic loading apparatus (shown in figure 3.27) was used to perform the rapid test. It comprised a 64 kg steel drop mass, and an aluminium guidance tube to guide the drop mass hits to the pile head. A series of disk springs were attached to the drop mass to lengthen the loading duration.



Figure 3.26: The constant loading rate apparatus



Figure 3.27: The dynamic loading devices

3.3.2.4 Measurement devices

The following parameters were measured during the test series: the point resistance and sleeve resistance of the cone, the applied force on the pile head, and the displacement and acceleration of the pile head. Pore water pressure was also measured during tests in saturated sand. These parameters were measured using the following devices:

- Built-in cone sensors of the cone measured the point and sleeve resistance, and pore water pressure.
- A strain gauge attached to the pile head measured the applied force on the pile head. It was used in both the static tests and rapid tests.
- An acceleration transducer installed on a mounting steel plate near the pile head measured the pile head acceleration. It was used in the rapid tests only.
- A displacement gauge (linear stroke potentiometer) measured the pile head displacement. Its stand-base was mounted on the steel beam, which was considered as a fixed boundary. The measuring pinpoint was placed on the mounting steel plate, where the acceleration transducer was installed. The displacement gauge was used in some static tests and in all pseudo-static tests. The stroke of displacement transducer was limited (only displacements up to 20 mm were measured).

3.3.2.5 Notes on the model scale

In this study, a prototype Statnamic pile load test was performed at a model scale of 1:10 under 1-g condition. This test is referred to here as the rapid test. The scaling factors were chosen in such a way that there was similarity between the behaviour of the model pile load test and the prototype Statnamic pile load test. It was thought that three aspects, might significantly affect the results of this model test series, and these are noted below.

The first aspect is the wave propagation phenomena in the model pile, which is characterised by the value of relative loading duration t_r (Middendorp et al, 1995). According to the classification presented in chapter 2, a pile is considered to be rapid loaded if the relative loading duration is larger than 10. In this model, the length of pile was 2.65m and the wave velocity in the model pile (steel rod) was approximately 5200 m/s. Therefore, the required loading duration will be:

$$T \geq 10 * \frac{2 * L}{c} \approx 0.010s$$

This requirement was met in both theoretical and practical terms by attaching a number of disk springs to the bottom of the drop mass (Dijkstra, 2004). The actual loading durations measured during the model rapid load tests ranged between 0.013 s and 0.024 s.

In comparison to the typical loading duration of the prototype rapid load test (from 0.1 s to 0.22 s),

the time scale parameter can be derived for this test as $n_t = \frac{t_p}{t_m} = 10$ (subscript m stands for model;

p for prototype). This is chosen as the basic scaling parameter ($N = 10$) to determine other quantities as shown in Dijkstra (2004).

The second aspect involves excess pore pressure during the model rapid test in saturated sand. If it is assumed that the sand and fluid in the prototype are the same as those used in this experiment, the consolidation time in the model will be N^2 times faster than that in the prototype as the dimension is scaled down N times. This conflicts with the loading duration time-scale presented in the previous paragraph. To unify the loading duration time-scale and the consolidation, the permeability of the prototype should be 10 times higher than the sand in this study. This means that

the model rapid test in this study can be seen as modelling a prototype Statnamic test in sand, with a permeability that is 10 times higher than that of the sand used in this experiment.

The third aspect to be considered relates to the soil stress state of the chamber. This is known to be a severe restriction of model pile tests under 1-g condition, where the stresses in the soil model are scaled down with the same magnitude as the dimensions. This means that the soil stress state in the model is N times lower than in the prototype. The soil behaviour in the model is not similar to that in the prototype because of the strong dependency of soil behaviour on the stress state. Therefore, the results of this model test series can only be guaranteed as quantitatively valid in this test condition.

3.3.3 Test results

This section presents the test results in unsaturated and saturated sand. Representative values of the measurement quantities during the load tests are first reviewed. How to determine pile resistance from these measurements is also discussed. The overall results are then summarised for a later evaluation of the loading rate effects.

3.3.3.1 Tests in unsaturated sand

A total of eight test beds were prepared. The sand bed was prepared in the same way for each time. The fluidisation period was 1.5 hours, and the vibration period was 10 minutes. Three different loading rate tests were applied in each time. The test sequence was as follows: (1) the CPT test (CPT); (2) the static test 1 (STA1); (3) the rapid test (PS); and (4) the static test 2 (STA2). The two static tests (STA1 and STA2) were performed before and after the pseudo-static test to examine the possibility of changes in soil resistance caused by the rapid test. Figures 3.28 to 3.37 show representative results from the tests.

The CPT tests

In the CPT test, the cone tip resistance and local sleeve friction were recorded in the last 20 cm of the penetration. The measurements as functions of time are shown in figures 3.28 and 3.29. It can be seen that resistance increased as the pile penetrated. Some of the large increase in gradient may be caused by the change in soil density with depth. The CPT test stopped at point A, and the shift from loading phase to unloading phase caused a sudden change in pile resistance. Relaxation in the soil under the pile tip when the pile stopped moving downwards would cause a sudden decrease of the measured point resistance values. Because of the force maintained on the pile head, the pile shaft friction would increase, resulting in an increase in measured sleeve friction values.

Figure 3.29 shows two types of plot of measured sleeve friction (type I and type II). In type I, the plot is similar to that for an ordinary CPT test i.e. sleeve friction increases directly to a certain value at the test start due to the existence of soil friction at that depth, and gradually increases to the final value (point A). This can be seen in most of the tests, but the type II plot is seen in some cases. Unlike the measurement in an ordinary CPT test, the sleeve friction in type II is an almost linear increase to the final value. The reason for this different behaviour is currently not clear.

Since these measurements are the mobilised soil resistance against the penetration of the cone at that depth, the values at point A are considered as the unit tip resistance and sleeve friction of the model pile during the CPT test. For the case shown in figure 3.28 and figure 3.29 (type II), the unit tip resistance is 10.5 MPa and the unit shaft friction is 0.05 MPa.

The pile resistance of the eight CPT tests is summarised in table 3.4.

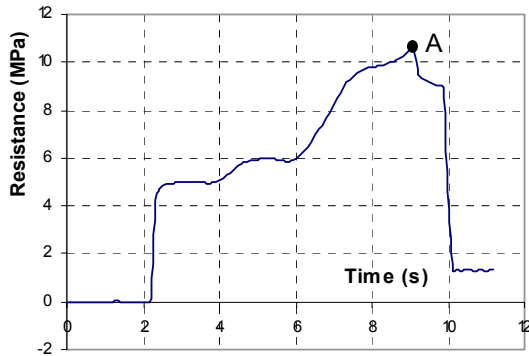


Figure 3.28: The measured point resistance in a CPT test

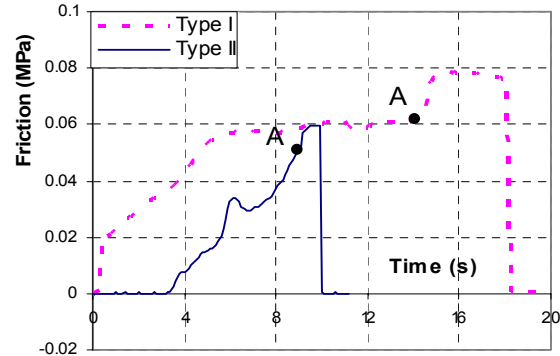


Figure 3.29: The measured sleeve friction in a CPT test

The static tests

An example of measurements made during the static load tests STA1 and STA2 as a function of time are shown in figures 3.30 to 3.33. The results from STA2 show a strange behaviour, which can be attributed to an interruption during the test. After the first increment of loading, the loading device stopped in nearly two seconds by unknown reason and then continued again. As a result, the pile displacement increased slightly and remained constant nearly two seconds at the start of the test (figure 3.33), and there was a constant value in the measured pile head force and point resistance value. The following points will be discussed based on these measurements: the actual penetration rate of the model pile, the quality of measured pile head force, the value of point resistance and sleeve friction, and a comparison between the results from STA1 and STA2.

From the measured pile head displacement in figure 3.33, it can determine the pile penetration rate during the static test was approximately 3.5 mm/s. This rate was faster than the desired rate (1 mm/s). This was because the loading device was operated manually, which meant that the rate could not be controlled precisely. The pile head displacement was measured in some static tests (tests 6, 7, and 8, as shown in table 3.4).

The pile head force measured by the strain gage is shown in figure 3.32. When considering the static equilibrium of the model pile, the pile head force must be equal to the sum of the point resistance and sleeve friction forces (total soil resistance). In this model, the point resistance force is calculated as:

$$F_{\text{point}} = q_c \cdot A_{\text{point}} = q_c \cdot \pi \cdot r^2 = q_c \cdot 0.001 \text{ (kN)}$$

The sleeve friction force is calculated by assuming that the uniform distribution of the measured sleeve friction along the pile shaft (the upper limit of the shaft friction) is:

$$F_{\text{sleeve}} = f_s \cdot C_{\text{sleeve}} = f_s \cdot 1.3 \cdot \pi \cdot 2 \cdot r = f_s \cdot 0.147 \text{ (kN)}$$

Where q_c and f_s are measured point resistance and sleeve friction; A_{point} and C_{sleeve} and r are the area of the toe, total surface area of the embedded shaft, and the radius of the model pile respectively. It follows that total soil resistance (F_{soilmax}) is:

$$F_{\text{soilmax}} = F_{\text{point}} + F_{\text{sleeve}}$$

The calculated soil resistance and measured pile head force are compared in figure 3.34. The measured pile head force is some 5 kN (~30%) larger than the maximum total soil resistance, and

this discrepancy is virtually the same in other tests. Since the cone sensors were calibrated regularly but the strain gauge was only calibrated once before it was first used, the cause is probably the strain gauge. According to Dijkstra (2004), the reason may be an installation problem, a data conversion factor, or some other factor. The point resistance and sleeve friction will therefore be used to represent pile resistance in a later evaluation of the loading rate effect.

The variation of point resistance and sleeve friction with time during a static test (as shown in figures 3.30 and 3.31) are very similar to those in the CPT tests. The point where the pile changes from the loading phase to the unloading phase (point A) is also seen. As in the CPT test, the values of point resistance and sleeve friction at point A are considered as maximum soil resistance during the static test and are taken as static resistance of the model pile. The first peak value of sleeve friction in figure 3.31 is only seen in the test series in unsaturated sand, but not in the test series in saturated sand. It is therefore seen here as the dry friction effect (not the intrinsic soil-pile friction), and will not be considered in an evaluation of the rate effect. The results of static tests are summarised in table 3.4.

When considering the possibility of a change in soil condition due to the pseudo-static test, the results from static test 1 (STA1) and static test 2 (STA2) are compared. There is little difference between the two measurements. Statistical analysis of the measured values in all the static tests confirms that the results are the same with 95% of confidence limit values (Dijkstra, 2004). It can therefore be concluded that the soil condition has not been changed by the rapid load test. The values of the static test 1 (STA1) are used as a representative value for the static pile resistance when evaluating the rate effect.

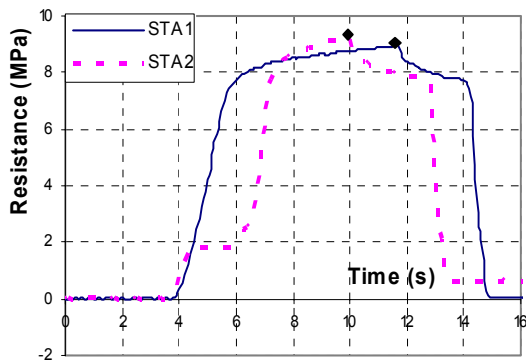


Figure 3.30: The measured point resistance in a static load test

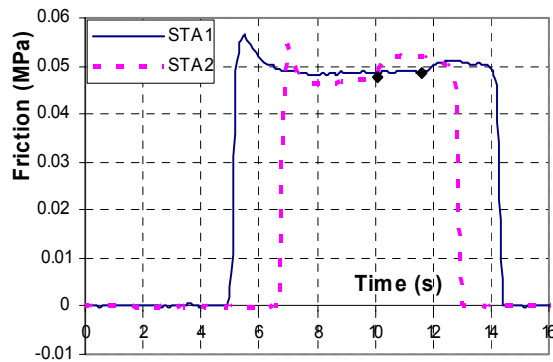


Figure 3.31: The measured sleeve friction in a static load test

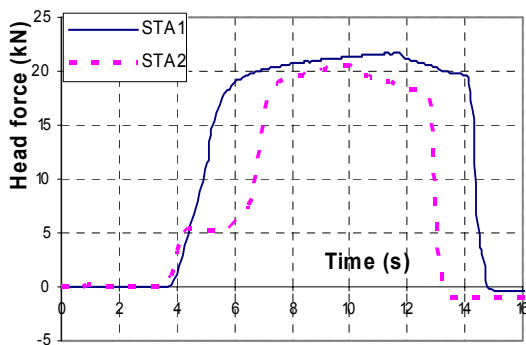


Figure 3.32: The measured pile head force in a static load test

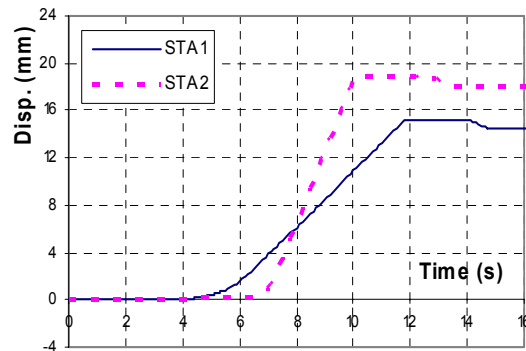


Figure 3.33: The measured pile head displacement in a static load test.

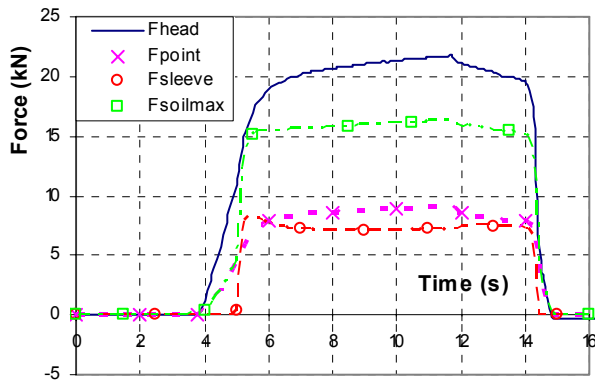


Figure 3.34: Comparison of the measured head force and total soil resistance in a static load test.

Table 3.4: Summarised results from CPT and static load tests in unsaturated sand

Test No		1	2	3	4	5	6	7	8
Date (dd-mm-2004)		20-7	27-7	17-8	19-8	19-8	8-9	8-9	10-9
Location		ii	i	i	i	ii	i	ii	iii
CPT	Point (MPa)	14.73	N/A	16	13.38	14.24	11.17	10.6	14.69
	Sleeve (MPa)	0.064	N/A	0.064	0.021	0.054	0.043	0.051	0.068
STA1	Head (kN)	23.26	28.21	29.6	25.05	26.53	22.8	20.6	27.57
	Point (MPa)	10.6	11.77	13.12	11.25	12	9.56	9.25	12.44
	Sleeve A (MPa)	0.067	0.072	0.055	0.031	0.055	0.042	0.047	0.069
	u (mm)	N/A	N/A	N/A	N/A	N/A	12.7	18.25	N/A
	v (mm/s)	N/A	N/A	N/A	N/A	N/A	0.81	2.44	N/A
STA2	Head (kN)	20	27.52	27.3	23.13	25	22.77	21.8	26.78
	Point (MPa)	9.8	11.02	12.89	10.5	11.88	9.59	9	12.4
	Sleeve A (MPa)	0.064	0.07	0.05	0.045	0.055	0.043	0.049	0.066
	u (mm)	N/A	N/A	N/A	N/A	N/A	18.18	15.14	17.92
	v (mm/s)	N/A	N/A	N/A	N/A	N/A	4.23	2.36	3.5
Notes:									
<ul style="list-style-type: none"> - "location" : position of the model pile in calibration chamber (see figure 3.22) - "point" : measured point resistance (MPa) - "sleeve A" : measured sleeve friction at point A (MPa) - "head" : measured force at pile head (kN) - "u" : measured maximum pile head displacement (mm) - "v" : average pile head velocity (mm/s) - N/A : not available 									

The rapid load tests

The typical measured pile head displacement and acceleration during a rapid load test are plotted in figures 3.35 and 3.36. It is thought that the extreme peak value in the acceleration signal at the start of the test was caused by the effect of metal-to-metal impact when the drop mass hit the pile head. The pile head velocity shown in figure 3.37 is integrated with the measured acceleration, and differentiated from the measured displacement. The pile head velocities derived from the

displacement and acceleration are in relative agreement until pile head displacement rebounds. After that point, the value of pile head velocity derived from the acceleration signals indicates an impossible motion, i.e. the pile moves continuously with constant velocity. This is due to the fact that signals from the acceleration transducer are not properly filtered causing a big noise at the starting of the test; thus causing a drift in the calculated velocity. For later evaluation of the rate effect, the pile head velocity should therefore be derived by differentiating the measured displacement.

Figure 3.38 presents the typical pile head force measured by the strain gauge. It can be seen that the loading duration was approximately 17 ms. However, results from the static test have shown that the strain gauge measurements may not be correct, and they will therefore not be considered further.

Figures 3.39 and 3.40 show the measured tip resistance and sleeve friction of the cone during a rapid test. These measurements directly indicate the reaction force of soil against penetration of the cone during the test. The maximum values are seen as the bearing resistance of the model pile. The maximum tip resistance value is clearly seen in figure 3.39, and can be taken as straightforward. In the case of sleeve friction, however, the substantial noise in the measured signal means that the average value indicated in figure 3.40 will be taken as the maximum shaft resistance. The results from the eight rapid tests are summarised in table 3.5.

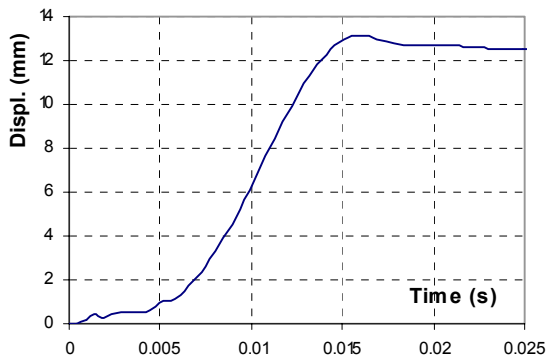


Figure 3.35: The measured pile head displacement in a rapid load test

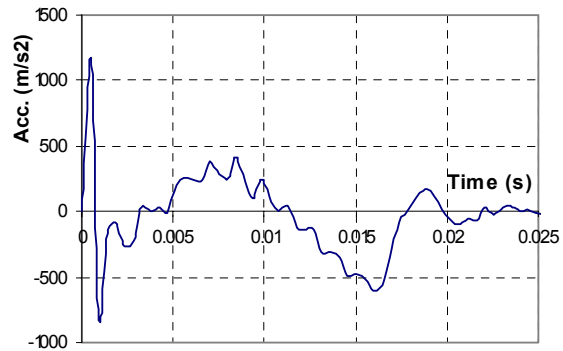


Figure 3.36: The measured pile head acceleration in a rapid load test

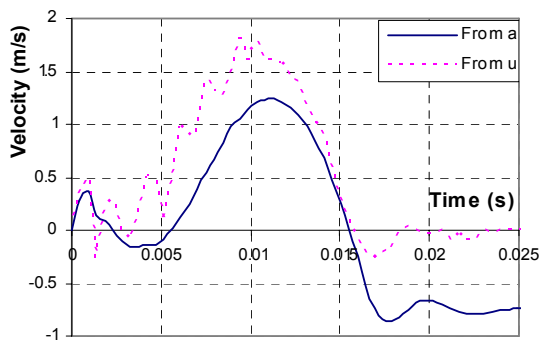


Figure 3.37: Calculated pile head velocity in a rapid load test

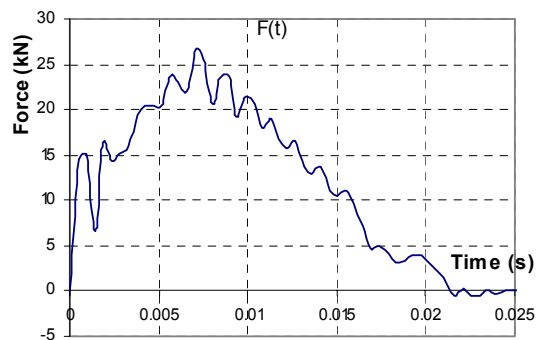


Figure 3.38: The measured pile head force in a rapid load test

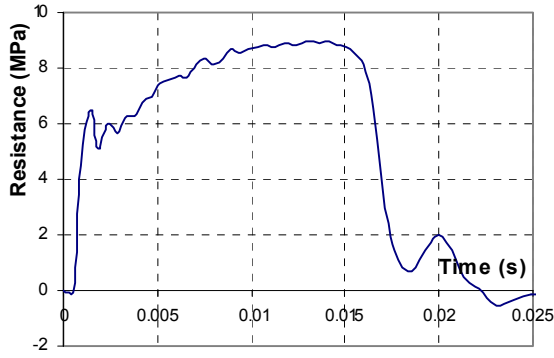


Figure 3.39: The measured pile tip resistance in a rapid load test.

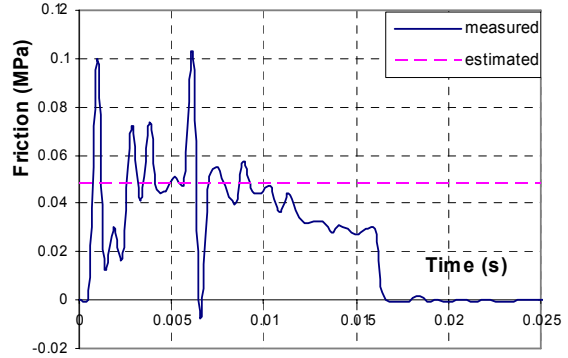


Figure 3.40: The measured and estimated average sleeve friction in a rapid load test.

Table 3.5: Summarised results of pseudo-static load tests in unsaturated sand

Test No	1	2	3	4	5	6	7	8
Date (dd-mm-2004)	20-7	27-7	17-8	19-8	19-8	8-9	8-9	10-9
Location	ii	i	i	i	ii	i	ii	iii
# disc springs	1	1	6	6	5	5	5	6
Drop height (cm)	18.5	20.9	29.9	30	32.5	29.3	32	27.5
u (mm)	5.4	3.5	>5.9	>3	6.5	>6	13	>9
Pulse width (ms)	13	14	23.5	23	22	21	22	22.5
v (m/s)	1.5	1*	0.7*	>0.4*	1.25	1.1*	1.6	2.2*
Point (MPa)	11.84	12.37	11.17	10.22	11.84	8.7	9	11.39
Sleeve (MPa)	0.068	0.065	0.057	0.03	0.057	0.052	0.050	0.074
Notes:								
<ul style="list-style-type: none"> - The maximum pile head displacement is not measured in tests 3, 6, and 8: the transducer exceeded its limit. - Measurement of displacement failed in test 4: the value is estimated. - "*" : the value is estimated 								

3.3.3.2 Tests in saturated sand

A total of eight tests were performed in a saturated sand bed. The test sequence was the same as in the unsaturated case, i.e. CPT – STA1 – PS – STA2. All tests were performed at the central point of the calibration chamber (location i). Preparation of the saturated sand bed involved a 1.5 hour-period of fluidisation and 5 minutes of vibration. Measurements include the value of pore water pressure near the pile toe. Typical results from tests in the saturated sand bed are presented in this section, in figures 3.41 to 3.48.

The CPT tests

In the CPT tests, cone resistance was recorded in the last 40 cm of penetration. The tip resistance and sleeve friction measurements shown in figures 3.41 and 3.42 are similar to those of the CPT test in unsaturated sand (figures 3.28 and 3.29). The measured excess pore water pressure is shown in figure 3.43. The magnitude of excess pore pressure is much smaller than the value of tip resistance.

The values at point A are taken as the pile resistance, as in the CPT test in unsaturated sand. A summary of the results is presented in table 3.6.

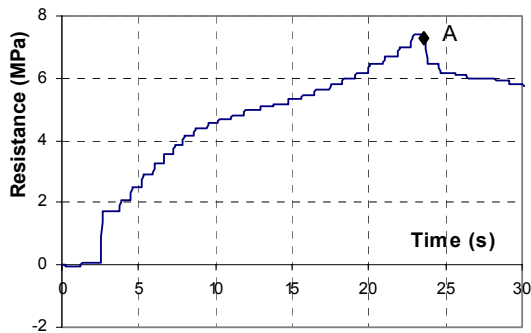


Figure 3.41: The measured tip resistance in a CPT test

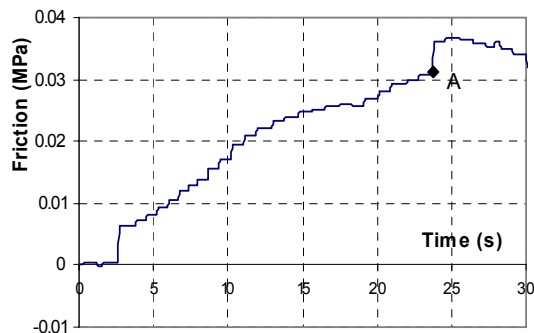


Figure 3.42: The measured sleeve friction in a CPT test

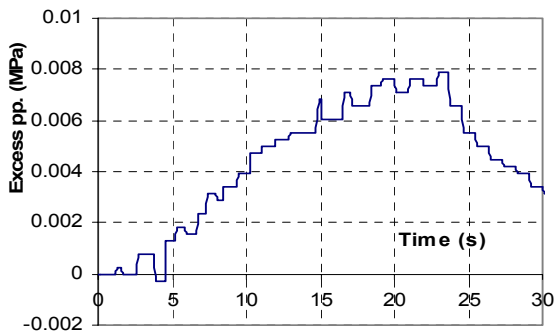


Figure 3.43: The measured excess pore pressure in a CPT test

The static tests

Typical measurements taken during a static test in saturated sand are presented in figures 3.44 to 3.48. The measured resistance as a function of time in this case was similar to that in the unsaturated case. The actual penetration rate during the test was somewhat slower than the desired value. The actual rates shown in figure 3.47 are 0.5 mm/s and 0.44 mm/s in the STA1 and STA respectively. Results from other static tests show nearly the same value (Table 3.6).

Figure 3.48 presents the excess pore pressure measured during the test. The value of the excess pore pressure measured during the static test was very small compared to cone resistance. At the beginning of the test, the pore pressure sharply increased due to the high rate of loading used to initiate pile movement. When the pile penetrated steadily, the loading rate slowed down, and pore pressure decreased to remain at an almost constant value.

Results from these static tests are summarised in table 3.6, in which sleeve friction is taken at point A (as in the static tests in unsaturated sand). The point resistance is taken at the moment that displacement equals the maximum displacement of the correlated pseudo-static test. It aims to be able to make the comparison of mobilised point resistance in these two tests at the same displacement.

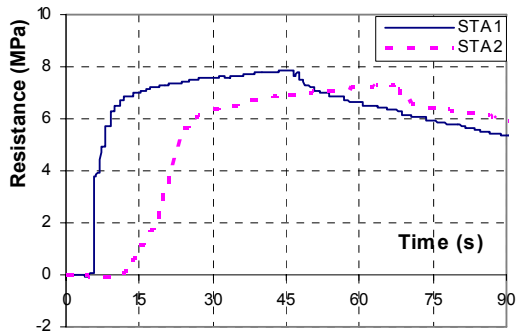


Figure 3.44: The measured point resistance in a static load test

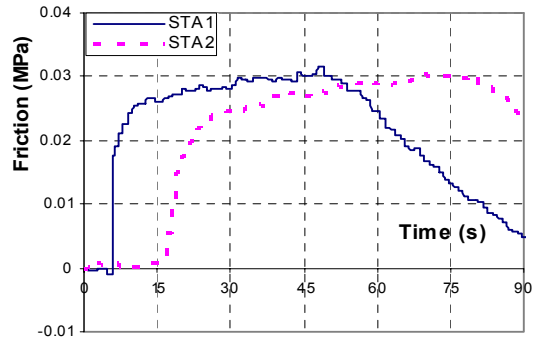


Figure 3.45: The measured sleeve friction in a static load test

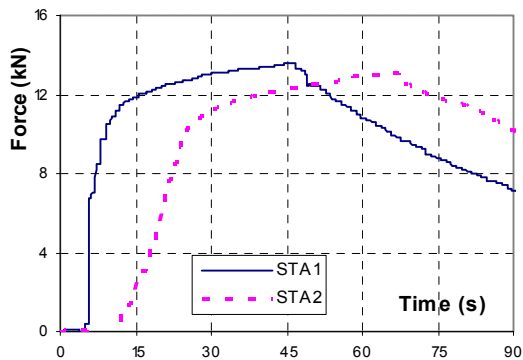


Figure 3.46: The measured pile head force in a static load test

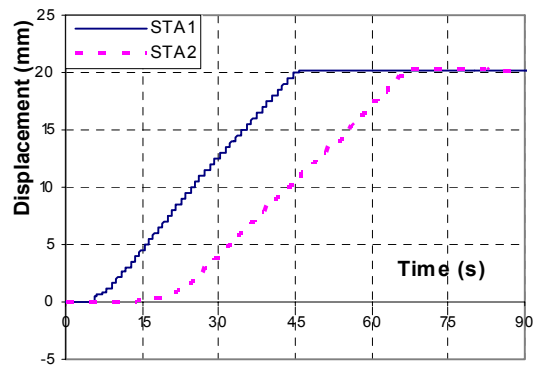


Figure 3.47: The measured pile head displacement in a static load test

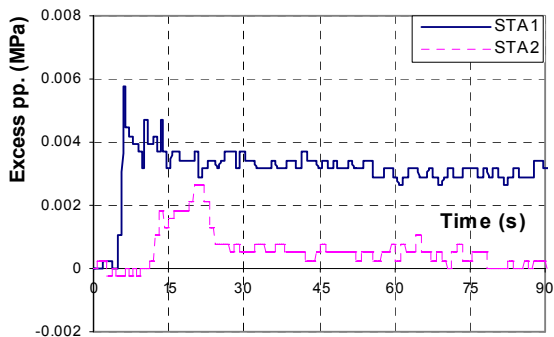


Figure 3.48: The measured excess pore pressure in a static load test

The rapid tests

Measurements taken during a rapid load test in saturated sand are shown in figures 3.49 to 3.53. The pile head velocity was derived from the pile head displacement, and is shown in figure 3.54. The general behaviour of the pile during the rapid test was similar to the case in unsaturated sand and will not be repeated here. Results from the eight rapid load tests are summarised in table 3.7. This section only discusses the excess pore pressure measurements.

In figure 3.53, the measured excess pore pressure and the calculated pile head velocity are plotted as a function of time. It can be seen that the tendency of excess pore pressure is directly related to the pile head velocity during the test's loading period. This implies that the magnitude of excess pore pressure depends on the velocity of the pile.

Table 3.6: Summarised results from CPT and static load tests in saturated sand

Test No		1	2	3	4	5	6	7	8
Date (dd-mm-2005)		20-1	21-1	24-1	25-1	26-1	27-1	4-2	7-2
Location		i	i	i	i	i	i	i	i
CPT	Point (MPa)	5.4	7.36	10	6.2	8.7	7.4	7.6	8.3
	Sleeve (MPa)	0.023	0.032	0.039	0.025	0.036	0.031	0.032	0.038
	Excess pp (MPa)	0.004	0.005	0.005	0.004	0.007	0.007	0.007	0.006
STA1	Head (kN)	11.2	14.4	18.3	13.6	15.9	13.3	15.9	14.4
	Point (MPa)	5.3	7	10	7.1	8.4	7.5	8.1	7.3
	Sleeve A (MPa)	0.028	0.031	0.038	0.03	0.037	0.03	0.035	0.039
	Excess pp (MPa)	0.003	0.004	0.004	0.003	0.004	0.004	0.003	0.004
	u (mm)	18	18	21.2	20.4	N/A	20	19.5	23
	v (mm/s)	0.5	0.5	0.8	0.5	N/A	0.5	0.45	0.5
STA2	Head (kN)	11.6	N/A	18	14	15.9	12.71	15.9	14.8
	Point (MPa)	5.6	N/A	10	7.7	9	7.3	8.1	7.7
	Sleeve A (MPa)	0.03	N/A	N/A	0.03	0.036	0.03	0.035	0.037
	Excess pp (MPa)	0.003	N/A	0.002	0.003	0.003	0.001	0.002	0.003
	u (mm)	20	N/A	18.5	N/A	19.69	18.18	21	15
	v (mm/s)	0.4	N/A	0.9	N/A	0.5	0.44	0.5	0.48
Note:									
<ul style="list-style-type: none"> - “location” : position of the model pile in calibration chamber (see figure 3) - “point” : measured point resistance (MPa) - “sleeve A” : measured residual sleeve friction (MPa) - “head” : measured force at pile head (kN) - “u” : measured maximum pile head displacement (mm) - “v” : average pile head velocity (mm/s) - N/A : not available 									

Table 3.7: Summarised results of rapid load tests in saturated sand

Test No	1	2	3	4	5	6	7	8
Date (dd-mm-2004)	20-1	21-1	24-1	25-1	26-1	27-1	4-2	7-2
Drop height (cm)	15	15	15	15	15	15	15	15.0
u (mm)	10.7	10.7	8.5	N/A	10.1	11.1	9.4	5.0
Pulse width (ms)	18	20	18	18	18	20	20	25
v (m/s)	1.7	1.5	1.3	N/A	1.6	1.6	1.8	0.8
Point (MPa)	6.8	7.6	10.0	7.8	8.7	8.0	8.0	7.8
Sleeve (MPa)	0.030	0.035	0.040	0.035	0.035	0.031	0.036	0.028
Excess pp (MPa)	0.030	0.050	0.020	0.028	0.024	0.022	0.023	0.015
Note: x – data missing ; N/A – not available								
Hydro static value is approximately 10 kPa								

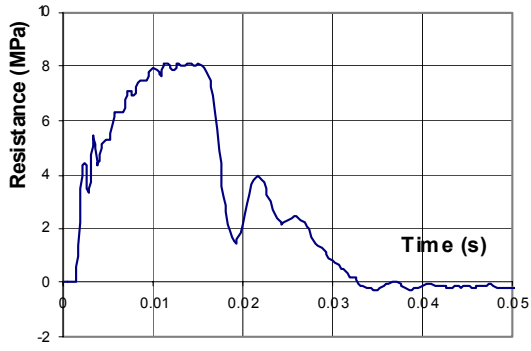


Figure 3.49: The measured tip resistance in a rapid load test

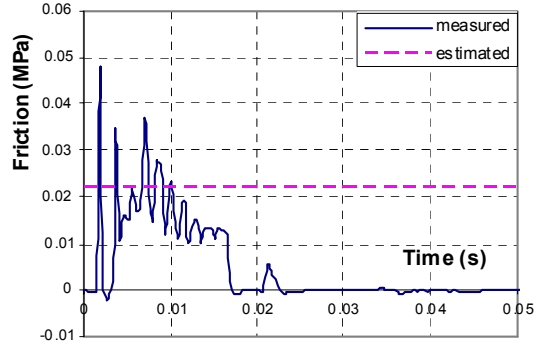


Figure 3.50: The measured sleeve friction in a rapid load test

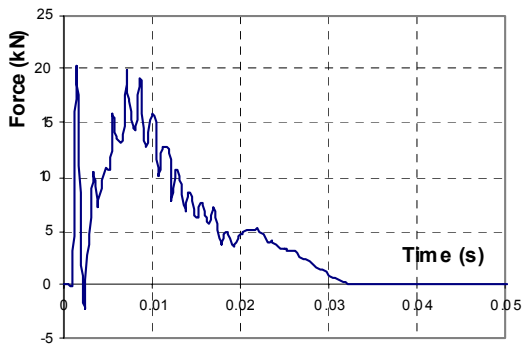


Figure 3.51: The measured pile head force in a static load test

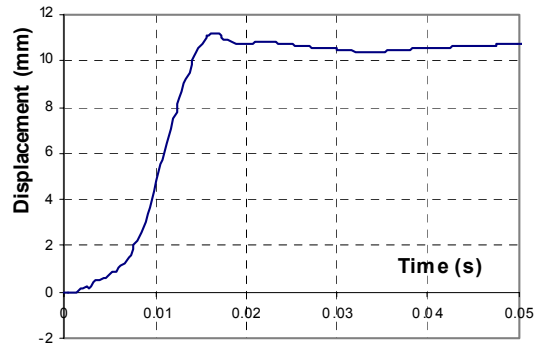


Figure 3.52: The measured pile head displacement in a static load test

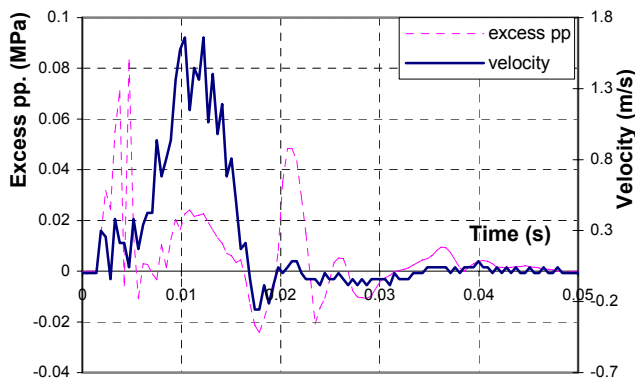


Figure 3.53: Pile velocity and excess pore pressure during a rapid load test

3.3.4 Evaluation of the rate effects

The previous sections have presented the results of different load tests on the model pile. Pile resistance in these tests has been derived in terms of the unit pile tip resistance and sleeve friction. This section evaluates the loading rate effect on the resistance of the model pile. Because the three different loading rate tests were performed using the same sand bed preparation, the test conditions are considered to be identical. An evaluation of the loading rate effect can therefore be based on a direct comparison of the derived resistance in these load tests. The effect on tip resistance and sleeve friction of the model pile will be examined separately.

3.3.4.1 Rate effect in unsaturated sand

Effect on ultimate resistance

To evaluate the loading rate effect on the ultimate resistance of the model pile, the resistance values derived from the CPT test and the rapid test (RP) are compared with that from the static test (STA). The derived resistance values are summarised in tables 3.4 and 3.5. In table 3.8, four ratios between these values are calculated: the ratio R_1 between the tip resistance in the CPT test (R_{t-CPT}) and that in the static test (R_{t-STA}); the ratio R_2 between the tip resistance in the rapid test (R_{t-RP}) and that in the static test (R_{t-STA}); the ratio R_3 between the sleeve resistance in the rapid test (R_{s-RP}) and that in the static test (R_{s-STA}); and the ratio R_4 between the sleeve resistance in the rapid test (R_{s-RP}) and that in the static test (R_{s-STA}).

$$R_1 = \frac{R_{t-CPT}}{R_{t-STA}}; R_2 = \frac{R_{t-RP}}{R_{t-STA}}; R_3 = \frac{R_{s-CPT}}{R_{s-STA}}; R_4 = \frac{R_{s-RP}}{R_{s-STA}}$$

The data in table 3.8 are plotted against the pile head velocity in figures 3.54 and 3.55. The pile head velocity (V) is normalised using a reference velocity $V_0 = 1$ mm/s.

In the case of sleeve friction, figure 3.54 shows no rate effect. Statistical calculation indicates a mean value for R_3 of 0.98 with a standard deviation of 0.13, and a mean value for R_4 of 1.04 with a standard deviation of 0.09. The difference is insignificant. The measured sleeve friction during a static test is equal to the sleeve friction measured during a CPT test and a rapid test, i.e. the loading rate does not affect the sleeve friction of the model pile in unsaturated sand.

Different rate effects are observed in the case of point resistance (figure 3.56). The point resistance in the CPT tests is higher than that of the static tests. The mean value of the point resistance ratio R_1 is 1.21 with a standard deviation of 0.07, i.e. the difference is significant. However, point resistance in the rapid tests and the static test is virtually the same. The mean value of the point resistance ratio R_2 is 0.96 with a standard deviation of 0.08. A statistical check using a student t-test with null hypothesis of equality resistance in 95% of confidence was performed to check the difference. The results are shown in table 3.9, and it can be seen that the difference in point resistance between the CPT tests and the static tests is confirmed. It seems that the loading rate does affect a pile's point resistance in unsaturated sand at a certain medium rate (~ 20 mm/s), and disappears at a high rate (> 400 m/s). This is an unexpected result and will be further discussed later.

Table 3.8: Resistance ratios for tests in unsaturated sand

Test No	1	2	3	4	5	6	7	8	9	Mean value	Standard deviation
Date (dd-mm-2004)	20-7	27-7	17-8	19-8	19-8	8-9	8-9	10-9	18-10		
Location	ii	i	i	i	ii	I	ii	iii	iii		
$R_1 = R_{t-CPT}/R_{t-STA}$	1.39		1.22	1.19	1.19	1.17	1.15	1.18	1.23	1.21	0.07
$R_2 = R_{t-RP}/R_{t-STA}$	1.12	1.05	0.85	0.91	0.99	0.91	0.97	0.92	1.03	0.96	0.08
$R_3 = R_{s-RP}/R_{s-STA}$	1.12	1.05	0.85	0.91	0.99	0.91	0.97	0.92	1.03	0.96	0.08
$R_4 = R_{s-RP}/R_{s-STA}$	0.94	0.72	0.90	0.86	1.14	1.08	1.02	0.96	1.03	1.04	0.09

Table 3.9: Results of student t-test (unsaturated case)

Comparison		T_p	$T_{m+n-1,0.05}$	$H_0 : \text{equal}$
CPT vs. STA	Point	2.577	2.36	False
	Sleeve	0.33	2.36	True
RP vs. STA	Point	0.71	2.31	True
	Sleeve	0.27	2.31	True

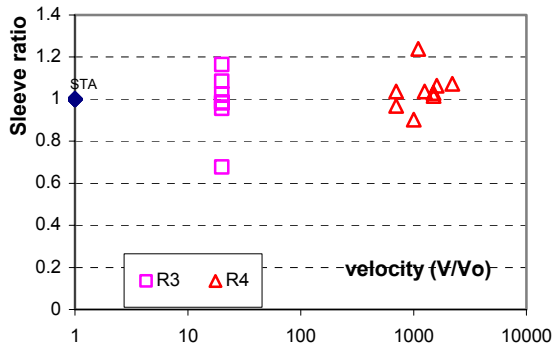


Figure 3.54: Rate effect on sleeve friction (unsaturated sand)

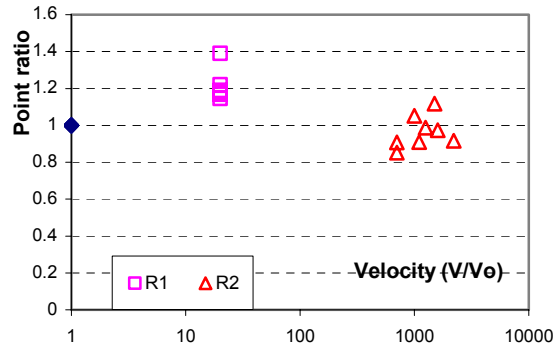


Figure 3.55: Rate effect on tip resistance (unsaturated sand)

Effect on the load-displacement curve

This section compares the load-displacement behaviour of static tests with that of rapid tests to examine the effect. A comparison example is shown in figures 3.56 and 3.57. The results are taken from test No. 7 (see tables 3.4 and 3.5). Little difference can be observed between the curves in these figures. A comparison with other tests shows the same result. It can therefore be concluded that there is no difference between the mobilisation of resistance in rapid tests and in static tests in this case.

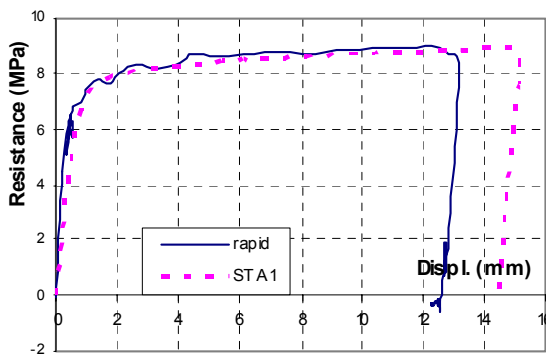


Figure 3.56: Unit tip resistance-displacement behaviour (unsaturated case)

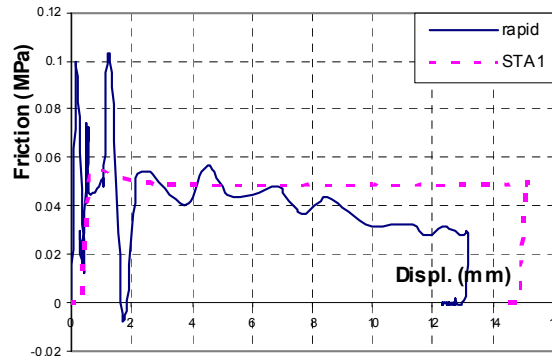


Figure 3.57: Unit sleeve friction-displacement behaviour (unsaturated case)

3.3.4.2 Rate effects in saturated sand

Effect on ultimate resistance and excess pore pressure

In the case of saturated sand, the following two ratios are added to compare the excess pore pressure:

$$R_{1pwp} = \frac{PP_{CPT}}{PP_0} ; R_{2pwp} = \frac{PP_{RP}}{PP_0}$$

where PP is the value of measured excess pore pressure in the CPT test and the rapid test, and PP₀ is hydrostatic pressure (0.01 kPa).

The calculated resistance ratios are presented in table 3.10. The plots of these ratios against pile head velocity are shown in figures 3.58 to 3.60. The student t-test was performed to determine whether results from the static tests are different from other test results or whether the difference is stochastic. The results of the student t-test are shown in table 3.11.

In the case of sleeve friction, no rate effect is seen in figure 3.58. The statistical calculation reveals the same conclusion. The ultimate sleeve friction measured during different loading rate tests is equal.

In the case of tip resistance (figure 3.59), there is no difference in the values measured in the static tests and the CPT test, but the ultimate value in the rapid tests is slightly higher than in the static tests. The statistical calculation shows the mean value of the tip resistance ratio R₂ is 1.09 with a standard deviation of 0.8. The student t-test in table 3.11 shows no significant difference between the two measurements, as the difference is negligible. The loading rate has no effect.

Figure 3.63 shows the loading rate has a significant effect on excess pore pressure near the pile toe. The excess pore pressure during a pseudo-static test is an order of magnitude larger than that of a static test and CPT test. The role of high excess pore water pressure will be presented in the next section.

Table 3.10: Resistance ratios for tests in saturated sand

Test No	1	2	3	4	5	6	7	8	Mean value	Standard deviation
Date (dd-mm-2004)	20-1	21-1	24-1	25-1	26-1	27-1	4-2	7-2		
Location	i	i	i	i	i	i	i	i		
R ₁ = R _{t-CPT} /R _{t-STA}	1.02	1.05	1.00	0.87	1.04	0.99	0.94	1.14	1.01	0.07
R ₂ = R _{t-RP} /R _{t-STA}	1.28	1.09	1.00	1.10	1.04	1.07	0.99	1.07	1.09	0.08
R ₃ = R _{s-CPT} /R _{s-STA}	0.82	1.03	1.03	0.83	0.97	1.03	0.91	1.00	0.95	0.08
R ₄ R _{s-RP} /R _{s-STA}	1.07	1.13	1.05	1.17	0.95	1.00	1.00	0.74	1.01	0.12
R _{1pwp}	1.33	1.25	1.25	1.33	1.75	1.75	2.33	1.50	1.56	0.35
R _{2pwp}	10.00	12.50	5.00	9.33	6.00	5.50	7.67	3.75	7.47	2.77

Table 3.11: Results of the student t-test (saturated case)

Comparison		T _p	T _{m+n-1,0.05}	H ₀ : equal
CPT vs. STA	Point	0.047	2.31	True
	Sleeve	0.59	2.31	True
	Pore pressure	4.04	2.31	False
RP vs. STA	Point	0.86	2.31	True
	Sleeve	0.061	2.31	True
	Pore pressure	6.12	2.31	False

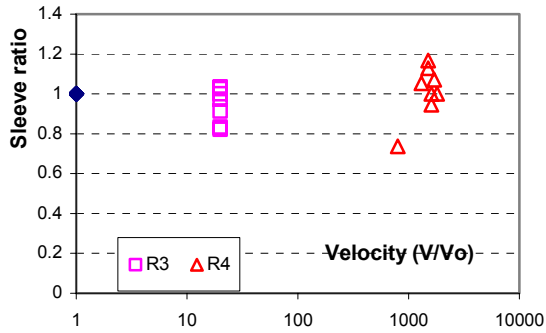


Figure 3.56: Rate effect on sleeve friction (saturated sand)

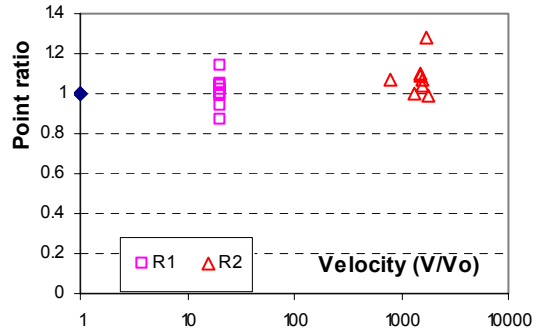


Figure 3.57: Rate effect on tip resistance (saturated sand)

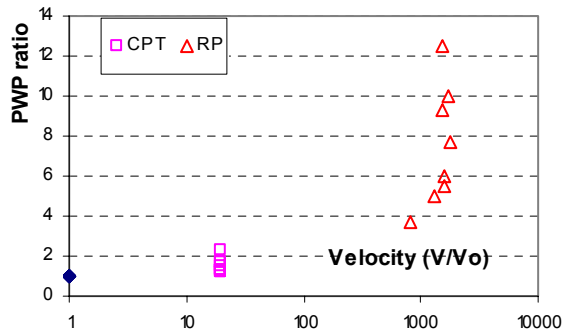


Figure 3.58: Rate effect on excess pore pressure (unsaturated sand)

The rate effect on load-displacement behaviour

Figures 3.59 and 3.60 show a comparison between the resistance-displacement behaviour of the model pile in a static load test and a rapid load test in saturated sand. The results are taken from test No. 6 (table 3.7). As with load tests in unsaturated sand, the static load-displacement response of the model pile is nearly the same as that in the rapid test. Only the stiffness of the tip resistance seems to be affected by the loading rate, but this effect is not easy to quantify due to the quality of measured signal in the current-set up of this test series. It is therefore noted here for future study.

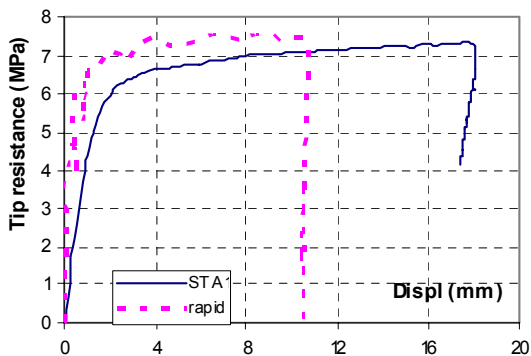


Figure 3.59: Comparison of tip resistance-displacement curves in saturated case

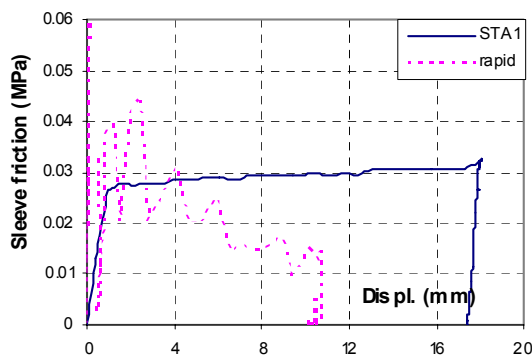


Figure 3.60: Comparison of sleeve-displacement curves in saturated case

3.3.5 Summary and discussion

Summary

In this model pile test series, different loading rate tests were performed on a model pile installed in unsaturated and saturated sand. The pile resistance during these load tests was derived in terms of the unit tip resistance and unit local sleeve friction. The loading rate effect on the model pile resistance has been evaluated by the comparisons between the derived resistances.

From the constant rate of penetration tests (the static tests and the CPT tests) where the penetration rate varied from ~1 mm/s to ~20 mm/s, the findings are:

- The sleeve friction of the model pile is independent of the penetration rate in both unsaturated sand and saturated sand.
- Tip resistance at the penetration rate of 20 mm/s is nearly 20% higher than that at the rate of 1 mm/s in unsaturated sand. No difference is observed in saturated sand.

Comparison between the static test and the rapid test (dynamic), the findings are:

- The ultimate values of tip resistance and sleeve friction of the model pile in static tests are identical to the rapid test. No loading rate effect is found.
- There is excess pore pressure during the rapid test near the pile tip. The magnitude of excess pore pressure depends on pile velocity.
- The stiffness of the pile tip load-displacement curve in the rapid test seems higher than in the static test but it needs further study to meet the final conclusion.

Discussion

The observed increase in pile tip resistance of approximately 20% in the CPT tests compared to the static tests in unsaturated sand is unexpected, and is briefly discussed here. In practice, it is known that the value of cone resistance in the CPT test is generally higher than the pile's unit tip resistance due to the scale effect (Chow, 1996). In this case, however, the scale effect should not play a role because the same cone was used in both the CPT test and the static load test. Also, the phenomenon was not observed in saturated sand. The observation is also not due to the rate effect in unsaturated sand, since it was not observed in the rapid tests where the loading rate was much higher. A possible explanation may be related to the behaviour of unsaturated sand. In this case, the water level may be near (under) the pile tip and a higher suction pressure may be generated in the soil region near the pile tip (due to the large deformation and high rate of the CPT test), causing higher pile toe resistance. This is only the assumption of the author, and further study is outside the scope of this research. It is noted here for future study.

For the applied loading rate in this model pile test series from 1 mm/s to approximately 1 m/s, the results of rate effect on pile resistance are in good agreement with the results from literature presented in figures 2.20 and 2.21, especially in the case of sleeve friction. It supports an idea of the existence a critical penetration rate and upon that value the rate effect is no longer significant. Perhaps the chosen static rate of around 1 mm/s approaches the critical value, thus no rate effect is found in this test series. This concept needs further validation.

Chapter 4

Numerical investigation into the effect of excess pore pressure

4.1 Introduction

This chapter studies the effects of excess pore pressure on a pile's mobilised resistance during a rapid load test using the numerical simulations approach. An axial rapid load test on a pile located in sand was the object of the simulations. The simulations were fully dynamic: wave propagation in pile and soil was taken into account.

The first part of the chapter describes the simulations performed in fully drained and fully undrained soil conditions. These are the two limiting cases of soil behaviour. Any difference in the simulation results will be due to the influence of drainage condition on the pile's mobilised resistance during the test. The specific effects of excess pore pressure on a pile's mobilised toe resistance and shaft friction are also described. The simulations were carried out using the Plaxis FEM package. Later in the chapter, the influence of partial drainage is considered. These simulations were carried out using Titan, a finite element code that links wave propagation and consolidation theories. The results from these simulations are used to evaluate the effects of excess pore pressure on stiffness and the ultimate value of the derived load-settlement curve. The chapter finishes with a discussion of these effects.

In chapter 2, a review of published experiments studying excess pore water pressure during a rapid pile load test was presented. In general, excess pore water pressure occurs in the sand surrounding the pile and the consolidation time of the excess pore pressure is of the same order of magnitude as the loading duration (Hölscher, 1995; Maeda et al, 1998). This implies that soil behaves in neither an undrained nor a drained condition during a rapid load test. Changes in soil resistance due to partial drainage should therefore be considered in order to correctly predict the derived load-settlement curve. After extensive research, the Japanese Research Committee on Rapid Pile Load Test Methods has noted the excess pore pressure phenomenon as a dynamic effect. This should be taken into account in order to derive a pile's load-settlement curve from the rapid pile load test method: "The Committee is aware that the influence of excess pore pressure is inevitable in the pile load test methods" (in Kusakabe et al, 1998. pp: 291 – 236). However, the effect of excess pore pressure on a pile's derived load-settlement has not yet been clarified. This chapter aims to demonstrate the importance of excess pore pressure on the resistance of a pile during a rapid load test.

4.2 Pile resistance in drained and undrained conditions

4.2.1 Introduction

The influence of pore pressure on the shear strength of soil in drained and undrained conditions is generally known, but the influence on pile resistance in a partially drained soil condition cannot be found in the literature. However, it is reasonable to expect that it would fall between the fully drained and fully undrained cases. It was therefore decided to simulate a rapid pile load test in both

a fully drained and fully undrained condition to evaluate the importance of drainage conditions on a pile's bearing capacity. The commercially-available FEM package, Plaxis V8.2, was used for this purpose as the package can perform a fully dynamic analysis in drained as well as in undrained conditions with various constitutive models of soil behaviour. A static load test as well as a rapid load test was simulated on the same pile. Simulation of the static pile load test was in a fully drained condition, and the rapid pile load test was in both a drained and undrained condition. The load-settlement curves were derived from the dynamic simulations results and compared to those from the static simulations. Since all input parameters were identical for these simulations except for the drainage condition, any difference should be induced by this parameter.

The first step described in this section was to simulate a case history pile load test in order to validate the simulation results. An evaluation is based on a comparison between the simulation results and in-situ measurements. The validity of the simulations is discussed, followed by how the derived load-settlement curve was derived from the rapid pile load test simulations. The derived static load-displacement curves are compared with those from the static pile load test simulation to examine the effects of excess pore pressure.

The second step described in this section was to separately consider the effects of excess pore pressure on tip resistance and shaft friction by simulating two hypothetical cases: (1) where there is predominantly shaft friction, and (2) where there is predominantly tip resistance. Further simulations were also performed, where soil parameters thought to control excess pore pressure were varied (such as pile diameter and the dilatancy angle of the sand) to obtain an overview of the effects. Generalisations about the effect of pore pressure can be derived from these simulations

4.2.2 Numerical simulation of the pile load tests

In the first simulation series, the case history of pile load tests performed at the testing event of the Fourth International Conference on Application of Stress Wave Theory to Piles, Delft, The Netherlands, in 1992 (Hölscher, 1995) was chosen. Both the static (maintained load test) and rapid (Statnamic test) load test methods had been performed on pile nr 3. Unfortunately, pile head measurement data (force and displacement) from the Statnamic test has since been lost, but the case history was selected because it is well-documented. Most of the soil and pile parameters needed for the numerical simulation are available from earlier studies on this case history (Hölscher, 1996). Moreover, measurements of excess pore water pressure near the pile toe during the Statnamic test are available, which is useful information for this study.

The pile in this case history was a pre-fabricated reinforced concrete pile, with a cross section of $25 \times 25 \text{ cm}^2$ and a length of 18.2m. The result of a cone penetration test at the test site is shown in figure 4.1. The soil at the test site was a soft soil, which is typical for the western part of the Netherlands. Soft soil (silty clay, silty sand and peat) with several sand layers was found between the surface and a depth of approximately 15 m. A dense sand layer was present at 15 m below the surface. The pile's bearing capacity was taken from this sand layer (Hölscher, 1995).

Figure 4.2 shows an axisymmetric finite element model used to simulate the problem, where the pile and soil were modelled using 15-noded triangular elements. The pile was modelled as an equivalent circular pile with a radius of 0.141 m. The soil was modelled around and below the pile. The finite element mesh measured 14.1 m in a horizontal direction and 21.7 m in a vertical direction. These dimensions were sufficient to eliminate the boundary effects (Deeks and Randolph, 1992). For the static simulation, the standard boundary conditions were set along the boundaries of the FE model, i.e. horizontal fixation in vertical boundaries and both horizontal and

vertical fixation at the bottom boundary. For the dynamic simulation, absorbent boundaries were set at the bottom and right-hand boundaries of the FE mesh to eliminate any wave reflection during the dynamic simulations. By this option a damper is set at the boundary in a certain direction instead of fixities to absorb any increase in stress without rebounding. However, at the time being, the shear waves are not fully absorbed (Brinkgvere, 2004); thus the boundary effect may exist in the simulation results. The pile was modelled as a linear elastic non-porous material. The soil was modelled using the linear elastic perfectly-plastic, Mohr-Coulomb model. The yield condition was specified by the friction angle φ' and the cohesion c' . A constant dilatancy angle ψ was used to model the dilatancy behaviour of the sand layer at the pile toe in the initial simulations. Pile and soil parameters are listed in table 4.1. Interface elements were set along the pile shaft to model the pile-soil interaction, i.e. the interaction properties between pile surface and soil. In this case the properties parameters of interface element are set equal to those of the surrounding soil for the simplification. Moreover, it is shown from the experience that the utilisation of interface elements are significantly reduced the mesh-dependency of the simulation results (Wehnert and Vermeer, 2004).

The static pile load test was simulated by static analysis, with a prescribed displacement applied at the pile head. A maximum displacement of 4 cm (equal to approximately 15% of the pile diameter) was chosen. The soil behaviour in this static simulation case was set to a drained condition.

The rapid pile load test was simulated by dynamic analysis, with a half sine dynamic loading applied on the pile head. The loading duration was 100 msec, which is a typical loading duration for the Statnamic pile load test. The soil behaviour was set at two conditions: fully drained and fully undrained. The actual situation should be in between, since the soil behaviour in a rapid pile load test is in a partially drained condition. The results of these simulations should therefore be considered as the two limiting cases of the problem.

For the dynamic undrained analysis, the input effective soil parameters are transferred to the undrained soil parameters as follows (Plaxis manual, 2004):

$$E_u = 2.G.(1+v_u)$$

$$v_u = \frac{3\nu' + B.(1 - 2\nu')}{3 - B.(1 - 2\nu')}$$

where G is the shear modulus, E_u is undrained Young's modulus, ν' and v_u are effective and undrained Poisson's ratio, and B is Skempton's parameter.

The distinction between total stress and effective stress and excess pore pressure is:

$$\text{total stress: } \Delta p = K_u \cdot \Delta \varepsilon_v$$

$$\text{effective stress: } \Delta p' = (1-B) \cdot \Delta p = K' \cdot \Delta \varepsilon_v$$

$$\text{excess pore pressure: } \Delta p_w = B \cdot \Delta p = \frac{K_w}{n} \cdot \Delta \varepsilon_v$$

where K' and K_w are the bulk modulus of soil skeleton and pore water respectively, K_u is the undrained bulk modulus of the mixture, n is porosity of the soil, and $\Delta \varepsilon_v$ is an increment of volumetric strain.

Table 4.1: The model parameters

Parameter	Symbol	Pile	Sand	Soft-soil	Unit
Dry volumetric weight	γ_{dry}	24	15.6	11.6	kN/m^3
Saturated volumetric weight	γ_{sat}	24	19.6	15.6	kN/m^3
Cohesion	c		0.1	0.1	kN/m^2
Friction angle	ϕ		37	5	$^\circ$
Dilatation angle	ψ		7.5	1	$^\circ$
Young's modulus	E'	$2 \cdot 10^7$	$3.4 \cdot 10^4$	$2.4 \cdot 10^4$	kN/m^2
Poisson ratio	ν'	0.2	0.25	0.25	

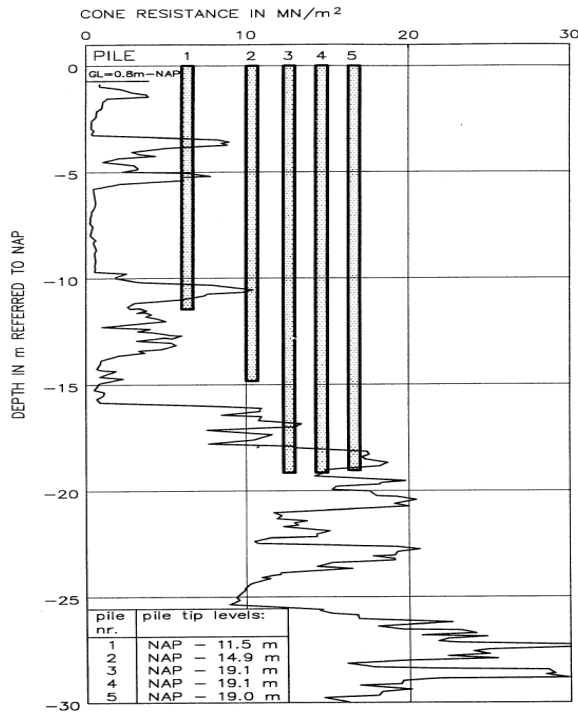


Figure 4.1: Result of cone penetration test at the pile position

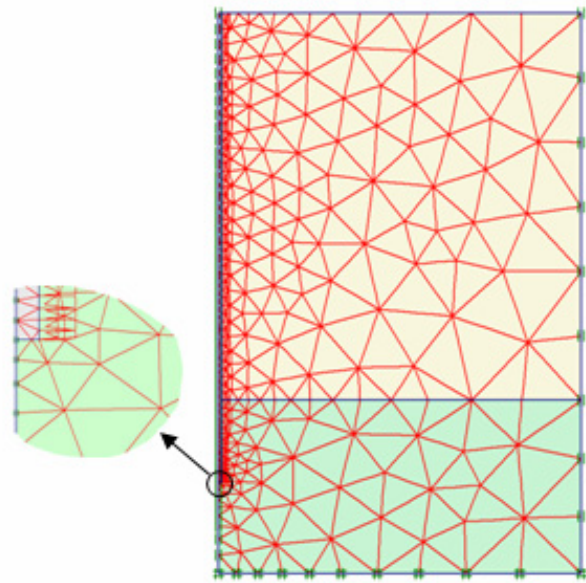


Figure 4.2: The FEM mesh for modelling the case history

4.2.3 Simulation results

Static simulations

This paragraph presents and evaluates the results from the static pile load test simulation against the in-situ measurement. The test was simulated by modelling a certain prescribed displacement on the pile top, and soil resistance was calculated in relation to that displacement. Pile shaft and toe resistance could be achieved by examining the interface stresses between the pile and the surrounding soil. Figure 4.3 shows the load-displacement curves of pile 3 from the in-situ static pile load test and from the simulation. The calculated total capacity is seen to be lower than the in-situ measurement at the same displacement, but the shape of the curves is very similar. This suggests that the simulation model is valid, as the lower calculated capacity can be explained. It is probably caused by ignoring the effects of the pile installation process (pile driving), which displaced and compacted the soil. This process would increase soil stresses, as well as strength, stiffness and pile capacity. Broere and van Tol (2006) have shown that this change in soil state due to pile installation can be modelled in the current FEM analysis program, and that an acceptable prediction can be achieved if the correct pile-soil interface properties are used in the simulations. However, this is outside the scope of this study. The main aim of these simulations is to examine differences in pile capacity in drained and undrained conditions. The current result is therefore acceptable.

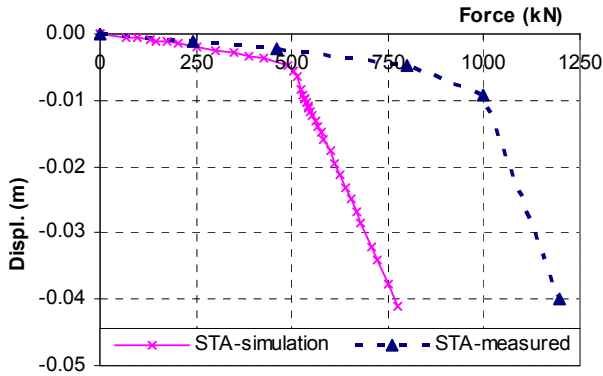


Figure 4.3: Static load-displacement curves from the simulation and in-situ load test

Dynamic simulations

This paragraph presents and evaluates the results of the dynamic simulation of the Statnamic load test case history. Typical calculated pile responses are shown in figures 4.4 to 4.7. In these figures, the solid line represents simulation results with a drained soil condition, while the dotted line represents the case with an undrained soil condition. The calculated pile head responses are seen to be very similar to typical pile responses during a Statnamic test (see figure 2.3). Figure 4.4 shows a time lag of the maximum pile head displacement behind the time of maximum applied force. The unloading point is clearly seen in figure 4.5. The maximum pile head velocity is approximately 1.2 m/s (figure 4.6) and the peak acceleration is approximately 100 m/s^2 . These figures are comparable to the typical value of a Statnamic test (see Kusakabe, 1998 – table 2). The differences in response of a pile in drained and undrained situations can clearly be seen in these figures. The difference in the derived load-settlement of a pile will be considered in the following sections.

In figure 4.8, the pile head displacement and the calculated response pore pressure are presented as a function of time. The pore water pressure is calculated at point A near the pile toe (0.5 m in a horizontal direction and 0.2 m below the pile toe). This is the same position as the pore pressure transducer in the case history. The negative value of pore pressure is compression. It can be seen that the response of pore pressure at the location is very similar to the pile displacement. It differs slightly from the in-situ measurement reported by Hölischer (1995 - see figure 2.22), as the figure does not indicate negative excess pore pressure due to dilatancy induced by shearing effect. It is, however, virtually identical to the measurements reported in Maeda et al. (1998). It is currently not possible to evaluate the accuracy of the simulation in this situation, due to the limitation of in-situ measurements and the lack of knowledge related to this aspect.

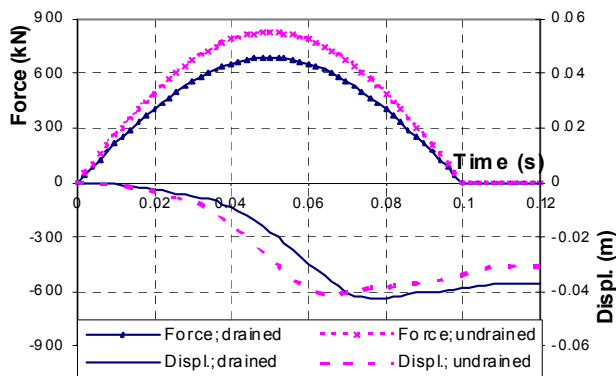


Figure 4.4: Applied force and calculated pile head displacement in drained and undrained cases

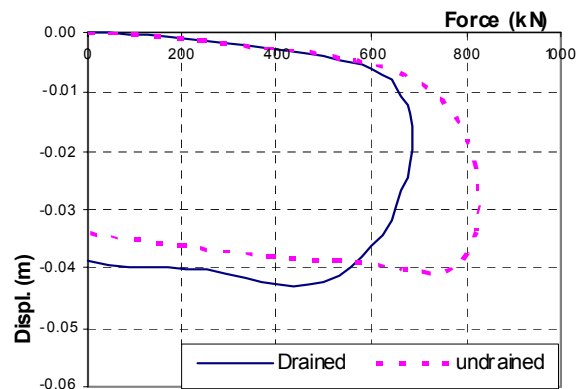


Figure 4.5: Statnamic load-displacement curves

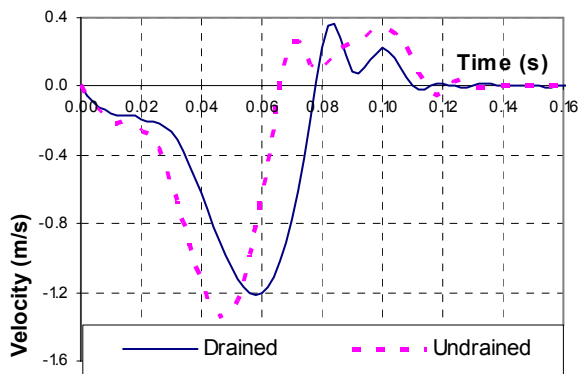


Figure 4.6: Calculated pile head velocity

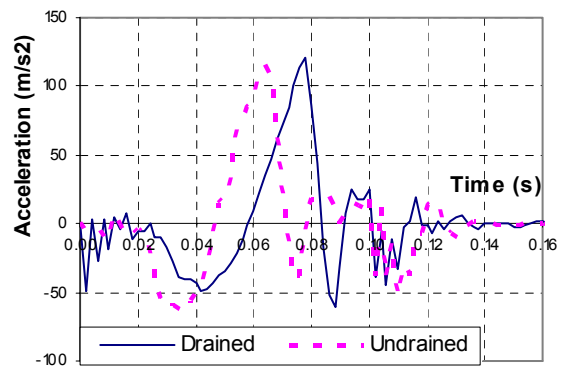


Figure 4.7: Calculated pile head acceleration

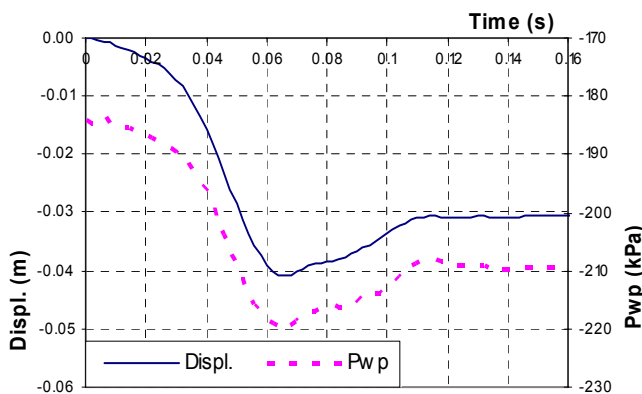


Figure 4.8: Calculated pile head displacement and pore pressure at point A

Determining the derived load-displacement curve from the dynamic simulations

This section describes two methods used to determine total mobilised soil resistance - the derived load-displacement curve - based on the Statnamic load test simulations. The first method is based on the calculated pile head responses, whilst the second is based on direct examination of calculated stresses at the pile-soil interface. The two results are compared to show validation of these analyses. They are also compared with results from the static simulations to evaluate the damping component of pile resistance.

The first method is similar to the unloading point method (UP method). The total soil resistance is derived by subtracting the inertial force (F_a) from the input dynamical load (F_{stn}). The total soil resistance includes static resistance (F_{sta}) and damping resistance (F_v).

$$F_{soil} = F_{sta} + F_v = F_{stn} - F_a = F_{stn} - m \cdot a(t)$$

where m is the pile mass, and $a(t)$ is pile head acceleration.

Figure 4.9 compares the calculated total soil resistance (F_{soil}) and applied force (F_{stn}) for the simulation in a drained condition with the load-displacement curve from the static simulation. Figure 4.9 shows the calculated curve (F_{soil}) is almost identical to the static load-displacement curve, which implies that the damping force (F_v) in this case is negligible. This can be explained by the damping source in this numerical scheme. Tan et al, (2004) have pointed out that radiation damping is the main source of damping for the pile-driving problem simulated by an axisymmetric model in the Plaxis program. According to Novak et al, (1978), the significance of radiation

damping depends on the loading frequency and the pile radius. In this case, the dynamic loading duration of 100 ms ($f=5\text{Hz}$) and a pile radius of only 0.141m result in very small value for the dimensionless frequency a_0 . The radiation damping is therefore close to zero (Novak et al, 1978; Matsumoto, 1998).

The second method derives total soil resistance from soil stresses at the pile-soil interfaces at a certain time during loading. The derived load-displacement curve from the dynamic simulation in a drained condition is shown in figure 4.10. The curve from the undrained condition is shown in figure 4.11. In both figures, results from the first method are also plotted for comparison. The results show good agreement, i.e. both methods can be used to derive soil resistance from the dynamic simulations. The second method is preferred and will be applied however, because of its ability to judge the interface stresses.

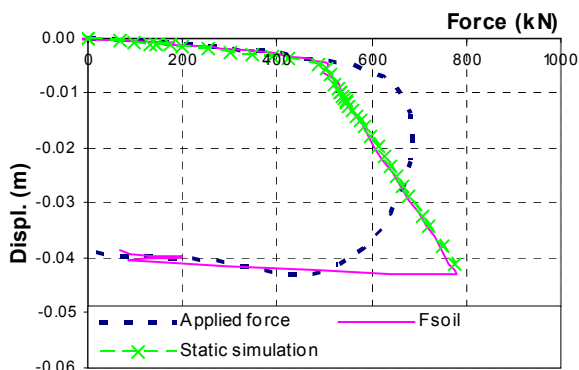


Figure 4.9: Comparison of derived load-displacement curves from simulations in a drained condition

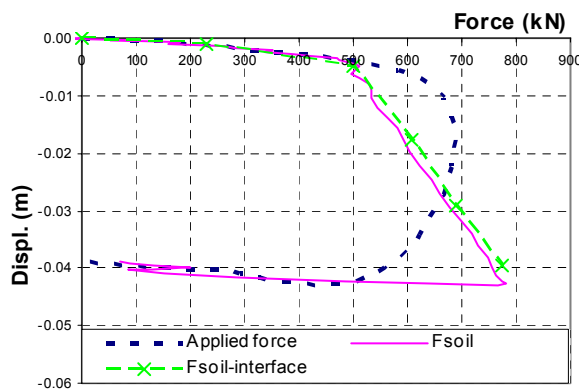


Figure 4.10: Derived load-displacement curves from simulations in a drained condition

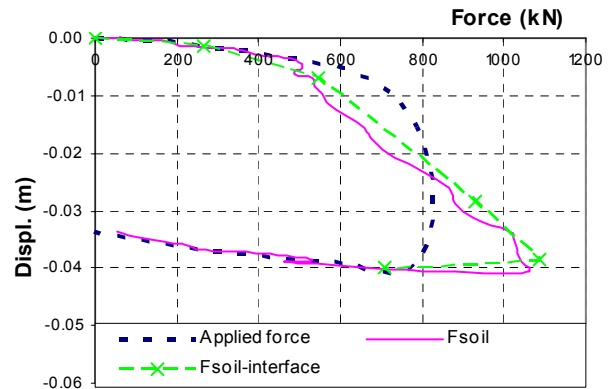


Figure 4.11: Derived load-displacement curves from the simulation in an undrained condition

Influence of drainage conditions

The derived load-displacement curves from the dynamic simulations in drained and undrained conditions are available from figures 4.10 and 4.11 and can be evaluated. A comparison of these two curves is shown in figure 4.12. The difference between the two curves is clearly seen. Since all input parameters for these two simulations are identical, the difference in figure 4.12 must be due to the difference in drainage condition. In this case, the undrained condition gives higher mobilised soil resistance than the drained condition. It can be concluded that the drainage condition does affect the derived load-settlement curve of a pile. The effect on shaft and tip resistance will be considered in the following sections.

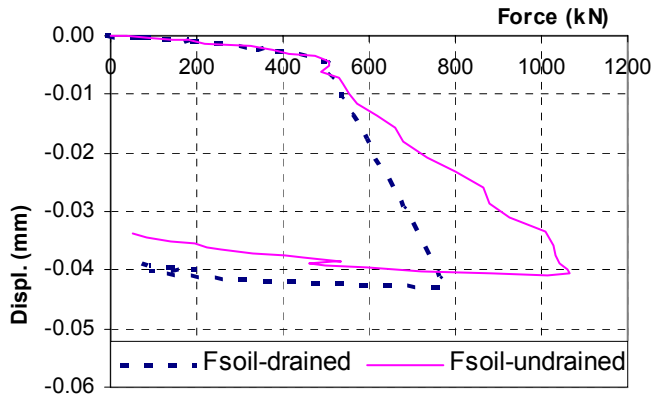


Figure 4.12: Comparison of drained and undrained load-displacement

4.2.4 Effect of drainage condition on tip resistance and shaft friction

This section aims to specify the effect of drainage condition on a pile's toe resistance and shaft friction. Two hypothetical cases of pile foundation are used: (1) where there is predominantly toe resistance; and (2) where there is predominantly shaft friction. The rapid pile load test on these piles was simulated in a drained and undrained condition. Derived load-settlement curves, which are determined from calculated interface stresses at a pile's interface as discussed above, are compared to clarify the effects.

To describe these two hypothetical cases, the subsoil was divided into two distinct layers: a layer along the pile shaft (from the surface down to pile toe level), and a layer underneath the pile tip (from the pile toe level down to infinity). Depending on the proposed case (1) or (2), the corresponding soil layer (known here as the bearing capacity layer) was modelled with high strength parameters. The other layer (known here as the soft layer) was modelled with very low strength parameters to minimise its resistance. The FE model of the pile and soil system used in the current simulations is shown in figure 4.13. It shows the case of predominant toe resistance, where the bearing capacity layer is set below the pile toe and the soft layer is set along the pile shaft. The boundary conditions were the same as those in the FE model described in section 4.2.2.

Material modelling of the pile and soil was similar to that described in section 4.2.2, i.e. the pile was modelled as a linear elastic material, and the soils were modelled as linear elastic perfectly-plastic. All the material model parameters were identical to those listed in table 4.1, except for the strength values of soft layer and the dilatancy angle of the bearing capacity layer. The strength parameters of the soft layer were reduced to nearly zero to minimise their contribution to the total pile resistance ($c=0$; $\phi=1$; $\psi=0$).

In this section, the dilatancy angle is varied from 0 to 15 degrees to examine the effect on the bearing capacity of a pile. As the dilatancy angle controls the tendency of volume change in soil when it fails in shear and therefore controls excess pore pressure, it could significantly affect the difference between pile resistance in undrained and drained conditions.

The Mohr-Coulomb soil model is used in the current model (i.e. the stiffness and strength values of the bearing capacity layer are constant and independent of the stress level). The consolidation process has been eliminated in the simulations. It is therefore reasonable to expect that the difference between pile resistance in undrained and drained conditions will be independent of the pile size. The pile dimensions can be chosen for the sake of convenience for the FE modelling. Two pile radii of 0.25 m and 0.5 m are chosen to verify the assumption.

The case of predominant toe resistance

The finite element mesh for the simulations in this case is shown in figure 4.13. The pile was 18 m in length with a radius of 0.25 m. A fine FE mesh was generated around the pile tip to reduce the effects of highly-concentrated stresses and the numerical singularity at the right-hand corner point of the pile tip. As discussed in Wehnert and Vermeer (2004), this is always the numerical singularity point and an unrealistic stress pattern could be created that might affect the pile toe resistance determined from the interface stress. They also suggested that a feasible way to minimise such an effect is to set more elements over the radius of the pile tip. After several trial calculations, generation of at least three elements over the pile toe radius seemed to be sufficient in these simulations. Table 4.2 lists the cases and variation parameters used for the simulations described in this section. Similar simulations were also performed with a pile of the same length but with a radius of 0.5 m.

Table 4.2: Simulation cases (for the case of predominant tip resistance)

Case No.	r (m)	ψ (degrees)	Conditions
1	0.25	0	Drained/undrained
2	0.25	7.5	Drained/undrained
3	0.25	15	Drained/undrained
4	0.5	0	Drained/undrained
5	0.5	7.5	Drained/undrained
6	0.5	15	Drained/undrained

The derived pile tip resistance-settlement curves from the simulation cases 1, 2, and 3 (pile radius = 0.25 m) are shown in figure 4.14. The solid lines are the results from simulations in a drained condition, whilst the dotted lines are results from simulations in an undrained condition. The curves marked with a solid square, open circle, and solid triangle are cases where the dilatancy angle of the bearing capacity layer is 0° , 7.5° , and 15° respectively. The effects on the tip resistance of differences between the drained and undrained condition can be clearly seen in the figure. The tendency of the effects depends on the value of the bearing layer's dilatancy angle. In figure 4.15, the ratio of the pile tip resistance in the drained condition (F_d) and in the undrained condition (F_{ud}) is plotted against the normalised pile head displacement. Where the dilatancy angle is zero ($\psi = 0^\circ$), the pile tip resistance in the drained condition is higher than that in the undrained condition (approximately 40% at the pile head displacement of 10% pile diameter). By contrast, where the dilatancy angle is 7° and 15° , the pile tip resistance in the drained condition is approximately 40% and 50% respectively lower than that in the undrained condition. The simulation cases 4, 5, and 6 (pile radius = 0.5m) show the same results as included in figure 4.15.

The observed effects in figures 4.14 and 4.15 can be explained by the characteristics of excess pore pressure in the soil region underneath the pile tip. Figures 4.16, 4.17 and 4.18 present the calculated pore pressure in undrained simulation cases 1, 2, and 3 (see table 4.2) at points underneath the pile tip. Point A is in the 'wedge' region of high compression directly under the pile tip, points B and C are in the shear failure region underneath the pile tip. Where the dilatancy angle is zero, the excess pore pressure in the undrained condition is positive (compression) as shown in figure 4.16. The excess pore pressure may cause a reduction of the effective stresses in the soil in comparison with the drained case. As a result, the shear strength of the soil decreases as well as the mobilised tip resistance. On the other hand, where the dilatancy angle is high (figures 4.17 and 4.18), the excess pore pressure in the shearing region becomes negative (tension). It reaches the value at which cavitation occurs (-100 kPa) due to the dilatancy of the soil in that soil region. This increases the shear strength of the soil; hence the mobilised tip resistance increases.

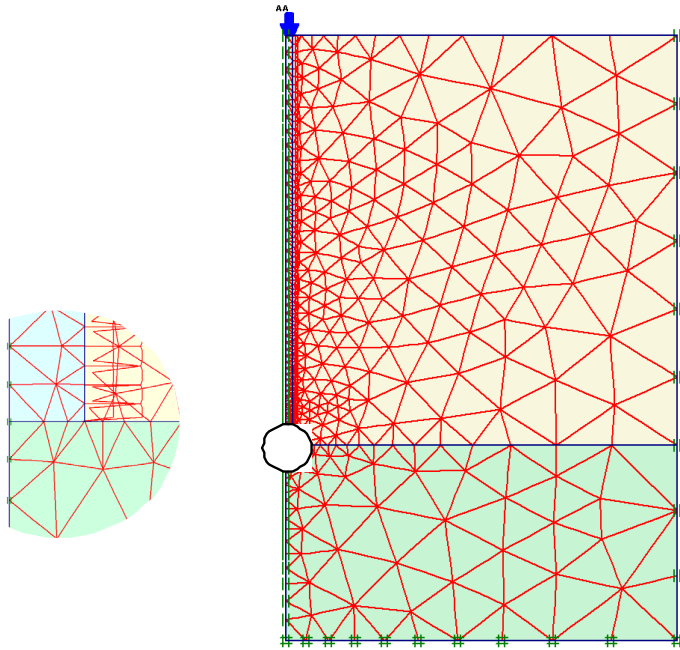


Figure 4.13: FE mesh for the case of predominant toe resistance

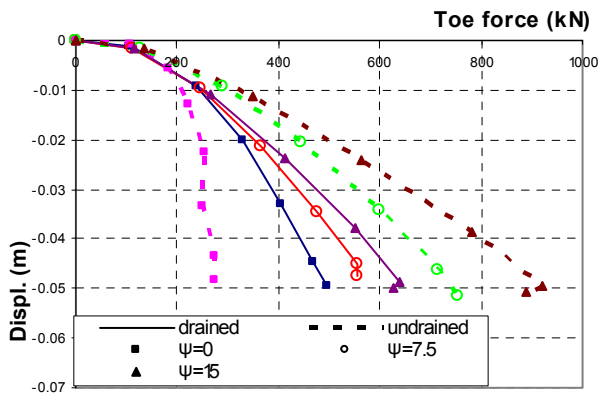


Figure 4.14. Difference in tip resistance between drained and undrained conditions with various dilatancy angles (radius = 0.25 m)

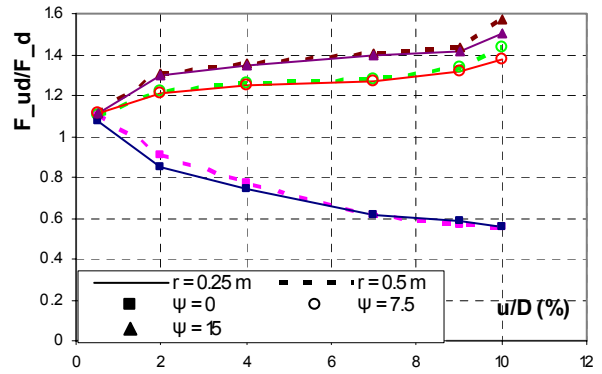


Figure 4.15: Effect of drainage condition on tip resistance with various dilatancy angles

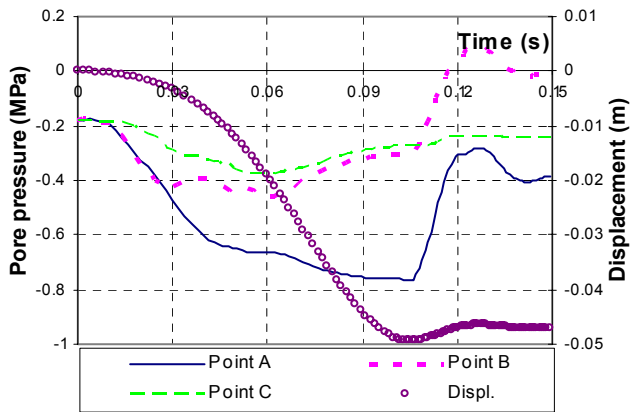
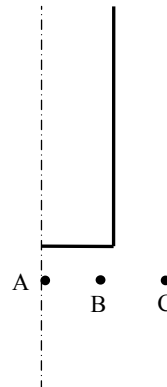


Figure 4.16: Pore pressure underneath pile tip in the rapid test simulation (undrained/ $\psi = 0^\circ$)



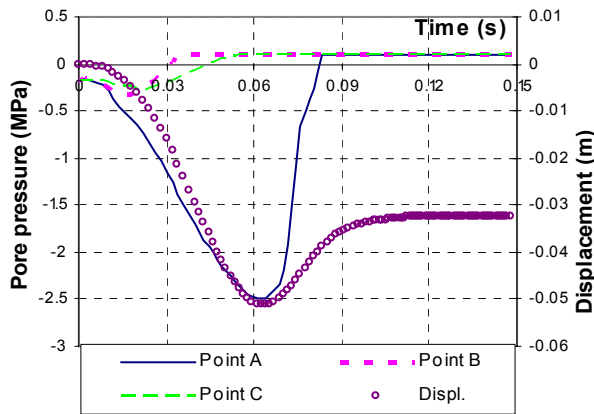


Figure 4.17: Pore pressure underneath pile tip in the rapid test simulation (undrained/ $\psi = 7.5^\circ$)

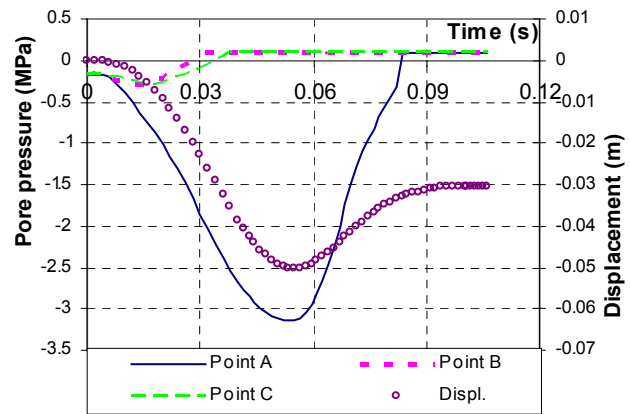


Figure 4.18: Pore pressure underneath pile tip in the rapid test simulation (undrained/ $\psi = 15^\circ$)

The case of predominant shaft resistance

In the simulations for this case, the FE model of the pile-soil system and the model parameters were the same as for the predominant toe resistance case, as shown in figure 4.13 and table 4.1. However, the soft soil layer was located under the pile toe and the bearing capacity layer was set along the pile shaft. The dilatancy angle values of the bearing capacity layer were varied as 0° , 1° , and 7.5° . The pile measured 0.2 m in radius and 18 m in length.

The derived shaft resistance-displacement curves from the simulations with different dilatancy angles are shown in figure 4.19. The pile shaft resistance is derived from the calculated shear stress at the pile shaft and soil interface. In figure 4.19, the solid lines are results from simulations in a drained condition, whilst the dotted lines are the results from simulations in an undrained condition. It can be seen that the pile shaft resistance is higher in the undrained condition than that in the drained condition, and that the increment strongly depends on the value of the dilatancy angle.

Where the dilatancy angle is zero, only a minor increment of undrained shaft resistance over the drained shaft resistance is observed. A comparison of stresses at the pile shaft interface in the undrained and drained conditions is shown in figure 4.20, where the stresses are calculated at the same time ($t = 55$ msec). The figure shows that the distribution of stresses in the drained and undrained case is almost identical along the pile shaft, except for values near the pile ends. It seems that the stress pattern along the pile shaft near the pile ends is affected by numerical errors at the singular points. In the undrained simulations, the pore pressure values close to the pile tip is somewhat lower than the hydrostatic value due to the effect of the singularity. This effect increases effective normal stress, as does the shaft resistance as seen in figure 4.19. It is therefore reasonable to conclude that the drainage condition has no effect on the pile shaft resistance where the dilatancy angle of the soil is zero.

Where the dilatancy angles are 1° and 7.5° , the increments of the undrained shaft resistance over the drained value at a displacement of 10% pile diameter are approximately 50% and 100% respectively. These increments directly relate to the negative excess pore pressure at the pile shaft as discussed here. Figure 4.21 presents the pore pressure response at three points close to the pile shaft during a simulation in an undrained condition with a dilatancy angle of 1° . Negative excess pore pressure (suction) is observed at all locations, caused by soil dilation as a result of shear failure along the pile shaft. The negative excess pore pressure increases the effective normal stress on the pile shaft, as does the shear strength at the pile-soil interface (i.e. the shaft resistance

increases). Figure 4.22 presents the normal stress difference values along the pile shaft between the drained and undrained simulations and the excess pore pressure in the undrained simulation. The values shown are calculated at a time of $t = 55$ msec where the dilatancy angle is 1° . The figure shows that the excess pore pressure is nearly equal to the effective normal stress difference. This means that the excess pore pressure is responsible for all the effective normal stress difference between the drained and undrained simulations. The values of the calculated shaft resistance at $t = 55$ ms are marked with number '4' in figure 4.19. The undrained value is approximately 400 kN higher than the drained value. This value of 400 kN is nearly the same as the shaft resistance value calculated from the values of effective normal stress difference shown in figure 4.22 (397.6 kN). It can therefore be concluded that the increment of shaft resistance seen in figure 4.19 or the effect of the drainage condition of pile shaft resistance is mostly due to negative excess pore pressure at the pile-soil interface.

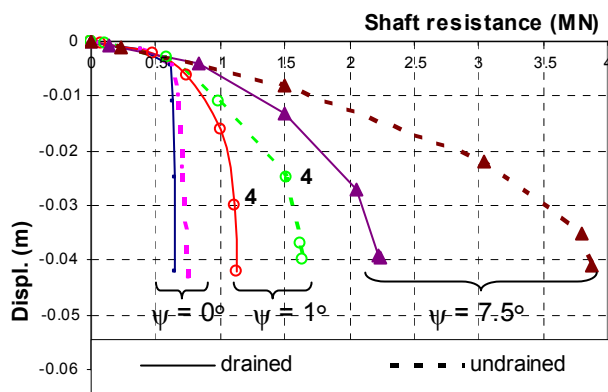


Figure 4.19: Difference in shaft resistance between drained and undrained conditions with various dilatancy angles

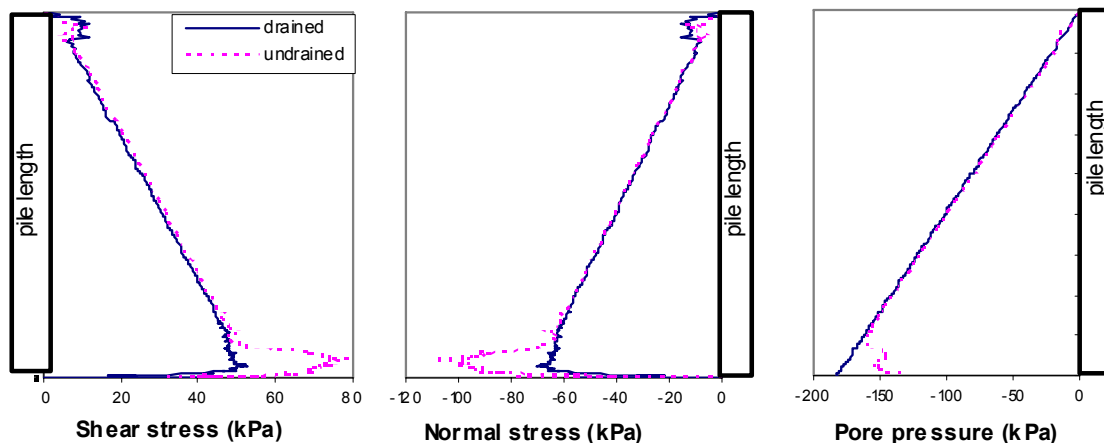


Figure 4.20: Comparison of stresses at pile shaft interface at a time ($t = 55$ ms) between the undrained and drained simulations for the case dilatancy angle = 0

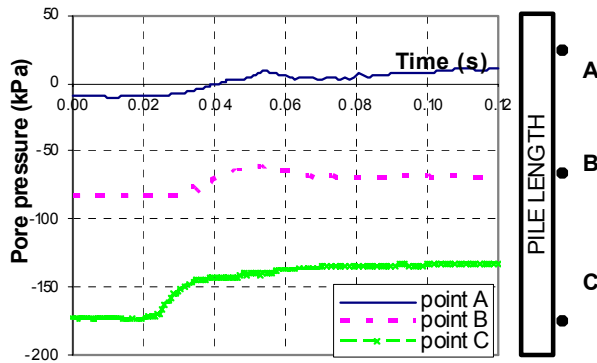


Figure 4.21: Excess pore pressure at pile shaft in undrained condition ($\psi = 1^\circ$)

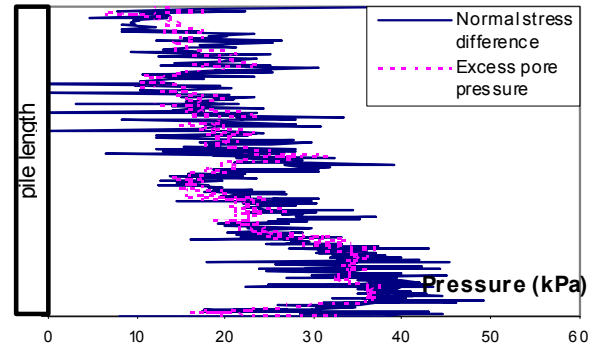


Figure 4.22: Effective normal stress difference between undrained and drained conditions; and excess pore pressure (at time $t = 55$ msec; the case $\psi = 1^\circ$)

4.2.5 Summary

The above presentations have described the differences between mobilised pile resistance in a drained condition and in an undrained condition. Pile shaft resistance and pile tip resistance are both affected by drainage conditions. The magnitude of the effect depends on the dilatancy angle of the bearing capacity soil layer. Because these results are from simulations of the Statnamic pile load test in drained and undrained conditions (the two limiting cases of soil behaviour), the effect will in reality be in between due to the partially drained condition.

4.3 Consideration of the partially drained condition

4.3.1 Introduction

This section investigates the effect of a partially drained condition on pile resistance. The simulations were performed using the Titan FE code created by Holscher (1995), which links wave propagation and consolidation theories. The rapid load test on a pile was dynamically simulated, and the consolidation process during the test was taken into consideration using the Titan code. Two parameters that are extremely important for the practical design and interpretation of rapid pile load tests are pile stiffness and pile resistance. The simulations described in this section aim to study the effect of drainage conditions on these parameters.

For the practical in-situ case of a pile founded in sand, the pile is often the end bearing pile. This means that the behaviour of pile tip resistance is predominantly the behaviour of the pile. Moreover, the effect on pile shaft resistance described above may be considerably reduced in practice (partially drained sand) due to the radial consolidation of the negative excess pore pressure (Randolph et al, 1979). The effect of the drainage condition on pile shaft resistance can therefore be considered as insignificant within the framework of this study. The study in this section is restricted to pile tip resistance.

4.3.2 Validation of the Titan finite element code

The Titan code uses the finite element method to solve the Biot-equations for the dynamic behaviour of saturated porous materials. The code has been used to solve practical dynamic problems (Holscher, 1995). Two material models are currently available in the code: the linear elastic model, and the bi-linear model. In the latter soil model, the stiffness of the soil depends on the stress level and is controlled by a stress state relative to the yield surface. In the stress space, the yield surface is defined by the equation:

$$f_y = (\eta_{ij} \cdot \eta_{ji})^{1/2} + M_m \cdot \ln\left(\frac{\sigma_m}{\sigma_{m,\max}}\right) = 0$$

where η_{ij} is the stress ratio tensor, M_m a material constant, σ_m the mean stress, and $\sigma_{m,\max}$ the (pre-) consolidation stress.

The value of $\sigma_{m,\max}$ is updated if $f_y > 0$ in order to keep $f_y = 0$. Inside the yield surface, the elastic stiffness is determined using the swelling index (κ). When the stress state is on the surface, the material becomes weak and elastic stiffness is determined using the compression index (λ) as:

$$G_s = \frac{3 \cdot (1 - 2\nu)}{2 \cdot (1 - \nu)} \frac{1 + e_0}{S_i} \cdot \sigma_{m,i} \cdot \left(\frac{\sigma_m}{\sigma_{m,i}}\right)^m$$

$$K_s = \frac{1 + e_0}{S_i} \cdot \sigma_{m,i} \cdot \left(\frac{\sigma_m}{\sigma_{m,i}}\right)^m$$

where ν is Poisson's ratio, e_0 is the initial void ratio, S_i is the swelling index κ if $f_c < 0$, and compression index λ if $f_c = 0$, $\sigma_{m,i}$ is the initial mean stress, and m is a material constant for stiffness.

This section demonstrates and discusses the applicability of the code for studying the dynamic response of foundations. Firstly, the Titan code was used to simulate the dynamic loading of a shallow foundation on saturated soil, and the results were compared to an analytical solution of the problem. A Statnamic pile load test was then simulated using the code, and the results were compared to field measurements of the case. A sketch of the simulated problems is shown in figure 4.23, and the results of these simulations are presented here.

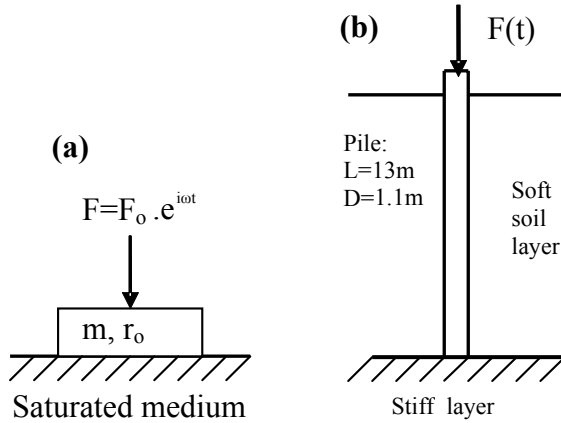


Figure 4.23: Sketch of the problems - (a) footing; (b) pile.

Vibration of a shallow foundation

The Titan code was used to analyse the response to harmonic loading of an elastic circular footing founded on a half-space of homogeneous saturated soil. The soil was considered as a two-phase porous medium: solid and fluid phases. The results were used to determine the dynamic stiffness of an equivalent single-degree-of-freedom (SDOF) model representative for the problem as widely accepted in practice. The calculated dynamic stiffness was compared with an analytical solution from literature to validate the code.

In relation to vibration of a footing on a homogeneous elastic half-space (single-phase material), Lysmer and Richart (1966) have showed that the problem can be represented by a single-degree-of-freedom (SDOF) ‘mass-spring-dashpot’ system with frequency-dependent stiffness and damping. In general, the dynamic stiffness K_d relates to the static stiffness K_s by:

$$K_d = K_s.[k(a_0) + i.a_0.c(a_0)]$$

where $k(a_0)$ and $c(a_0)$ are frequency-dependent dynamic stiffness and damping coefficients.

$a_0 = \frac{\omega.r}{V_s}$ is a dimensionless frequency

ω is the angular frequency of load

r is the footing radius

V_s is the shear wave velocity of soil medium.

i is an imaginary unit.

Many researchers have shown that the stiffness and damping coefficient of saturated soil also depends on the two-phase nature of soil behaviour (Halpern and Christiano, 1986; Philippacopulos, 1989; Kassir et al., 1989; Bo, 1999). An analytical solution found by Bo (1999) was chosen to validate the Titan code simulation. The same problem was simulated using the Titan code with a linear elastic soil model, with the material parameters taken from Bo (1999). From the simulation results and a known footing mass, the stiffness and damping coefficient of an equivalent SDOF model were derived by the method of least square. Figure 4.24 presents the Titan code’s results and a graph of Bo’s analytical solution from figures 10 and 11 in his paper (see Bo, 1999). There is close agreement between the two results. This simulation validates the Titan code.

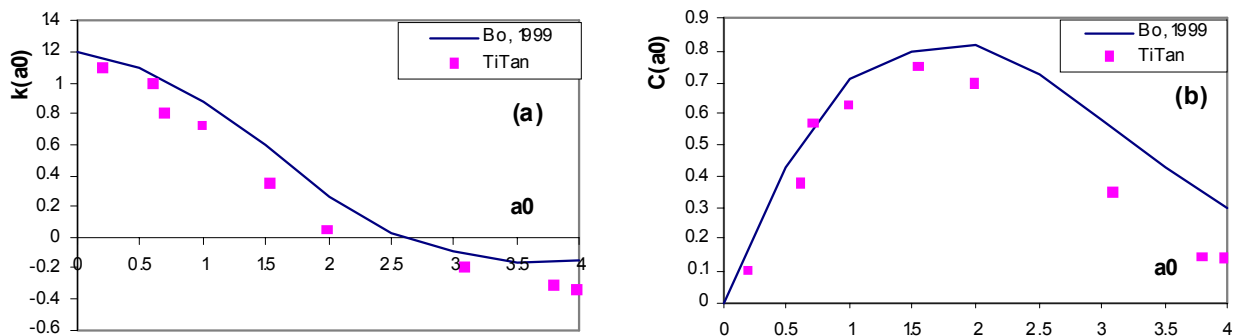


Figure 4.24: Comparison between the results of Titan and the analytical solution
(a) spring stiffness ; (b) damping coefficient

Statnamic test simulation using Titan

To validate the simulation of a Statnamic test using the Titan code, the case history of Maeda et al, (1998) was simulated. The simulated problem is shown in figure 4.23b. The pile was a cast-in-place concrete pile, with the toe placed on a dense sand layer. During the test, pore water pressure was measured at two points near the pile toe.

The axi-symmetric model was applied. For the simplified modelling, the soft soil layer was set from the surface to the depth of pile toe, with a stiff soil layer underlying the pile toe. The pile was loaded by a force correlated to the Statnamic loading, as shown in figure 4.25. An interface element was placed between the pile and the soil to transfer fluid stress to the pile. The pile was modelled as a linear elastic material, and the soil was modelled using a bi-linear two-phase model. Four simulations were performed: one in a fully drained condition, the remaining three in partially

drained conditions with different soil permeability values: $k = 2.6 \cdot 10^{-2}$ m/s; $k = 2.6 \cdot 10^{-3}$ m/s, and $k = 2.6 \cdot 10^{-4}$ m/s.

Figure 4.25 presents the applied load and calculated pile head displacements as a function of time. Figure 4.26 presents the calculated load-displacement curves. It can be seen that the calculated responses are very similar to those in the prototype Statnamic pile load test (see Maeda et al, 1998). As soil permeability increases, behaviour becomes closer to the drained case. For this simulation, where the soil permeability value is $2.6 \cdot 10^{-2}$ m/s, the soil behaviour is close to a drained condition.

Figure 4.27 presents the calculated excess pore pressure at a point (at a distance of 0.4 m and 1 m below the pile toe), which is the same location as the pore pressure transducer in the case history. The measurement reported by Maeda et al (1998) is similar to the line named ' $k=2.6 \cdot 10^{-4}$ ' in the figure. As expected, the figure also shows that the lower soil permeability case induced higher excess pore pressure.

These results confirm that the Titan code can be used to simulate the dynamic response of a pile in a partially drained condition, and that the simulation results can be used to evaluate the effect of a partially drained condition in simulations of a Statnamic pile load test.

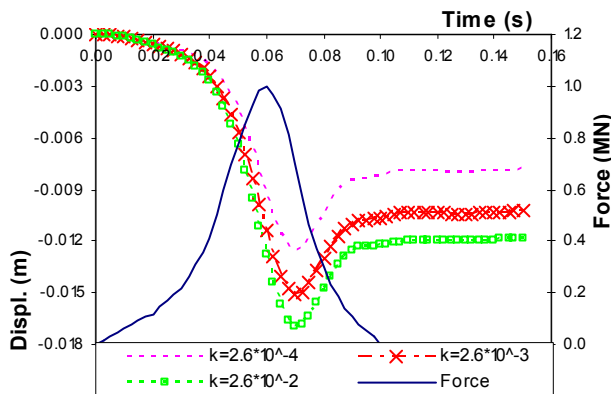


Figure 4.25: Load and displacement vs. time of the Statnamic test simulated by Titan code

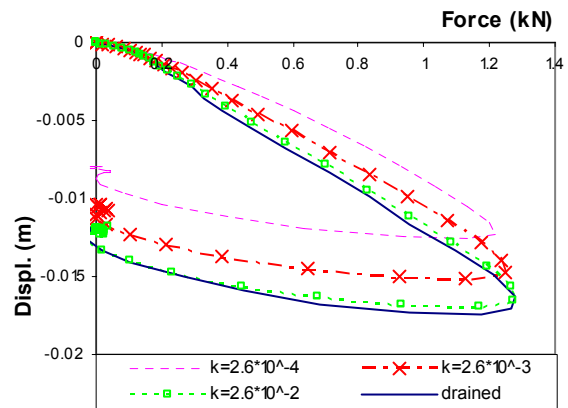


Figure 4.26: Load-displacement curves of the Statnamic test simulated by Titan code

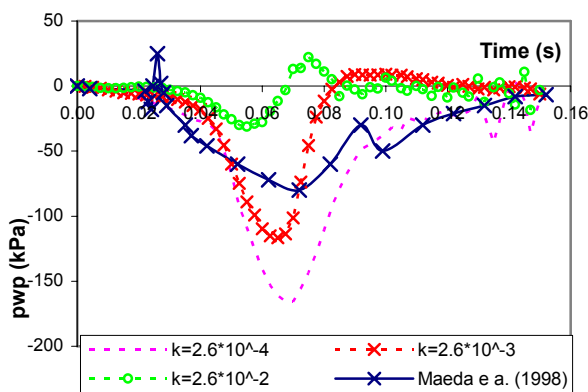


Figure 4.27: Excess pore pressure vs. time from the Titan simulations (negative value is compression)

4.3.3 Effect of different drainage conditions on dynamic stiffness

This section examines the effect of drainage condition on spring stiffness and the damping coefficient of the lumped mass model at the pile tip. The shallow footing problem is considered

first, as its behaviour is virtually the same as the pile toe in the same dynamic loading. The model of a pile embedded in homogeneous soil is then studied. The effect between the lumped mass model for shaft friction and toe resistance is investigated separately.

The foundation-soil system was simulated in a fully dynamic way with different drainage conditions. The foundation's motions from the simulation were entered into the dynamic equation of the SDOF model to determine the best-fit values for spring stiffness and the dashpot constant using the method of least squares. To find the effect of the drainage condition, these values were normalised with the values from the simulation in a fully drained condition with the same system.

The drainage condition is represented by a dimensionless parameter η , known here as *the drainage factor*, which is related to a certain fraction of consolidation during the loading period of the test. The drainage factor η was defined by Hölischer and Barends (1992) as:

$$\eta = \frac{G.T}{\gamma.r^2}.k$$

where G is the shear modulus (N/m^2), T is the loading duration (s), r is the pile radius (m), γ is the volumetric weight of the water (N/m^3), and k is the hydraulic conductivity (m/s).

Footing stiffness

The problem shown in figure 4.23a is considered here. The input parameters of the saturated soil medium and footing are shown in table 4.3. To achieve different soil drainage conditions, the value of the dynamic drainage factor η is varied by changing the value of soil permeability and shear modulus in the corresponding range of sand in reality.

The dependency of spring stiffness and damping constant on the drainage factor η (drainage condition) is shown in figures 4.28 and 4.29. In these figures, the values of the dynamic stiffness from simulations in a partially drained condition (k_{PD} and c_{PD}) are normalised to those from simulations in a drained condition (k_D and c_D). It can be seen that the values of the stiffness and damping coefficient depend on the value of the drainage factor; but that it has no influence at certain extreme drainage factor values. This implies that the soil behaves in a fully drained and fully undrained condition at these extreme values. For this simulation case, the value of η higher than 5 can be considered as the boundary value between the partially drained and fully drained conditions; whereas the value of 0.01 is the boundary between the partially drained and fully undrained conditions.

To verify these extreme drainage factor values, the same problem was simulated using the Plaxis program in the drained and undrained condition. A comparison between the results from the Titan code and the Plaxis program is shown in table 4.4. There is quite significant difference in the last value shown in table 4.4 (approximately 30%). This may be caused by friction between the pore water and the soil skeleton, which is ignored in a fully undrained simulation using the Plaxis program. The other values are in good agreement. These results validate the applicability of the Titan model when considering the partially drained condition.

Table 4.3: Material parameters

Footing/pile			
Radius	r	0.5	m
Volumetric mass	ρ	2500	kg/m^3
Bulk modulus	K	$12 \cdot 10^9$	N/m^2
Shear modulus	G	$9.6 \cdot 10^9$	N/m^2
Saturated soil			
Volumetric mass solid	ρ_s	2400	kg/m^3
Bulk modulus solid	K_s	$80 \cdot 10^6$	N/m^2
Shear modulus solid *	G_s	$48 \cdot 10^6$	N/m^2
Volumetric mass water	ρ_w	1000	kg/m^3
Bulk modulus water	K_w	$1000 \cdot 10^6$	N/m^2
Porosity	n	0.4	
Added mass	ρ_a	400	kg/m^3
Permeability *	k	$1 \cdot 10^{-3}$	m/s
* value will be changed			

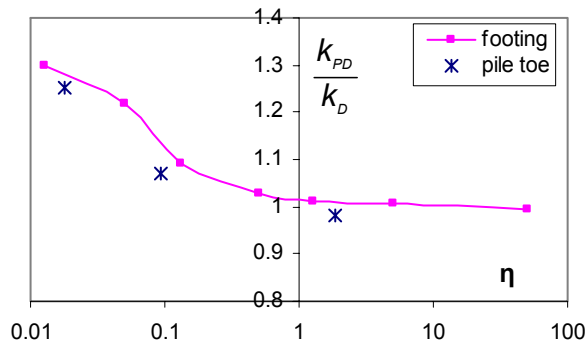


Figure 4.28: Dependence of spring stiffness on the drainage factor

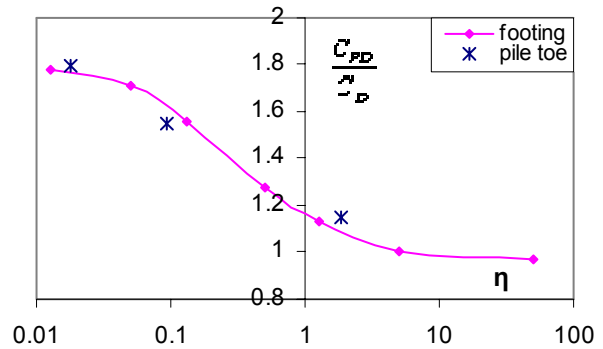


Figure 4.29: Dependence of dashpot coefficient on the drainage factor

Table 4.4: Comparison limiting cases of Titan and Plaxis

Parameter	case / limit	Titan	Plaxis	Diff.
stiffness (MN/m)	drained	128	119	7%
	undrained	170	158	8%
dashpot (kN.s/m)	drained	309	298	3%
	undrained	566	430	30%

Pile stiffness

Simulation of a pile embedded in a saturated homogeneous elastic soil medium is described here. The geometry of the pile-soil system is shown in figure 4.23b, except that the soil is homogeneous. The input parameters and drainage condition of the simulations were the same as those used in the footing simulations (table 4.3). The pile radius was 0.25m.

From the simulation results, the calculated pile tip force and pile tip motions were used to determine the spring stiffness and damping constant, in the same way as for the footing simulations. The determined results of three simulation cases with different values of drainage factor are shown in figures 4.28 and 4.29. They are in good agreement with the footing simulations. The response of

the pile tip is the same as the response of a footing with the same radius. The effect of the drainage condition on the stiffness and damping coefficient model for the pile tip is the same as that in the footing model.

4.3.4 Effect of different drainage condition on pile toe resistance

The effect of the drainage conditions on ultimate pile resistance at the time of maximum displacement is studied in this section. An end bearing pile was the object of the simulations. The pile measured 11m in length, of which 1m was embedded in the bearing soil layer. Two pile radii of 0.25m and 0.55m were chosen to have a large drainage factor range. The pile was modelled using a linear elastic model, where the material properties were the same as those for the footing simulation in table 4.3. The soil layers were modelled with the bi-linear model described earlier. The model parameters of the bearing capacity layer were chosen as typical for dense sand. A thin weak soil layer was placed along the pile shaft to minimise shaft resistance. The applied load was based on the Statnamic loading and is shown in figure 4.25. In this case, a large range of drainage factor values was achieved by varying the input soil properties (permeability, shear modulus) and the loading duration. The derived load-displacement curves were determined by subtracting the inertial force of the pile ($m \cdot a$) from the input Statnamic force, i.e. $F_{\text{soil}} = F_{\text{STN}} - m \cdot a$. The ultimate resistance was taken at the time of maximum displacement (approximately 10% of pile diameter).

Figure 4.30 shows the dependency of pile resistance on the dynamic drainage factor. The pile resistance in different partially drained conditions (F_{PD}) is normalised by that in a fully drained condition (F_D). At high drainage factor values (i.e. towards the drained side), the partial pile resistance is close to the fully drained value. Where the drainage factor value is low (i.e. towards the undrained side), the partial pile resistance is higher than the fully drained value. The maximum increment of the pile resistance is approximately 30%.

Figure 4.31 shows the ratio between excess pore pressure (compression) and total vertical stress under the pile toe at the time of maximum pile displacement with different drainage factor values. The ratio is close to zero towards the drained side. Towards the undrained side, the excess pore pressure may exceed 80% of the total vertical stress. The relationship between excess pore water pressure and the increase in ultimate pile resistance is shown in figure 4.32. When the excess pore water pressure less than 70% of total stress at the pile toe, its effect on a pile's ultimate toe resistance is very small (less than 10%). If the value of excess pore pressure exceeds 70% of total stress, its effect will increase significantly (up to 30% or higher).

It can be seen that the curve shown in figure 4.30 is very similar to that in figure 4.28. This suggests that the increment of pile resistance should be in relation to the stiffness increment. This seems reasonable, due to the soil model used in these simulations. The current soil models of the Titan code do not imply any dilatancy tendency of the soil. Excess pore pressure under the pile toe therefore remains in compression unless the pile rebounds as seen in figure 4.27. If the drainage factor decreases, i.e. the flow of pore fluid inside the soil mass is more difficult, the soil condition is closer to the undrained condition. At a certain value of the drainage factor, the soil nearly behaves in an undrained condition where any increment in the applied load is almost completely carried by the fluid stress (figure 4.31). Because the compressibility of the fluid is much lower than the soil, the stiffness of undrained material increases as shown in figure 4.25. Pile resistance also increases.

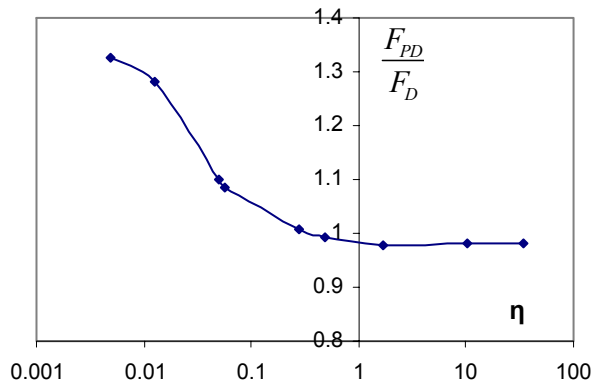


Figure 4.30: Dependence of ultimate resistance on drainage factor

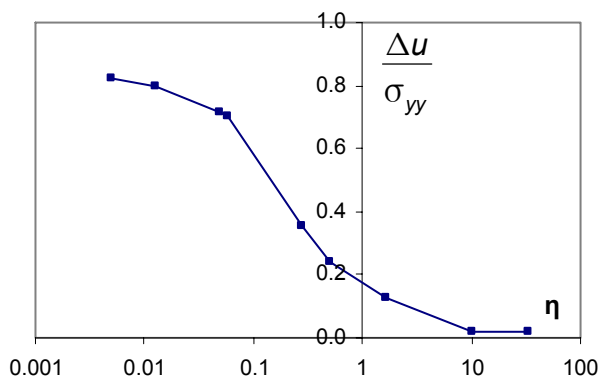


Figure 4.31: Dependence of excess pore pressure on drainage factor

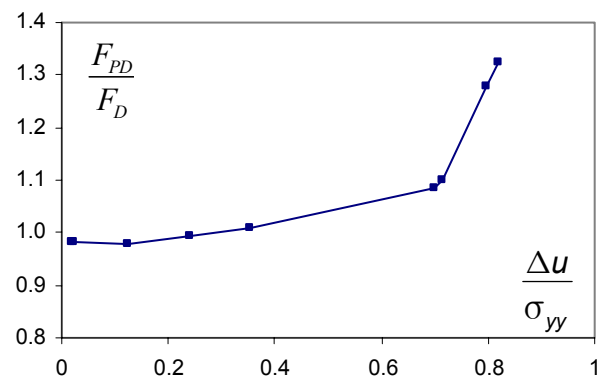


Figure 4.32: Relationship between excess pore pressure and pile tip resistance

4.3.5 Summary

The dependency of pile resistance on the soil's drainage condition has been indicated in this section. The most important finding is that the defined drainage factor (η) can be used to evaluate the effect of drainage condition.

In the case of the SDOF-model used to model pile behaviour, the dependency of the stiffness and damping coefficients on the drainage factor value has been shown. The coefficients determined from the elastic simulations using the Titan code at extreme drainage factor values show good agreement with those from the elastic simulations using the Plaxis program in undrained and drained conditions (table 4.4). This shows the validity of using the defined drainage factor, as well as the similarity between the Titan code's results and the analytical solution. It implies that the Titan code's results are validated, at least in the elastic range of soil behaviour. The results presented in figure 4.28 and 4.29 can therefore be used with confidence.

The demonstrated effect of drainage conditions on pile resistance (figure 4.30) can be seen with less confidence due to the limitations of the soil model in these simulations. The effect differs markedly from actual soil behaviour at failure as dilatancy is not taken into consideration. It does, however, confirm that the drainage condition affects pile resistance and that the magnitude of the effect can be evaluated using the value of the defined drainage factor. These conclusions are important in practice as they can be used to consider whether or not excess pore pressure affects pile resistance for a pile load test.

Chapter 5

Model pile load tests in the geotechnical centrifuge

5.1 Introduction

Small-scale model tests have long been used to study prototype behaviour in many geotechnical problems. Full-scale tests are costly, time-consuming, and are not always possible. In pile foundation engineering, model tests offer the opportunity to investigate many aspects of pile behaviour in conditions that can be controlled and reproduced (Sedran et al. 1998). With respect to investigating the relationship between mobilised resistance and the penetration velocity of a pile founded in sand, a large number of small-scale model tests have been reported. These have been reviewed in chapter 2. Within the framework of this thesis, a series of model pile load tests were carried out in a large calibration sand chamber and have been presented in chapter 3. However, all the experiments were performed in a calibration chamber at a 1-g condition. It is widely known that this situation does not resemble initial stress at a homologous point between the model and the prototype. Because the soil behaviour is highly non-linear and dependent on the stress level, soil behaviour in the chambers may not be the same in the prototype and findings from these experiments may also differ. As indicated by Altaee and Fellenius (1994), these test results have little relevance to the real behaviour of a pile-soil system in a full-scale prototype and the validity can only be ensured in the small-scale condition.

The geotechnical centrifuge can be used to overcome the limitation of 1-g devices. A model scaled using a factor N can be tested in the centrifuge, if centrifugal acceleration of N times higher than earth's gravity is applied to the sample. If so, the increment in vertical stress per scaled length in the model equals the increment of stress per length in the prototype. The initial stress in the model and prototype is therefore identical, and soil behaviour in a small-scale model will be almost identical to that in a prototype.

The number of centrifuge experiments described in literature that are relevant to the topic of this thesis is very limited (Allard, 1990; de Nicola and Randolph, 1994; Bruno and Randolph, 1999). Their tests focus on the behaviour of piles or surrounding sand during a dynamic pile load test, but none adequately consider the pore pressure response. Allard (1990) performed the experiments in dry sand. De Nicola and Randolph (1994) and Bruno and Randolph (1999) used silica flour instead of sand to reduce the permeability of the soil sample (although the similarity in constitutive behaviour of silica flour and sand is not fully warranted). Their paper does not mention the effect of excess pore pressure.

As indicated in chapter 4, the response of pore pressure may significantly affect a pile's mobilised resistance during a load test, and the effects depend on the sand's drainage condition and the generation of pore water pressure during a test. To obtain more knowledge about mobilised pile resistance during a rapid load test and to verify the numerical results, it was therefore decided to carry out a series of pile load test in the geotechnical centrifuge at Delft Geotechnics (GeoDelft), giving particular attention to modelling the pore pressure response. The test series and results are presented and discussed in this chapter.

The test series included a number of axial load tests on a model pile founded in a well-defined saturated sand bed. The loading rate of these load tests was varied. Simulation of a prototype static pile load test was the slowest load test; the fastest was simulation of a prototype rapid pile load test. Some intermediate loading rates were tested. The principle aims of the test series were:

1. To study the effect of the penetration rate on the resistance of a pile embedded in sand.
2. To obtain knowledge about excess pore pressure in the soil region around the pile tip, and its effect on resistance during a rapid pile load test.
3. To validate numerical results concerning the effects of excess pore pressure on pile resistance, as presented in chapter 4.

This chapter first details the testing programme, before giving the scaling rules applied for the tests. The test set-up is then described, and the possible effects of the set-up on test results are discussed. Test data with typical measurement results from each load test is presented next, and the chapter concludes by elaborating the test data to fulfil the aims of the test series.

5.2 Test programme

The test series included four centrifuge tests that differed in the initial density of the sand sample and the viscosity of the pore fluid. The first pilot test is not considered here, since major changes in the test set-up have been introduced since the test. Table 5.1 provides an overview of conditions during the remaining three tests, in both the geo-centrifuge situation as well as the equivalent prototype situation.

Table 5.1: Overview of the centrifuge tests

Parameters	Test 2	Test 3	Test 4
Relative density	54%	36%	65%
Material	sand	sand	sand
Pore fluid	viscous fluid	viscous fluid	water
Viscosity	265	292	1
Prototype			
Material	sand	sand	sand
Permeability	fine sand	fine sand	coarse sand

A number of static load tests (SLT) and rapid load tests (RLT) were performed in each centrifuge test. Figure 5.1 shows the sequence of load tests performed during each centrifuge test. For the sake of convenience, the term ‘centrifuge test’ is referred to as ‘the test’, and ‘load test’ means a particular pile load test performed in a centrifuge test.

During preparation, the pile tip was placed at a depth equivalent to 10 times the pile diameter ($10 \cdot D$) below the surface. The load test sequence shown in figure 5.1 was applied after the centrifuge had been spun to an acceleration level of 40-g. The test began with installation of the model pile. The first hydraulic actuator pushed the model pile deeper into the sand bed with a velocity of 10 mm/min and a total displacement of 11.3 cm ($10 \cdot D$). Once installation was complete, the pile tip reached a depth of $20 \cdot D$ and the first static load test (SLT) was carried out. Three sets of four rapid load tests (RLT) were then performed, followed by another SLT. The SLT was performed with a velocity of 0.00167 mm/s and a displacement of 10% of the pile diameter ($0.1 \cdot D$). The duration of the load was shorter for each set of four RLTs, which led to an increasing test loading velocity. Each of the four RLTs was carried out with increasing maximum

displacement (1%, 2% 5%, and 10% of the diameter). All load tests were displacement-controlled with the displacement pattern shown in figure 5.2. Extra RLTs were performed in tests 3 and 4, using the same imposed pile head displacement (0.1D) but different penetration rates. Details of the loading scheme of the tests are presented in Appendix 5a.

step	Test	RLT1	RLT2	RLT3
		slow	medium	fast
0	Installation			
1	SLTi-1			
2	RLTi - 1 - 0.01D	█		
3	RLTi - 1 - 0.02D	█		
4	RLTi - 1 - 0.05D	█		
5	RLTi - 1 - 0.1D	█		
6	SLTi-2			
7	RLTi - 2 - 0.01D		█	
8	RLTi - 2 - 0.02D		█	
9	RLTi - 2 - 0.05D		█	
10	RLTi - 2 - 0.1D		█	
11	SLTi-3			
12	RLTi - 3 - 0.01D			█
13	RLTi - 3 - 0.02D			█
14	RLTi - 3 - 0.05D			█
15	RLTi - 3 - 0.1D			█
16	SLTi-4			

i = 2, 3, 4 is the centrifuge test number

Figure 5.1: Loading scheme of the tests

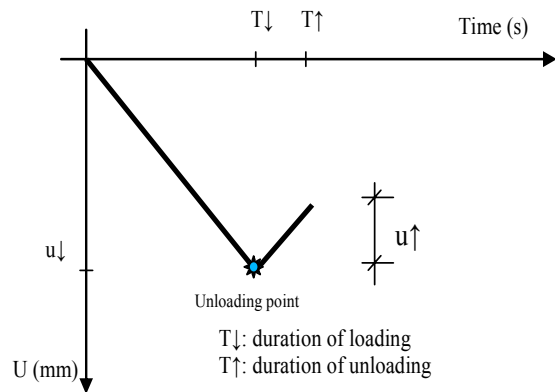


Figure 5.2: Displacement pattern of a rapid load test

5.3 Scaling rules

The standard scaling rules for centrifuge modelling have been well established in literature (*e.g.* Ko, 1988; Altaee and Fellenius, 1994; Sedran et al., 2001) and will not be repeated here. This section first introduces a set of scaling rules, which can be used to extrapolate the results from the test series into an equivalent prototype situation. Secondly, the main point of discussion is the treatments with pore fluid to correctly model the pore pressure response during a prototype rapid load test.

Centrifuge modelling is used to obtain identical stresses and strains in the model as in the prototype. Generally, if the scaling factor N is chosen for the length (the length quantities will be reduced N times), the acceleration level in the centrifuge model will be N times higher than in the prototype. Other quantities can be found from the dimensional analysis. The static and rapid pile load tests simulated in this test series were not the reduced scale model of a specific prototype case. The scaling rules introduced here are therefore used to extrapolate the test results into an equivalent prototype situation. Table 5.2 presents the scaling rules.

The requirements for pore fluid treatments are considered next. When considering the permeability

of a soil sample as defined by Darcy's law $k = \frac{Kg}{\nu}$ (where K is the intrinsic permeability of the

sand, g is the acceleration level, and ν is the viscosity of the pore fluid), it can be seen that permeability depends on the acceleration level. In the centrifuge environment, acceleration is increased N times as well as soil permeability. This implies that if the sand and water in the centrifuge and prototype are the same, the pore pressure dissipation process (consolidation) in the

centrifuge will occur N^2 times faster. This conflicts with the time scale presented in table 5.2. To compensate for this and to retain the same sand, a fluid with a viscosity N times higher than water should be used, as proposed by Fuglsang and Ovesen (1986). However, the viscosity of pore fluid used in this test series will differ somewhat from the requirement necessary to meet the aims of this study. This is discussed in the following paragraphs.

Results from chapter 4 have indicated that the significance of the effect of excess pore pressure on a pile's mobilised resistance during a rapid load test depends on the drainage condition of the soil, which is determined by the defined drainage factor:

$$\eta = \frac{GT}{g\rho R^2} k = \frac{GT}{\rho R^2} \frac{K}{\nu}$$

From the definition, the correlation between the value of the drainage factor in the model and in the prototype depends on the relative value of the permeability. If water is used in the centrifuge tests, the drainage factor will be N times smaller than in the prototype, since time scales with $1/N$. If a fluid with N times higher viscosity is used, the drainage factor will be identical.

The scaling factor $N = 40$ is chosen in this test series for the convenience of the test performance.

In the planning phase, it was proposed that the response of pore pressure and its effects in all relevant values of the drainage factor should be tested. However, the hydraulic actuator (plunger) was not fast enough to reach the low value of drainage factor ($= 0.01$). Taking the loading duration of the Statnamic test (100 milliseconds) as a representative loading duration for a rapid pile load test in prototype, the loading duration of the model test should be 2.5 milliseconds with a scaling factor of 40. In reality, the fastest loading duration of the plunger was approximately 7.5 milliseconds, slower than the requirement by a factor of three. To compensate for this, the viscosity of the pore fluid had to be increased three times (i.e. $3 \times 40 = 120$ times higher than water). With that increment however, the drainage factor in the fastest rapid test was close to 1, still too high to show any effects of excess pore pressure according to figure 4.30. It was therefore decided to increase the viscosity of the fluid to lower the drainage factor. In centrifuge tests 2 and 3, the viscosity of the fluid was chosen as approximately 300 times higher than the viscosity of water. In test 4, it was decided to use water as a pore fluid to achieve a nearly fully drained drainage condition. In this way, centrifuge tests 2 and 3 can be seen to simulate a prototype rapid load test on a pile founded in a sand, whose constitutive behaviour is similar to Baskarp sand but whose permeability is approximately 2.5 times lower ($300/120 = 2.5$). The same is true for centrifuge test 4, but permeability is 40 times higher. Table 5.3 presents the drainage factor values for every RLT with an imposed displacement of $0.1 \cdot D$. The values in the column ' η_{model} ' are the actual values in the model scale, and the values in the column ' $\eta_{\text{prototype}}$ ' are the values for an equivalent prototype RLT with a loading duration ($T = 40 \cdot T_{\text{model}}$), performed on a pile in Baskarp sand.

The viscous fluid chosen for this test series was developed at Delft Geotechnics (Allard and Schenkeveld, 1994). It is a mixture of water and sodium carboxy Methyl Cellulose. The viscous fluid can reach a viscosity up to 300 times the viscosity of water, while its physical properties are similar to those of water. Extensive laboratory tests have shown the similarity in constitutive behaviour between a sand specimen saturated with viscous fluid and a sand specimen saturated with water (Allard et al. 1994).

Table 5.2: The scaling rules

Parameter	Model	Prototype
Length and displacement	1	N
Area	1	N ²
Volume	1	N ³
Time	1	N
Acceleration	N	1
Velocity	1	1
Density of soil	1	1
Mass	1	N ³
Force	1	N ²
Stress	1	1
Strain	1	1

Table 5.3: Drainage factor in the model and prototype

	Test No	ld (%)	G (MPa)	T_model (s)	viscosity ()	k0_water (m/s)	ko_fluid (m/s)	η_model (-)	η_prototype ()
Test 2	RLT2-1-0.1D	54	39.51	0.0529	265	8.85E-04	3.34E-07	2.19	14.49
	RLT2-2-0.1D	54	39.51	0.0203	265	8.85E-05	3.34E-07	0.84	5.56
	RLT2-3-0.1D	54	39.51	0.0100	265	8.85E-05	3.34E-07	0.41	2.74
Test 3	RLT3-1-0.1D	36	20.68	0.0529	292	8.85E-05	3.03E-07	1.04	7.58
	RLT3-2-0.1D	36	20.68	0.0203	292	8.85E-05	3.03E-07	0.40	2.91
	RLT3-3-0.1D	36	20.68	0.0100	292	8.85E-05	3.03E-07	0.20	1.43
Test 4	RLT4-1-0.1D	65	51.04	0.0529	1	8.85E-05	8.85E-05	748.52	18.71
	RLT4-2-0.1D	65	51.04	0.0203	1	8.85E-05	8.85E-05	287.24	7.18
	RLT4-3-0.1D	65	51.04	0.0100	1	8.85E-05	8.85E-05	141.50	3.54

5.4 Experimental set-up

This section describes components of the test set-up, preparation of the sand bed, and the instrumentation used in the test. The effects that the set-up may have on test results are considered at the end of the section.

5.4.1 Test set-up

Figures 5.3 and 5.4 show the complete test set-up. The load tests were carried out in four stacked Ø600 mm steel sand fill containers, which were mounted on an assembly plate. A loading frame with plungers was mounted above the sand fill containers. The model pile was connected to the plungers. The various components of the set-up will be described briefly in the following paragraphs.

Sand fill container

The sand fill container measured 793 mm in height, and included four steel cylindrical rings with an inner diameter of 589 mm. One had a height of 100 mm, the remaining three measured 231 mm in height (see figure 5.3). These cylindrical containers were mounted onto one another by means of watertight connections using O-seals. In the lowest of the three containers, watertight feeds were made for transducer cables inside the containers.

Loading system

The pile loading system consisted of two hydraulic actuators (plungers) that were connected in series. The first and largest plunger was fixed on the loading frame, and was used to install the pile to its starting point before the load tests began. The second smaller plunger was the fast loading plunger, and was fixed to the plunger rod of the first plunger. This second plunger was used to perform the model pile load tests. The pile was attached to the small plunger. The two plungers were mounted in the loading frame, which was connected to the top of the sand fill container. A photograph of the loading system can be seen in figure 5.5.

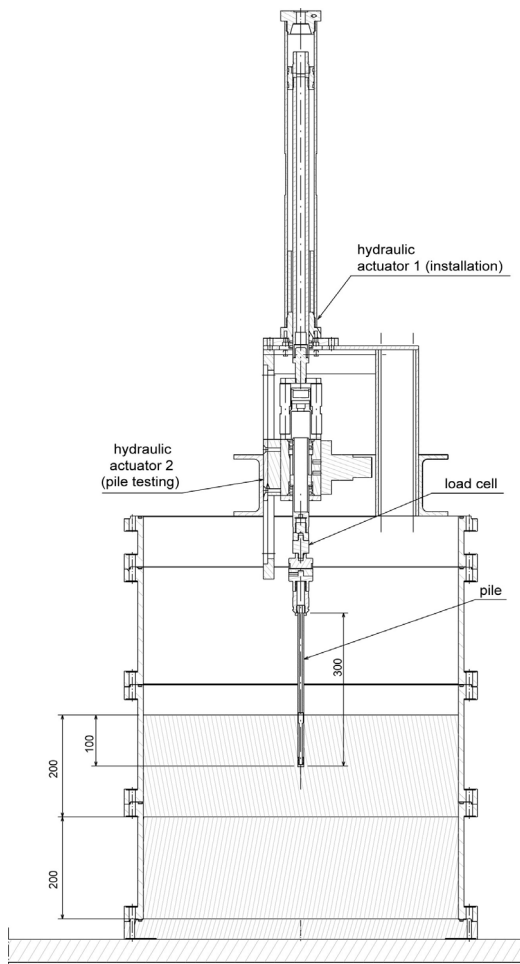


Figure 5.3: Sketch of centrifuge test set-up



Figure 5.4: Photograph of centrifuge test set-up



Figure 5.5: The loading system

The model pile

The model pile was made of steel, with a length of 300 mm and a diameter of 11.3 mm. The model pile weighed 570 grams. A load cell was placed on the model tip to measure pile tip resistance during the tests. The pile tip was also equipped with a pore pressure transducer to measure pore pressure directly below the pile tip. For this purpose, a small hole measuring 5 mm in diameter was made to accommodate the transducer. A photograph of the model pile is shown in figure 5.6.



Figure 5.6: The model pile

5.4.2 Soil material

Soil properties

Baskarp sand with a $d_{50} = 130 \mu\text{m}$ was used for the tests. It is widely used for laboratory tests, and its soil parameters have been reported in a variety of literature (e.g. Allard et. al. 1994; Mangal, 1999). The grain size distribution curve of the sand used is shown in figure 5.7. The sand's basic soil parameters, determined from the GeoDelft laboratory test, are presented in table 5.4.

Table 5.4: Properties of Baskarp sand.

Parameter	Value	Dimension
Density grains	2,647	kg/m^3
d_{10}	90	μm
d_{50}	130	μm
d_{90}	200	μm
Min. porosity	34	%
Max. porosity	46.9	%
Permeability at min. porosity	$6.5 \cdot 10^{-5}$	m/s
Friction angle at $R_D=50\%$ ($n=40\%$)	41	Degr.

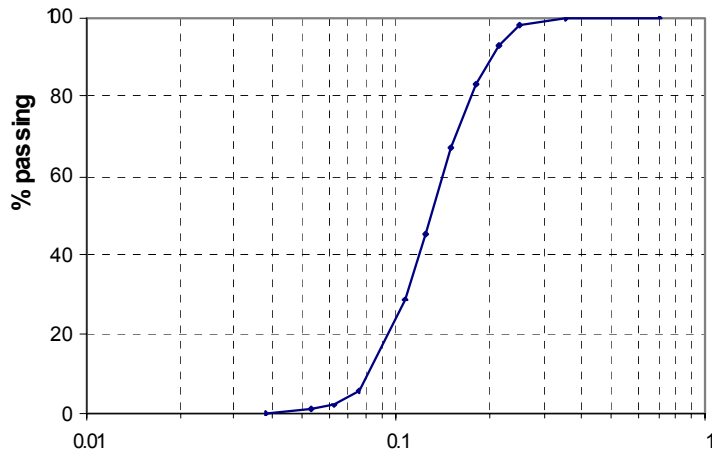


Figure 5.7: Grain size distribution of Baskarp sand

Sample preparation

The following steps were followed to prepare the sand sample with a homogenous body in a pre-determined density. The container was first filled with de-aerated water and the pre-determined amount of wet sand was pluviated under the water surface. The water level in the cylinder was sufficient and the sand was softly blown into the water in an upwards direction to slow the grains to the equilibrium speed. A very loose sand sample was created. The loose sand sample was then compacted. A loaded permeable plate was placed on the surface of the sand sample, the complete container was lifted a few centimetres above the floor, and the container was released. The impact caused by falling compacts the sand sample. By repeating the process and carefully registering the achieved height, the predetermined relative density (D_r) could be achieved. When the desired density was reached, the top layer was carefully removed and flattened. The preparation method has been described in detail by Van der Poel and Schenkeveld (1998). It is possible to prepare a soil sample with a predefined relative density within 1-2% accuracy using this method.

In those cases where viscous fluid was used, the saturated water in the prepared sand sample was replaced by the viscous fluid. The viscous fluid was first slowly positioned above the saturated sand sample. A vacuum was then applied at the bottom of the container. The vacuum pressure extracted the water and the viscous fluid penetrated into the sand sample. As the colour of the viscous fluid was purple, a colour change was observed in the drainage pipe once it reached the bottom of the sand sample. The viscosity of the exiting fluid was measured, and the saturation process was stopped when the measurement confirmed the value of viscosity. This saturation process was described in detail in Allard et al. (1994).

5.4.3 Measurement set-ups

The following parameters were measured as a function of time during each test:

- V_PL_KL: Displacement of the small plunger. This was measured using a transducer, which was an integral part of the servo-control system and was used to obtain the load-displacement characteristics in static and rapid pile loading.
- F_PL_BK: The load on the pile head. The force was measured by a load cell, which was mounted at the pile head. This parameter was required to obtain the load-displacement characteristics of the pile head.
- F_PL_OK: The force on the pile tip. The force was measured by a specially-constructed flat cone tip equipped with a load cell. This parameter was required to obtain the load-displacement characteristics of the pile tip.

- WSM_PL: Pore pressure beneath the pile tip. The pore pressure immediately under the pile tip was measured using a pore pressure transducer integrated into the pile tip.
- WSM 1 – 4: Pore pressure in the sand bed. The pore pressure was measured at four different positions beneath the pile tip level. The transducers provided information about pore pressure variation as a function of time during a load test. Figure 5.8a and 5.8b shows the location of the four pore pressure transducers with respect to the pile tip location at a depth of 20D (226 mm) below the sand surface and their installation in the container.

All the measurement devices were calibrated before each centrifuge test. The load cell was a miniature force transducer U9B made by HBM Inc., with a measurement range of 0-10 kN. The calibration in this range showed a maximum absolute fault less than 0.007 kN. The pore pressure transducers were high performance pressure transducers produced by Druck Ltd. The pore pressure transducer in the pile tip was a PDCR 42 Druck type, with a maximum range of 2000 kPa. The calibration up to 1000 kPa showed the maximum fault to be less than 0.3 kPa. The pore pressure transducers in the sand bed were a PDCR 82 Druck type, with a maximum range of 1000 kPa. It was calibrated up to 700 kPa and showed the maximum fault to be less than 0.26 kPa.

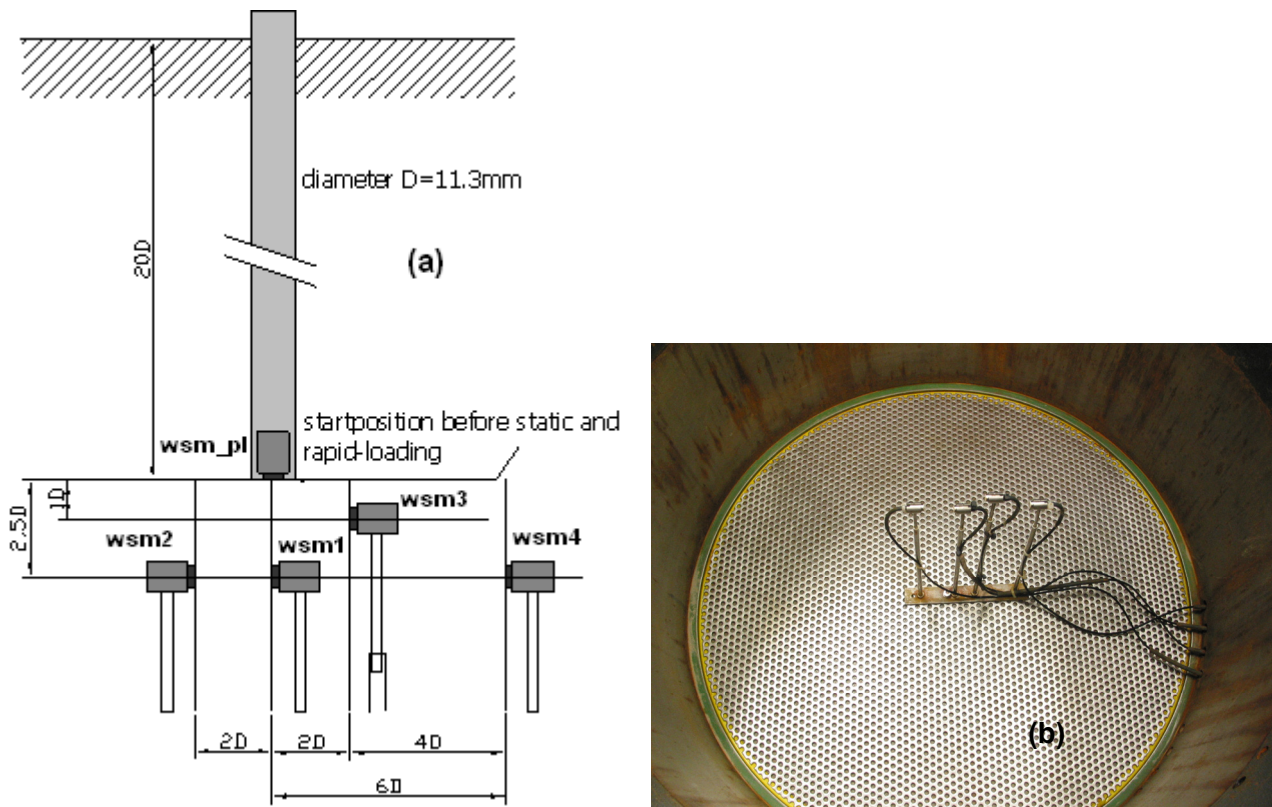


Figure 5.8: (a) Positions of pore pressure transducers; (b) installation.

5.4.4 Discussion of the set-up effects

Some aspects of the model test set up may have an undesirable effect on the test results. For the set-up that has been described, the following items may be capable of causing such effects and are discussed below in the same order:

- Grain size of the sand
- Size of the sand fill container
- Dimension of the pore pressure transducers

- Soil condition changes due to installation and the load tests
- Difference between the model load test and the prototype rapid load test.

The grain size used for the centrifuge modelling corresponds to those N times larger in the prototype. This may induce differences in behaviour between the model and the prototype, due to the dependence of the failure mechanism (defined in terms of the width and extent of the shear band) on the grain size. However, scaling the sand grain size in the centrifuge model would require using the particle size of silt or clay, which has significantly different strength characteristics. In most cases, the same soil is therefore used in the model and in the prototype. Ovesen (1981) performed a series of pull-out tests on model anchors where the ratio of the anchor diameter to the mean grain size of sand was from 25 to 128. No effect was found on grain size. Yamaguchi et al. (1977) studied the effect on the bearing capacity of the footing. The ratio of the footing diameter to the mean grain size was varied from 36 to 286, but no effect was observed. Phillips and Valsangkar (1987) performed a series of centrifuge tests to study the grain size effects on penetration resistance. In their tests, the acceleration level was from 20g to 80g, and the ratio between the probe diameter and mean grain size was from 10 to 58. They found that the effect of grain size is observed if the ratio of probe diameter to mean sand grain size is smaller than 20. In this study, the mean grain size of Baskarp sand D_{50} was 0.13 mm (table 5.4) and the model pile diameter was 11.3 mm. This resulted in a ratio of more than 86. The grain size effect was not present in the centrifuge tests.

In the model test, the soil sample volume was limited by the size of container. This differed from the prototype situation, where the soil was an infinite half-space. The difference may have caused unexpected boundary effects on the test results. The significance of these effects depends on the size of container, the diameter of the penetration object, and the type of test carried out. For these model tests, the major boundary effects were: (1) effect of the container size to resistance of the model pile; (2) effect of the reflection of stress wave from the container walls.

The first effect generally exists when a penetration test is carried out in a narrow container, but it can be negligible at a certain value of the ratio between the container diameter and the model pile diameter (diameter ratio). From their calibration chamber tests, Parkin and Lunne (1982) showed that the effect is more pronounced as the density of the soil sample increases. They suggested that the diameter ratio between a container diameter and a model pile diameter should not be below 50 to eliminate the effect at all densities. Gui (1995) suggested that a diameter ratio value of 40 is enough to ignore the boundary effect, based on his centrifuge test on silica Fontainebleau sand. Other authors have also suggested different values for the diameter ratio, but the value of 50 is generally accepted. In this test, the container's inner diameter was 589 mm and the pile diameter was 11.3 mm, which makes the diameter ratio larger than 52. The container size in this case will therefore have a negligible effect on the resistance of the model pile.

The second effect is related to a dynamic model test where stress waves are generated. These waves radiate from the model pile into the sand sample and reflect back from the container walls. The wave reflection phenomenon does not occur in the prototype since the soil field is infinite. For the container used in this test, the effect may be more significant as the vertical container wall was circular. This facilitated the reflection, and focused the reflected waves to the centre of the container where the model pile was placed. Solutions to reduce the effect include using a type of wave-absorbent material along the container walls, or enlarging the size of the container so that the test is finalised before the reflection waves reach the pile. However, wave reflection in this case is not expected to be significant due to the type of tests performed. Wave reflection is known to be more important for low amplitude vibration tests, while in this case of pile load testing there was

large plastic deformation and sliding between pile and soil, which reduced the importance of (elastic) wave transmission from the pile into the surrounding soil. Moreover, because all the load tests in this test series were constant rate of penetration tests, the vibration may have been minimised. To check the existence of wave reflection during the RLTs, measured pore pressure signals were used with the assumption that if wave reflection was significant, this would be seen in the signal of the pore pressure transducers. Later descriptions will show that there was no evidence of wave reflection for a RLT with a penetration rate up to 80 mm/s. It only seems to be observed in the fastest tests ($v \approx 300$ mm/s), but the tendency of resistance development and pore pressure variation are the same with slower RLTs. It can therefore be concluded that the reflected waves are small and their influence is negligible in the test set-up.

The dimension of the pore pressure transducer is relatively large in comparison to the pile diameter and the space from the pile tip to their location of the pore pressure transducers (figure 5.8), which is different from the in-situ case where the dimension of the transducer is very small in comparison with the pile dimension and the soil field. The sizable of these transducers might be the cause for the unusual measured response of pore pressure at the location of the transducer wsm1 during the rapid load test as discussed later in the section 5.5.3.

Due to the installation of the pile and the load tests the soil condition near the pile tip would be changed and the discussion on the effect of this change will be presented in sections 5.5.1 and 5.5.3.

It is presented in section 5.2 that the model rapid load tests in this test series are displacement control test, which is different from the practical where the test is load control test. However, as presented in section 5.5.2, the fastest model rapid load test (RLTi – 3 – 0.1D) is very similar to the load control test and it shows the same behaviours as other performed RLTs. Therefore, it is believed that the findings from this test series are not affected by the difference between the model load test and the prototype rapid load test.

5.5 Test results

This section presents an overview of the measured results from the model pile load test. The first part gives typical results of measured forces and motions of the model pile during the load tests. The second part shows the typical measured response of pore pressure during rapid load tests. All results are presented in the model scale.

For the sake of convenience, the following terms and parameters will be used throughout the chapter.

- Pile head force (F_{head}) is a directly measured parameter.
- Pile tip force (F_{tip}) is also a directly measured parameter.
- Shaft force (F_{shaft}) is derived from the difference between F_{head} and F_{tip}
- The name used for a static load test will be SLTi – 1, which is a first static load test (step 1 in Figure 5.1) of the centrifuge test i ($i = 2, 3, 4$)
- The name used for a rapid load test will be in the form of RLTi – 3 – 0.02D, which is the third rapid load test with the imposed pile head displacement of 2% of pile diameter (step 13 in Figure 5.1) of the centrifuge test i .

5.5.1 Static load test (SLT)

The typical measured forces and displacement of the model pile in a static load test are shown in figure 5.9. The force-displacement curves are shown in figure 5.10. The results are taken from the first static load test in test 3, where viscous fluid was used as the pore fluid and the initial density of the sand bed was 35%. The SLT was performed with a velocity of 0.00167 mm/s and a displacement of 10% of pile diameter (0.1*D). Figure 5.10 shows that most of the mobilised soil resistance of the model pile is end-bearing resistance, which is approximately 80% of the pile's total resistance. The total shaft resistance reaches an ultimate value at relatively small displacement of the model pile (approximately 3% of pile diameter), whereas the ultimate tip resistance requires larger displacement (about 7% of pile diameter).

As described in section 3.3, four SLTs were carried out in each centrifuge test. A comparison between them gives information about the change in soil condition due to RLTs performed in between. All the force-displacement curves of the SLTs in centrifuge tests 2, 3, and 4 are shown in figures 5.11, 5.12, and 5.13 respectively. Some deviation can be seen between the curves in each figure, and the later SLT shows generally higher resistance than the previous SLT. Because the four RLTs were performed between two consecutive SLTs, densification of the sand due to these RLTs can be expected. An investigation using the same Baskarp sand by Dijkstra et al. (1997) indicated that there is densification of sand around the pile as the pile penetrates. It is therefore believed that the deviation is caused by densification of the sand due to the RLTs performed in between. This explanation is strengthened by the fact that the largest deviation is observed in test 3. The initial density of the sand bed was lowest ($I_D = 35\%$) in this test, thus the highest densification would be expected. Also, the deviation in test 2 ($I_D = 53\%$) is less, and similar deviation is observed in test 4 where the initial density was highest ($I_D = 65\%$). An exception is seen with the curve known as SLT4-1 in figure 5.13, where the deviation is slightly higher than for other SLTs in test 4. The reason is not clear. Nevertheless, this exception does not affect the research results since the comparisons are made between the resistance of a RLT and its closest SLT. The result of this test is therefore of limited use, as shown in later sections.

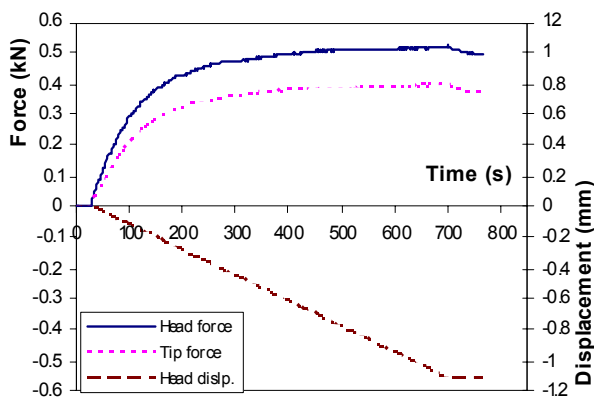


Figure 5.9: Measured forces and displacement in a static load test (SLT3-1)

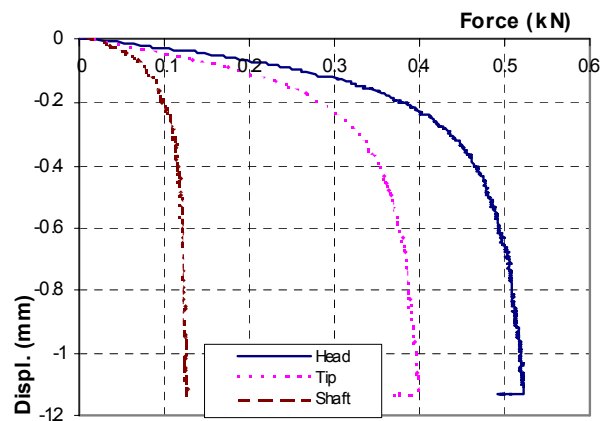


Figure 5.10: Force-displacement curves (SLT3-1)

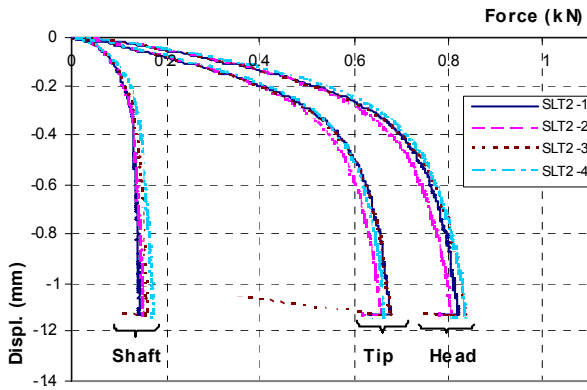


Figure 5.11: Force-displacement curves of the SLTs in test 2

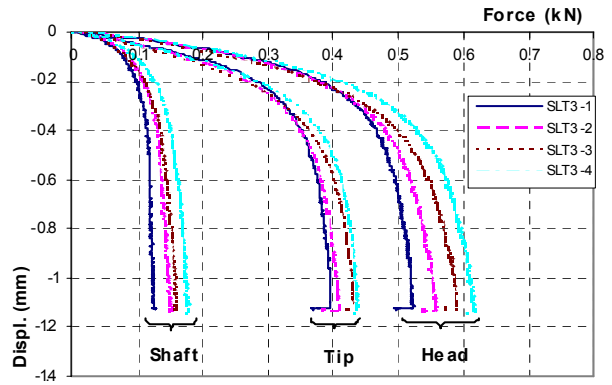


Figure 5.12: Force-displacement curves of the SLTs in test 3

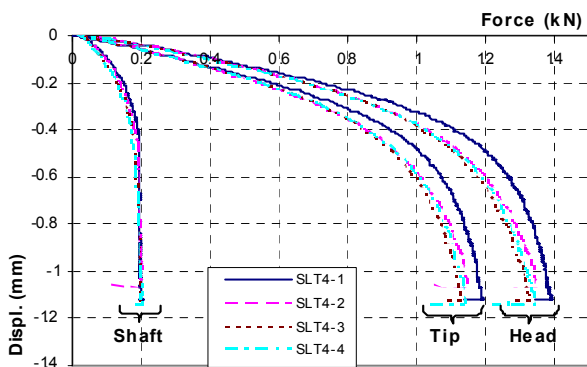


Figure 5.13: Force-displacement curves of the SLTs in test 4

5.5.2 Rapid load tests (RLT)

This section presents the RLT measurement data. During one centrifuge test, twelve RLTs were carried out with different imposed displacement and penetration rates. Data measured during the RLTs are generally very similar if the imposed pile head displacements were the same. From the RLTs with the same displacement, only the data of a representative RLT are therefore introduced. The representation includes the measured forces, displacement during a RLT, pile velocity and acceleration derived from the measured displacement, and the load-displacement curves of the RLT. It shows that RLT results with a penetration rate smaller than 0.08 m/s are not affected by the inertial force (i.e. the inertial force is very small in comparison with the pile head force) and that tests with higher rates are very similar to the prototype rapid load test. The effect of different pore fluid usage on the RLT data is discussed at the end of this section.

RLT with a displacement of 1% pile diameter

Typical measured parameters during a RLT with an imposed pile head displacement of 0.113 mm ($0.01 \cdot D$) as a function of time are shown in figure 5.14. These are the results of test RLT3-1-0.01D where the imposed velocity was ≈ 0.012 m/s. The pile head velocity and acceleration shown in figure 5.15 are derived from the measured displacement. The pile velocity varies somewhat during the test's loading time because of how the loading plunger responds to small displacement at a high loading velocity. The acceleration of the pile is in the magnitude of 1-g, thus the magnitude of inertial force (6 N, with a pile mass of 0.57 kg) is negligible to the maximum pile head force (250 kN). The force-displacement curves are shown in figure 5.16. The resistance of the model pile does not reach the ultimate value due to the small imposed displacement.

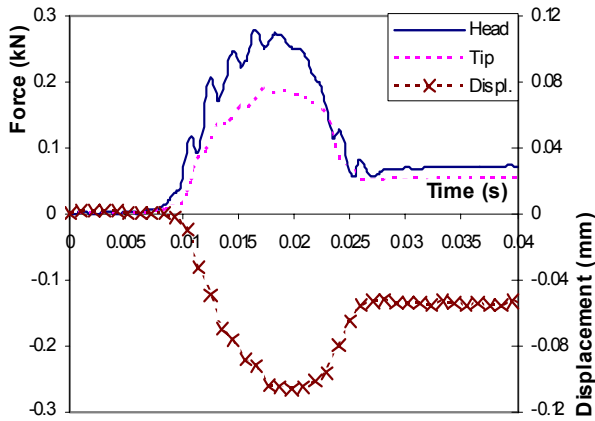


Figure 5.14: Typical measured parameters in a RLT with a displacement of $0.01 \cdot D$.

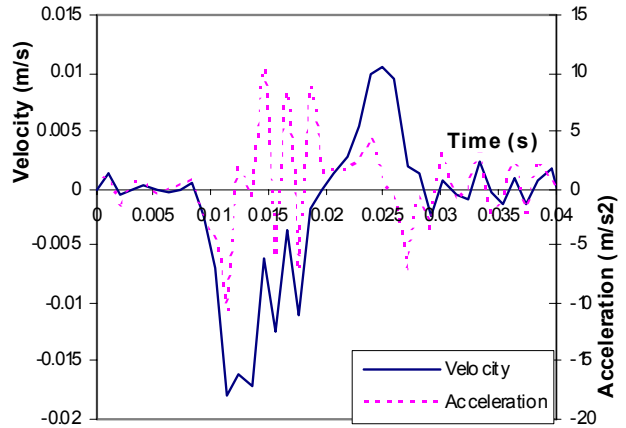


Figure 5.15: Typical derived velocity and acceleration in a RLT with a displacement of $0.01 \cdot D$.

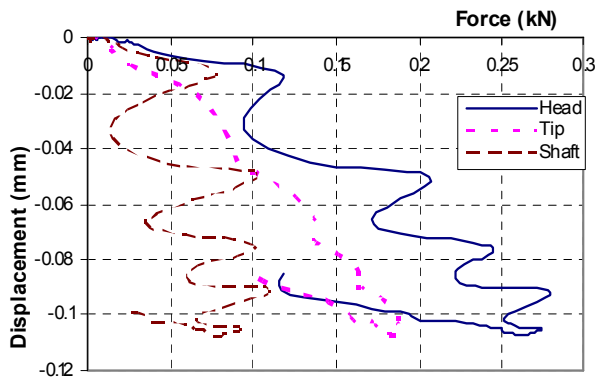


Figure 5.16: Typical load-displacement curves of a RLT with a displacement of $0.01 \cdot D$.

RLT with a displacement of 0.02 pile diameter (RLT03 – 3 – $0.02D$)

Typical results of a RLT with an imposed pile head displacement of $0.02 \cdot D$ are shown in figures 5.17, 5.18, and 5.19. These results are taken from the test RLT03 – 3 – $0.02D$ where the imposed penetration rate was 0.0251 m/s. In general, the results are similar to those of the RLT with a displacement $0.01 \cdot D$. The pile head displacement is still too small to fully mobilise resistance.

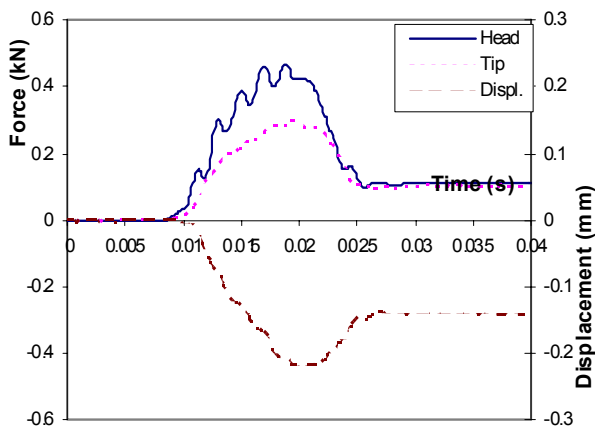


Figure 5.17: Typical measured parameters in a RLT with a displacement of $0.02 \cdot D$.

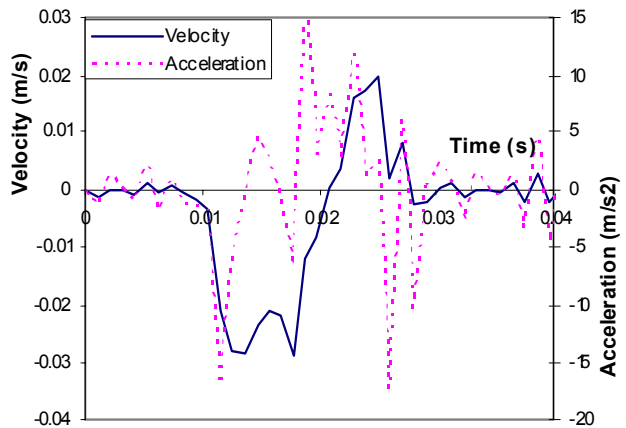


Figure 5.18: Typical derived velocity and acceleration in a RLT with a displacement of $0.02 \cdot D$.

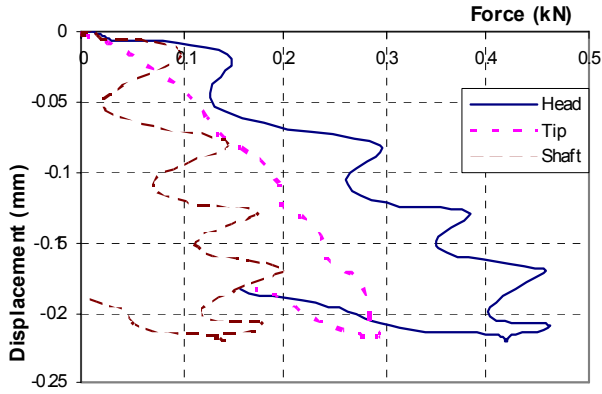


Figure 5.19: Typical load-displacement curves of a RLT with a displacement of $0.02 \cdot D$.

RLT with a displacement of 0.05 pile diameter (RLT02 – 2 – 0.05D)

Typical results of a RLT with a pile head displacement of $0.05 \cdot D$ are shown in figures 5.20, 5.21, and 5.22. These results are taken from the test RLT02 – 2 – 0.05D where the imposed penetration rate was 0.0305 m/s. These figures show that the displacement and velocity patterns are very similar to those prescribed. If the displacement patterns of the RLTs with imposed displacement of $0.01 \cdot D$ and $0.02 \cdot D$ (as presented above) are compared, this implies that the loading plunger requires larger displacement to perform properly. Shaft resistance reaches its ultimate value during the test, but displacement is not high enough to reach the ultimate toe resistance value.

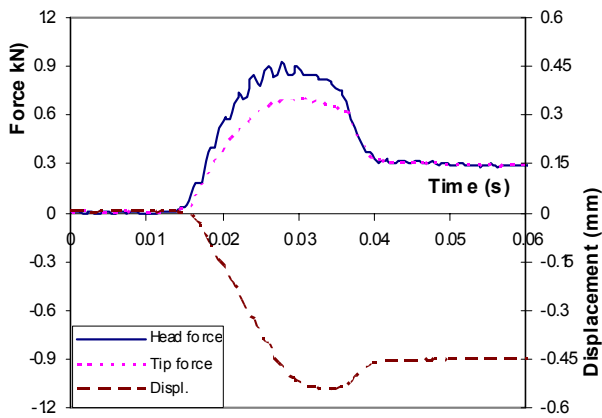


Figure 5.20: Typical measured parameters in a RLT with a displacement of $0.05 \cdot D$.

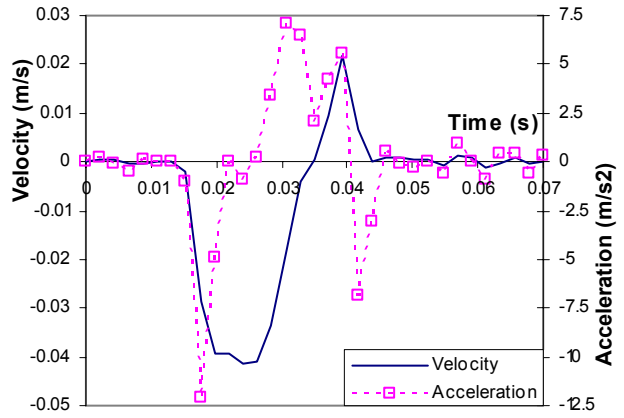


Figure 5.21: Typical derived velocity and acceleration in a RLT with a displacement of $0.05 \cdot D$.

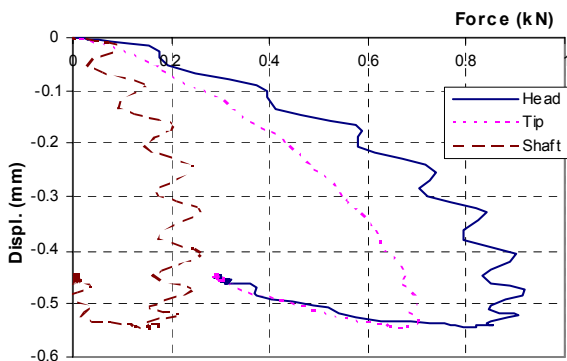


Figure 5.22: Typical load-displacement curves of a RLT with a displacement of $0.05 \cdot D$.

RLT with a displacement of 0.1 pile diameter, velocity slower than 0.08 m/s

Typical results of a RLT with a pile head displacement of $0.1 \cdot D$ and pile velocity smaller than 0.08 m/s are shown in figures 5.23, 5.24, and 5.25. These results are taken from the load test RLT2 – 2 – 0.1D where the imposed penetration rate was 0.061 m/s. The actual velocity is seen to be somewhat higher than proposed, but the pattern is in good agreement with that expected. As shown in figure 5.23, the displacement pattern is similar to the proposed pattern presented in figure 5.20. This implies that RLT performance is well-controlled up until this penetration rate and that displacement and velocity patterns are the same as those expected. Acceleration is in the magnitude of 1-g, hence the inertial force is still small in comparison with the pile head force. Shaft resistance reaches its ultimate value during the test. The ultimate value of tip resistance does not seem to be reached completely as no clear failure mode is seen. This type of pile tip resistance-displacement behaviour is only observed in centrifuge tests 2 and 3 where viscous fluid is used as the pore fluid. It is not seen in centrifuge test 4 where water is used as the pore fluid. This is discussed later in this section.

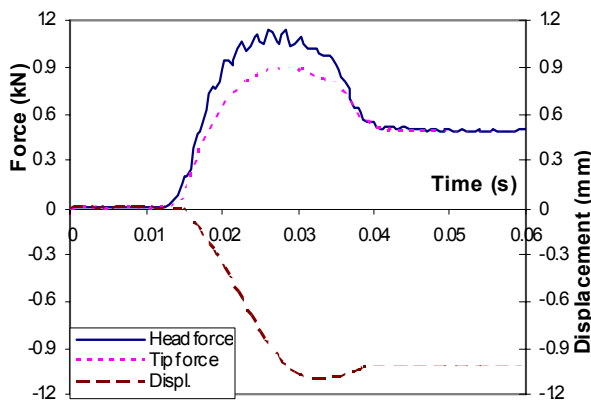


Figure 5.23: Typical measured parameters in a RLT with a displacement of $0.1 \cdot D$; velocity < 0.08 m/s

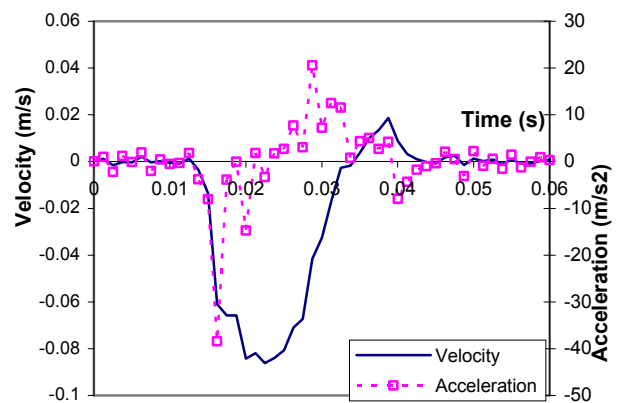


Figure 5.24: Typical derived velocity and acceleration in a RLT with a displacement of $0.1 \cdot D$; velocity < 0.08 m/s.

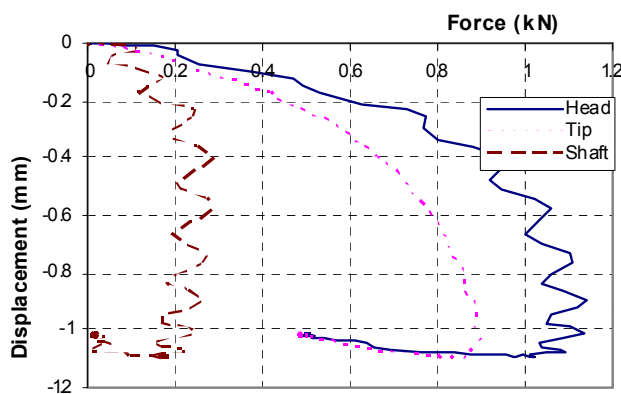


Figure 5.25: Typical load-displacement curves of a RLT with a displacement of $0.1 \cdot D$; velocity < 0.08 m/s

RLT with a displacement of 0.1 pile diameter, velocity higher than 0.1 m/s

This RLT was intended to be the highest rate test with a penetration rate of 125.6 mm/s and a loading duration of 9 ms. However, after revising the test data it could be seen that the actual velocity was much higher (≈ 300 mm/s) and the loading duration was shorter (≈ 7 ms). Technical examination of the loading system showed that the loading plunger did not act in accordance with the proposed loading velocity. This probably exerted an impact load on the pile head at the highest

possible velocity. Evidence of impact includes vibrations in the pile head force signal, and rebound in the pile head displacement. It is also manifested by the fact that the actual penetration rate and displacement pattern of this RLT are markedly different from those proposed, as shown in the next paragraph.

Figure 5.26 presents typical measured forces and displacement during the RLT with high velocity as a function of time. The pile head response shows oscillations in the pile head force signal and the rebound of the loading plunger on the pile head. The maximum pile head displacement is approximately 1 mm, which is smaller than proposed. These observations denote that this RLT was out of control. However, the behaviour of the pile tip force seems to be very realistic (see dotted line in figure 5.26). Figure 5.27 shows the values of velocity and acceleration as a function of time. A maximum velocity as high as 0.3 m/s is reached at the steady state of pile penetration. This value is in the same magnitude of pile velocity as during a prototype rapid load test (≈ 0.5 m/s). In contrast to other slower load tests, the acceleration of this RLT is relatively high and the inertial force is comparable with the pile head force at the start of the test (see figure 5.28). The loading duration of the test is approximately 7ms (equal to the loading duration of $40 \times 7 = 280$ ms in the prototype scale), which results in a test wave number (wave length / pile length) of approximately 120. This falls within the usual range of the rapid pile load test, according to the classification criterion proposed by the Japanese research group on rapid pile load test method (Kusakabe et.al. 1998). Therefore, instead of all the RLTs being the proposed constant rate of penetration load test (displacement control test), this fastest RLT was in fact closer to an impact load test (force control test). It can be regarded as a reduced scale of the prototype rapid load test in the equivalent soil condition.

The load-displacement curves of the RLT are presented in figure 5.28. There is extreme over-valuation in shaft resistance at the start, which is caused by vibrations in the pile head force signal and an incorrect value for pile shaft resistance. The development of tip resistance is realistic and similar to the results of a slower RLT (e.g. that shown in figure 5.25), where test performance was well-controlled.

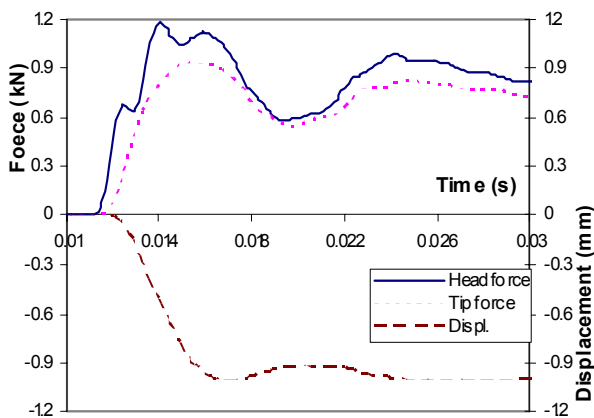


Figure 5.26: Typical measured parameters in a RLT with a displacement of $0.1 \cdot D$; velocity > 0.08 m/s (RLT2 - 3 - 0.1D)

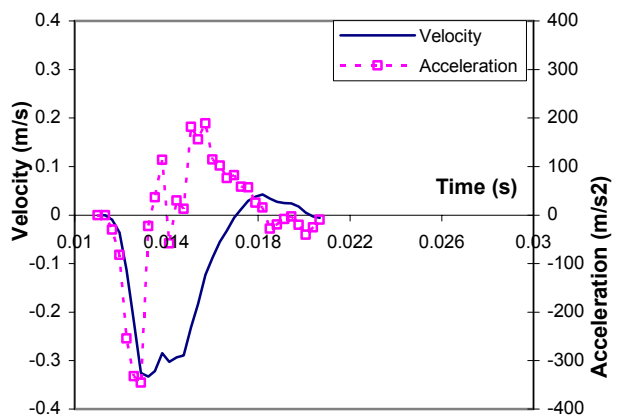


Figure 5.27: Typical derived velocity and acceleration in a RLT with a displacement of $0.1 \cdot D$; velocity > 0.08 m/s. (RLT2 - 3 - 0.1D)

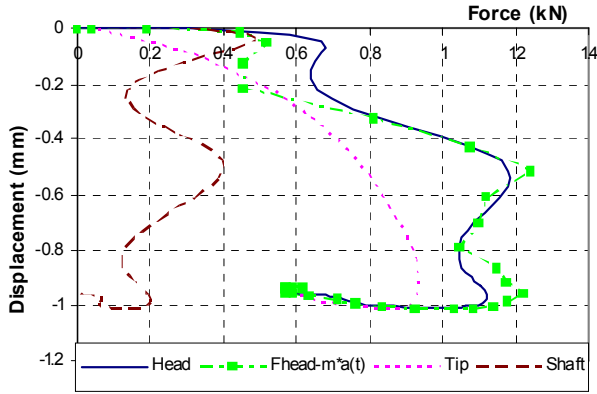


Figure 5.28: Typical load-displacement curves of a RLT with a displacement of $0.1 \cdot D$; velocity > 0.08 m/s (RLT2 – 3 – 0.1D)

Effect of different pore fluid usage

RLT data presented earlier are taken from centrifuge tests 2 and 3, where viscous fluid was used as the pore fluid. This section shows that the use of water as a pore fluid in test 4 does not affect the general behaviour of the model pile during a RLT, but does affect the failure mode in the tip force-displacement curve. The results of RLT4 – 3 – 0.1D are introduced in figures 5.29, 5.30, and 5.31. This RLT was performed in the same way as RLT2 – 3 – 0.1D (figures 5.26 to 5.28). Their results can therefore be compared to assess the effects. The general behaviour of the model pile shown in figures 5.29 to 5.31 is very similar to that shown in figures 5.26 to 5.28, apart from the pile tip force-displacement response. The tip force-displacement curve in figure 5.31 clearly shows fully-plugged failure mode, but is not seen in figure 5.28. This difference may be induced by the difference in excess pore pressure between these two RLTs, caused by different pore fluid usage as pointed out later in section 5.6.2.

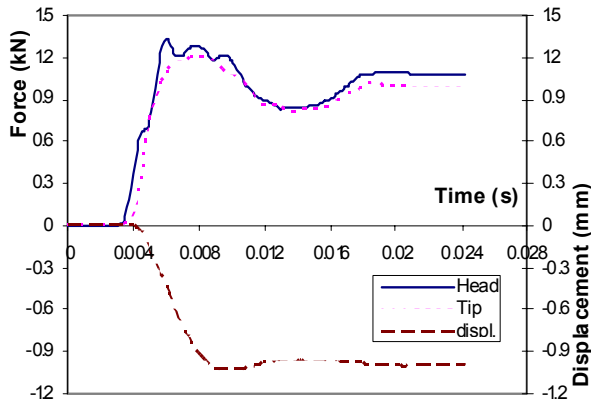


Figure 5.29: Example of measured parameters in test 4 (water as pore fluid; RLT4 – 3 – 0.1D)

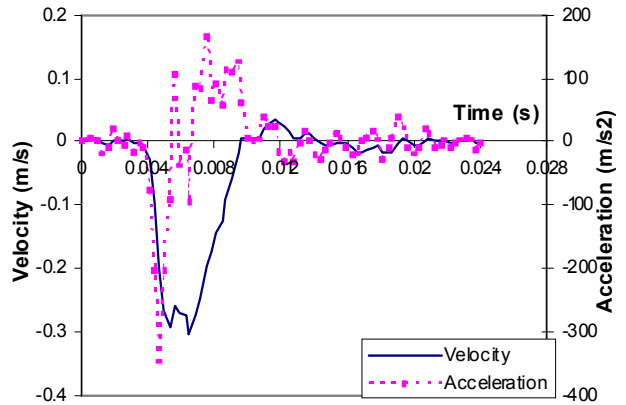


Figure 5.30: Example of derived velocity and acceleration in test 4 (water as pore fluid; RLT4 – 3 – 0.1D)

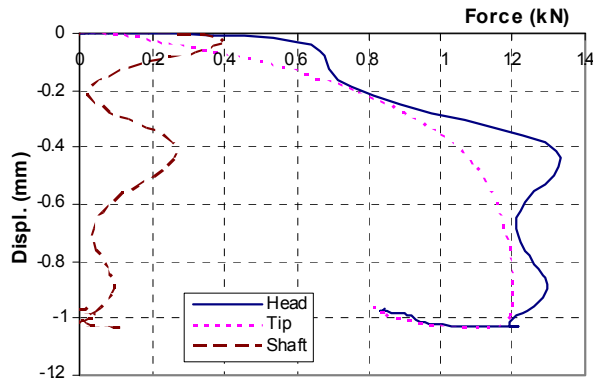


Figure 5.31: Example of load-displacement curves in test 4 (water as pore fluid; RLT4 – 3 – 0.1D)

5.5.3 Response of pore pressure during a RLT

In the test set-ups, four pore pressure transducers were placed at four different locations underneath the pile tip. A fifth transducer was fitted on the pile tip to measure the response of pore pressure during the load tests. The measurements made by these transducers are presented in this section, and an explanation of the measurements is given in section 5.7. It will be shown that sand behaves in a partially drained condition during these RLTs, and that the tendency for excess pore pressure at the same soil location is relatively consistent despite the displacement magnitude and penetration rate. However, the magnitude of excess pore pressure depends on the penetration rate and soil permeability, i.e. the drainage factor.

Figures 5.32(a)(b) to 5.34(a)(b) present representative pictures of excess pore pressure and the measured values as a function of time, during RLTs in centrifuge test 2 (viscous fluid, $I_D = 53\%$). The pore pressure transducer 4 (wsm4) was defective in test 2 and is therefore not included in the figure. Figures 5.32(a) and (b) present results from the slowest and smallest displacement magnitude rapid load test (RLT2-1-0.01D), figures 5.33(a) and (b) present results from the slow but largest displacement magnitude rapid load test (RLT2-1-0.1D), and figures 5.34(a) and (b) present results from the fastest and largest displacement rapid load test (RLT2-3-0.1D). The general responses of pore pressure during these RLTs are virtually the same. There is excess pore pressure at all locations. The time needed for that excess pore pressure to attenuate to the static value after the load test (consolidation time) is in the same order of magnitude as the loading duration of the RLT. This implies that the soil is in a partially drained condition during these RLTs. The pore pressure response values in figure 5.34 are generally higher than those in figure 5.33, as the penetration rate of RLT2-3-0.1D is higher than the rate of RLT2-1-0.1D i.e. the excess pore pressure depends on the penetration rate.

The tendency of pore pressure response recorded by each pore pressure transducer is described below.

- Pore pressure transducers at the pile tip (wsm_pl) and (wsm2) show relatively the same response. At the beginning of a RLT, the pore pressure increases before decreasing shortly afterwards. In figure 5.32(a)(b), pore pressure at the pile tip (wsm_pl) slowly decreases with penetration of the model pile but still remains in compression (positive excess pore pressure). When the pile stops moving, the excess pore pressure decreases at a higher rate and becomes lower than the static value (negative excess pore pressure) as the model pile moves upward. After the rapid increase at the start of the test, pore pressure (wsm2) continues to increase but at a much lower rate. When the pile stops moving, the response is

the same as the transducer wsm_pl. This pattern of pore pressure response is only observed in RLTs with an imposed displacement of $0.01 \cdot D$. For other RLTs with a higher imposed displacement ($\geq 0.02 \cdot D$), the similarity between wsm_pl and wsm2 is clearer, as shown in figures 5.33(a)(b) and 5.34(a)(b). After the rapid increase to peak positive value, the pore pressure decreases to the value lower than the static value (negative excess pore pressure). The negative excess pore pressure directly underneath the pile tip is not known beforehand, and it is interesting to note that pore pressure at these locations continues to decrease even when the pile stops moving (see figure 5.33) or even when it moves upward (see figure 5.34). This implies that there will be a region elsewhere in the soil where the pore pressure value is lower, which affects pore pressure response at the locations of wsm_pl and wsm2. This region is probably the shear failure surface.

- The transducer wsm1, placed at a distance $2.5 \cdot D$ directly underneath the pile tip, shows an extremely unusual pore pressure response. During all RLTs executed in the sand sample saturated with viscous fluid (centrifuge tests 2 and 3), the pore pressure decreases rapidly (negative excess pore pressure) at the start of the load test. At virtually the same time that pore pressure at the pile tip (wsm_pl) reaches its maximum value, the decreasing rate gradually decreases. In figure 5.32, the excess pore pressure (wsm1) remains negative throughout the load test, while pore pressure starts to increase after a while in figures 5.33 and 5.34. This differs from the expectation that positive excess pore pressure would occur at that location. It will be shown later that this response may be caused by the transducer set-up.
- The transducer wsm3 shows consistent pore pressure response at that location during a RLT, and positive excess pore pressure is observed. However, the increment seems relatively high compared to wsm_pl. This may also be caused by the transducer set-up as shown later.

In centrifuge test 3, viscous fluid was also used as the pore fluid. Measurements of pore pressure response show agreement with those in centrifuge test 2. Figure 5.35(a)(b) presents an example of pore pressure measurements during a RLT in centrifuge test 3, which was the fastest load test (RLT3-3-0.1D). The responses are very similar to those seen in figure 5.34, where the results from a corresponding RLT of the centrifuge test 2 (RLT2-3-0.1D) are shown. Given the test conditions of centrifuge tests 2 and 3, it will be shown later that the drainage factor of centrifuge test 3 is slightly lower than that in centrifuge test 2. It is therefore reasonable to observe that the value of excess pore pressure in figure 5.35 is higher than that in figure 5.34.

Figures 5.36(a)(b) and 5.37(a)(b) present the representative results of pore pressure response during RLTs in centrifuge test 4, where water was used as the pore fluid. Figures 5.36(a)(b) are the results from the slowest rate and smallest displacement magnitude load test (RLT4-1-0.01D). Figure 5.37(a)(b) shows the results from the fastest rate and largest displacement magnitude load test (RLT4-3-0.1D). The general responses at the transducer positions wsm_pl, wsm2, and wsm3 are very similar to those described above. However, the values of excess pore pressure are much smaller due to the higher permeability of the sand sample in centrifuge test 4. Only the pore pressure response at the location of the transducer (wsm1) is different. It increases at the start of the load test instead of decreasing immediately as in centrifuge tests 2 and 3, but there is a time lag between the starting pore pressure increment and the start of the load test. The detailed close-up of values from transducer wsm1 included in figure 5.37b reveals a small decrease in pore pressure at the start of load test RLT4-3-0.1D. It is therefore extremely likely that there is a tendency for negative excess pore pressure at the position of transducer wsm1 during RLTs in centrifuge test 4 which is similar to other measurements in centrifuge tests 2 and 3, but that the value is too small to be seen due to the high permeability of the sand sample.

It should be noted here that excess pore pressure shown in figure 5.37 attenuates soon after the start of the load test. Nearly halfway through the loading duration of RLT4-3-0.1D, pore pressure values are nearly equal to the static value, i.e. no or minimal excess pore pressure, and soil behaviour can be considered to be in a drained condition. This is different from the results in centrifuge tests 2 and 3, and is probably related to the explanation for the difference in failure mode of RLT load-displacement curves in tests 2, 3, and test 4 (see section 5.5.2). Further details for the explanation will be discussed in section 5.6.2.

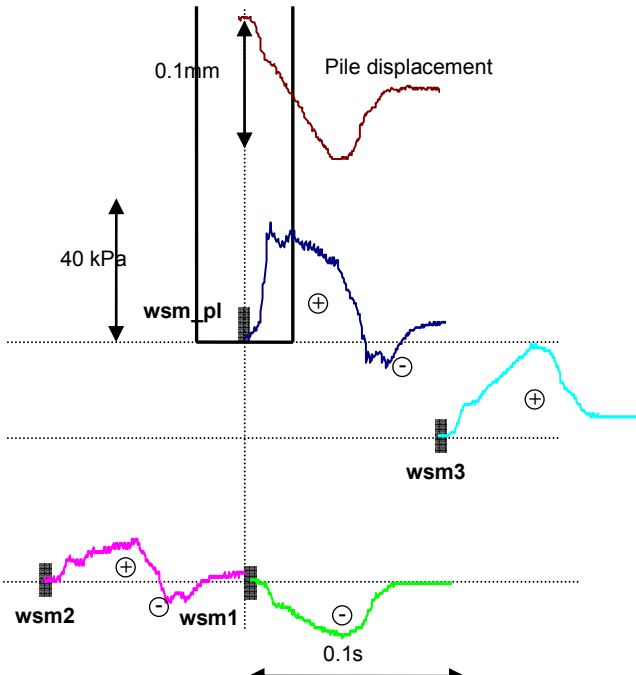


Figure 5.32a: Excess pore pressure during RLT2-1-0.01D; $v = 2.35$ mm/s.

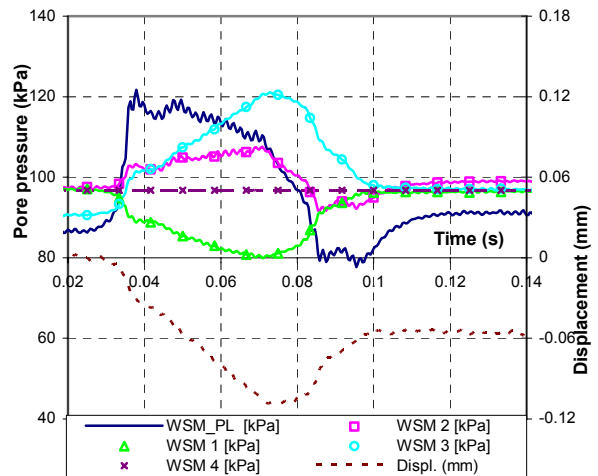


Figure 5.32b: Measured pore pressure during RLT2-1-0.01D; $v = 2.35$ mm/s.

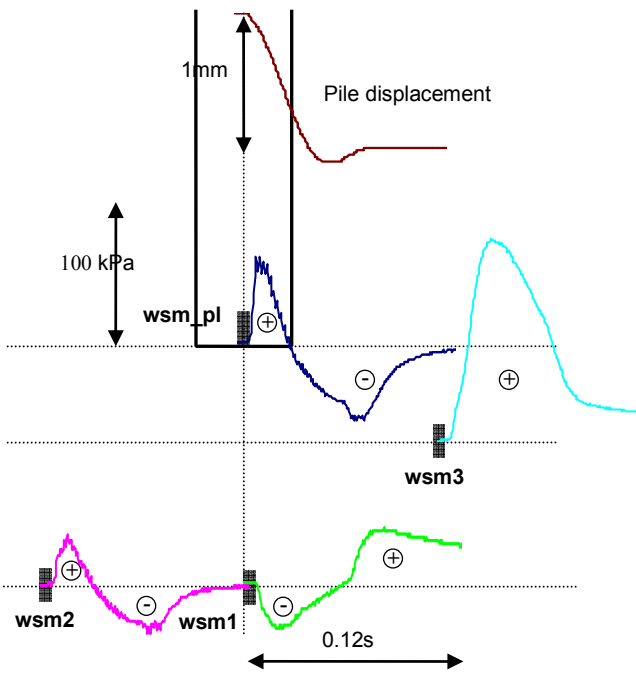


Figure 5.33a: Excess pore pressure during RLT2-1-0.1D; $v = 32$ mm/s.

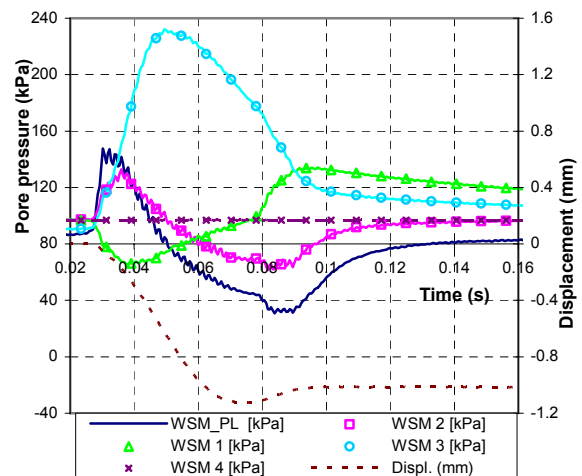


Figure 5.33b: Measured pore pressure during RLT02-1-0.1D; $v = 32$ mm/s

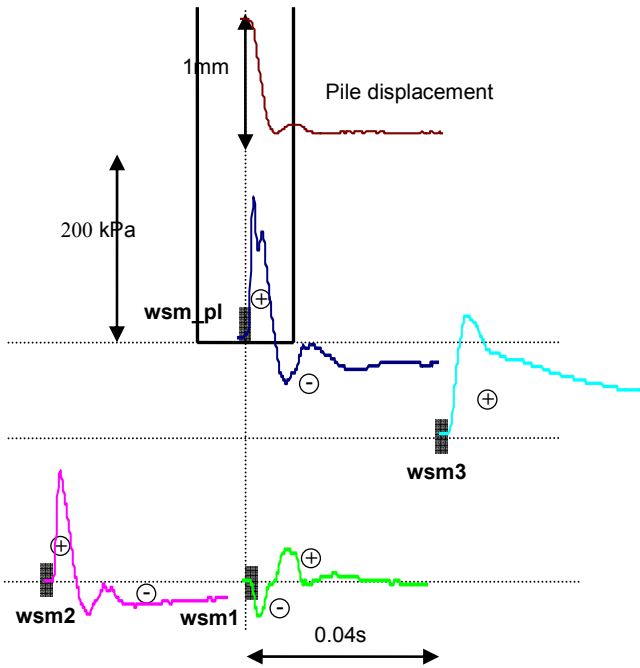


Figure 5.34a: Excess pore pressure during RLT2-3-0.1D; $v = 320$ mm/s.

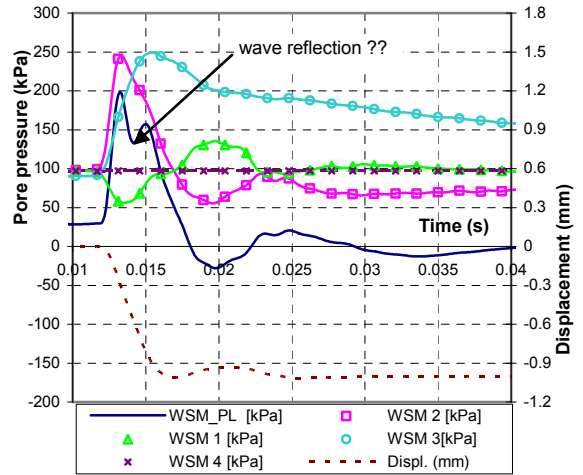


Figure 5.34b: Measured pore pressure during RLT02-3-0.1D; $v = 320$ mm/s

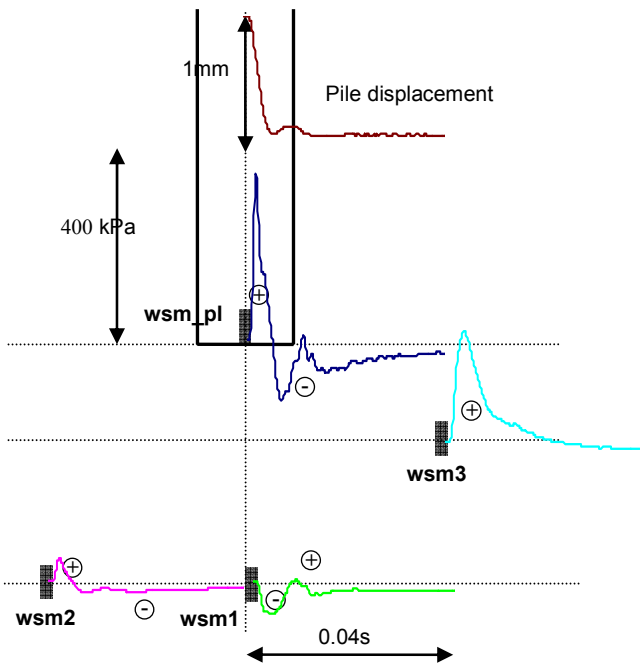


Figure 5.35a: Excess pore pressure during RLT3-3-0.1D; $v = 280$ mm/s.

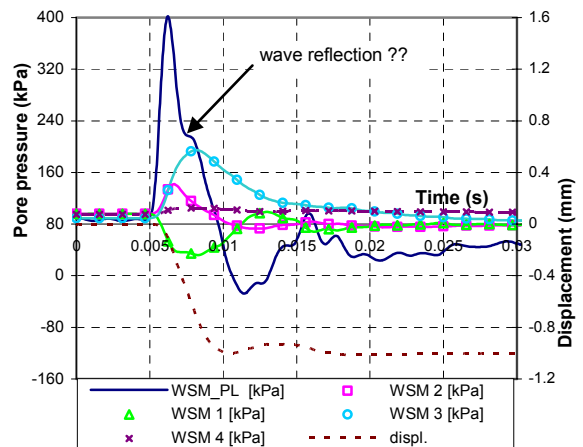


Figure 5.35b: Measured pore pressure during RLT3-3-0.1D; $v = 280$ mm/s.

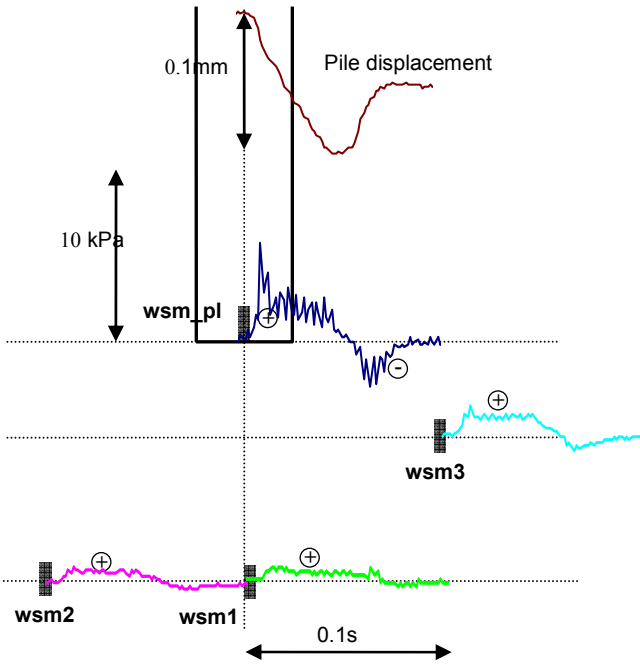


Figure 5.36a: Excess pore pressure during RLT4-1-0.01D; $v = 2.35$ mm/s.

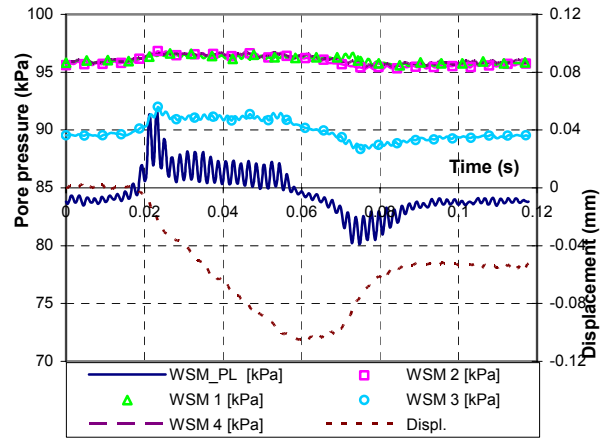


Figure 5.36b: Measured pore pressure during RLT4-1-0.01D; $v = 2.35$ mm/s

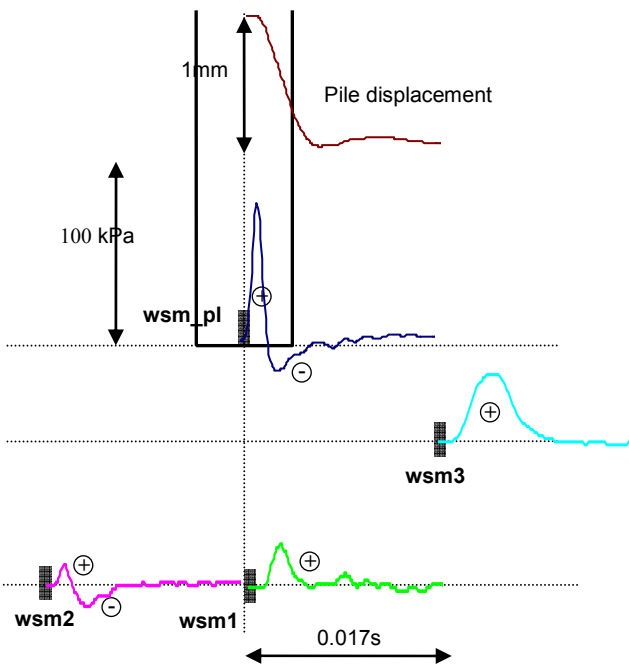


Figure 5.37a: Excess pore pressure during RLT4-3-0.1D, $v = 280$ mm/s.

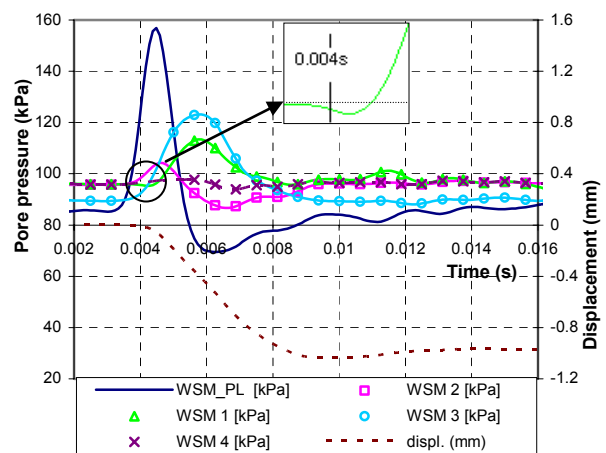


Figure 5.37b: Measured pore pressure during RLT4-3-0.1D, $v = 280$ mm/s.

5.6 Effect of the penetration rate on pile resistance

This section considers the effect of penetration rates on the model pile's resistance by comparing pile resistance in a SLT test with that in the RLTs. The effect on shaft resistance and tip resistance is considered separately. Since the ultimate value of pile resistance is the most important parameter, only load tests with an imposed displacement of $0.1D$ are considered here. It will be shown that the

penetration rate affects both shaft resistance and tip resistance. Using the interpretation method described in this thesis for the rapid pile load method (i.e. the UP method), the effect on shaft resistance is seen to be negligible whereas the effect on tip resistance is significant and must be taken into account. This section also points out that the penetration rate effect includes the so-called ‘true’ rate effect, which is limited; and the excess pore pressure effect, which is predominant in this case. The ‘true’ rate effect mentioned here is the increase in shear strength of the sand due to high shearing rate, which related to the intrinsic behaviour of sand. As sand is started shearing, the particles will adjust their position and slide over each other. If the loading time is slow enough, the particles can rearrange themselves to slide in the paths of least resistance. On the contrary, if the loading is too fast, the particles will not be able to do so; thus, the shear strength will increase and so does the bearing capacity. In relation to the rapid loading, there might be the crushing of sand particles, which is believed to contribute to the increase of shear strength (Lee et al, 1969).

5.6.1 Effect of penetration rate on shaft resistance

Figures 5.39 to 5.41 compare the total shaft resistance-displacement curves between the static load test and rapid load tests in centrifuge tests 2, 3, and 4 respectively. Total shaft resistance is derived from the difference between the measured pile head force and the pile tip force. The curves for the most rapid rate tests (penetration rate of approximately 280 mm/s) show extreme overvaluation at the beginning, which must have been caused by vibration in the pile head force signal. This does not reflect the effect of the penetration rate, and the peak is therefore not considered further.

Figures 5.39a and 5.40 show that total shaft resistance of the SLT is lower than that from the RLTs. What is more, shaft resistance is seen to increase as the RLT becomes faster. On the other hand, there is almost no difference between the curves shown in figure 5.41, i.e. no penetration rate effect. As the range of penetration rates of load tests shown in figures 5.39a, 5.40, and 5.41 is the same, the different observation must be related to a difference in test conditions between the centrifuge tests, i.e. the density of the sand sample and the pore fluid. The former may cause the difference in magnitude of the penetration rate effect, whereas the latter may affect the magnitude of excess pore pressure in the sand. Both can affect pile shaft resistance. However, the difference in sand bed density would not play a role in this case as no penetration rate effect is observed in figure 5.41, which shows results from centrifuge test 4 with the highest sand sample density ($I_D = 65\%$). Based on the results from the fast triaxial test series (chapter 3), the denser sand would show the higher effect. If the effect does not exist in test 4 (density = 65%), it would therefore not exist in tests 2 and 3 (density = 54% and 36%, respectively). This means that the increment in figures 5.39a and 5.40 should solely relate to the use of viscous fluid. Although the pore pressure is not measured at the pile shaft, it can be expected that the generation of negative excess pore pressure at the pile shaft will increase the effective stress and shaft resistance. Using this assumption, the difference between figures 5.39a, 5.40, and 5.41 can be explained by the difference in drainage ability. In test 4, water is used as the pore fluid (high permeability) and excess pore pressure along the pile shaft is low. Shaft resistance is therefore not affected. By contrast in tests 2 and 3, where viscous fluid is used as a pore fluid (i.e. the permeability is much lower), excess pore pressure would be significant enough to affect shaft resistance. As the drainage conditions in tests 2 and 3 are nearly the same, the penetration rate effects shown in figures 5.39a and 5.40 are very similar.

Figure 5.39b presents the shaft resistance and pile velocity values as a function of time for the test named “ $v = 80 \text{ mm/s}$ ” in figure 5.39a and the static values of shaft resistance. Since the increment of shaft resistance is due to the negative excess pore pressure, values higher than the static value can only be observed at a certain time during the velocity increase phase where excess pore pressure increases. As pile velocity decreases, excess pore pressure starts to dissipate and shaft

resistance therefore gradually decreases to the static value. Close to the time of maximum pile displacement, velocity reaches zero and excess pore pressure no longer occurs, i.e. there is no further change in the effective stresses, and shaft resistance is virtually the same as the static value. Shaft resistance is not affected by excess pore pressure and equals the static value close to the time of maximum pile displacement.

To summarise, in the case of a pile founded in sand as described here, shaft resistance is not affected by the rate effect but may be affected by excess pore pressure. Sand permeability is the determining parameter. However, the increment of shaft resistance will not affect the value of total pile resistance at the time of maximum displacement (unloading point), since excess pore pressure is negligible at that time. In this case, the effect on shaft friction will therefore not affect the current interpretation procedure for a RLT.

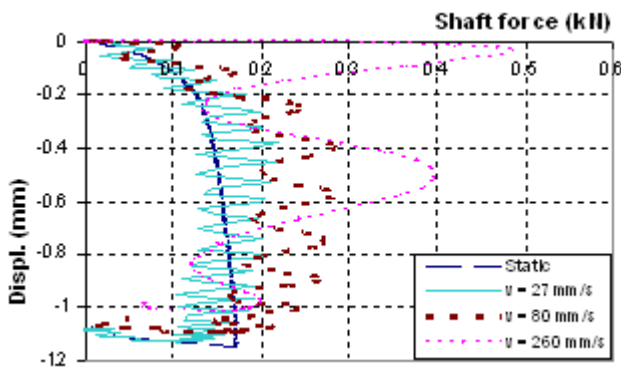


Figure 5.39a: Shaft resistance-displacement curves (centrifuge test 2)

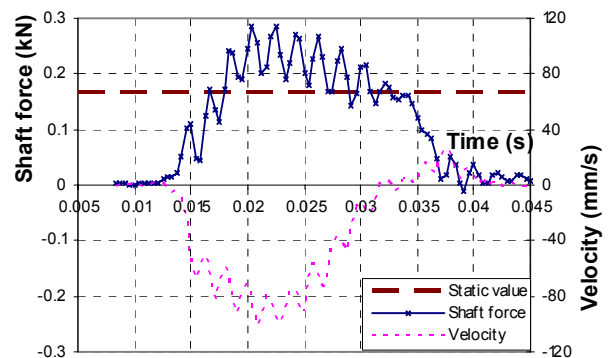


Figure 5.39b: Pile shaft force and velocity vs. time (test 2, $v = 80$ mm/s)

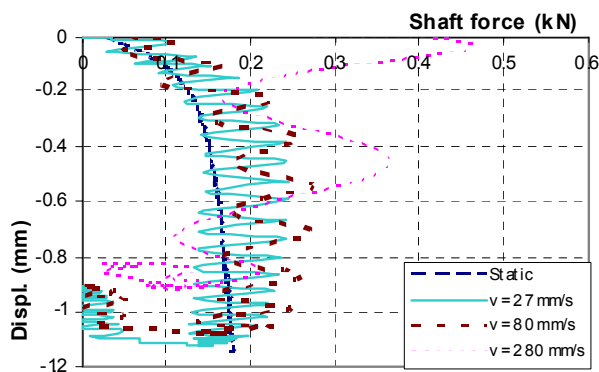


Figure 5.40: Shaft resistance-displacement curves (centrifuge test 3)

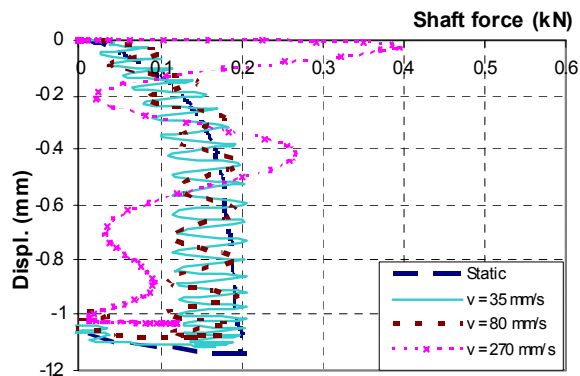


Figure 5.41: Shaft resistance-displacement curves (centrifuge test 4)

5.6.2 Effect of penetration rate on tip resistance

The pile tip resistance-displacement response measured during the load tests performed in tests 2, 3, and 4 are shown in figures 5.42, 5.43, and 5.44 respectively. The penetration rate effects are clearly seen in these figures, although the degree of effect differs and depends on the pore fluid used. In tests 2 and 3 where viscous fluid was used, the tip resistance strongly depends on the penetration rate of the pile: the higher the RLT rate, the higher the tip resistance. In test 4 where water was used, the tip resistance of the RLTs is clearly higher than that in the SLT, but the ultimate value of these RLTs is independent of the penetration rate.

Figure 5.45 shows a generalisation of the dependence of maximum pile tip resistance on the penetration rate of the model pile. The results are taken from all RLTs performed in tests 2, 3, and 4 with an imposed displacement of 0.1D (see Appendix 5a). In the figure, the maximum tip resistance of a RLT (R_{max}) is normalised by the value of SLT at the same magnitude of displacement (R_{sta}). The figure shows that the penetration rate causes an increase in tip resistance of approximately 10% in test 4, whereas the increment varies from 20% to more than 40% in tests 2 and 3, dependent on the rate. This difference in the penetration rate effect will be discussed further in section 5.7.2.

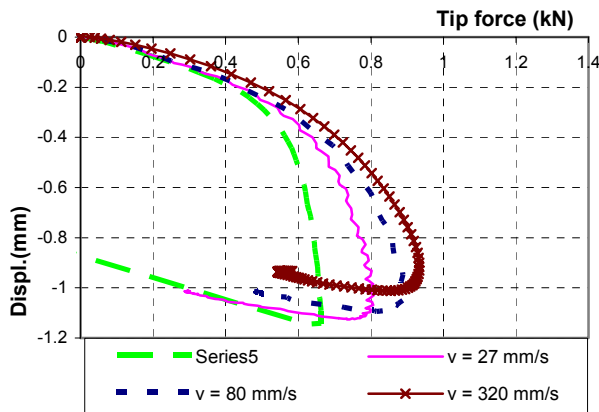


Figure 5.42: Tip resistance-displacement curves (test 2 low permeability)

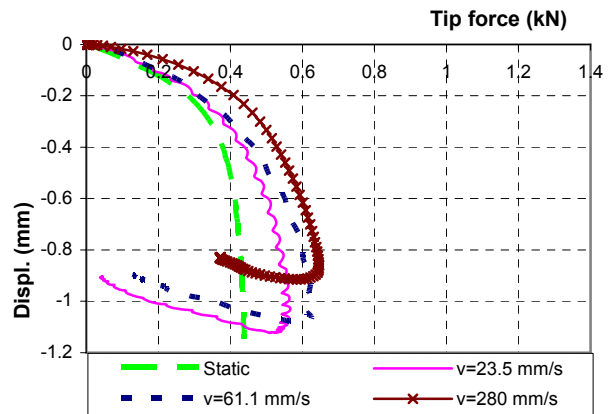


Figure 5.43: Tip resistance-displacement curves (test 3 low permeability)

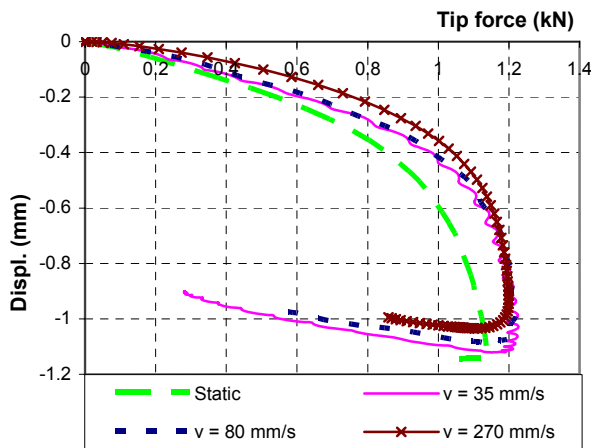


Figure 5.44: Tip resistance-displacement curves (test 4 high permeability)

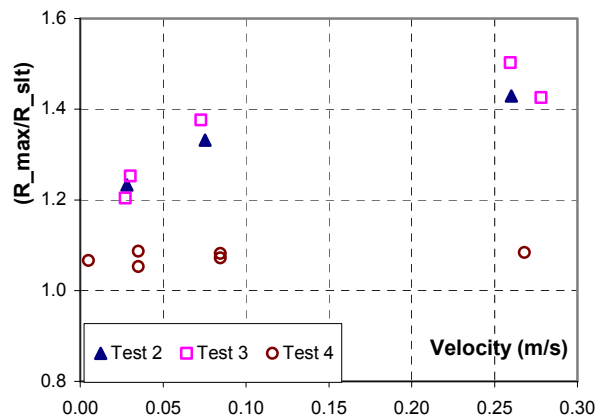


Figure 5.45: Effect of penetration rate on maximum tip resistance

5.7 Characteristics of excess pore pressure and its effects on tip resistance

Section 5.5.3 presented the results of pore pressure measurements during a RLT. This section discusses the validation of these measurements. Overall, the transducers show a consistent pore pressure response during a RLT despite differences in penetration rate and the imposed magnitude of displacement between these RLTs. The measurements are somewhat different than expected however, for example the response measured by transducers *wsm_pl* and *wsm1*. The qualitative explanation for these pore pressure responses during a RLT is given here. The role of excess pore pressure on the increment of tip resistance due to the penetration rate is also examined.

5.7.1 Characteristics of excess pore pressure

Penetration of a pile into a soil mass will generally cause deformation in the surrounding soil body. If the soil is in a saturated undrained condition, excess pore pressure is generated which will indicate the tendency volume change of the soil elements. However, as indicated in section 5.5.3, the sand was not in a fully undrained condition during a RLT in this case: pore fluid therefore flowed through the soil mass from the high pressure region to the lower pressure region to equalise any pressure gradient. As a result, excess pore pressure that would exist in an undrained condition would have been re-distributed. The magnitude was not solely controlled by volume deformation of the soil element, but also by pore flow through the saturated soil mass, i.e. the drainage condition. This concept will be used in the next paragraph to explain the measured pore pressure.

In order to qualitatively explain the pore pressure response at the location of transducer wsm_pl, the deformation pattern in the sand region around the pile tip during penetration is used as reported by White (2002). White (2002) indicated the formation of a 'nose cone' of high compression and densification of sand particles underneath the pile tip during an increment of pile penetration. As the pile penetrates into the sand, the 'nose cone' moves with the pile and the surrounding sand is slide and sheared along the edges of the 'nose cone'. This pattern helps to explain the observed tendency of the pore pressure responses, which is solely dependent on the deformation pattern and the existence of pore flow in the soil region underneath the pile tip. Based on this pattern, the pore pressure response at wsm_pl can be described as follows. At the beginning of the load test, the soil region nearly underneath the pile tip was elastically compressed and became denser. Pore pressure increased. As the pile moved downwards, shear failure occurred and the sand began to slide along the edges of the 'nose cone'. Due to densification, the shearing caused the void volume in the shear zone to increase and therefore generated negative excess pore pressure. A sketch of the negative excess pore pressure regions and direction of water flow is presented in figure 5.46. Water in the 'nose cone' and from the outer regions flows toward the shear zone, and pore pressure in the 'nose cone' decreases. The magnitude of the decrease depends on the value of excess pore pressure in the shear zone, which in turn depends on the rate of volume change, and the rate of fluid flow from outside the region to equalise the pressure gradient. If the former is higher, pore pressure decreases and a negative value can be seen (and vice versa). The flow of water continues until no pressure gradient exists. Due to the low permeability value in tests 2 and 3, the flow of water stops when the pile stops moving (no further shearing). The response of pore pressure is therefore seen throughout the test. In test 4, the flow stops as pore pressure in the shear zone stops decreasing (rate of volume change equals the rate of in-flow). No pore pressure response is therefore observed for a brief period after the start of the test. It is noted here that the pattern of pore pressure response at the location of wsm_pl is the same as that reported by Möller and Bergdahl (1981), who had measured pore pressure response at the pile tip during the model pile driving experiment in a calibration chamber.

At the location of transducer wsm-1, the decrease in pore pressure seems very unrealistic. Pore pressure would be expected to increase at the start of the test due to compression and then decrease, but the measurements show the opposite trend. If this is due to the extension of shear failure surface to that location, the increase of pore pressure observed after a certain time (e.g. figure 5.34) would not be seen. This is because negative excess pore pressure in the failure surface would remain throughout the RLT, as indicated in the previous paragraph. Another explanation, which seems to be more reasonable, is the set-up and size of the transducer. The porous stone of the transducer measured approximately 6 mm in diameter, which is large in comparison with the pile tip diameter. It would therefore act as an obstacle in the soil. The transducer set-up meant that it is fixed in the location where the soil particles moved downwards (White, 2002). It is therefore possible that the

soil particles slid around the transducer during the test and formed a shear surface. At the beginning of a RLT, it can be seen that the shearing effect is dominant and there is negative excess pore pressure. After a while however, the pile head force increases, compression also increases, and pore pressure predominantly increases.

At the transducer locations wsm-2 and wsm-3, the responses of pore pressure are seen to be more realistic: nearly the same pore pressure response as recorded by wsm_pl would be expected. Eiksund (1994) performed a series of dynamic load tests on a model pile founded in sand in a calibration chamber, where pore pressure measurements were taken at nearly the same locations as these transducers. One of his results is shown in figure 5.47. It can be seen that all transducers show an increase in pore pressure at the start of the load test, which then decreases due to the sand dilatancy. This is the same as the pore pressure response at the location wsm-2. However, the measurements in this study show a relatively high increase in pore pressure. The pore pressure at wsm-3 is mainly positive. The boundary conditions of these transducers may affect the increase in pore pressure. As pointed out by White (2002), there is horizontal displacement of sand particles in that region, and the boundary conditions in the transducer's position increase compression of the soil region in front of the porous stone. The set-up therefore causes pore pressure to increase more than the real value without the transducer.

In conclusion, it seems that the set-up and size of the pore pressure transducers in the sand sample (wsm1, 2, 3, 4) affect the pore pressure response at the locations where they were placed.

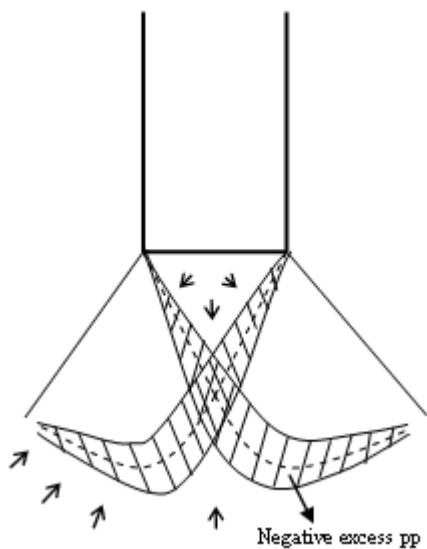


Figure 5.46: Sketch of negative excess pore pressure under the pile tip

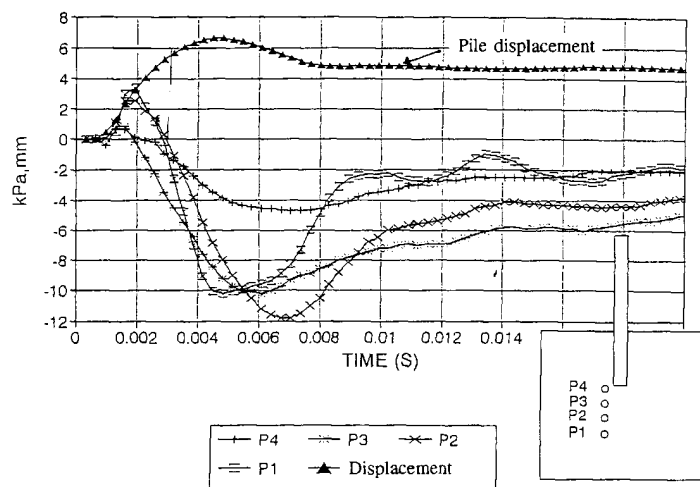


Figure 5.47: Pore pressure response during a model dynamic pile load test (Eiksund, 1994)

5.7.2 Effects of excess pore pressure

The effect of excess pore pressure on the model pile's shaft resistance has been discussed in section 5.6.1. This section concentrates on the effect on tip resistance.

To consider the effect of excess pore pressure, it is necessary to explain the relationship between excess pore pressure underneath the pile tip and pile tip resistance. Section 5.5.3 showed that there is negative excess pore pressure underneath the pile tip during a RLT, which would increase effective stress in the sand and thus increase the strength. Tip resistance also increases. However, direct comparison between excess pore pressure values and the increment of total stress under the

pile tip does not provide an explanation for the role of excess pore pressure: the value of excess pore pressure is too small in comparison with stress at the pile tip. In RLT2-3-0.1D (figure 5.34) for example, the largest negative excess pore pressure directly underneath the pile tip is less than -80 kPa, whereas the increment in total stress over the static value of SLT3-0.1D shown in figure 5.42 is much higher (approximately 2000 kPa). This is similar to findings by Eiksund (1994) and Maeda et.al. (1998). The increment of 2000 kPa is indeed also caused by the ‘true’ rate effect, but it will be shown later that the ‘true’ rate effect plays a minor role in the increment (approximately 30%) and that the remainder probably relates to excess pore pressure. It can therefore be concluded that there is no direct relationship between the value of excess pore pressure at the pile tip and the increment of pile tip resistance due to the penetration rate effect.

Another possible explanation for the effect of excess pore pressure can be based on the classic bearing capacity theory. From the theory, it is known that pile tip resistance equals contact stress at the pile tip, but that the value of contact stress is supported by the limit stress state at the shear failure surface and pressure from the Rankine passive pressure area. The role of excess pore pressure should therefore be evaluated by comparing the value of excess pore pressure and the effective stresses at these regions. These stresses are generally not known, i.e. no quantitative comparison is possible. In qualitative terms however, it can be expected that the magnitude of stresses in the shear failure surface and the Rankine wall are much smaller than the value at the pile tip as the area of shear failure surface is much larger than the tip area. However, according to the explanations for the characteristics of pore pressure response given in the previous section, the negative excess pore pressure in the shear failure surface should be lower than that in the pile tip. Therefore, the magnitude of stresses and the excess pore pressure would be in the same order of magnitude, i.e. any difference in excess pore pressure may cause the change in pile tip resistance. This explanation seems realistic, and can be supported by observations in the test results described in the following paragraphs.

Section 5.6.2 pointed out the effect of the penetration rate on the tip resistance of the model pile, namely that the effect is more significant in tests 2 and 3 (figures 5.42 and 5.43) than in test 4 (figure 5.44). By considering the measured excess pore water pressure, it was explained that this difference cannot be caused solely by the ‘true’ rate effect, but must be influenced by the difference in excess pore pressure during these centrifuge tests. Figures 5.48 and 5.49 present the measured force and pore pressure at the pile tip during the two fastest RLTs in test 2 (RLT2-3-0.1D) and test 4 (RLT4-3-0.1D). Figure 5.48 is representative for RLTs where excess pore pressure is high (in centrifuge tests 2 and 3 using viscous fluid), and figure 5.49 is representative for RLTs where excess pore pressure is low (in centrifuge test 4 using water). The significant difference between these figures is the time of pore pressure response, although the loading duration is identical for the two tests.

- In figure 5.48, pore pressure continues to decrease at the time of maximum pile tip force, implying a lower negative value of excess pore pressure at the shear failure surface. It is possible that negative excess pore pressure decreases continuously up to the time of maximum pile tip force due to increasing pile penetration. Pile tip resistance therefore also increases, as seen in figures 5.42 and 5.43.
- By contrast in figure 5.49, the decrease in pore pressure stops much faster and there is almost no excess pore pressure at the pile tip and at other locations (figure 5.37) at the time of maximum pile tip force. This implies that soil behaviour is close to a drained condition, i.e. no effect of excess pore pressure. After tip resistance reaches the static value, there is therefore no or only a negligible increase in tip resistance due to negative excess pore pressure. The full failure mode in the load-displacement curves is seen as in figure 5.44.

The increment of approximately 10% over the static value is caused purely by the ‘true’ rate effect. Ibsen et al. (1994) performed a series of triaxial tests with Baskarp sand, and found the ‘true’ rate effect to be approximately 10%. The ‘true’ rate effect in centrifuge tests 2 and 3 may be smaller as the density of sand sample is lower. Therefore, the effect of excess pore pressure mainly contributes to the maximum increment of 40% seen in figure 5.45.

From the above, it can be concluded that the ‘true’ rate effect in this simulation case causes approximately a 10% increment of pile tip resistance, whereas excess pore pressure causes more than a 30% increment of pile tip resistance.

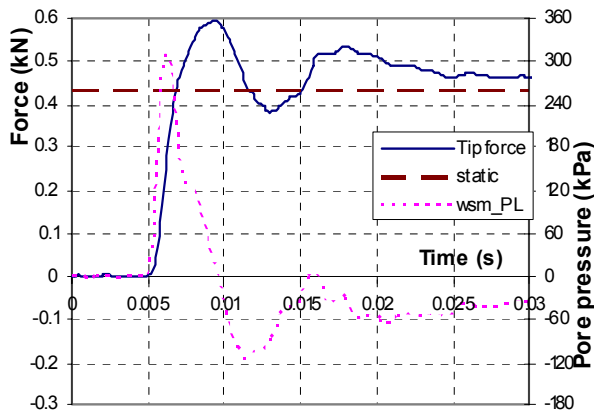


Figure 5.48: Force and pore pressure measured at the tip in RLT2-3-0.1D

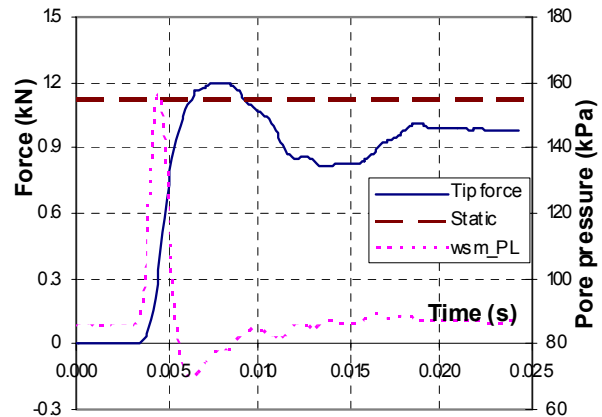


Figure 5.49: Force and pore pressure measured at the tip in RLT4-3-0.1D

5.8 Validating the numerical results

Chapter 4 presented a numerical study into the effect of excess pore pressure on a pile’s tip resistance. The results show that the effect depends on the drainage condition of the soil during the RLT; and the magnitude of the effect can be evaluated using the defined drainage factor value. This finding is extremely important in practice as it means that determination of the drainage factor is feasible. This section evaluates the results of the geocentrifuge tests against the calculated value of the drainage factor for each RLT.

Figure 5.50 shows the ratio of maximum pile tip resistance to the static value against the calculated drainage factor. The figure also includes the result from the numerical study. It can be seen that the tendency is very similar, but that the effect boundary is different. A possible reason will be given below.

The similarity in tendency can be explained by the fact that the effect is controlled by the flow of pore fluid. The numerical scheme takes adequate consideration of consolidation during the RLT, hence it shows the same tendency as the experiment results. However, the mechanism for generating excess pore water pressure differs in the numerical scheme with that in the experiment. The boundary is therefore different. The effect of dilatancy is not considered in the numerical scheme, thus the pore pressure increases as loading increases. If the drainage factor is below a certain value, the water bears a considerable part of the load. The soil behaviour under consideration is therefore similar to that in an undrained condition, and the stiffness of the soil increases due to low compressibility of the water. As a result, tip resistance increases as soil stiffness increases. On the other hand, the excess pore pressure in the experiment is highly dependent on the volume expansion of the soil during shear failure and the flow of pore fluid.

Dilatancy at the shear failure surface occurs as the pile starts to move downwards, and may affect the mobilised tip resistance with time. Therefore, the effect leads to a higher value of the boundary for the drainage factor.

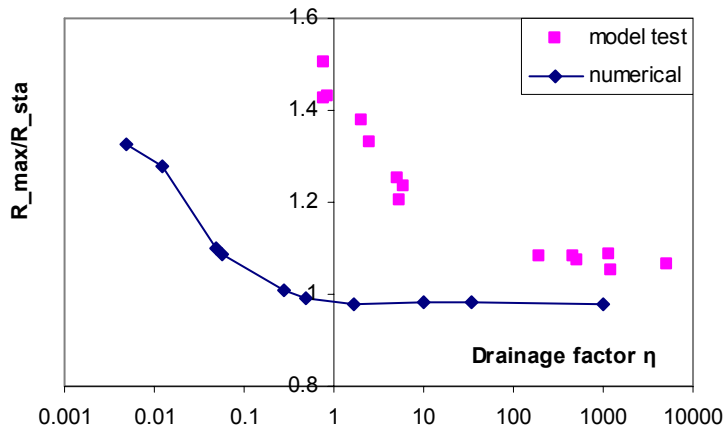


Figure 5.50: Normalised tip resistance against dynamic drainage factor

5.9 Concluding remarks

The results of the three centrifuge pile load test series have been presented in this chapter. The rapid load tests performed in each centrifuge test are comparable with the prototype rapid load test, both in terms of stress wave number in the pile and pile behaviour. The results presented in this chapter are therefore applicable to the prototype scale. The following conclusions can be drawn from the test results:

- Due to the high penetration rate of the pile during a RLT, pile resistance is higher than during a static load test. The effect includes both the ‘true’ rate effect and the effect of excess pore pressure.
- For shaft resistance, only the effect of pore pressure is observed.
- For tip resistance, both the ‘true’ rate effect and the effect of excess pore pressure can be seen. The ‘true’ rate effect is limited (less than 10%). The effect of pore pressure is more significant (more than 30%).
- The effect of pore pressure can be evaluated using the value of the defined drainage factor.
- Excess pore pressure in the soil region underneath the pile tip is controlled by the deformation pattern of the soil and the pore fluid flow. The measurements show certain characteristics which were not known beforehand, but which can be explained.

Chapter 6

Implications for the analysis of rapid pile load tests

6.1 Introduction

This chapter discusses the implications of the experimental results in relation to improving the interpretation methods of the rapid load test. An axial rapid load test on a pile in sand is considered. The implications of the results are examined in relation to the most widely used interpretation method – the unloading point method (UP method).

Several experiments were carried out within the framework of this thesis:

- the fast triaxial test;
- model pile load tests in a calibration chamber;
- model pile load tests in a geotechnical centrifuge.

The first two experiments showed that rate effects in sand are limited, and these therefore have limited consequences when interpreting the rapid pile load test. The centrifuge experiment provided important results however, which showed the effect of a high penetration rate on the mobilised resistance of a pile founded in sand. The results also help to clarify that the high penetration rate effect comprises two effects: the true rate effect, and the effect of excess pore pressure. Results from the centrifuge tests significantly improve current knowledge about the rate effect in a rapid pile load test. The discussions in this chapter therefore concentrate on the implications of results from the centrifuge test series. The ultimate aim is to develop a guideline that incorporates the true rate effect and the effect of excess pore pressure in the UP method.

6.2 Elaboration of the centrifuge test results

This section reconsiders the centrifuge test results in order to assess the implications for the UP method. The discussions focus on the effects on the model pile's measured tip resistance. Tip resistance is predominant in total resistance, not only because important effects are found on tip resistance, but also because of the practical situation of a pile in sand. Although the penetration rate affects shaft resistance but it does not affect the analysis results using the UP method (as indicated in section 5.6.1).

Based on the reviews of the UP method presented in chapter 2, the following aspects are examined:

- The effects of the penetration rate on pile resistance at the time of maximum displacement, the unloading point resistance (R_{up}).
- The effects of the penetration rate on maximum resistance (R_{max})
- The rate dependency law (linear or non-linear)
- Specification of the true rate effect and the pore pressure effect.

The RLTs in the test series were performed with different magnitudes of pile head displacement. This is important for the practical situation of the RLTs, where pile head displacement is often smaller than 10% of the pile diameter (i.e. the common criterion to define the ultimate bearing

capacity of a pile). In such cases, fully mobilised resistance of a pile is not reached. To elaborate the test results in this section, the model RLTs are divided into three categories: small displacement (0.01D and 0.02D), medium displacement (0.05D), and large displacement (0.1D). The penetration rate effect in these RLTs is considered separately. The results are required for evaluating the usefulness of a prototype RLT, which has a small pile head displacement (less than 10%).

6.2.1 Small displacement RLTs (0.01D and 0.02D)

This section considers the load-displacement curve of RLTs with small imposed pile head displacement (0.01*D and 0.02*D), and the load-displacement curve of the SLT. Figure 6.1 compares the load tests of centrifuge test 3. The figure shows the tip force-displacement curves of the most rapid RLTs with small pile displacement (RLT3-3-0.01D; $v = 12.55$ mm/s) and 0.02*D (RLT3-3-0.02D; $v = 25.1$ mm/s), together with the static curve (SLT3-3). The corresponding results for the RLTs in centrifuge test 2 are similar and are not presented here. The corresponding results for centrifuge test 4 are shown in figure 6.2. Both figures show almost no difference between the load-displacement curves of the two RLTs as pile head displacement increases. In the rapid load-displacement curves, there is no distinction between the point of maximum tip resistance and the unloading point, i.e. they nearly coincide. The tip resistance of the RLTs is somewhat higher than static resistance at the same pile head displacement.

Figure 6.3 presents a generalisation of the effect of the penetration rate on maximum mobilised tip resistance (relative to the static value) during the small displacement RLTs. The results are taken from all small displacement RLTs performed in centrifuge tests 2, 3, and 4. The vertical axis shows the ratio of maximum tip resistance over the static value at the same displacement. The horizontal axis shows the average penetration rate of the RLTs. There is an overall increase due to the penetration rate effect, but the average increment is small (less than 10%) within the penetration rate range of these RLTs. The results from test 4 are in the same order of magnitude as those from tests 2 and 3, i.e. no effect of excess pore pressure is observed. The plastic deformation in the sand may not be significant, due to the small pile head displacement in this case. As a result, the generation of excess pore pressure is not high enough to show any effect on mobilised tip resistance.

It should be noted that the penetration rate of these RLTs (the maximum is 25.1 mm/s) is much slower than that of a prototype RLT (the average is 500 mm/s). Since the excess pore pressure depends on the penetration rate, it is not clear whether the same results would be observed in the prototype situation.

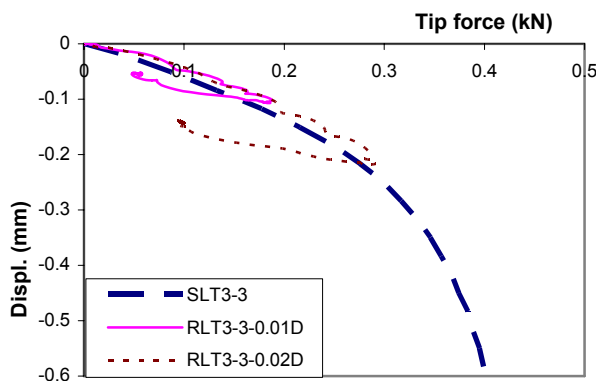


Figure 6.1: Tip resistance-displacement curves of small displacement RLTs and SLT (test 3)

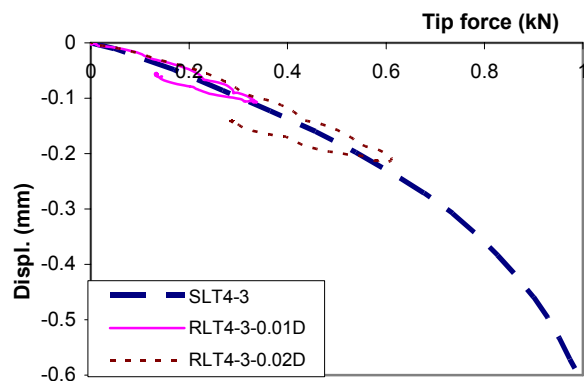


Figure 6.2: Tip resistance-displacement curves of small displacement RLTs and SLT (test 4)

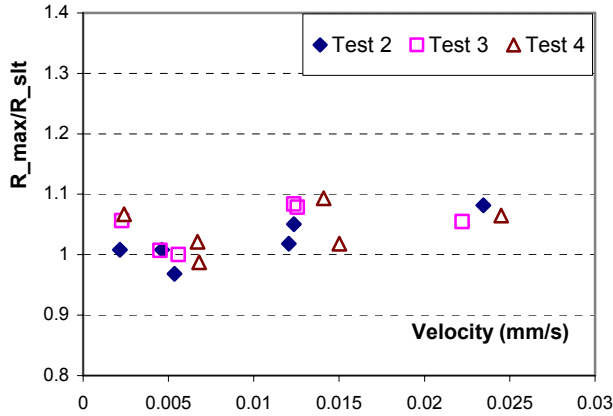


Figure 6.3: Effect of penetration rate on maximum tip resistance (small displacement RLTs)

6.2.2 Medium displacement RLTs (0.05D)

Figures 6.4 and 6.5 compare the tip resistance-displacement curves for the medium displacement RLTs. At 0.5 mm displacement, the differences between the rapid test and the static test are substantial. The tendency of the penetration rate effect in these figures is very similar to the case of large displacement RLTs, which were presented in section 5.6.2.

Figures 6.6 and 6.7 respectively show the generalisation of the penetration rate effect on maximum pile tip resistance (R_{tip_max}), and the resistance value at the time of maximum displacement, i.e. the unloading point (R_{tip_up}). The magnitude of the effect differs between the results from centrifuge tests 2 and 3, and those from test 4. From section 5.7.2, it is known that the increment of tip resistance in the RLTs in centrifuge test 4 is solely caused by the rate effect, and that both the rate effect and excess pore pressure cause the increment in centrifuge tests 2 and 3. In contrast with the case of small displacement RLTs, the generation of excess pore pressure is now significant enough to influence mobilised tip resistance. The true rate effect causes an increase of approximately 5% in maximum tip resistance (results from test 4), and excess pore pressure causes an increase of up to 15% in maximum tip resistance (results from tests 2 and 3). The magnitude of the increment due to excess pore pressure depends on the loading duration (i.e. the drainage condition during the RLTs). From Figure 6.7, it can be noted that the value of tip resistance at the time of the unloading point in test 4 is not affected by the rate effect, and that it is only affected by excess pore pressure in tests 2 and 3.

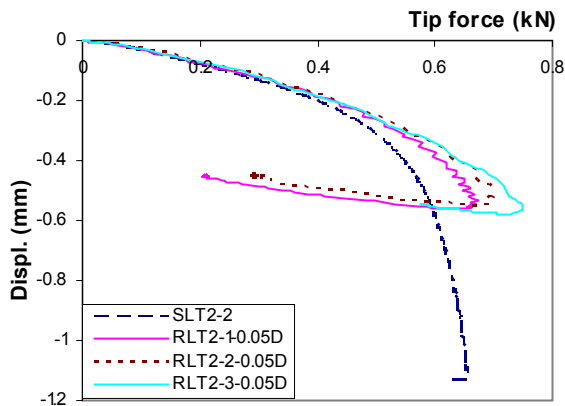


Figure 6.4: Tip resistance-displacement curves of medium displacement RLTs and SLT (test 3)

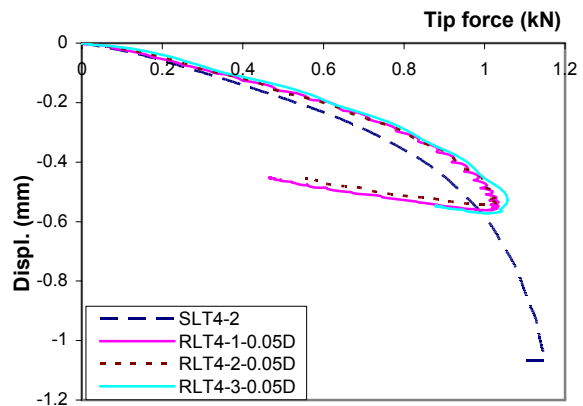


Figure 6.5: Tip resistance-displacement curves of medium displacement RLTs and SLT (test 4)

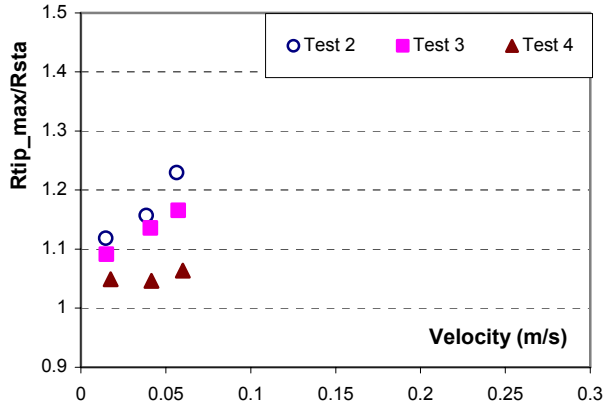


Figure 6.6: Effect of penetration rate on maximum tip resistance (medium displacement RLTs)

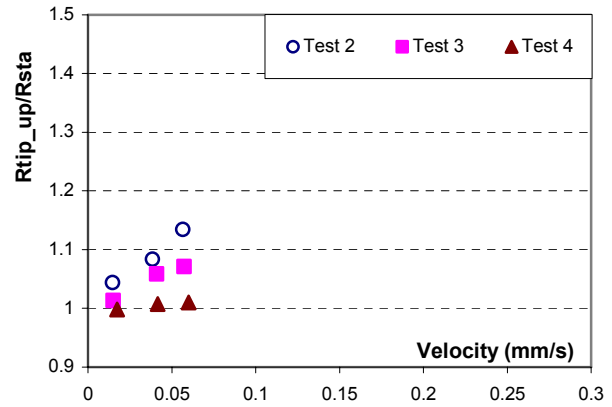


Figure 6.7: Effect of penetration rate on tip resistance at unloading point (medium displacement RLTs)

6.2.3 Large displacement RLTs (0.1D)

Section 5.6.2 discussed the effect of the penetration rate on the load-displacement curves of tip resistance during the large displacement RLTs. Figures 6.8 and 6.9 respectively plot the dependency of maximum tip resistance and the tip resistance value at the time of the unloading point on the penetration rate. In figure 6.8, data points from centrifuge test 4 show a nearly constant increment of maximum tip resistance between 5% and 10% over the static value, within the tested velocity range of the rapid load test. The damping term may therefore not exist here, and the increment is purely the rate effect. By comparing these figures, it can be concluded that the rate effect increases the maximum tip resistance by approximately 10%, but does not affect the unloading point value. The excess pore pressure affects both values. The magnitude of this effect depends on the loading duration of the RLT, i.e. it depends on the drainage factor. As presented in section 5.5.2, the fastest RLT in this case can be seen as a simulation of a prototype test. The observations from figures 6.8 and 6.9 are therefore valid when analysing a prototype rapid load test.

The trend lines for results from tests 2 and 3 are also plotted in figures 6.8 and 6.9. These data points fit a power law. This means that the rate dependency for pile tip resistance is non-linear when excess pore pressure plays a role. Coefficients of the power law are virtually the same for the two centrifuge tests 2 and 3, which suggest a possible single power for these cases (use of the same sand and excess pore pressure affects resistance). Since this conclusion is based on a limited number of data points, further verification is necessary.

6.2.4 Integration of all displacement results

In the case of large displacement, the tendency of the penetration rate effect is very similar to results from the medium displacement RLTs case shown in figures 6.6 and 6.7. This similarity suggests that extrapolation of the data points in figures 6.6 and 6.7 to higher velocities will show the same tendency as those in figures 6.8 and 6.9. It would certainly seem to be true for the pure rate effect (data point from centrifuge test 4). It is therefore possible to conclude that a RLT with a pile head displacement larger than 5% of pile diameter may have the same rate dependency characteristics as the test with a displacement of 10% of pile diameter, and that it can be used to predict the static load-displacement behaviour up to its displacement during the test.

Figure 6.10 shows the normalised tip resistance against the drainage factor. The solid square represents the ratio of maximum pile tip resistance in the RLT over the static value at the same displacement; the open circle represents the ratio of pile tip resistance at the unloading point over

the static value at the same displacement. From figure 6.10, it is estimated that a drainage factor of approximately 10 can be used to separate the drained side (negligible effect of excess pore pressure) and the partially drained side (effect of excess pore pressure must be considered) for the in-situ rapid load test. However, more test data with a drainage factor between 4 and 100 are required to specify the value.

Figure 6.10 also shows the practical range of the drainage factor for piles in sand. The following parameters are used to plot these lines: shear modulus $G = 80 - 160$ MPa, coefficient of permeability $k = 10^{-5} - 10^{-2}$ m/s, loading duration $T = 80 - 160$ ms, and pile diameter $R = 0.15 - 0.4$ m.

Figures 6.11 and 6.12 present the normalised maximum and the unloading point value of the tip resistance against the drainage factor for medium displacement and large displacement RLTs and the small displacement RLTs, respectively. As presented in section 6.2.1, there is no difference between the maximum value and the value at the time of maximum displacement in the small displacement RLTs. These are therefore excluded in figure 6.12 for the convenience of observation. These figures show that the extent of the excess pore pressure effect also depends on the test's displacement magnitude. This seems reasonable as a higher displacement magnitude may cause a lower negative excess pore pressure in the same drainage condition (see section 5.5). The resistance increase is therefore larger. It can thus be concluded that the effect of excess pore pressure not only depends on the defined drainage factor, but on the magnitude of displacement as well. Use of a single parameter such as the defined drainage factor may be insufficient to evaluate the effect of excess pore pressure.

In the literature, Finnie and Randolph (1994) studied the effect of the penetration rate in constant rate tests in sand. They concluded that the effect of partial drainage on the penetration resistance can be evaluated against the non-dimensional velocity V , defined as $V = v \cdot D / c_v$, where v is the penetration velocity, D is the pile diameter, and c_v is the coefficient of consolidation. This non-dimensional velocity is used here, and its value in each RLT is calculated with the penetration velocity v taken as the average velocity of the pile during the loading time of the RLT. Graphs of the normalised resistance against the non-dimensional velocity V are plotted in figures 6.13 and 6.14. It can be seen that there is some improvement compared with figures 6.11 and 6.12, but that the effect of displacement magnitude still exists. Neither the drainage factor nor the non-dimensional velocity can fully explain the effect of displacement magnitude. Another parameter may be involved.

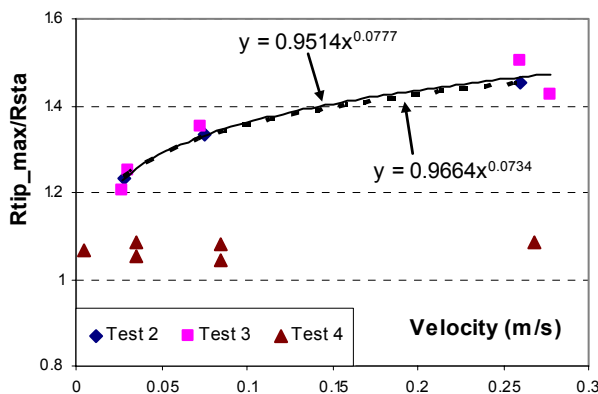


Figure 6.8: Effect of penetration rate on maximum tip resistance (large displacement RLTs)

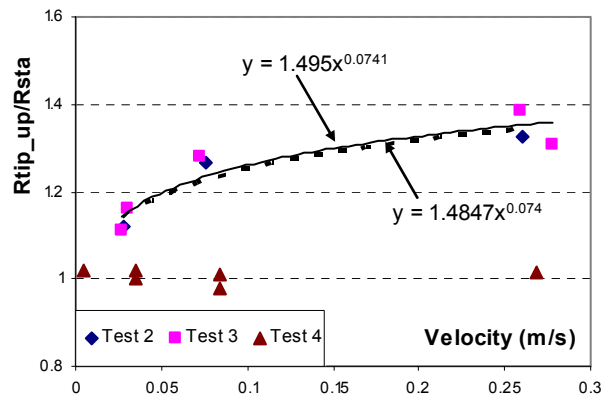


Figure 6.9: Effect of penetration rate on tip resistance at unloading point (large displacement RLTs)

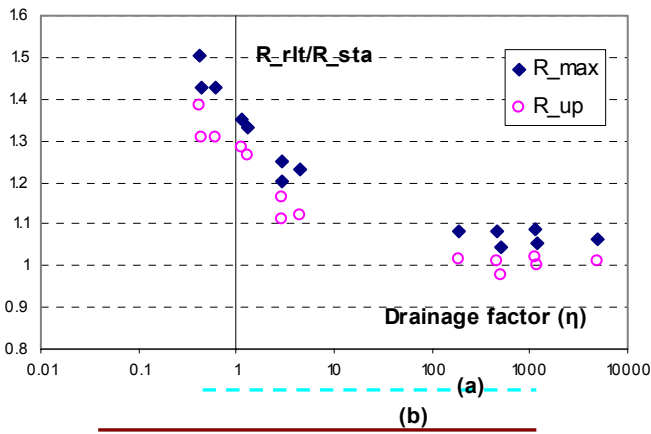


Figure 6.10: Normalised pile tip resistance against drainage factor (large displacement RLTs)

Line (a): Practical range of drainage factor for Baskarp sand
 Line (b): practical range of drainage factor for sand

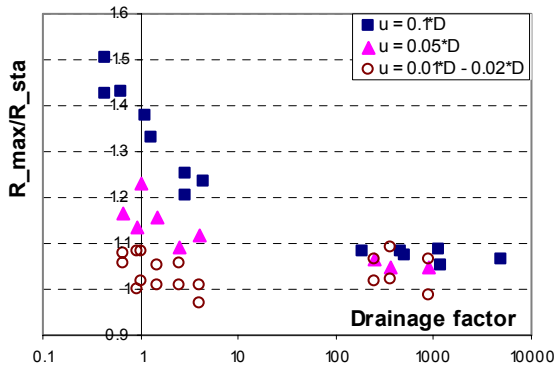


Figure 6.11: Normalised maximum pile tip resistance against drainage factor ($u = 0.05 \cdot D$ & $u = 0.1 \cdot D$)

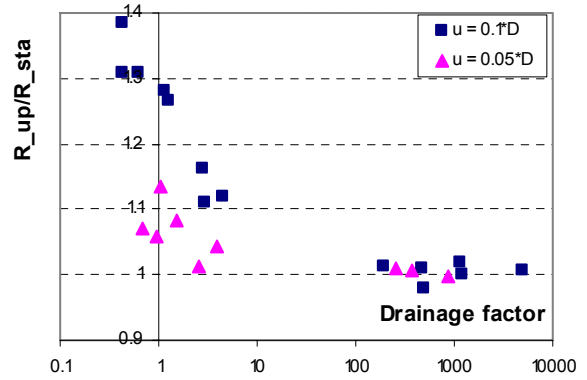


Figure 6.12: Normalised pile tip resistance at UP time against drainage factor ($u = 0.05 \cdot D$ & $u = 0.1 \cdot D$)

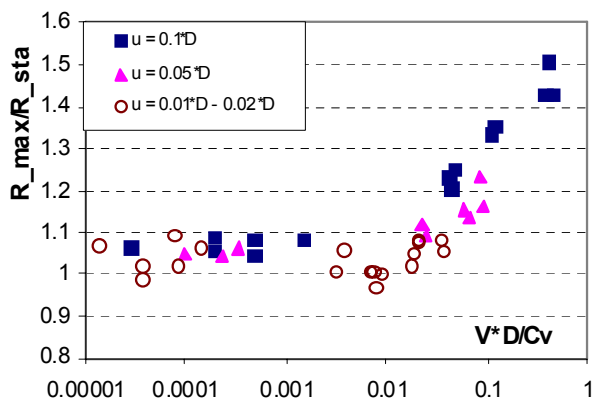


Figure 6.13: Normalised maximum pile tip resistance against velocity V ($u = 0.05 \cdot D$ & $u = 0.1 \cdot D$)

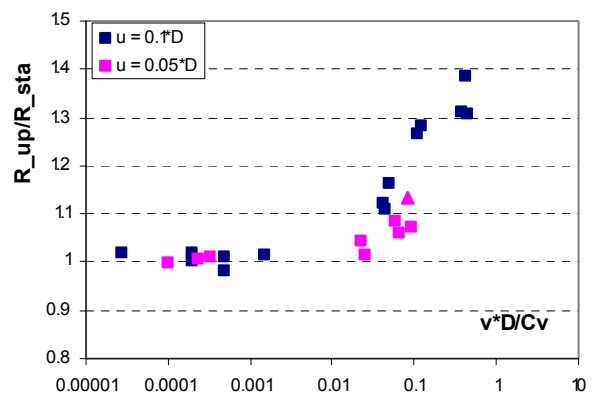


Figure 6.14: Normalised pile tip resistance at UP time against velocity V ($u = 0.05 \cdot D$ & $u = 0.1 \cdot D$)

6.3 Implications

The above elaborated results indicate that knowledge about the drainage factor is vital for analysing an in-situ rapid load test, especially in cases where a large diameter pile is founded in low permeability sand. The shear modulus and permeability should be known for the test site, so that the value of the drainage factor can be estimated.

A drainage factor value of 10 can be considered as a boundary when deciding whether the effect of excess pore pressure should be taken into account or not. If the drainage factor is larger than 10, the effect of excess pore pressure is negligible and only the true rate effect needs to be considered. It is important to bear in mind that the rate effect increases the maximum resistance of the pile, but does not influence the value of pile resistance at the time of maximum pile head displacement (unloading point). The UP method assumes that pile resistance at the unloading point is equal to the static value. Therefore, the UP method can be used in a straightforward way. The maximum resistance is approximately 10% higher than the static value, due to the true rate effect. This value is more or less constant within the range of penetration rate, shown in figure 6.8. Since this rate is used in practical applications, it could be used as a correction factor for the static value at the time of maximum force.

If the drainage factor is smaller than 10, the excess pore pressure increases both maximum resistance and resistance at the unloading point. Significant errors will therefore arise if the conventional UP method is used without taking this aspect into account. A correction for the excess pore pressure effect must be applied to accurately predict the static bearing capacity of a pile. However, it is currently not possible to give general recommendations for selecting this correction factor. The curves shown in figure 6.10 are based only on the results of these tests, and therefore cannot be guaranteed to be correct in general. More tests using different sands and pile diameters are essential.

If the excess pore pressure effect occurs, the relationship between mobilised resistance and velocity fits a power law as shown in figure 6.8 and 6.9. This is similar to the finding of Coyle and Gibson (1968). In these cases, a non-linear model similar to that proposed by the research group in Sheffield University (Brown, 2004; Anderson et. al. 2006) can be used to analyse the rapid load test. The required damping parameter for the power law can be taken from the study, from Gibson and Coyle (1968), or be based on experience from dynamic pile load testing.

The implications presented above are applicable when analysing a rapid pile load test in cases where the pile is founded in sand, where the pile tip resistance is predominant for the total resistance of the pile, and where pile head displacement during the RLT is approximately 10% of pile diameter.

6.4 Conclusions

The discussions in this chapter have resulted in the following statements:

- if no effect of excess pore pressure occurs, the UP method can be used in a straightforward way to determine the static bearing capacity of a pile from rapid load testing results. The rate effect correction factor suggested by Paikowsky et al, (2006) (see section 2.3.5) is not necessary.
- if the effect of excess pore pressure does occur, the UP method can be applied only when a correction factor is used. The value of this correction factor depends on the drainage condition of the test, and on the displacement magnitude of the pile head. This finding highlights the need for further study to derive the correction factor.

Chapter 7

Conclusions and recommendations

7.1 Conclusions

The introduction to this thesis states that the objective of this research is to provide answers to two fundamental questions that are relevant to the response of sand and a pile founded in sand under the high loading rate of a rapid load test.

- (1) The effect of the loading rate on the strength of sand, and on the mobilised resistance of a pile founded in sand.
- (2) The effect of excess pore pressure on the mobilised resistance of a pile founded in sand during the rapid load test.

Based on the findings of experimental research reported in chapters 3 and 5 and the numerical work described in chapter 4, the following conclusions can be drawn regarding these two fundamental questions.

7.1.1. Rate effect in sand

This thesis defines the rate effect as the strength dependency on the loading rate, excluding other dynamic effects such as inertia, damping, and pore pressure built up during testing. This ‘true’ rate effect should be seen as constitutive soil behaviour. In the laboratory experiments, this rate effect was generally measured directly. In the model tests on piles, the rate effect was derived by eliminating the other effects.

Investigation of the rate effect on sand’s strength in the triaxial tests has shown that the loading rate does increase the strength of sand. In dry sand, sand strength is seen to increase as the loading rate increases from a static rate to a rate of 0.2 m/s, but no significant increase in strength is found in the rate range 0.2 m/s to 0.6 m/s. This research provides the total increment for dry sand in terms of the friction angle from 1 to 1.5 degrees (or from 10 to 20% in terms of shear strength). When combined with the results reported in the literature, it can be concluded that the rate effect is only significant up to a certain ‘critical’ rate. After that value, there is no rate effect or it is only minor. For saturated sand, a 5% increase in peak strength is found. However, the true rate effect may be obscured by cavitation inside the specimen.

Regarding the rate effect on the resistance of a pile, there are a number of findings from the 1-g and the n-g tests. Firstly, pile tip resistance increases as the loading rate increases. Shaft friction is not affected by the loading rate. An increment of tip resistance that has the same magnitude as the effect on sand strength is possible. The existence of a ‘critical’

loading velocity as mentioned above is also supported by test results from the model pile. It appears that the penetration rate of the static load tests on the model pile at the 1-g condition (chapter 3) is too high (≈ 1 mm/s) in comparison with the generally accepted rate in conventional static load tests. This penetration rate may be in the same order of magnitude as the ‘critical’ rate, and no clear increment in resistance is therefore seen at higher rates. More evidence can also be found in literature (figures 2.20 and 2.21). This finding is also strengthened by results from the centrifuge test series (figure 6.8). In centrifuge test 4 (where only the loading rate effect exists), the constant value of an approximately 10% increase of pile tip resistance over the static value is found (the loading rates ranged from 5 mm/s to 285 mm/s). The triaxial tests on Baskarp sand reported by Ibsen (1995) indicate exactly the same rate effect as from the centrifuge test results (figure 2.11), although the loading rate in his study is much slower (from 10^{-3} - 10 mm/s). However, observations in 1-g tests may reflect that the rate effect is dependent on the sand type. This is currently not clear.

To summarise, it can be concluded that both sand strength and the tip resistance of a pile founded in sand increase as the loading rate increases. An increment of up to 20% is possible, depending on the sand type. The rate effect in sand is pronounced up to a certain ‘critical’ loading rate, but becomes insignificant above that value. This implies that evaluation of the rate effect largely depends on the chosen ‘static’ rate. The value of the ‘critical’ velocity has not been determined in this study, but is much smaller than the typical pile velocity value during a rapid load test. The rate effect can be therefore be expected to exist in the rapid load test.

7.1.2. Excess pore pressure effect

Investigations into the effect of excess pore pressure on the resistance of a pile embedded in sand have revealed that pile tip resistance as well as pile shaft friction may be significantly increased by excess pore pressure during the loading time of the RLTs. However, results from the centrifuge tests show that excess pore pressure does not affect pile shaft friction at the time of the unloading point. The magnitude of the effect depends on the sand properties, pile radius, loading duration, and the displacement magnitude. This research found that tip resistance increases up to 40% when the value of the defined drainage factor is as low as 0.4.

The increase in pile resistance is caused by negative excess pore pressure, which is due to the volume expansion of sand in shearing, known as dilatancy. This suggests that the dilatancy angle of the sand plays an essential role in the magnitude of the effect of excess pore pressure. In practice, excess pore pressure can be expected to have a different influence if rapid loading tests are performed on piles with the same dimensions, but where the dilatancy behaviour of the soil is different. The importance of dilatancy in the sand also implies that soil models capable of incorporating the dilatancy characteristics of the soil need to be implemented in the finite element code that is used (Titan code) for further parametric study into this aspect.

The increase of pile resistance due to the generation of negative excess pore pressure, even in the case of initially loose-packed sand, can be seen from the experiment results of this study. The density of the sand around the pile must be higher in this case. This is possible due to the effect of pile installation and/or the increment of pile penetration during the rapid test. This suggests that, in practical situations, the rapid load test on displacement piles may show a greater excess pore pressure effect than cases with auger piles or bored piles. It also implies that, in future, densification of the soil during pile penetration should be incorporated in the numerical works mentioned above.

The dynamic drainage factor (defined in chapter 4) can be used to distinguish between cases where excess pore pressure effects are expected, and cases where full drainage prevents any excess pore pressure effect. This factor is defined using the common soil properties (G , k), the known pile radius, and the loading duration of the test. The drainage factor can therefore be determined to assess the excess pore pressure effect,. Although the degree of excess pore pressure effect also depends on the displacement magnitude, the boundary value between these cases seems identical. The research suggests a boundary value of 10 for the defined drainage factor.

The calibration chamber is not a suitable device for studying the effect of excess pore pressure if the grain size and/or the viscosity of the pore fluid are not scaled. The small radius of the model pile and the sand's high permeability mean that the drainage factor value will be so high in this experimental situation that drainage will prevent the effect of excess pore pressure.

7.1.3. The UP method

With the regard to the UP method, the experiment results from this study show that the mobilised resistance of a pile embedded in sand during a rapid load test is not affected by the rate effect at the time of the unloading point, but may only be affected by excess pore pressure. Therefore, the UP method's significant assumption that pile resistance at the time of unloading point is identical to the static bearing capacity of the pile can only be valid in cases where there is no effect of excess pore pressure. However, this conclusion is only based on the limited number of experiment results from this study. For validation purposes, more evidence must be gathered from other tests using different sands as well as some well-defined field tests.

In cases where the effect of excess pore pressure exists, a correction factor is necessary for analysis using the UP method. The correction factor depends on the value of the drainage factor, which is determined by the permeability of the sand, the loading rate, and the pile dimensions. Assuming a pile displacement of approximately 10% of the diameter, figure 6.10 can be used to determine the correction factor.

The rate dependency of pile resistance in cases where excess pore pressure is generated fits a non-linear power law. The linear law used in the UP method is over-simplified in such cases. Application of a power law such as that proposed by the Sheffield University research group is more suitable.

With regard to the load-displacement curve, it can be concluded that stiffness is not affected by excess pore pressure based on the results of centrifuge tests. This seems to disagree with the numerical analysis findings in this research (section 4.3.3). However, this can be explained by the fact that the drainage factor value in the centrifuge tests is much lower than the value at which stiffness is seen to increase (figure 4.28).

7.2 Recommendations

The experimental results of this thesis, in particular from the centrifuge tests, provide valuable knowledge about the effect of the loading rate and excess pore pressure on the response of a pile during a rapid load test. They also make clear that more experiments need to be performed, and indicate a number of recommendations for further study.

- (1) Similar centrifuge tests with defined drainage factor values ranging from 5 to 100 are necessary to determine the drainage factor value at which the test condition changes from drained to partially drained. It is also recommended that the test is performed without the installation of pore pressure transducers in the sand bed to verify their influence on test results.
- (2) Centrifuge tests with other sand types are recommended to study the uniqueness of the influence curve, as shown in figure 6.10.
- (3) Implementation of a more advanced soil model that incorporates dilatancy and densification in the Titan code would be a good subject for further study. Use of such a numerical tool would enable more aspects of the problem to be examined, without the high cost of experiments.
- (4) A more fundamental explanation needs to be found for the difference between the numerical results and the centrifuge tests results regarding the dependency of the effect of excess pore pressure on the drainage factor.

References

- Abrantes, A.E. and Yamamuro, J.A., 2002. Experimental and Data Analysis Techniques Used for High Strain Rate Tests on Cohesionless Soil. *Geotechnical Testing Journal*, ASTM, Vol. 25, No. 2, pp. 128-141.
- Al-Mhaidib, A.I., 1999. Bearing capacity of a model pile in sand under different loading rates. *Proceedings of the 9th international offshore and polar engineering conference*, Brest, France, pp. 724–730.
- Allard, M.A., 1990. Soil stress field around driven piles. Doctor of philosophy thesis. California Institute of Technology.
- Allard, M.A. and Schenkeveld, F.M., 1994. The Delft Geotechnics model pore fluid for centrifuge tests, *Proc. of Centrifuge 94*, Balkema, Rotterdam, pp. 133-136.
- Altaee, A., and Fellenius, B. H., 1994. Physical modeling in sand. *Can. Geotech. J.* 31(3), pp. 420–431.
- Anderson, W.F., Hanh, N.D., and Hyde, A.F.L., 2006. A new analysis of data from a Statnamic tests on piles in clay. *Proc. 10th Int. Conf. Piling and Deep Foundations*, Amsterdam, the Netherlands, pp.
- Archeewa, E. 2005. The effect of loading rate on bearing capacity of saturated sand. MSc. Thesis, Unesco – IHE, Institute for water education, Delft, The Netherlands.
- Bermingham, P. & Janes, M.C. 1989. An innovative approach to load testing of high capacity piles. *Proc. of Int. Conf. on piling and deep foundation*, pp. 409-413.
- Bo, J. 1999. The vibration of an elastic circular plate on a fluid-saturated porous half space. *International Journal of Engineering Science*, Vol. 37, pp. 379-393.
- Brinkgvere, R.B.J. 2004. *Plaxis 2D-Version 8: User manuals*.
- Broere, M. 2004. Tunnel face stability and new CPT applications. PhD thesis, Faculty of. Civil Engineering and Geosciences, TU Delft.
- Broere, W. and van Tol, A.F. 2006. Modelling the bearing capacity of displacement piles in sand. *Proceedings of the Institution of Civil Engineers, Geotechnical Engineering*, 159(3):195-206, July 2006.
- Brown, D.A., 1994. Evaluation of static capacity of deep foundations from Statnamic testing, *Geotechnical testing journal*, Vol. 17, No. 4, pp. 403-414.
- Brown, M.J., 2004. The rapid load testing of piles in fine grained soils. Ph.D thesis. University of Sheffield, United Kingdom.
- Brown, M.J., Hyde, A.F.L., and Anderson, W.F., 2006. Analysis of a rapid load test on an instrumented bored pile in clay. *Geotechnique*, Vol 56, No. 9, pp. 627-638

Brumund, W. F. and Leonards, G. A., 1973. Experimental Study of Static and Dynamic Friction Between Sand and Typical Construction Materials. *Journal of Testing and Evaluation*, JTEVA, Vol. 1, No. 2, pp. 162-165.

Bruno, D. and Randolph, M. F., 1999. Dynamic and static load testing of model piles driven into dense sand. *Journal of Geotechnical and Geoenvironmental Engineering*, Vol. 125, No. 11, pp. 988-998.

Casagrande, A. and Shannon, W.L., 1948. Strength of soils under dynamic loads. *Proceeding of the American Society of Civil Engineering*, Vol. 74, No.4, pp. 591-608.

Charue, N. 2004. Loading rate effects on pile load-displacement behaviour derived from back-analysis of two load testing procedures. Ph.D thesis. Université catholique de Louvain (Belgium).

Chow, F.C. 1996. Investigations into the behavior of displacement piles for offshore foundations. Ph.D dissertation, University of London (Imperial College).

Coyle, H.M. and Gibson, G.C., 1970. Empirical damping constants for sands and clays. *Journal of Soil Mechanics and Foundations*. ASCE, Vol 96, N° SM3, pp 949-965.

Dayal, U. and Allen, J.H., 1975. The effect of penetration rate on the strength of remoulded clay and sand sample. *Canadian Geotechnical Journal*, Vol 12, pp 336-348.

De Nicola, A. and Randolph, M.F. 1994. Development of a miniature pile driving actuator', *Proc. Int. Conference Centrifuge '94*, Singapore, pp 473-478

Dijkstra, J. 2004. Influence of loading rate on pile capacity in sand. MSc. thesis, Delft University of Technology.

El Naggar, M.H., Novak, M. 1992. Analytical model for an innovative pile test. *Canadian geotechnical journal*, Vol 29, pp. 569-579.

El Naggar, M.H., Baldinelli, M. 1998. Stress wave analysis of Statnamic load test for bearing capacity prediction. *Proc. 2nd Int. Statnamic seminar*, Tokyo, pp. 327-335.

Eiksund, G. & Nordal, S., 1996. Dynamic model pile testing with pore pressure measurements. *Proc. 5nd Int. Conf. Application of stress-wave theory to piles*, Florida, pp. 581-588.

Finnie, I.M. and Randolph, M.F. 1994. Bearing response of shallow foundations on uncemented calcareous soil, *International Conference Centrifuge '94*, Singapore, Balkema, Rotterdam, 1: pp 535-540

Flemming, W. G. K., 1958. The Bearing Capacity of Pile Groups. PhD Thesis, Queen's University of Belfast.

- Fuglsang, L.D. and Ovesen, N.K. 1987. The application of theory of modelling to centrifuge studies. *Centrifuge in soil mechanics*. Craig, W., James, Schofield, A. (eds), Balkema, Rotterdam, pp. 119–138.
- Gennaro, V. De, Frank, R. Bosco, G. & Canou, J., 2001. Effet de la vitesse de chargement sur le comportement mecanique de pieux modele en chambre d'etalonnage. *Proc. 15th Int. Conf. Soil Mech. Geotech. Eng.*, Istanbul, Aug. 2001, Lisse, Balkema, 2001, Vol.2, pp.885-888.
- Gibson, G.C. & Coyle, H.M. 1968. Soil damping constants related to common soil properties in sands and clays (Bearing Capacity for Axially Loaded Piles). Texas Transportation Institute Research Report 125-1 (Study 2-5-67-125). Texas: Texas A&M University.
- Gonin, H., Coelus, G. & Leonard, M. 1984. Theory and performance of a new dynamic method of pile testing. *Proc. 2nd Int. Conf. Application of stress-wave theory to piles*, Stockholm, pp. 403-410.
- Hajduk, E.L., Paikowsky, S.G., Mullins, A.G., Ealy, C., Lewis, C., Hourani, N.M. 1998. The Behavior of Piles in Clay during Statnamic, Dynamic, and different Static Load Testing Procedures. *Proc. 2nd International Statnamic Seminar*, Tokyo, Japan, pp.59-73.
- Hanh, D.H. 2006. Rapid load testing of piles in clay. Ph.D thesis, Sheffield University, United Kingdom.
- Halpern, M. R. and Christiano, P. 1986. Steady-state harmonic response of a rigid plate bearing on a liquid-saturated poroelastic half space. *Earthquake Eng. Struct. Dyn.*, Vol: 14, pp. 439–454.
- Hyde, A.F.L., Anderson W.F., and Robinson S.A., 1998. Rate effects in clay soils and their relevance to Statnamic pile testing. In the Proceedings of the 2nd International Statnamic Seminar, Tokyo, Japan, pp 303-309.
- Head, K. H., 1998, *Manual of soil laboratory testing*, Vol. 1&2&3, Pentech press.
- Heerema E.P. 1979. Relationships between wall friction, displacement, velocity and horizontal stress in clay and in sand for pile driveability analysis. *Ground Engineering*, 12, N°1, pp 55-61.
- Hölscher, 1996. personal contact
- Hölscher, P. 1995. Dynamical response of saturated and dry soils. Ph.D thesis, Delft University of Technology, Delft, The Netherlands.
- Hölscher, P., and Barents, F,B,J. 1992. Statnamic load testing of Foundation piles. *Proc. 4th Int. Conf. Application of Stress Wave Theory to Piles*, the Netherlands, pp. 413-419
- Holeyman, A.E. 1992. Keynote lecture: Technology of pile dynamic testing, *Proc. 4nd Int. Conf. Application of stress-wave theory to piles*, The Hague: 195-216.

- Holeyman A.E., 2006. Pile monitoring, testing and data processing. Piling and Deep Foundations. Conference Proceedings, DFI EFFC, Amsterdam. 86-100
- Horikoshi, K., Kato, K. & Matsumoto, T. 1998. Finite element analysis of Statnamic loading test of pile. Proc. 2nd Int. Statnamic seminar, Tokyo: 295-302.
- Hungr, O., and Morgenstern, N.R., 1984. High velocity ring shear tests on sand. Géotechnique, Vol. 34, pp. 415-421.
- Huy, N.Q.**, Dijkstra, J., van Tol, A.F., and Hölscher, P, 2005 Influence of loading rate on floating piles in sand. In: Proc. Of the 16th Int. Conf. on Soil Mechanics and Geotechnical Engineering. Osaka, Japan. Vol.4, pp.2125-2128.
- Huy, N.Q.**, van Tol, A.F., and Hölscher, P, 2006. Numerical simulation of quasi-static pile load test. In: Proc. Of the 10th Int. Conf. on Piling and Deep Foundations. Amsterdam, The Netherlands. pp.677-683.
- Huy, N.Q.**, Hölscher, P., van Tol, A.F. 2007. A numerical study to the effects of excess pore water pressure in a rapid pile load test. Proc. XIV European Conference on Soil Mechanics and Geotechnical Engineering, ECSMGE 2007, 24-27 September 2007, Madrid, Spain.
- Huy, N.Q.**, van Tol, A.F., Hölscher P. 2008. Rapid model pile load tests in the geotechnical centrifuge, Part 1, Recent Developments in Rapid Load Testing on Piles. Hölscher P, van Tol, A.F. (Eds), Francis Taylor, September 2008.
- Huy, N.Q.**, van Tol, A.F., Hölscher P. 2008. Interpretation of a rapid pile load tests in sand in regard of rate effect and excess pore pressure. Accepted for printing in the Proc. 8th Int. Conf. on the Application of stress wave to piles. Lisbon, Portugal. September 2008.
- Hölscher, P., van Tol, A.F., **Huy, N.Q.** 2008. Influence of the rate effect and pore water pressure during rapid load test of piles in sand. Recent Developments in Rapid Load Testing on Piles. Hölscher P, van Tol, A.F. (Eds), Francis Taylor, September 2008.
- Hölscher, P., Bezuijen, A., van Lottum, H., **Huy, N.Q.**, van Tol, A.F. (2008) "Rapid pile test simulation in the geocentrifuge", Proceedings of the 2nd BGA Int. Conf. on Foundations to be held in Dundee, 24-27 June 2008
- Ibsen, L.B., 1995. The Static and Dynamic Strength of Sand. Proceedings of the 11th European Conference on Soil Mechanics and Foundation Engineering, Copenhagen, 28 May - 1 June 1995 : XI ECSMFE E : DGF-bulletin 11., Lyngby : Danish Geotechnical Society, 1995. pp. 69-76
- Janes, M.C., Justason, M.D. & Brown, D.A. 1998. Proposed ASTM Standard test for piles under rapid axial compressive load with its draft paper " Long period dynamic load testing ASTM Standard draft " presented to the seminar for technical discussion, Proc. 2nd Int. Statnamic seminar, Tokyo, pp. 199-118.

Jezequel, J.F., 1969. Les pénétromètre statiques. Influence du mode d'emploi sur la résistance de pointe. Laboratoire Central des Ponts et Chaussées, Bulletin de Liaison, 36, pp: 151-160.

Justason, M.D. et al. 1998. A comparison of static and Statnamic load tests in sand: A case study of the Bayou Chico bridge in Pensacola, Florida. Proc. 2nd Int. Statnamic seminar, Tokyo, pp. 43-53.

Karkee, M., Horiguchi, T., Kishida, H. 1997. Static and dynamic tests for evaluation of the vertical load bearing capacity of piles. In 22nd Annual member's Conference, Deep Foundations institute, pp. 199 – 214.

Kassir, M. K. Bandyopadyay, K. K. and Xu, J. 1989. Vertical vibration of a circular footing on a saturated half space. Int. J. Eng. Sci., 27, pp. 353–361.

Kusakabe et al., 1998. Proceedings of the 2nd International Statnamic Seminar, Tokyo, Japan, 1998. Kusakabe, O. et al. Editors

Kusakabe et al., 1998. Research Committee on Rapid Pile Load Test Methods – JGS, Japan. Research activities toward standardization of rapid pile load test methods in Japan. Proc. 2nd Int. Statnamic Loading Test Seminar, Tokyo, Japan, 1998. pp. 219 – 238.

Lee, K.L., Seed, H.B., and Dunlop, P., 1969. Effect of transient loading on the strength of sand. Proceedings of the 7th Int. Conf. on soil mechanics and foundation Eng., Vol. 1, pp. 239-247.

Lewis, C.L. 1999. Analysis of Axial Statnamic Testing by the Segmental Unloading Point Method. Master of Science Thesis submitted to the University of South Florida, Tampa, FL.

Litkouhi, S. and Poskitt, T.J., 1980. Damping constants for pile driveability calculations, Geotechnique, Vol. 30, No. 1, pp. 77-86.

Lysmer, J and Richart F.E. Jr. 1966. Dynamic response of footings to vertical loading. J. Soil Mech. and Found. Div., ASCE, 92, No. SM 1, 65-91.

Mangal. J.K. 1999. Partially – drained loading of shallow foundations on sand. Doctor of philosophy thesis. University of Ocford.

Matsumoto, T., Tsuzuki, M., 1994, Statnamic Tests on Steel Pipe Piles Driven in a Soft Rock. International Conference on Design and Construction of Deep Foundations, Orlando, U.S. Federal Highway Administration

Matsumoto, T. and Nishimura, S., 1996. Wave propagation phenomena in statnamic tests of a steel pipe pile. Proceedings of the 5th International Conference on the Application of Stress-Wave Theory to Piles, Orlando, Florida, USA. pp 1015-1030.

Matsumoto, T. 1998. Finite element analyses of Statnamic loading test of pile. Proc. 2nd Int. Statnamic Seminar, Tokyo, Japan, pp. 295-302

Matsumoto, T., Asai, Y. and Hayashi, T. 1998. Two Successive Statnamic Load Tests on a Cast-in-Situ Concrete Pile. Proc. 2nd Int. Statnamic seminar, Tokyo, Japan, pp. 159-168

Matsumoto et al. 2004. Development of a rapid pile load test method using a falling mass attached with spring and damper. Proc. 7th Int. Conf. on the Appl. of Stress-Wave Theory to Piles, pp. 351-358

Matsumoto, T., 2005 personal contact.

Maeda, Y., Muroi, T., Nakazono, N., Takeuchi, H., and Yamamoto, Y., 1998. Applicability of Unloading-point-method and signal matching analysis on the Statnamic test for cast-in-place pile. Proceedings of the 2nd International Statnamic Seminar, pp. 99-108.

McVay, M.C, Kuo, C.L. and Guisinger, A.L. 2003. Calibrating Resistance Factors in the Load and Resistance Factor Design of Stanamic Loading Testing. Final report submitted to Florida Department of Transportation (internet source).

Middendorp, P., Bermingham, P., and Kuiper, B., 1992. Stanamic Load Testing of Foundation Piles. Proc. Fourth International Conference on the Application of Stress Waves on Piles, the Hague, Balkema, pp 581-588.

Middendorp, P. & Bielefeld, M.W. 1995. Stanamic load testing and the influence of stress wave phenomena. Proc. 1st Int. Stanamic seminar, Vancouver, pp:207-220.

Middendorp, P. 2000. Keynote lecture: Stanamic the engineering of art. Proc. 6th Int. Conf. Application of stress-wave theory to piles, Sao Paolo: pp: 551-562.

Moller, B. and Bergdahl, U., 1981. Dynamic Pore Pressure During Pile Driving in Fine Sand. Proceedings of the 10th International Conference on Soil Mechanics and Foundation Engineering, Vol. 2, pp. 791-794.

Mullins, G., Lewis, C.L. and Justason, M.D. 2002. Advancements in Statnamic data regression techniques. In M.W. O'Neill (ed), Proc. ASTM Conf. Int. Deep Foundations Congress, 2002, Florida, ASTM Geotechnical Special Publication No.116, Vol. 2. pp 915-930.

Nishimura, S. and Matsumoto, T. 1995. Wave propagation analysis during Statnamic loading of a steel pipe. Proc. of 1st Int Statnamic Seminar, Vancouver, Canada, pp. 23-33.

Ochiai, H., Kusakabe, O., Sumi, K., Matsumoto, T. and Nishimura, S. 1996. Statnamic tests on offshore steel pipe piles for foundations of access bridge for New Kita-Kyushu airport inland. Proc. 5th Int. Conf. Application of stress-wave theory to piles, Florida, pp: 997-1014.

Ovesen, N.K. 1981. Centrifuge tests to determine the uplift capacity of anchor slabs in sand. Proceedings, 10th International Conference on Soil Mechanics and Foundation Engineering, Stockholm, Sweden, vol. 1, pp. 717-722.

Parkin, A.K. and Lunne, T. (1982). Boundary effects in the laboratory calibration of a cone penetrometer for sand. Proc. of the 2nd. European symp. on Penetration Testing, Amsterdam, v2, ~761-767.

Paikowsky, S.G. 2006. Innovative pile load testing. Internet source.

Poulos, H.G. 1998. Keynote lecture: Pile testing-From the designer's viewpoint, Proc. 2nd Int. Statnamic seminar, Tokyo: 3-21.

Philippacopoulos, A. J. 1989. Axisymmetric vibration of disk resting on saturated layered half space. J. Eng. Mech. Div., Vol 115, No 10, pp. 2301-2322.

Phillips, R. and Valsangkar, A.J. 1987. An experimental investigation of factors affecting penetration resistance in granular soils in centrifuge modelling. Technical Report No CUED/D-Soils TR210, Cambridge University, UK.

Randolph, M.F. and Deeks, A.D. 1992. Keynote lecture: Dynamic and static soil models for axial pile response, Proc. 4nd Int. Conf. Application of stress-wave theory to piles, The Hague, pp. 3- 14.

Randolph M.F., Carter J.P. and Wroth C.P. 1979. Driven Piles in Clay - The Effects of Installation and Subsequent Consolidation. Géotechnique, Vol 29, pp. 361-393

Sedran, G., Stolle, D.F.E. and Horvath, R.G., 1998. Physical Modelling of Load Tests on Piles. Proceedings of the 2nd International Statnamic Seminar, editors - O. Kusakabe, F. Kuwabara and T. Matsumoto, 2000, pp.355-364.

Seed, H. B. and Lundgren, R. .1954. Investigation of the Effect of Transient Loading on the Strength and Deformation Characteristics of Saturated Sands. Proc. American Society for Testing and Materials, Vol. 54, pp. 1288-1306.

Schimming, B. B., Haas, A. M., and Saxe, H. C., 1966. Study of Dynamic and Static Failure Envelopes. Journal of the Soil Mechanics and Foundations Division, ASCE, Vol. 92, No. SM2, pp. 105-124.

Seidel, J.P. 1996. The use of the signal matching approach to the analysis of Statnamic tests. In Townsend, M. Hussein & M.C. McVay (eds), Pro. 5th Int. Conf. on the Application of Stress Wave Theory to Piles, Florida, 11-13 September, 1996. Rotterdam, A.A. Balkema. pp. 1051-1061.

Schellingerhout, A.J.G. & Revoort, E. 1996. Pseudo static pile load tester, Proc. 5th Int. Conf. Application of stress-wave theory to piles, Florida: pp. 251-260.

Van Foeken, R.J., Middendorp, P. and Courage, W.M.G., 1998. Application of stress wave method for automatic signal matching and Statnamic predictions. Proceedings of the 2nd International Statnamic Seminar, Tokyo, Japan, pp 345-354.

Poel J.T.van der, and Schenkeveld, F.M. 1998. A preparation technique for very homogenous sand models and CPT research. *Centrifuge 98*, Vol. 1, pp. 149-154.

Vesic, A.S., Banks, D.C., and Woodard, J.M. 1965. An experimental study of dynamic bearing capacity of footings on sand. *In* Proceedings of the 6th International Conference on Soil Mechanics and Foundation Engineering, Montréal, Que., 8–15 September, University of Toronto Press, Toronto, Ont. Vol. 2, pp. 209–213.

Wehnert, M., and Vermeer, P.A., 2004. Numerical analyses of load tests on bored piles. Proc. of the 9th Symposium on Numerical Models in Geomechanics (NUMOG IX), Ottawa/Canada, Leiden: A.A. Balkema Publishers, 2004, pp. 505-511.

White, D., 2002. An investigation into the behaviour of pressed in piles. PhD Thesis, University of Cambridge, UK.

Whitman, R.V. 1957. The behaviour of soils under transient loadings. Proc. , 4th Int. Conf. on Soil Mechanics and Foundation Engineering, 1957. pp. 207-210..

Whitman, R. V. and Healy, K. A., 1962. Shear strength of sands during rapid loading. Journal of the soil mechanics and foundations division, ASCE, Vol.88, No. SM2, pp. 99-132.

List of abbreviations and symbols

In general all abbreviations and symbols are explained in detail in the text.

List of abbreviations

CUR: Civieltechnisch Centrum Uitvoering Research en Regelgeving - Centre for Civil Engineering Research and Codes
CRP: Constant rate of penetration
FEM: Finite element method
MLT: Maintained load test
MUP method: Modified unloading point method
PP: Measured excess pore pressure in the model pile toad test
PS: Pseudo-static load test
RLT: Rapid load test
SDOF: Single degree of freedom
SLT: Static load test
STA: Static
STN: Statnamic
SUM method: Segmental unloading point method
UP: unloading point

List of symbols

a: Acceleration (m/s^2)
c: Velocity of stress wave propagation in the pile (m/s)
 c_v : Coefficient of consolidation
C: Damping coefficient (N.s/m)
D: Pile diameter (m)
e: Void ratio of sand
 E, E_u : Effective and undrained Young's modulus (N/m^2)
 F_{stn} : Applied Statnamic force (N)
 F_{soil} : Total mobilized soil resistance (N)
 F_a : Inertial force of the pile mass (N)
 F_v : Damping force (N)
 $F_u = F_{STA}$: Derived static force (resistance – N)
 F_{point} : Point resistance of the model pile (N)
 F_{sleeve} : Sleeve friction of the model pile (N)
 F_d, F_D : Pile resistance in drained condition (N)
 F_{ud} : Pile resistance in undrained condition (N)
 F_{PD} : Pile resistance in partially drained condition (N)
 F_{head} : Applied pile head force (N)
 F_{tip} : Pile tip resistance (N)

F_{shaft} : Pile shaft resistance (N)
 g : Gravity acceleration (m/s^2)
 G : Shear modulus (N/m^2)
 I_d : Relative density (%)
 J : Damping parameter in the Smith's model
 k : - Soil permeability (m/s)
 - Spring stiffness (N/m)
 K_s, K_w : Bulk modulus of soil skeleton and water (N/m^2)
 L : Pile length (m)
 m : Pile mass (kg/m^3)
 N : Scaling factor
 N_w : wave number
 r : Pile radius (m)
 R_d : Total dynamic resistance (N)
 R_s : Total static resistance (N)
 R_{up} : Pile tip resistance at the unloading point (N)
 R_{max} : Maximum pile tip resistance (N)
 t : Time (s)
 t_r : Relative duration
 T : Loading duration (s)
 u : Displacement (m)
 Δu : Excess pore pressure (Pa)
 v : Velocity (m/s)

α, β : Damping coefficient of the rate effect model used by the Sheffield University research group.

τ_d : Limiting value of the dynamic shaft resistance (N/m^2)
 τ_s : Limiting value of the static shaft resistance (N/m^2)
 η : - Loading rate correction factor proposed by Paikowsky et al. (2006)
 - The defined drainage factor
 ν', ν_u : Effective and undrained Poisson's ratio
 ρ : Volumetric mass (kg/m^3)
 σ : stress (Pa)
 φ : Friction angle (deg.)
 ψ : dilatancy angle (deg.)

APPENDIX 5A: Loading procedure of the centrifuge tests

Centrifuge test 2: 19-4-2007

Boundary conditions:

- Pile is installed in the sand with the pile tip at 10D below surface
- The sand is fully saturated with a high viscous fluid of approx. 265 cSt.
- The sand had a relative density of $D_r = 54\%$
- The test was carried out at $N_g = 40$
- Diameter of the pile $d = 11,3\text{ mm}$

Installation of the pile		
	GEF nr.	
1	1	Installation of the pile with another 10D = 113 mm with a constant speed of 10 mm/min. ($t = 11.3\text{ min}$)
2	1	Unloading of the pile to approx. 0 kN
Static loading 1		
3	2	Displacement $0,1D = 1,13\text{ mm}$ in 676.6 sec ($v = 0.00167\text{ mm/s}$)
4	2	Unloading of the pile to approx. 0 kN
Quasi-Static loading series 1 (Slow)		
5	3	Displacement $\downarrow 0,01D = 0,113\text{ mm}$ in 0,048 sec ($v = 2.35\text{ mm/s}$) Displacement $\uparrow 0,005D = 0,0565\text{ mm}$ with ($v = 2.35\text{ mm/s}$)
6	3	Unloading of the pile to approx. 0 kN
7	3	Displacement $\downarrow 0,02D = 0,226\text{ mm}$ in 0,048 sec ($v = 4.70\text{ mm/s}$) Displacement $\uparrow 0,01D = 0,113\text{ mm}$ with ($v = 4.70\text{ mm/s}$)
8	3	Unloading of the pile to approx. 0 kN
9	3	Displacement $\downarrow 0,05D = 0,565\text{ mm}$ in 0,048 sec ($v = 11.77\text{ mm/s}$) Displacement $\uparrow 0,01D = 0,113\text{ mm}$ with ($v = 11.77\text{ mm/s}$)
10	3	Unloading of the pile to approx. 0 kN
11	3	Displacement $\downarrow 0,1D = 1,13\text{ mm}$ in 0,048 sec ($v = 23.5\text{ mm/s}$) Displacement $\uparrow 0,01D = 0,113\text{ mm}$ with ($v = 23.5\text{ mm/s}$)
12	3	Unloading of the pile to approx. 0 kN
Static loading 2		
13	4	Displacement $0,1D = 1,13\text{ mm}$ in 676.6 sec ($v = 0.00167\text{ mm/s}$)
14	4	Unloading of the pile to approx. 0 kN

Quasi-Static loading series 2 (Average)		
15	5	Displacement ↓ 0,01D = 0,113 mm in 0,0185 sec (v = 6.10 mm/s) Displacement ↑ 0,005D = 0,0565 mm with (v = 6.10 mm/s)
16	5	Unloading of the pile to approx. 0 kN
17	5	Displacement ↓ 0,02D = 0,226 mm in 0,0185 sec (v = 12.2 mm/s) Displacement ↑ 0,01D = 0,113 mm with (v = 12.2 mm/s)
18	5	Unloading of the pile to approx. 0 kN
19	5	Displacement ↓ 0,05D = 0,565 mm in 0,0185 sec (v = 30.5 mm/s) Displacement ↑ 0,01D = 0,113 mm with (v = 30.5 mm/s)
20	5	Unloading of the pile to approx. 0 kN
21	5	Displacement ↓ 0,1D = 1,13 mm in 0,0185 sec (v = 61.1 mm/s) Displacement ↑ 0,01D = 0,113 mm with (v = 61.1 mm/s)
22	5	Unloading of the pile to approx. 0 kN
Static loading 3		
23	6	Displacement 0,1D = 1,13 mm in 676.6 sec (v = 0.00167 mm/s)
24	6	Unloading of the pile to approx. 0 kN
Quasi-Static loading series 3 (Fast)		
25	7	Displacement ↓ 0,01D = 0,113 mm in 0,009 sec (v = 12.55 mm/s) Displacement ↑ 0,005D = 0,0565 mm with (v = 12.55 mm/s)
26	7	Unloading of the pile to approx. 0 kN
27	7	Displacement ↓ 0,02D = 0,226 mm in 0,009 sec (v = 25.1 mm/s) Displacement ↑ 0,01D = 0,113 mm with (v = 25.1 mm/s)
28	7	Unloading of the pile to approx. 0 kN
29	7	Displacement ↓ 0,05D = 0,565 mm in 0,009 sec (v = 62.8 mm/s) Displacement ↑ 0,01D = 0,113 mm with (v = 62.8 mm/s)
30	7	Unloading of the pile to approx. 0 kN
31	7	Displacement ↓ 0,1D = 1,13 mm in 0,009 sec (v = 125.6 mm/s) Displacement ↑ 0,01D = 0,113 mm with (v = 125.6 mm/s)
32	7	Unloading of the pile to approx. 0 kN
Static loading 4		
33	8	Displacement 0,1D = 1,13 mm in 676.6 sec (v = 0.00167 mm/s)

Centrifuge test 3: 12-6-2007

Boundary conditions:

- Pile is installed in the sand with the pile tip at 10D below surface
- The sand is fully saturated with a high viscous fluid of approx. 292 cSt.
- The sand had a relative density of $D_r = 36\%$
- The test was carried out at $N_g = 40$
- Diameter of the pile $d = 11,3$ mm

Installation of the pile		
	GEF nr.	
1	2	Installation of the pile with another 10D = 113 mm with a constant speed of 10 mm/min. (t = 11.3 min)
2	2	Unloading of the pile to approx. 0 kN
Static loading 1		
3	2	Displacement 0,1D = 1,13 mm in 676.6 sec ($v = 0.00167$ mm/s)
4	2	Unloading of the pile to approx. 0 kN
Quasi-Static loading series 1 (Slow)		
5	3	Displacement ↓ 0,01D = 0,113 mm in 0,048 sec ($v = 2.35$ mm/s) Displacement ↑ 0,005D = 0,0565 mm with ($v = 2.35$ mm/s)
6	3	Unloading of the pile to approx. 0 kN
7	3	Displacement ↓ 0,02D = 0,226 mm in 0,048 sec ($v = 4.70$ mm/s) Displacement ↑ 0,01D = 0,113 mm with ($v = 4.70$ mm/s)
8	3	Unloading of the pile to approx. 0 kN
9	3	Displacement ↓ 0,05D = 0,565 mm in 0,048 sec ($v = 11.77$ mm/s) Displacement ↑ 0,01D = 0,113 mm with ($v = 11.77$ mm/s)
10	3	Unloading of the pile to approx. 0 kN
11	3	Displacement ↓ 0,1D = 1,13 mm in 0,048 sec ($v = 23.5$ mm/s) Displacement ↑ 0,01D = 0,113 mm with ($v = 23.5$ mm/s)
12	3	Unloading of the pile to approx. 0 kN
Static loading 2		
13	4	Displacement 0,1D = 1,13 mm in 676.6 sec ($v = 0.00167$ mm/s)
14	4	Unloading of the pile to approx. 0 kN

Quasi-Static loading series 2 (Average)		
15	5	Displacement ↓ 0,01D = 0,113 mm in 0,0185 sec (v = 6.10 mm/s) Displacement ↑ 0,005D = 0,0565 mm with (v = 6.10 mm/s)
16	5	Unloading of the pile to approx. 0 kN
17	5	Displacement ↓ 0,02D = 0,226 mm in 0,0185 sec (v = 12.2 mm/s) Displacement ↑ 0,01D = 0,113 mm with (v = 12.2 mm/s)
18	5	Unloading of the pile to approx. 0 kN
19	5	Displacement ↓ 0,05D = 0,565 mm in 0,0185 sec (v = 30.5 mm/s) Displacement ↑ 0,01D = 0,113 mm with (v = 30.5 mm/s)
20	5	Unloading of the pile to approx. 0 kN
21	5	Displacement ↓ 0,1D = 1,13 mm in 0,0185 sec (v = 61.1 mm/s) Displacement ↑ 0,01D = 0,113 mm with (v = 61.1 mm/s)
22	5	Unloading of the pile to approx. 0 kN
Static loading 3		
23	6	Displacement 0,1D = 1,13 mm in 676.6 sec (v = 0.00167 mm/s)
24	6	Unloading of the pile to approx. 0 kN
Quasi-Static loading series 3 (Fast)		
25	7	Displacement ↓ 0,01D = 0,113 mm in 0,009 sec (v = 12.55 mm/s) Displacement ↑ 0,005D = 0,0565 mm with (v = 12.55 mm/s)
26	7	Unloading of the pile to approx. 0 kN
27	7	Displacement ↓ 0,02D = 0,226 mm in 0,009 sec (v = 25.1 mm/s) Displacement ↑ 0,01D = 0,113 mm with (v = 25.1 mm/s)
28	7	Unloading of the pile to approx. 0 kN
29	7	Displacement ↓ 0,05D = 0,565 mm in 0,009 sec (v = 62.8 mm/s) Displacement ↑ 0,01D = 0,113 mm with (v = 62.8 mm/s)
30	7	Unloading of the pile to approx. 0 kN
31	7	Displacement ↓ 0,1D = 1,13 mm in 0,009 sec (v = 125.6 mm/s) Displacement ↑ 0,01D = 0,113 mm with (v = 125.6 mm/s)
32	7	Unloading of the pile to approx. 0 kN

Static loading 4		
33	8	Displacement $0,1D = 1,13$ mm in 676.6 sec ($v = 0.00167$ mm/s)
34	8	Unloading of the pile to approx. 0 kN (NOT PERFORMED)

Quasi-Static loading rate test		
35	8	Displacement $\downarrow 0,1D = 1,13$ mm in 0,23 sec ($v = 5$ mm/s) (low sample rate) Displacement $\uparrow 0,02D = 0,226$ mm with ($v = 5$ mm/s)
36	9	Unloading of the pile to approx. 0 kN
37	9	Displacement $\downarrow 0,1D = 1,13$ mm in 0,048 sec ($v = 23.5$ mm/s) Displacement $\uparrow 0,02D = 0,226$ mm with ($v = 23.5$ mm/s)
38	9	Unloading of the pile to approx. 0 kN
39	9	Displacement $\downarrow 0,1D = 1,13$ mm in 0,0185 sec ($v = 61.1$ mm/s) Displacement $\uparrow 0,02D = 0,226$ mm with ($v = 61.1$ mm/s)
40	9	Unloading of the pile to approx. 0 kN
41	9	Displacement $\downarrow 0,1D = 1,13$ mm in 0,009 sec ($v = 125.6$ mm/s) Displacement $\uparrow 0,01D = 0,226$ mm with ($v = 125.6$ mm/s)

Centrifuge test 4: 24-10-2007

Boundary conditions:

- Pile is installed in the sand with the pile tip at $10D$ below surface
- The sand is fully saturated with water
- The sand had a relative density of $D_r = 65\%$
- The test was carried out at $N_g = 40$
- Diameter of the pile $d = 11,3$ mm

Installation of the pile		
	GEF nr.	
1	4	Installation of the pile with another $10D = 113$ mm with a constant speed of 10 mm/min. ($t = 11.3$ min)
2	4	Unloading of the pile to approx. 0 kN
Static loading 1		
3	5	Displacement $0,1D = 1,13$ mm in 676.6 sec ($v = 0.00167$ mm/s)
4	5	Unloading of the pile to approx. 0 kN

Quasi-Static loading serie 1 (Slow)		
5	6	Displacement ↓ 0,01D = 0,113 mm in 0,048 sec (v = 2.35 mm/s) Displacement ↑ 0,005D = 0,0565 mm with (v = 2.35 mm/s)
6	6	Unloading of the pile to approx. 0 kN
7	6	Displacement ↓ 0,02D = 0,226 mm in 0,048 sec (v = 4.70 mm/s) Displacement ↑ 0,01D = 0,113 mm with (v = 4.70 mm/s)
8	6	Unloading of the pile to approx. 0 kN
9	6	Displacement ↓ 0,05D = 0,565 mm in 0,048 sec (v = 11.77 mm/s) Displacement ↑ 0,01D = 0,113 mm with (v = 11.77 mm/s)
10	6	Unloading of the pile to approx. 0 kN
11	6	Displacement ↓ 0,1D = 1,13 mm in 0,048 sec (v = 23.5 mm/s) Displacement ↑ 0,01D = 0,113 mm with (v = 23.5 mm/s) (LOADING NOT PERFORMED)
12	7	Unloading of the pile to approx. 0 kN
Static loading 2		
13	7	Displacement 0,1D = 1,13 mm in 676.6 sec (v = 0.00167 mm/s)
14	7	Unloading of the pile to approx. 0 kN
Quasi-Static loading serie 2 (Average)		
15	8	Displacement ↓ 0,01D = 0,113 mm in 0,0185 sec (v = 6.10 mm/s) Displacement ↑ 0,005D = 0,0565 mm with (v = 6.10 mm/s)
16	8	Unloading of the pile to approx. 0 kN
17	8	Displacement ↓ 0,02D = 0,226 mm in 0,0185 sec (v = 12.2 mm/s) Displacement ↑ 0,01D = 0,113 mm with (v = 12.2 mm/s)
18	8	Unloading of the pile to approx. 0 kN
19	8	Displacement ↓ 0,05D = 0,565 mm in 0,0185 sec (v = 30.5 mm/s) Displacement ↑ 0,01D = 0,113 mm with (v = 30.5 mm/s)
20	8	Unloading of the pile to approx. 0 kN
21	8	Displacement ↓ 0,1D = 1,13 mm in 0,0185 sec (v = 61.1 mm/s) Displacement ↑ 0,01D = 0,113 mm with (v = 61.1 mm/s)
22	8	Unloading of the pile to approx. 0 kN

Static loading 3		
23	9	Displacement $0,1D = 1,13$ mm in 676.6 sec ($v = 0.00167$ mm/s)
24	9	Unloading of the pile to approx. 0 kN
Quasi-Static loading serie 3 (Fast)		
25	10	Displacement $\downarrow 0,01D = 0,113$ mm in 0,009 sec ($v = 12.55$ mm/s) Displacement $\uparrow 0,005D = 0,0565$ mm with ($v = 12.55$ mm/s)
26	10	Unloading of the pile to approx. 0 kN
27	10	Displacement $\downarrow 0,02D = 0,226$ mm in 0,009 sec ($v = 25.1$ mm/s) Displacement $\uparrow 0,01D = 0,113$ mm with ($v = 25.1$ mm/s)
28	10	Unloading of the pile to approx. 0 kN
29	10	Displacement $\downarrow 0,05D = 0,565$ mm in 0,009 sec ($v = 62.8$ mm/s) Displacement $\uparrow 0,01D = 0,113$ mm with ($v = 62.8$ mm/s)
30	10	Unloading of the pile to approx. 0 kN
31	10	Displacement $\downarrow 0,1D = 1,13$ mm in 0,009 sec ($v = 125.6$ mm/s) Displacement $\uparrow 0,01D = 0,113$ mm with ($v = 125.6$ mm/s)
32	10	Unloading of the pile to approx. 0 kN
Static loading 4		
33	11	Displacement $0,1D = 1,13$ mm in 676.6 sec ($v = 0.00167$ mm/s)
34	11	Unloading of the pile to approx. 0 kN
Quasi-Static loading rate test		
35	12	Displacement $\downarrow 0,1D = 1,13$ mm in 0,23 sec ($v = 5$ mm/s) Displacement $\uparrow 0,02D = 0,226$ mm with ($v = 5$ mm/s)
36	12	Unloading of the pile to approx. 0 kN
37	12	Displacement $\downarrow 0,1D = 1,13$ mm in 0,048 sec ($v = 23.5$ mm/s) Displacement $\uparrow 0,02D = 0,226$ mm with ($v = 23.5$ mm/s)
38	12	Unloading of the pile to approx. 0 kN
39	12	Displacement $\downarrow 0,1D = 1,13$ mm in 0,0185 sec ($v = 61.1$ mm/s) Displacement $\uparrow 0,02D = 0,226$ mm with ($v = 61.1$ mm/s)
40	12	Unloading of the pile to approx. 0 kN
41	9	Displacement $\downarrow 0,1D = 1,13$ mm in 0,009 sec ($v = 125.6$ mm/s) Displacement $\uparrow 0,01D = 0,226$ mm with ($v = 125.6$ mm/s) (loading not recorded)

Curriculum Vitae

Name

Nguyen Quang Huy

Date of birth

7 June 1975 in Hanoi, Vietnam

- | | |
|------------------------|--|
| Sep. 1992 - June. 1997 | Bachelor of Civil Engineering, Hanoi University of Civil Engineering. |
| Sep. 1997 - Sep. 2000 | Master of Engineering, Hanoi University of Civil Engineering. |
| Sep. 19975 - Dec. 2002 | Lecturer in the Section of Structural Mechanics, Faculty of Civil Engineering, Hanoi University of Civil Engineering. |
| Jan. 2003 – Mar. 2008 | Ph.D. researcher in the Section of Geotechnics Laboratory, Faculty of Civil Engineering and Geosciences, Delft University of Technology. |

